THE PHYSICAL REVIEW

VOLUME 82 Second 3

MAY 1, 1951

Published
AMERICAN PHYSICAL SOCIETY

THE PHYSICAL REVIEW

A journal of experimental and theoretical physics established by E. L. Nichols in 1893

Published by the American Institute of Physics for the

AMERICAN PHYSICAL SOCIETY

Officers

President

C. C. LAURITSEN
California Institute of Technology
Pasadena, California

Vice-President

J. H. VAN VLECK
Harvard University
Cambridge, Massachusetts

Secretary

K. K. DARROW
Bell Telephone Laboratories
Office:
Columbia University
New York 27, New York

Treasurer

G. B. PEGRAM
Columbia University
New York 27, New York

Local Secretary
for the Pacific Coast

J. KAPLAN
University of California at Los Angeles
Los Angeles, California

Managing Editor

S. A. GOUDSMIT
Brookhaven National Laboratory
Upton, Long Island
New York

BOARD OF EDITORS

Editor

S. A. GOUDSMIT

Assistant Editor

S. PASTERNACK

Associate Editors

J. BARDEEN — HARVEY BROOKS — M. GOLDHABER
T. BONNER — R. E. CHERRY — R. HOFSTADTER
R. G. HERB — C. L. CRITCHFIELD — A. W. LAWSON
W. E. LAMB, JR. — M. DEUTSCH — A. PAIS
A. J. F. SIEGERT — T. H. JOHNSON — R. SERBER
W. E. STEPHENS — ERLING ROSTI — C. H. TOWNES

Manuscripts for publication should be submitted to S. A. Goudsmit, Brookhaven National Laboratory, Upton, Long Island, New York. Authors' institutions are requested to pay a publication charge of $10 per page which, if honored, entitles them to 100 free reprints. Instructions will be sent with galley proofs.

Proof and all correspondence concerning papers in the process of publication should be addressed to the Publication Manager, American Institute of Physics, 57 East 55 Street, New York 22, New York.

Subscription Price

United States and Canada $25.00
Elsewhere $27.00

Back Numbers[1]

Yearly back number rate when complete year is available:
Prior to 1949: $25.00
Thereafter: $27.00
Single copies: $2.00 each, prior to July, 1929;
$1.00 each, July, 1929–December, 1941;
$2.00 each, January, 1942–December, 1946;
$1.00 each, January, 1947–December, 1948;
$1.25 each, thereafter.
General index, 1893–1930: $4.00.

Subscriptions, renewals, and orders for back numbers should be addressed to the American Institute of Physics, 57 East 55 Street, New York 22, New York.

Changes of address in the case of members of the American Physical Society should be addressed to the Treasurer; in the case of other subscribers to the American Institute of Physics.

[1] For Sale: Library of Physics Department, Cornell University, Ithaca, New York.

The Physical Review is published semi-monthly at Prince and Lemon Streets, Lancaster, Pennsylvania.

Entered as second-class matter March 6, 1947, at the Post Office at Lancaster, Pennsylvania, under the Act of March 3, 1879.

Acceptance for mailing at special rate of postage provided for in paragraph (d-2), section 34.40, P. L. & R. of 1948, authorized January 29, 1948.

THE
PHYSICAL REVIEW

A journal of experimental and theoretical physics established by E. L. Nichols in 1893

SECOND SERIES, VOL. 82, NO. 3 MAY 1, 1951

The Properties of Particles Producing High Energy Nuclear Collisions in Gold*

MELVIN B. GOTTLIEB†
Department of Physics, University of Chicago, Chicago, Illinois
(Received December 18, 1950)

A large multiplate counter controlled cloud chamber containing 300 g/cm² of gold has been used for the study of penetrating showers at an altitude of 11,500 ft. The minimum energy required to trip the counter control efficiently was about 15 Bev. Counters located inside the chamber made it possible to observe events initiated by both ionizing and non-ionizing particles. It was found that at least 83.5 percent of the particles initiating these high energy events were ionizing. From the distribution of events in the plates of the chamber, the mean free path in gold for the particles producing these penetrating showers was found to be 145±15 g/cm². The projected zenith angle distribution of the shower primaries could be approximately represented by $\cos^m\theta$, where m was in the range 8 to 10. Since the measurements were made at 680 g/cm² atmospheric depth, this corresponds to an absorption mean free path in air of 70 to 90 g/cm². The flux of particles capable of producing these high energy showers was found to be $(1.7\pm1)\times10^{-6}$ particles cm^{-2} sec^{-1} sterad^{-1}. This value, when compared with the flux of the primary protons at the top of the atmosphere, yielded an absorption mean free path of 71±5 g/cm². Application of the Gross transformation changed this value to 77±5 g/cm². The large mass of the gold nucleus plus the presence of two mean free paths of material inside the chamber made it very unlikely that only a small fraction of the energy of the primary particles be lost in the cloud chamber.

I. INTRODUCTION

COSMIC-RAY penetrating showers have been extensively investigated using many experimental techniques.[1] It has been found that these showers, particularly those of high energy, are very complex events involving large numbers of various particles. Counter controlled multiplate cloud chambers have been very helpful in understanding the nature of these events. This paper gives some additional results which have been obtained utilizing a large instrument of this type designed to observe very high energy nuclear interactions. The experiment was performed at Climax, Colorado (alt. 11,500 ft) in November and December of 1949.

It is very desirable to have enough material inside the chamber so that both primary and secondary nuclear events can be observed and studied in detail. About two nuclear mean free paths of absorbing material would give a high probability for the occurrence of both primary and secondary events. If a nuclear collision cross section equal to the geometric area of the nucleus is assumed, then about 300 g/cm² of a heavy material like lead would be necessary for this purpose. It did not seem quite feasible to build a chamber containing this much lead, but it was apparent that the use of a more dense material such as tungsten or gold would make it possible to construct a chamber of reasonable size containing this amount of absorbing material. Through a very special effort, the Office of Naval Research secured, at the request of Professor Marcel Schein, a number of machined gold plates, which made it possible to include over 300 g/cm² of gold inside the chamber. The use of this high density material plus the use of counters inside the chamber enabled the observation of events initiated by both ionizing and non-ionizing particles in the region above the counters and, in addition, yielded another region below the counters where the geometry was simple enough to make possible a direct determination of the mean free path of the primary particles.

II. APPARATUS

The cloud chamber and counter control arrangement are shown in Fig. 1. The inside dimensions of the chamber were as follows: 24 in. high, 16 in. wide, and 7 in. deep. Sixteen frames, mounted inside the chamber and inclined toward the camera, held the sixteen 14½ in.×5¾ in.×0.4 in. gold plates. The seventeenth

* Assisted by the joint program of the ONR and AEC.
† Now at the State University of Iowa, Iowa City, Iowa.
[1] For bibliography, see T. G. Walsh and O. Piccioni, Phys. Rev. 80, 619 (1950).

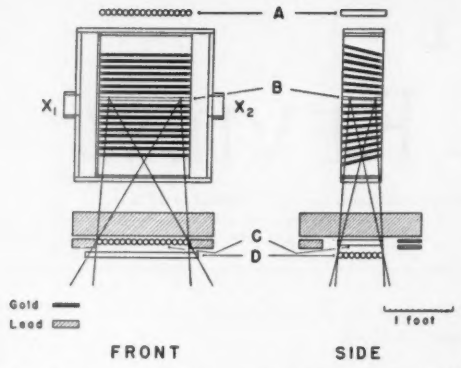

FIG. 1. Schematic view of the cloud chamber and counter banks.

frame, at position B, was replaced by a bank of nine $\frac{1}{2}$-in. diameter counters.

In order to photograph the full depth of the chamber, it was necessary to use small lens apertures. This, in turn, required more light. It was, therefore, decided to utilize rear illumination through the transparent back wall. This method is more efficient than side illumination owing to the smaller light scattering angle involved.

The front and rear walls of the chamber were tempered plate glass, $\frac{3}{4}$ in. in thickness. The expansion took place at X_1 and X_2 (Fig. 1) by means of a valve on each side. The valves were actuated simultaneously by two solenoids connected in series. The chamber was filled with argon at a total pressure of 86 cm Hg and used an excess of water-alcohol mixture.

The lights consisted of two Amglo xenon filled flash tubes, each 46 in. long and 0.35 in. in diameter, mounted in silvered semicircular cylindrical reflectors. Condenser banks of 200-μf capacity were discharged at 2000 volts through each flash tube. The lights were triggered simultaneously by two Tesla coils connected in series. The illuminated region is shown by the shaded portion

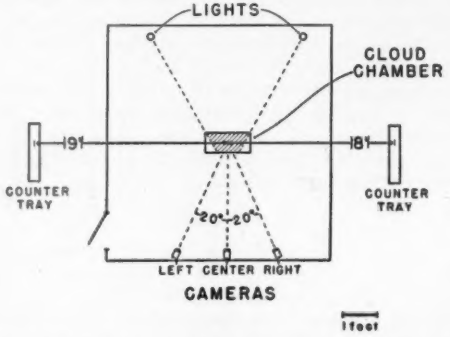

FIG. 2. Schematic plan view of the disposition of components of the apparatus.

of the chamber in Fig. 2, which also shows the disposition of lights and cameras.

The chamber was photographed by three cameras from positions shown in Fig. 2. The cameras utilized Kodak Ektar f:3.5, 50-mm lenses which were operated at apertures of f:8 to f:10 and used 35-mm Linagraph Ortho film. During part of the experiment, a camera utilizing 70-mm film was used at the center position.

The plates inside were insulated from the chamber wall by means of polystyrene bars. Thus, the clearing field of about 3 v/cm could be applied between alternate

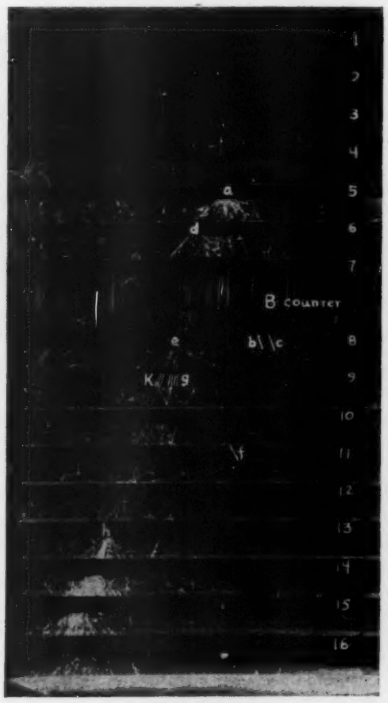

FIG. 3.

plates. The clearing field was reduced to zero for a period of about 0.2 sec starting at the time of the coincidence pulse which triggered the chamber.

The apparatus was operated continuously, day and night. The expansion ratio was checked visually about four times a day and the control circuits once a day.

The entire apparatus, except circuits, was situated inside a cubical enclosure $6\frac{1}{2}$ ft on an edge, made of $\frac{3}{8}$-in. plywood, so that the temperature could be controlled to about $\frac{1}{2}$°C.

The counter control system contained three banks of counters: B, C, and D, as shown in Fig. 1. The bank B consisted of nine counters each $12\frac{1}{2}$ in. long and $\frac{1}{2}$ in.

in diameter, the bank C of sixteen counters each 8 in. long and 1 in. in diameter, and the bank D of eight counters each 20 in. long and 1 in. in diameter. A layer of 4 in. of lead was placed above and at the sides of the counters C and proved to be very effective in reducing the number of soft showers registered by the counter control system. A fivefold coincidence BC_3D (the C_3 refers to any three of the sixteen C counters) was required for the master pulse which caused an expansion of the chamber. An additional bank of counters at position A (Fig. 1), consisting of sixteen counters, each 8 in. long and 1 in. in diameter, was not used for control of the chamber expansion but was very useful for the purpose of gaining information on the number of ionizing particles incident on the chamber.

Coincidences between the master pulse (BC_3D) and any of the individual counters at A, C, or D resulted in the flashing of a neon light (one neon light was used for each individual counter) mounted on a panel located directly above the chamber in such a position as to be photographed by the cloud chamber cameras. Two banks of counters, each consisting of four counters 20 in. long and 1 in. in diameter, were placed at distances of 8 ft and 9 ft from the chamber and were used during part of the experiment to measure coincidences between extensive atmospheric showers and nuclear events occurring in the chamber.

III. TYPICAL EVENTS

Since a considerable variety of cosmic-ray events were photographed in the course of this experiment, it seemed desirable to include a number of photographs demonstrating the nature of these events. In these photographs, the horizontal gold plates are numbered consecutively from top to bottom. Between the 7th and 8th plates is the counter tray B of Fig. 1.

Figure 3 shows a penetrating shower which was initiated at position *a* in plate 5, with the following features:

(1) There were three regressive particles,[2] one of which may have been scattered in plate 5, since it does not trace back to the same point as the others. One of these particles passed out of the left side of the chamber, the other two stopped in plate 4.

(2) There are at least three clearly visible tracks of heavily ionizing particles which emerged from the bottom of plate 5 at *a*.

(3) Most of the tracks visible below plate 5 were certainly those of electrons, which were part of a cascade shower which continued through plate 6 and almost completely died out after traversing plate 7.

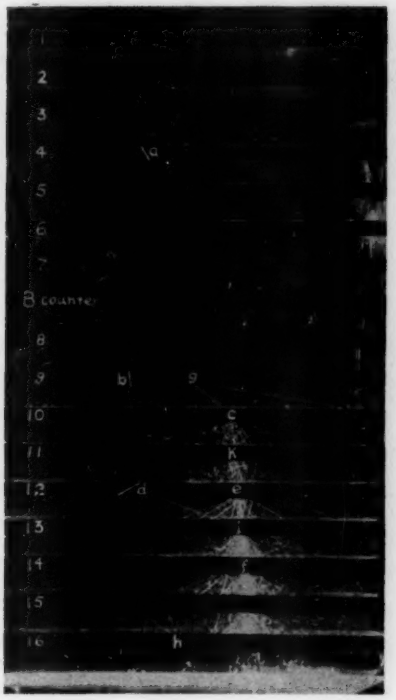

FIG. 4.

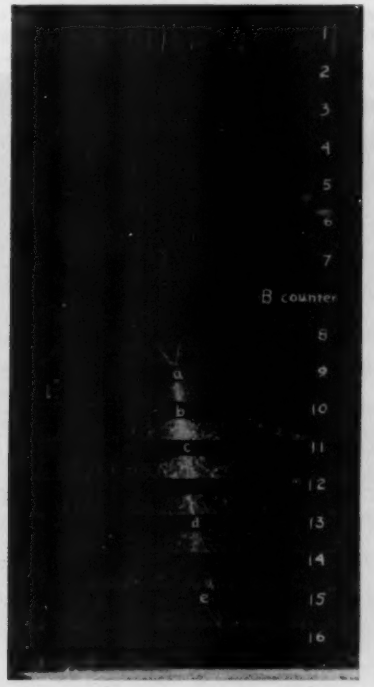

FIG. 5.

[2] There seems to be no commonly accepted designation for those particles which are observed to move in a sense opposite to that of the initiating particle. We adopt the word *regressive* as meaning *moving backwards*.

(4) Wide angle penetrating particles, for example, those indicated by the reference marks at *b* and *c*, were produced in the event *a*.

(5) There are tracks of a number of minimum ionization penetrating particles close to the axis of this event. It is difficult in this case to count these tracks because of the presence of a number of electron tracks, but there were at least five particles within a 5° cone.

(6) A low energy secondary nuclear event was produced at *d*. It is not possible to know whether this event was produced by an ionizing or non-ionizing particle because of the large number of tracks in the region.

(7) A large secondary event occurred at *e* in which heavily ionizing particles, electron cascades and penetrating particles (see *f*, for example) were produced. Two electron cascades, *g* and *k*, apparently were produced by the event *e*. The cascade *g* was at an angle of 14° to the axis of the penetrating shower.

(8) A large electron cascade originated at *h*. The direction of the axis of this event was very close to that of the initiating particle and to the core of the event produced at *a*.

In those cases in which successive production of electron cascades occurred, the electron shower produced in the original event was, in the large majority of cases, of higher energy. Hence, this event is somewhat atypical in this respect. Analysis of the secondary events in this picture is rendered somewhat difficult by the presence of at least four cascade showers. This frequent occurrence of electron showers is strong evidence against the hypothesis that these electron cores may have originated from electromagnetic interactions like bremsstrahlung or knock-on processes. On the contrary, the only explanation feasible seems to be that they originated from the decay of neutral mesons. These neutral mesons, as demonstrated at Berkeley, are known to decay into two gamma-rays, thus starting electron cascade showers.

Figure 4 shows a penetrating shower initiated by an ionizing particle in plate 10 at *c* accompanied by at least two penetrating particles *a* and *b* and probably *d*. Particles *a* and *b* together traversed fourteen plates without undergoing a nuclear collision. There was also an accompanying event at *g* probably initiated by a neutron. The tracks of penetrating particles were quite straight. There was, however, a displacement which occurred near the counter owing to the fact that the counter tray was not mounted quite level. The right edge was visibly lower than the left. As a result, tracks were displaced toward the left below the counter, and toward the right above the counter. Secondary nuclear events occurred at *e*, *f*, and *h*, and probably also at *k* and *i*. The accompanied penetrating showers were usually the same in appearance as the nonaccompanied showers.

Figure 5 shows an event at *a* in plate 9 which, at first glance, would seem to have been initiated by a non-ionizing particle. Stereoscopic measurements show, however, that this event originated very near the back glass and that the incident particle entered the chamber through the back glass at the height of plate 8. Therefore, it would have been visible only in the one space between plates 8 and 9. The large number of regressive particles made it difficult to decide whether the incident particle was ionizing or not. Of the nine or ten regressive particles, only one was sufficiently energetic to penetrate plate 8 (and thus to trip counter B). In addition to the initial event *a*, other nuclear events occurred at *b*, *c*, *d*, and *e*. The electron shower had an

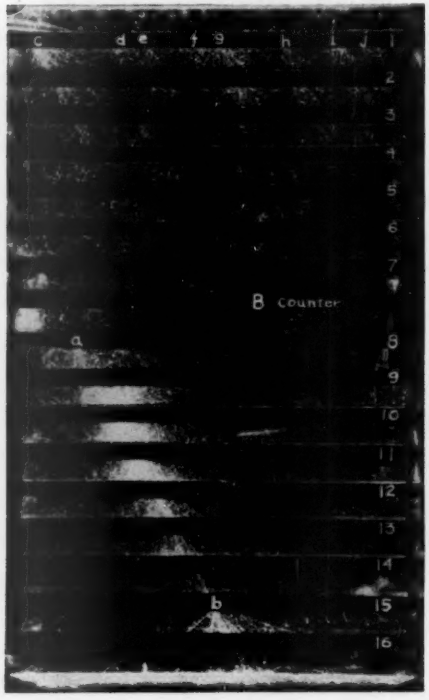

FIG. 6.

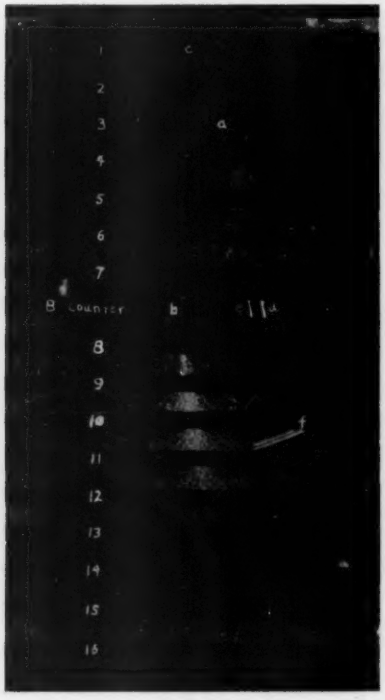

FIG. 7.

energy of about 5×10^9 ev. About eight minimum ionization particles passed out of the bottom of the chamber.

Figure 6 shows a photograph of a large air shower accompanied by a high energy nuclear event which started at *a*. One of the secondary particles in the core of the penetrating shower produced a large secondary event at *b*. Numerous electron cascades (*c* to *j*) can be seen at the top of the chamber. All of these cascades were of the order of a few times 10^8 ev in energy. The axes of all the events were quite parallel.

Figure 7, on the other hand, shows two separate locally produced penetrating showers which started at *a* and *b* accompanied by an air shower of very low density. An additional small event appeared at *c*. The event at *a* was initiated by an ionizing particle which entered through the top of the chamber. Many of the particles produced in this event passed out of the back of the chamber, but a few tracks (*d* and *e*, for example) are visible for some distance. The event at *b* actually originated in the front glass. A number of tracks starting midway in the space below *b* show where the shower particles emerged from the glass. At *f* an old α-ray track, split by the clearing field, may be seen. Few events of this type were observed.

Figure 8 shows what was probably the core of an extensive air shower. Electron showers up to an energy of a few times 10^9 ev appear. The nuclear events at *b*, *c*, and *e* seem to be part of one cascading penetrating shower of very high energy, while those at *d* and *f* were probably part of another penetrating shower parallel to the first one. Still another nuclear event of lower energy occurred at *a* in plate 1. Electron cascades are apparent in all parts of the photograph. Many particles entered the chamber above the first plate, and all the counters were tripped above the chamber.

Figure 9 shows what was probably the highest energy event observed in this experiment. The chamber was completely filled with tracks including the full depth (as can be seen at the bottom corners of the picture). Even the region of the chamber considered to be nonilluminated shows the presence of droplets. The print from which this photograph is reproduced was exposed about three times as much as the other photographs. When the exposure was increased by another factor of three, it was possible to resolve hundreds of parallel tracks in the space above the first plate at an angle of about 15° to the vertical. The particles producing these tracks apparently multiplied in passing through the first plate, for below that it is impossible to resolve individual tracks. Every counter in the control system was discharged. The use of several methods of estimating the minimum energy density incident on the chamber gave about the same figure, 5×10^9 ev/cm². Assuming a total extension of this air shower of about 100 m leads to a figure for the minimum total energy of this event of $\sim5\times10^{17}$ ev.

IV. RATIO OF IONIZING TO NON-IONIZING INITIATING PARTICLES

Since the counter control did not require that counters above the chamber be tripped, any nuclear event which started in plates 1 to 7 and was of high enough energy, could be photographed, regardless of whether the initiating particle was of the ionizing or non-ionizing type. Owing to the fact that counters B were part of the control system, events which occurred in plates 8 to 16 below B could be initiated only by

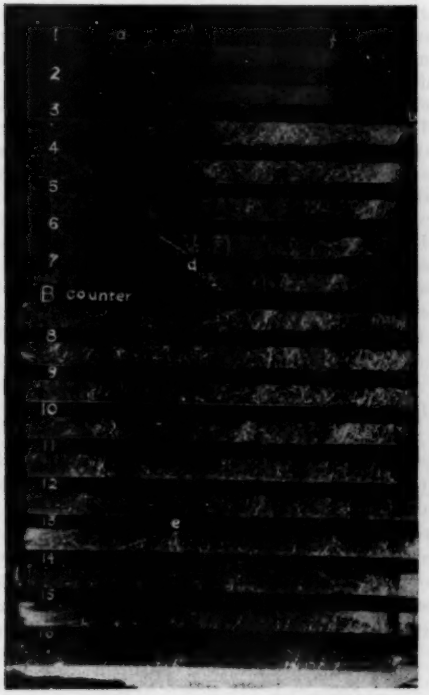

FIG. 8.

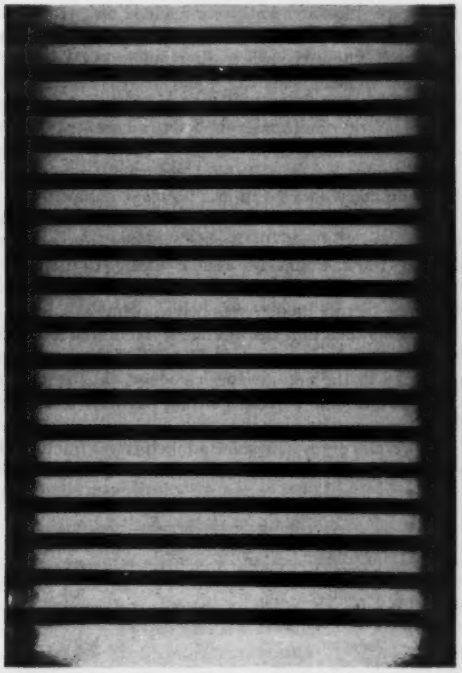

FIG. 9.

ionizing particles (neglecting the effect of regressive particles). This made it possible to analyze all events occurring in the plates above B (Fig. 1) in order to determine whether or not the incident particles were ionizing. Only incident particles were included in the data which satisfied the following criteria:

(1) It was required that the track of an incident particle, if ionizing, be visible in at least two spaces between gold plates. (Since most of the regressive particles had a range less than 1 cm of gold, confusion of the incident track with those of the regressive particles could thus be minimized. Because of this criterion, nuclear events initiated in the first plate were not counted.)

(2) All incoming particles were examined in two cameras to assure their exact positions in space relative to the axis of the nuclear event. (It was found that in all cases of ionizing incident particles, the direction of the incident particle was the same as that of the axis of the penetrating shower.)

(3) Events accompanied by other penetrating showers or electron showers were excluded.

(4) It was required that the proper one of the counters in bank A was fired whenever an ionizing incident particle visible in the chamber was within the solid angle of the counters ABCD.

(5) In the case of non-ionizing incident particles, stereoscopic measurements were made in order to make sure that the penetrating shower started at such a point and exhibited such a direction in the chamber that the incident particle would have been clearly visible if it had been ionizing.

(6) The criterion (5) was applied to all events in order to avoid systematic error.

The results shown in Table I essentially agree with the preliminary data given in a previous publication.[3]

The questionable cases are mainly (1) cases in which it was very difficult to decide whether or not the incident track would be visible owing to its very unfavorable position in the chamber, and (2) cases in which the picture quality was below average.

It follows then that the minimum fraction of ionizing incident particles is given by adding all of the questionable cases to the non-ionizing category, thus resulting in a figure of 83.5 percent ionizing particles initiating high energy penetrating showers.

The results given here show a much larger fraction of ionizing incident particles than do previous measurements. Fretter[4] showed that some penetrating showers are produced by non-ionizing particles but did not determine the relative numbers. The determination of this ratio using coincidence arrays has generally yielded a figure of about 50 percent for the ionizing incident particles producing penetrating showers. The nuclear emulsion work of the Bristol group[5] has also indicated a much smaller fraction of ionizing incident particles, but the number of cases of comparable multiplicity in their data is small. This marked difference seems to indicate strongly that the average energy of the penetrating showers observed in this experiment was higher than that of the other observers, in agreement with Hartzler's[6] determination of minimum energy as $E>15$ Bev.

From these results it appears that at high energies penetrating showers are initiated mainly by protons or possibly π-mesons which originate from nuclear collisions occurring between primary protons and air nuclei in the first mean free path above the apparatus. The contribution due to μ-mesons must be negligible because of their very small nuclear interactions.

However, at least 4 percent, and possibly as many as 16 percent, of the penetrating showers were initiated by non-ionizing particles. It is possible to account for this effect without introducing elastic collisions of protons and neutrons, for these non-ionizing particles could be the product of the break-up of α-particles and heavy nuclei at the top of the atmosphere. Because of the short mean free paths of these multiply charged particles, none of them would reach low altitudes, but they would certainly be expected to contribute to the nucleonic

TABLE I. Character of the initating particle.

Initiating particle	Number of cases	Percent of total
Ionizing	139	83.5
Non-ionizing	7	4.0
Questionable	21	12.5
Total	167	100.0

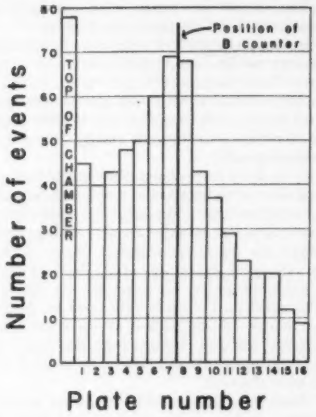

FIG. 10. Histogram showing the number of nuclear events which were initiated in each plate.

[3] Gottlieb, Hartzler, and Schein, Phys. Rev. **79**, 741 (1950).

[4] W. B. Fretter, Phys. Rev. **73**, 41 (1948).

[5] Brown, Camerini, Fowler, Heiller, King, and Powell, Phil. Mag. **40**, 862 (1949).

[6] A. J. Hartzler, Phys. Rev. **82**, 359 (1951).

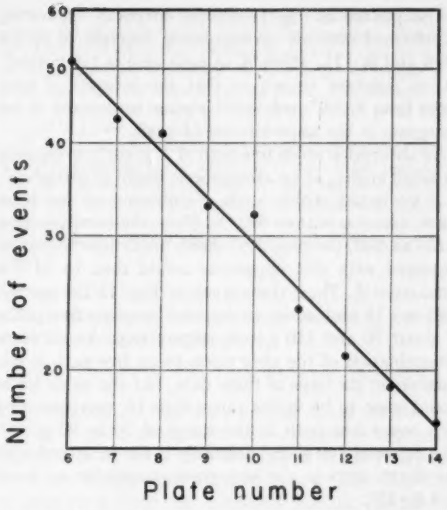

FIG. 11. The number of events which were initiated in plates 6 to 14 by particles within the same area and solid angle limits. The least squares slope corresponds to a collision mean free path of 145 g/cm².

component. The energy of the heavy nuclei would, of course, have to be at least 15 Bev/nucleon.

V. MEAN FREE PATH

The depth in the chamber at which nuclear events occurred was, of course, a function of the mean free path of the initiating particles and of the geometry of the apparatus. The distribution of occurrence of high energy nuclear events in the sixteen gold plates of the chamber is shown in Fig. 10. All events capable of tripping the control counters BC_3D were included in these data. If the sensitive area and solid angle were constant for events occurring at any depth in the chamber, an exponential distribution would have been expected. However, the product of area times solid angle dropped off rapidly above plate 6 (as can be seen in Fig. 1), as a result of which the curve actually shows a peak in the region of plates 7 and 8, next to the B counters. The large number of events initiated in the top of the chamber was due to the fact that the average amount of material in the top wall was about 25 g/cm² of iron, which, assuming a cross section proportional to $A^{\frac{1}{2}}$, is equivalent to about 60 g/cm² of gold—or three of the plates inside the chamber. It was sometimes difficult to decide whether an event started in plate 1 or in the top of the chamber, so it is quite likely that the number of events which originated in plate 1 was actually smaller than the number shown in Fig. 10. Thus, it is clear that the data for the top part of the chamber are not well suited, because of the large geometrical factors involved, to a determination of the mean free paths of the initiating particles. On the other hand, in the part of the chamber from plate 6 to the bottom, the product of area times solid angle was constant (for single particles traversing the chamber), as can be seen in Fig. 1. The only correction to be applied to the data in this part of the chamber arose from the fact that the counters B did not entirely fill the cross section of the chamber. This affected the data in the following manner.

(1) An ionizing particle which produced a nuclear event in the region of the chamber below the counters B tripped the counter control only if it passed through counters B. However, this control could be discharged by regressive particles or by accompanying particles even though the shower initiating particle missed B. This correction applied chiefly to events originating in plate 8. Figure 5 shows a photograph of such a case. In this case, the initial nuclear event occurred in plate 9, but the initiating particle entered the chamber at the 8th plate from the back. It could not be determined whether the initiating particle was ionizing, due to the large number of regressive particles. One of the three regressive particles had sufficient energy to pass through plate 8 and thus to trip the counters B.

(2) An event which occurred in plates 6 or 7 above the counter could result in a firing of counter B by a secondary particle even though the axis of the shower missed B. This correction, as would be expected, was larger for plate 7 than for plate 6. The correction amounted to 15 percent in plate 6 and 24 percent in plate 7.

By a measurement of the position of the point at which the axis of the penetrating shower passed through the chamber at the plane defined by the counter tray, it was possible to eliminate each event whose axis did not pass through the B counter. For obvious reasons one can overlook events occurring near the bottom of the chamber. Hence, the events corresponding to plates 15 and 16 were not considered in the determination of the mean free path. This does not affect the accuracy of this determination in any way.

The distribution of nuclear events, corrected as previously described, is shown on a semilogarithmic plot in Fig. 11. Each point represents the corrected number of events which occurred in the designated plate. A least squares determination of the slope of the line drawn through the points gave for the mean free path a figure of 7.20 plates. The small deviations of the points from the straight line seem to indicate that no large systematic error was involved. Each plate was 19.6 g/cm² thick. Since most of the particles traversed the plates at an angle θ to the vertical, the path length was greater than the thickness of the plates by a factor of $1/\cos\theta$. By measuring the angles of all events, it was found that this correction amounted to 2 percent. Thus, the mean free path was found to be

$$\lambda = 145 \pm 15 \text{ g/cm}^2.$$

The error figure (which is much larger than the statistical error) takes into account a possible nonrandom distribution of the zenith angles of incident particles. This mean free path yields a cross section for nuclear interactions of high energy cosmic-ray particles in gold of

$$\Phi_{exp} = 2.3 \times 10^{-24} \text{ cm}^2.$$

This may be compared with the approximate value of the geometric area of the gold nucleus (derived from the expression $r=1.5\times10^{-13}A^{\frac{1}{3}}$):

$$\Phi_{\text{theor}}=2.4\times10^{-24}\text{ cm}^2.$$

VI. ZENITH ANGLE DISTRIBUTION

In order to determine the zenith angle distribution of the particles producing penetrating showers, measurements were made of the zenith angle of each penetrating shower as projected on the surface viewed by the center camera. Owing to the fact that the expansion of the chamber was toward the sides, a displacement of the gas in the chamber occurred, resulting in a track zenith angle slightly larger than that of the original particle. If a cosmic-ray particle passed through the chamber at a projected angle θ_p to the vertical, then the resultant track after expansion made a projected angle θ_T to the vertical, where θ_p and θ_T were related by the equation $\tan\theta_T=1.08\tan\theta_p$. The factor 1.08 arises from the fact that this figure represented the expansion ratio at which the cloud chamber was operated.

The histogram of Fig. 12 shows the projected zenith angle distribution of all of the penetrating showers observed. The abscissa is the projected track angle, θ_T, while the ordinate in each case is the number of penetrating showers in each 4° interval of θ_T.

In order to evaluate this distribution it was necessary, in addition, to know the angular divergence of secondary particles with respect to the direction of the axis of the shower. This was necessary because of the discrimination of the counter control against large angle events. From the geometry of the counter control system it can be shown that there was no discrimination for single particles up to an angle of 4°, except that the effective area varied as $\cos\theta_p$. The average angular divergence of individual events was about 12°. Therefore, up to an angle of about 16° it can be assumed that discrimination of the apparatus was negligible.

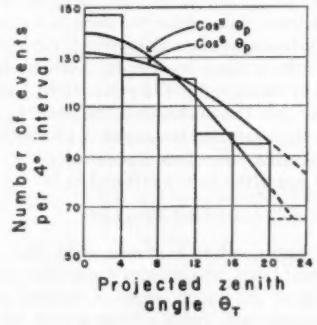

FIG. 12. Histogram showing the number of events originated within each 4° interval of projected zenith angle. The curves for $\cos^{11}\theta_p$ and $\cos^{6}\theta_p$ are normalized over the interval from $\theta_T=0°$ to $\theta_T=20°$.

Also plotted in Fig. 12 are the curves $N=K\cos^m\theta_p$ transformed into the corresponding function of θ_T for $m=6$ and $m=11$, where K in each case is the normalization constant chosen so that the integral of each curve from $\theta_T=0°$ to $\theta_T=20°$ is equal to the area of the histogram in the same interval of angle.

An absorption mean free path of X g/cm² corresponds for small angles, at an atmospheric depth of 680 g/cm², to a projected zenith angle distribution of the form $\cos^n\theta$, where n is then $680/X$. Since the sensitive area varies as $\cos\theta$, the projected zenith angle distribution as measured with this apparatus would then be of the form $\cos^{n+1}\theta$. Thus, the curves in Fig. 12 for $\cos^m\theta_T$, with $m=11$ and $m=6$, correspond to mean free paths of about 70 and 140 g/cm², respectively. An accurate determination of the absorption mean free path is not possible on the basis of these data, but the value for m would seem to be in the range 8 to 10, corresponding to a mean free path in the range of 70 to 90 g/cm². The figure of 140 g/cm² definitely is not in accord with the sharp drop in the histogram observable at $\theta=4°$ and $\theta=12°$.

This zenith angle distribution is in agreement with that of Green,[7] who reported a zenith angle distribution of the form $\cos^m\theta$, where the value of m was in the range 7 to 9. Since these measurements were made at an atmospheric depth of 655 g/cm², they, too, would correspond to a mean free path in the range 70 to 90 g/cm².

VII. FLUX OF PENETRATING SHOWER PRODUCING PARTICLES

Out of a total of 7324 counter controlled expansions, there were 1514 which showed at least one penetrating shower. Single unaccompanied penetrating showers tripped the chamber at the rate of 1.32 per hour of chamber running time. (The chamber running time is the actually elapsed time from which is subtracted the product of the number of expansions in that time interval times the cloud-chamber recycling time of $2\frac{2}{3}$ minutes.)

From the above rate, the vertical flux of shower producing particles can be calculated by taking into account the following factors:

(1) The counters B did not completely fill the whole horizontal cross-sectional area inside the chamber. Owing to the spread of the shower particles, the effective area for events starting above the counters B was larger than that for events starting below B. The actual cross-sectional area of the counters at B was 400 cm². The effective cross-sectional area of the counters, as obtained from the weighted number of showers occurring above and below B, was found to be 600 cm².

(2) Only events at a projected zenith angle θ_x (projected on the surface viewed by the center camera) less than 15° were counted. It was also necessary to measure the component of the zenith angle θ_y in a vertical plane normal to the surface viewed by the center camera, in order that the solid angle for observation of penetrating showers could be calculated. For θ_y less than 4°, the

[7] J. R. Green, Phys. Rev. **80**, 832 (1950).

whole counter area was useful for single ionizing particles traversing the chamber. On the basis of measurements carried out on a number of penetrating showers, it was found that the spread of ionizing particles with respect to the direction of the axis of an event was about 12°. The maximum value of θ_x averaged over the B counter area was about 20°. These values of θ_x and θ_y resulted in a solid angle of 0.4 steradian.

(3) On the average, an incident particle traversing the chamber had to pass through about 200 g/cm² of gold. It has been shown that the collision mean free path of these particles was about 145 g/cm². Then, the fraction of the incident particles capable of producing penetrating showers which pass through the chamber without taking part in a nuclear encounter is $N/N_0=e^{-200/145}$, or about $\frac{1}{4}$.

Taking all of these factors into account, one gets a flux of high energy penetrating shower producing particles at 51°N geometric at Climax of

$$I=(1.7\pm1)\times10^{-6} \text{ particles cm}^{-2} \text{ sec}^{-1} \text{ sterad}^{-1}.$$

The minimum energy of a nuclear event required to trip the counter control system has been estimated by Hartzler[6] as 15 Bev. It is considered unlikely that the minimum energy could be as high as 25 Bev. The flux, as calculated from the counting rate of Fretter,[8] is about three times the value given here, while the flux measured by Hazen, Randall, and Tiffany[9] is about six times the value given here.

More absorbing material was used in this apparatus than in those of the previously mentioned workers, so that the flux measurement in this experiment would be expected to give a somewhat lower figure. The three measurements, therefore, certainly agree within an order of magnitude.

It is of particular interest to compare this measured flux with that of primary protons capable of initiating these showers. From the data of Winckler, Stix, Dwight, and Sabin[10] the vertical flux of primary protons of energy greater than 15 Bev is $I_0=0.026$ particles cm^{-2} sec^{-1} sterad^{-1}.

Assuming a simple exponential law of absorption,

$$I=I_0e^{-d/\lambda},$$

where d is the atmospheric depth (680 g/cm² at Climax), one gets for λ, the absorption mean free path of primary protons of energy above 15 Bev,

$$\lambda=71\pm5 \text{ g/cm}^2.$$

When the Gross transformation is applied over the solid angle of the apparatus, this figure becomes

$$\lambda=77\pm5 \text{ g/cm}^2.$$

An upper limit of a mean free path compatible with the observed flux can be estimated by assuming that the actual flux was twice the measured value and that the minimum energy of the events observed was 25 Bev. An application of the Gross transformation to these data gives as an upper limit for the absorption mean free path a figure $\lambda=90$ g/cm². This is quite different from the absorption mean free path which has been determined by utilizing counter arrays. Tinlot[11] reported a figure of 120 g/cm², while Walsh and Piccioni,[1] by correcting for events coming in at large angles, found an absorption mean free path of 140 g/cm. These experiments undoubtedly included lower energy events than those described in the present experiment, however. On the basis of an absorption of 140 g/cm², the flux would be about 60 times the observed value.

On the other hand, if it is argued that fractional energy encounters made the energy of the incoming particle much higher than that transferred in a nuclear event, then it is necessary to assume that the minimum energy of the penetrating shower producing particles in this experiment was well over 100 Bev in order to get a mean free path of 140 g/cm². However, there are a number of factors which make this explanation unlikely.

(1) A particle passing through a gold nucleus will, on the average, encounter more than 5 nucleons. Thus, even if two encounters with air nuclei are necessary for a proton to be absorbed, then, in the case of the gold nucleus, these two encounters would be quite likely to occur in the same gold nucleus.

(2) The chamber contained an amount of material corresponding to two mean free paths, so that most of the energy would be expected in any case to be lost to secondary particles inside the chamber.

(3) Successive nuclear events produced in the chamber definitely showed an appreciable degradation of energy.

Thus, the flux measurements indicate an average absorption mean free path in the atmosphere above mountain altitudes to be about 80 g/cm², in agreement with other cloud-chamber measurements. However, Fretter found an absorption mean free path of 120 g/cm² between 3027 m and sea level. It will be checked whether the present apparatus shows a similar effect.

It is quite likely, of course, that the mean free path varies with altitude due to the contribution of π-mesons to the production of very high energy penetrating showers. For π-mesons of mean life at rest τ_0 and mean free path λ, the number of mesons which interact or decay is given by

$$dN=-N[(dl/\tau_0)+(dX/\lambda)],$$

where X is path length measured in g/cm². For particles of relativistic energy, the mean life in the laboratory system becomes $\gamma\tau_0$, and the equation can be written as

$$dN=-N[(dX/\gamma\tau_0\rho c)+(dX/\lambda)],$$

where ρ is the density of air and c the velocity of light. The ratio of the number of particles which decay, N_d, to the number which produce nuclear interactions, N_n, is then

$$N_n/N_d=\gamma\tau_0\rho c/\lambda.$$

[8] W. B. Fretter, Phys. Rev. **76**, 511 (1949).
[9] Hazen, Randall, and Tiffany, Phys. Rev. **75**, 694 (1949).
[10] Winckler, Stix, Dwight, and Sabin, Phys. Rev. **79**, 656 (1950).
[11] J. Tinlot, Phys. Rev. **73**, 1476 (1948); **74**, 1197 (1948).

Inserting values for c and τ_0 and assuming $\lambda_{air}=67$ g/cm², and replacing ρ by $0.001P$, where P is the atmospheric pressure in atmospheres,

$$N_n/N_d=P\gamma\times10^{-2}.$$

For mesons of 10-Mev energy ($\gamma=70$),

$$N_n/N_d=0.7P.$$

Thus, at one atmosphere, about 40 percent of the π-mesons of energy $\sim$10 Bev produce nuclear interactions, while at $\frac{1}{2}$-atmosphere this number is down to 20 percent. These π-mesons which interact thus result in an increase in the measured absorption length of the shower producing radiation.

Thus, it is possible, at least qualitatively, to reconcile a 70 to 90 g/cm² absorption mean free path for primary particles above mountain altitudes with the observed 120 g/cm² absorption free path of shower producing particles between mountain altitudes and sea level.

VIII. CONCLUSION

It has been shown that at least 83.5 percent of the high energy ($E>15$ Bev) penetrating showers are initiated by ionizing particles. These ionizing particles are probably largely primary protons. It is quite possible, of course, that some of these events are initiated by π-mesons produced in the nuclear mean free path of air immediately above the chamber. The measured collision cross section for gold was found to be 2.26×10^{-24} cm², which is very close to the usually accepted value of the area of the gold nucleus.

A determination of the vertical flux of shower producing particles ($E>15$ Bev) at Climax yields a value which, compared with the value of Winckler, Stix, Dwight, and Sabin[10] at the top of the atmosphere of 0.026 particles cm^{-2} sec^{-1} ster^{-1}, results in a mean free path of 77 ± 5 g/cm², which is quite close to the value corresponding to the geometric cross section (assuming an exponential absorption of the penetrating shower producing particles). This is in agreement with the figure derived from the zenith angle distribution and barometric effect of very large bursts.[12]

Other measurements of the absorption mean free path of penetrating showers have yielded a figure of 120 to 140 g/cm². There are two possibilities for explaining this discrepancy. It might be assumed that the energies of the incident particles in this experiment have been grossly underestimated if only fractional energy losses were to take place in the chamber. In order to yield an absorption mean free path of 140 g/cm², it would be necessary to assume a minimum primary energy of about 100 Bev which, in turn, would mean that only about $\frac{1}{6}$ of the energy was lost in all of the successive events visible in the chamber. However, there was more than 300 g/cm² of material in the chamber, which is equivalent in mass to about $\frac{1}{3}$ of the atmosphere. Thus, the loss of such a small fraction of the energy in this large amount of material would seem to be quite inexplicable.

Alternatively, the discrepancy might arise from the fact that other experiments have dealt with somewhat lower energies—as is shown by the latitude effect which was observed by Walsh and Piccioni. In addition, owing to the fact that the ratio of the ionizing to the non-ionizing particles was not known in other experiments, it is possible that a larger number of events produced by neutrons resulting from elastic collisions were included.

A mean free path in air close to that corresponding to the geometric cross section is also indicated by the measurements of the zenith angle distribution of the particles producing these high energy penetrating showers. It was found that the measured projected zenith angle distribution could be represented to a first approximation by an equation of the form $\cos^m\theta$, where m had a value from 8 to 10 which corresponds to an absorption mean free path in the range 70 to 90 g/cm².

These measurements all indicate that the particles producing high energy interactions lose a large fraction of their energy in the first encounter to π-mesons. This would agree with the observations of high energy stars in emulsions which show that most of the high energy secondary particles are π-mesons.

The author wishes to express his thanks to Professor Marcel Schein for his valuable advice and helpful discussions and, in connection with the cloud chamber, for suggesting the use of gold as well as the use of counters inside the chamber.

Many thanks are due to the Office of Naval Research for the great effort they expended in procuring the gold.

Thanks are due the Climax Molybdenum Corporation for their continued cooperation at the High Altitude Laboratory in Climax and to Thomas Stinchcomb, who was very cooperative and helpful at the Climax Laboratory.

[12] T. G. Stinchcomb, Phys. Rev. **80**, 479 (1950).

Nuclear Interactions in Gold of Secondary Particles Emitted in Penetrating Showers*†

A. J. HARTZLER‡
Department of Physics, University of Chicago, Chicago, Illinois

(Received December 18, 1950)

A large counter controlled cloud chamber containing 16 gold plates totaling 308 g/cm² in thickness was operated at an altitude of 11,500 ft. Forty of the pictures of penetrating showers obtained were selected for the determination of the mean free path for nuclear collisions of ionizing secondary particles. The result was found to be 230±60 g/cm², corresponding to 0.7±0.2 times the cross section equal to the geometric area of the gold nucleus. The 14 percent of the nuclear events used in making this determination were large angle scatterings of a penetrating secondary particle with no observable disintegration products emerging from the gold plate in which the scattering occurred. The number of secondary nuclear events occurring, which are not observed because of the absorption of all tertiary particles, was estimated to be 18 percent of the total. The momenta of the secondary particles used in this determination ranged between 10^9 and 10^{10} ev/c. The lowest energy penetrating shower which has a high probability of tripping the counter coincidence circuit used was estimated to be 1.5×10^{10} ev. The number of high energy protons among the secondary particles used in the determination of the collision mean free path was less than 11 percent, and the total fraction of protons is less than 30 percent. The 88±3 percent of the penetrating showers observed in the experiment showed the presence of an observable electron cascade. The average number of penetrating secondaries of minimum ionization emitted in penetrating showers of an average energy of 3×10^{10} ev, and either not showing any electronic cascade or showing the presence of an electronic cascade having an energy less than or equal to 7×10^9 ev, is 7±1 per shower. The corresponding average multiplicity of secondary particles of minimum ionization in penetrating showers of 6×10^{10} ev average energy, which show the presence of an electron cascade of an energy greater than 7×10^9 ev, is 11±2 per shower. Evidence is given that the angular distribution of the mesons in the center-of-mass system of a nucleon–nucleon collision at energies above 1.5×10^{10} ev is not isotropic and is probably collimated in two cones of about 50° half-angle around the directions of the velocities of the nucleons in the center-of-mass system.

I. INTRODUCTION

A NUMBER of workers have analyzed the interactions of the secondary particles of penetrating showers with matter, and, in particular, determinations of the collision mean free path of penetrating secondaries have been made.[1,2] Some of the experiments were performed by means of arrays of counters and absorbers, others with counter controlled cloud chambers, and still others have been carried out by analyzing showers of minimum ionization particles occurring in photographic emulsions. However, most of these experiments were not designed with the primary intention of measuring the cross section for the interactions of the various components present in penetrating showers.

II. APPARATUS AND EXPERIMENTAL PROCEDURE

The major purpose of the present experiment was the determination of the probability of nuclear collisions of the secondary particles from penetrating showers. For this reason a large cloud chamber with a sensitive volume 24 in. high, 16 in. wide, and 7 in. deep was constructed. A scale drawing of the front and side views of the chamber, the counters, and the absorbing materials in the interior and vicinity of the chamber is given in Fig. 1. The outside of the chamber was made out of steel $\frac{3}{4}$ in. in thickness, the front and back were made out of $\frac{3}{4}$-in. plate glass, and, as is indicated in the figure, the expansion of the gas inside the chamber was toward the sides. The lights were placed a few feet back of the chamber so that the light entered the sensitive volume through the rear glass wall. The cloud chamber was photographed with 3 cameras, the central one of which was placed 35 in. from the center of the chamber on a line through the center and perpendicular to the front glass wall. The two other cameras viewed the chamber at angles of 20° in either side of the center camera. Film of 35-mm size was used in the side cameras for all of the pictures. For part of the experiment the

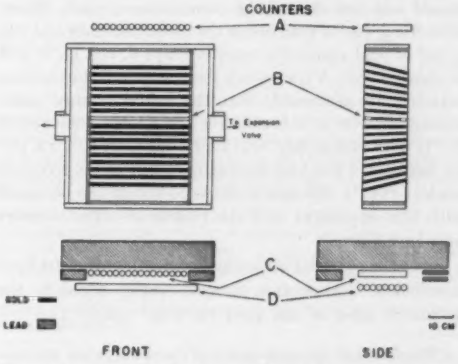

FIG. 1. Front and side median sections of the apparatus showing the arrangement of G-M counters and absorbers in the interior and vicinity of the cloud chamber.

* Assisted by the joint program of the ONR and AEC.

† This paper was written as a Ph.D. thesis for the Department of Physics, University of Chicago.

‡ AEC Predoctoral Fellow (October 1, 1948 to June 30, 1950). Now at the Carnegie Institute of Technology, Pittsburgh 13, Pennsylvania.

[1] A recent bibliography can be obtained in the paper by T. G. Walsh and O. Picconi, Phys. Rev. 80, 619 (1950).

[2] The results of several determinations of the collision mean free path are compiled by Camerini, Fowler, Lock, and Muirhead, Phil. Mag. 41, 413 (1950).

center camera which used 35-mm film was replaced by a camera using film 70 mm wide. The larger film size gives better resolution, and, therefore, for the analysis of complicated events occurring inside the chamber, these larger pictures give considerably more information. The chamber was filled with argon saturated with the vapor of a mixture of equal parts of alcohol and water to a total pressure of 86 cm Hg.

The expansion of the cloud chamber was controlled by a counter coincidence which was made selective for penetrating showers. The number and dimensions of the counter labelled in Fig. 1 are as given in Table I. In addition to the counter trays indicated in Fig. 1, there were two trays of shower detecting counters, designated as S, placed in a horizontal distance of 1.5 to 2 m from the chamber. The fivefold counter coincidence which was required to expand the chamber was a discharge of any one of the counters B, any three of the counters C, and any one of the counters D. This coincidence will be called BC^3D. The following additional coincidences were recorded by means of neon lights which were photographed simultaneously with the event occurring in the cloud chamber.

A_iBC^3D	$i=1$ to 16
C_jBC^3D	$j=1$ to 16
D_kBC^3D	$k=1$ to 8
S_mBC^3D	$m=1$ to 6.

The record of these coincidences gives additional valuable information concerning the paths of the incident particles and of the secondary particles below the lead which was beneath the cloud chamber.[3]

Inside the cloud chamber were mounted 16 pure gold plates of 14.5-in. effective length, 5.75-in. effective width, and 0.40-in. thickness.[4] These plates served two purposes: (1) to produce and (2) to absorb the radiations present in the penetrating showers. A lead shield 4 in. thick was placed directly above the counter tray C (Fig. 1) in order to reduce the chance that air showers should trip the controlling coincidence circuit. There were 308 g/cm² of gold inside the cloud chamber and 124 g/cm² of lead above the counter trays C and D. It will be shown in Sec. VI, in which the energies of the showers detected are discussed, that the lowest energy penetrating showers which can trip the master coincidence BC^3D with probability near unity has close to 1.5×10^{10} ev. Because of this high minimum energy of the recorded nuclear events, differences between the results obtained with this apparatus and the results of other workers may be expected.

Since the particles initiating penetrating showers have a collision cross section in gold nearly equal to the geometric area of the gold nucleus,[5] nearly two collision mean free paths of gold were present in the sensitive volume of the cloud chamber.[6] These facts yield a probability of 55 percent that a vertically incident penetrating shower producing particle will interact with a gold nucleus in the upper 7 plates in the chamber. Hence, the nuclear interactions of mesons and nucleons present in these showers can be studied in detail in the remaining plates in the cloud chamber. Since, according to recent measurements in photographic emulsions, the collision cross section of the secondary particles seemed to be of the order of magnitude of the nuclear area, it was expected that a large number of secondary nuclear events would be produced in the sensitive volume of the chamber.

TABLE I. Numbers and dimensions of G-M counters.

Designation	Number	Diameter	Active length
A	16	1″	7.9″
B	9	½″	13.5″
C	16	1″	7.9″
D	8	1″	19.7″

The fact that each 1-cm thick gold plate corresponds to 3.3 radiation units makes the removal of the electron cores, which are associated with the great majority of the high energy penetrating showers, considerably more effective than for other dense materials such as lead. For example, an electron shower with even as high an energy as 10^{10} ev will penetrate only 7.3 cm of gold. Owing to this fact, many of the interesting details of the secondary nuclear events occurring in the remaining plates in the lower part of the chamber frequently will not be obscured by the presence of electrons.

A large solid angle for the selection of penetrating showers was obtained by means of placing the counter tray B (Fig. 1) in the interior of the chamber. Also, the fraction of the pictures which showed events of interest is high (~20 percent). Because of the high efficiency of the counter control arrangement and because of the large amount of material in the sensitive volume of the chamber, more than 1000 penetrating showers were obtained in this experiment, which show the presence of secondary nuclear events.

The cloud chamber at the High Altitude Laboratory of the University of Chicago at Climax, Colorado (altitude 11,500 ft) was in almost continuous operation for 60 days during the late fall and early winter of 1949–50. During the operation of the chamber, periodic checks were made of the expansion ratio and of the performance of all coincidence circuits.

In order to determine the frequency of single penetrating particles occurring by chance in the chamber, 450 random expansions were photographed. One picture in 20 showed the presence of a single particle penetrating 5 or more plates. Only particles of nearly the same age as that of the tracks obtained in the counter

[3] The details of the construction of the chamber and the associated apparatus will be published elsewhere.

[4] These gold plates for this and similar experiments were kindly supplied by the ONR.

[5] M. B. Gottlieb, Phys. Rev. **82**, 349 (1951).

[6] The theoretical mean free path, corresponding to a cross section equal to the area of a gold nucleus, is 160 g/cm².

controlled pictures were considered. From this result one can estimate that less than 1 percent of the pictures of penetrating showers will contain sharp random tracks which lie in such a region of the cloud chamber as to be confused with the secondary particles emitted from the shower.

The photographs of penetrating showers selected for the analyses given in this paper did not show the presence of large numbers of electrons entering the chamber from the air. Hence, the events discussed were not associated with high density atmospheric showers.

III. METHOD OF DETERMINATION OF THE MEAN FREE PATH Λ FOR NUCLEAR COLLISION OF THE SECONDARY PARTICLES IN PENETRATING SHOWERS

The principles underlying the method used for the determination of the collision mean free path Λ will now be discussed. Let us consider N, the number of penetrating secondary particles of penetrating showers, and dN, the number of secondary particles making nuclear collisions in a thickness of dx.

$$dN = n_0 N \phi dx, \tag{1}$$

where ϕ is the cross section in cm² for collision with a nucleus, n_0 is the number of nuclei per cm³, and x is measured in cm. The probability that a particle does not collide with a nucleus in a distance x is then given by

$$P(x) = \exp[-\phi n_0 x]. \tag{2}$$

By integration of Eq. (2), the mean free path for collision, λ, is found to be

$$\lambda = 1/\phi n_0,$$

and in g/cm²

$$\Lambda = \rho/\phi n_0, \tag{3}$$

where ρ is the density of gold, 19.3 g/cm³.

It should be clearly understood that Eq. (2) does not represent the decrease with thickness of the number of secondary particles but refers to the decrease with thickness of the fraction of the secondary particles which have not made a nuclear collision. If a secondary particle does not lose a large fraction of its energy in a nuclear collision, it may well be capable of producing a tertiary event. Figure 5 shows a photograph of a high energy nuclear interaction in which, at the points (F) and (H), the production of two clearly visible successive nuclear events occurred.

Combination of Eqs. (1) and (3) yields

$$\Lambda = \rho N dx/dN. \tag{4}$$

Thus, the collision mean free path Λ can be determined from the number of secondary particles N which traverse gold plates of thickness dx and from the number of secondary nuclear collisions dN. The number of traversals of the 1-cm gold plates can be counted for particles wherever they can be best observed. In the determination of Λ for the secondaries of the high energy penetrating showers observed in this experiment, only those traversals occurring in regions of the chamber that were quite free of tracks were used.

If there are particles with long mean free paths present among the secondaries of penetrating showers the results are biased in favor of particles whose path lengths are longer than the average, and, hence, the values of Λ as derived from data obtained in this manner might be considerably higher than the actual average value.

Selection of Secondary Nuclear Events

In order for any event to be classed as a nuclear event, and to eliminate electromagnetic interactions, one of the following criteria is required to be fulfilled.

(1) If a secondary penetrating particle enters a gold plate and two or more particles including the initial particle are observed to emerge at large angles with respect to the initial particle, the event is classed as a nuclear disruption or star. The requirement that two or more particles be ejected rules out the possibility that particles which are stopped by ionization loss be counted as nuclear events.

(2) If a penetrating secondary particle is observed to enter a gold plate and to eject two or more particles, one or more of which is heavily ionizing, the event is considered to have been a nuclear collision. The requirement that a heavily ionizing particle be ejected prevents the counting of events from which knock-on electrons are observed to emerge. Particles which ionize more than 4 times the minimum ionization of a singly charged particle were classed as having heavy ionization.

(3) If a penetrating secondary particle ejects one or more penetrating particles from a gold plate on its passage through that plate, the event is classed as a nuclear collision. A particle is said to be a penetrating particle if it passes through a gold plate and does not produce a single secondary particle. Since an electron with sufficient energy to penetrate 1 cm of gold is well above the critical energy, the chance that the electron will penetrate a minimum of 1 cm (3.3 radiation units) of gold without producing any additional electrons is small, and the chance that such an electron neither produces a secondary nor is scattered is negligible. If one further considers that the penetrating secondary particle must have produced a knock-on electron in one gold plate, which neither multiplies nor is scattered in the following plate, it is seen that the production of knock-on electrons is effectively excluded from the data.

(4) If a penetrating secondary particle exhibited a sharply defined single scattering in a gold plate, an analysis was made in order to determine whether or not the scattering could be attributed to multiple coulomb scattering or whether it must be assumed that the scattering was due to a single nuclear encounter. If it is assumed that the distribution of the projected scattering angles is gaussian,[7] then the probability that the measured scattering angle is due to multiple scattering can be computed provided that the momentum and velocity of the scattered particle are known. Since the velocity of minimum ionization particles is close to the velocity of light, only the momentum must be determined. A lower limit of the momentum of the scattered particle was obtained in each case from the upper limit on the root mean square (rms) multiple scattering angle of the particle transversing several gold plates.

[7] E. J. Williams, Proc. Roy. Soc. (London) **A169**, 513 (1939). The gaussian approximation is not exact; but for the purposes of the present experiment, the exact form of the distribution does not greatly increase the accuracy. H. S. Snyder and W. T. Scott, Phys. Rev. **76**, 220 (1949).

In regions of the cloud chamber in which the density of confusing tracks is low, the smallest deviation from a straight line which can be detected with certainty is 2° on sharp tracks which travel at least 10 cm in the chamber. The probability that an actually observed scattering angle ϑ is due to a fluctuation in the distribution of the multiple scattering can be determined from the ratio

$$R=\vartheta/\theta_{\text{rms}}, \tag{5}$$

where $\theta_{\text{rms}}=(\langle\theta^2\rangle_{\text{Av}})^{\frac{1}{2}}$ is the rms scattering angle observed for that particle. If $R\geq 2.0$, the chance that the angle arises from a fluctuation in the distribution of the scattering is less than 1 in 20. Therefore, events for which $R\geq 2$ were classed as nuclear events in contrast to cases for which $R<2$ which were not included in the data. Possible errors introduced by the use of this criterion will be discussed with the other errors in the determination of Λ.

IV. DISCUSSION OF TYPICAL EVENTS

Some photographs of typical events observed in this experiment are shown in Figs. 2, 5, and 7. These events will be discussed in detail in order to clarify the later discussion of the results derived from these and similar pictures.

(A)

Figure 2 is a photograph and Fig. 3 is the corresponding diagram of an event which was initiated by an ionizing cosmic-ray particle (a) in the second gold plate. Figure 3 is given in order to clarify the discussion of the event.

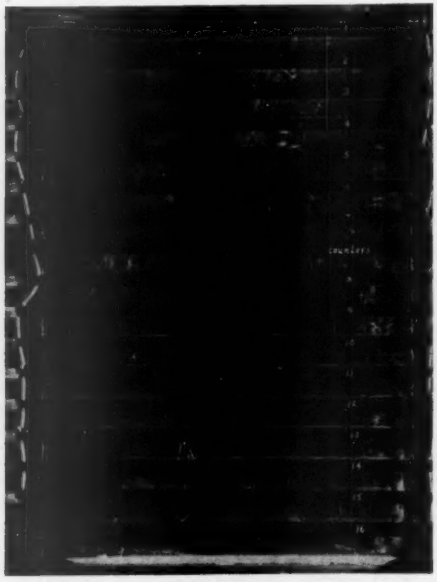

FIG. 2.

Eight penetrating particles (b, c, d, e, f, g, h, i) and an electron shower (S) are seen to emerge from a point (A) in the second plate. The cascade shower (S) penetrates between 8 and 11 radiation units of gold. Twelve ± 2 particles are seen in the shower below the third plate, and 20 ± 4 particles are seen below the fourth plate. These figures are in agreement with the penetration and numbers of particles expected at the corresponding points in a shower of 10^9 ev total energy.[8] The axis of the electron shower (S) is located at an angle of 10° from the direction of the incident particle (a). The deviation of electron showers from the axis of the penetrating shower in which it was produced has been observed previously.[9] A more complete discussion of the data collected in this experiment on the origin of electron showers associated with penetrating showers will be published later.

As is shown in Fig. 2, particles (b, c, d, e) traverse several gold plates in clear regions of the chamber, and, hence, they can be

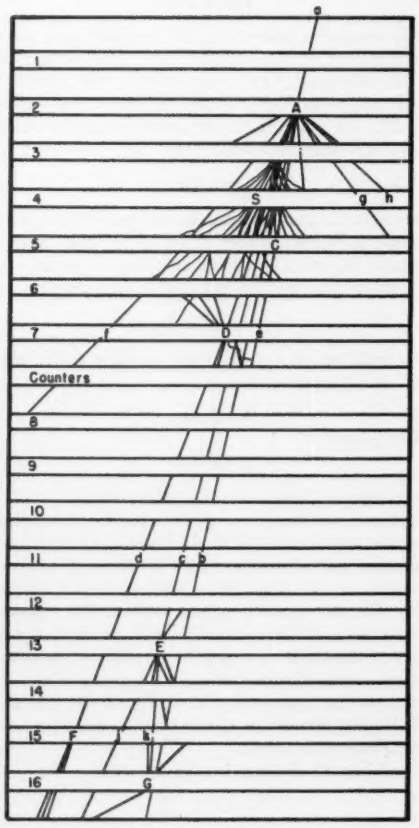

FIG. 3. Diagram of the events of Fig. 2.

[8] D. J. X. Montgomery, *Cosmic Ray Physics* (Princeton University Press, Princeton, New Jersey, 1949), pp. 261–283.

[9] C. Y. Chao, Phys. Rev. **75**, 581 (1949); W. B. Fretter, Phys. Rev. **76**, 511 (1949); Gregory, Rossi, and Tinlot, Phys. Rev. **77**, 299 (1950).

used for the determination of the mean free path for nuclear collision.

Particle (d) makes a collision and is scattered through an angle $\vartheta=3°$ at D in the seventh gold plate. Three lightly ionizing particles are seen in the space above the seventh plate near D, and 4 lightly ionizing particles are seen near D below the seventh plate. Since only 3 of these 7 particles can be extrapolated to the point D, it is not certain that all of them are tertiary particles ejected from the nuclear event. Since (d) suffered a scattering on making a collision with a gold nucleus in the seventh plate, it is possible to estimate its momentum if the value of the recoil momentum is known. It is difficult, however, to determine the exact value of the recoil momentum transferred in a collision occurring in a gold plate because possibly not all of the tertiary particles are observed to emerge from the plate in which the collision occurred. In order to estimate the energy of particle (d), the following simplifying assumptions are made.

(1) In the collision, a recoil momentum P_r was transferred to a nucleon. This recoil momentum then produced the nuclear disruption at D. The energy of this event at D can be estimated to be 7×10^8 ev, and the corresponding recoil momentum is $P_r=1.3\times10^9$ ev/c.

(2) The energy lost by particle (d) in the collision at point D is only a small fraction of its total energy. This is a reasonable assumption in view of the smallness of the angle ϑ.

For this simplified case the momentum vector diagram can be represented as is given in Fig. 4, where P_0 is the momentum of particle (d) before the collision, and P_1 is the momentum after the collision. Since, according to assumption (2), $P_0\simeq P_1$, the initial momentum of (d) can be found simply. The corresponding energy of particle (d) is as follows:

$$E=2.4\times10^{10} \text{ ev for a proton;}$$
$$E=2.5\times10^{10} \text{ ev for a } \pi\text{-meson.}$$

While the assumptions made in this estimate are necessarily not exact, the order of magnitude of the energy of particle (d) can be considered to be correct. Typical examples of estimates of the energies of secondary particles which were scattered in nuclear collisions are given in Tables III and IV.

Particle (d) continues after having been scattered at D and makes another nuclear collision at F in the fifteenth gold plate. A total of 3 minimum ionization particles are ejected from F at angles less than 4° from the direction of (d) as it enters the fifteenth plate. This strong collimation of the tertiary particles from the event at F is in good agreement with the high value of the energy of particle (d) estimated from its scattering at D.

Particle (c), which was emitted from the initial nuclear collision at A, makes an encounter at E in the thirteenth gold plate. From the event E there are emitted 2 heavily ionizing particles and 4 lightly ionizing particles. Two of the emitted particles of minimum ionization (j, k) have sufficient energy to penetrate several gold plates, and (k) has enough energy to produce a star in the sixteenth plate. Since (k) makes a tertiary star which has an estimated total energy of about 7×10^8 ev and since the star at E seems considerably more energetic than at G, it seems reasonable to estimate the total energy of (c) to be 2×10^9 ev.

Particle (b) ejected in the core of the shower from the initial collision at A traverses 10.5 cm of gold without having made a visible collision in the lower part of the chamber. In addition, the path of (b) through the 10 gold plates does not show any measurable deviation from a straight line, and, hence, the minimum momentum of this particle can be determined from the theory of multiple scattering. The smallest total deviation from a straight line that could have been measured on this particular track in traversing 10 gold plates is 3°. The corresponding rms scattering angle places a lower limit of $p=4\times10^9$ ev/c on its momentum. The calculated minimum energy of (b) is

$$E=1.6\times10^9 \text{ ev if it is a proton,}$$

and

$$E=2.1\times10^9 \text{ ev if it is a meson.}$$

These lower limits on the energy of (b) are high enough to show that it could have made an observable nuclear disruption. If it is assumed that particle (b) has a collision cross section equal to the geometric area of a gold nucleus, it has a probability of 0.28 of traversing 10.5 cm of gold without making a nuclear collision. In view of the large number of particles present in the event shown in Fig. 2, it is not improbable that one of the particles can have a long path through the chamber.

The particle (e), which is seen in the core of the penetrating shower above the counter, passes out of the rear glass wall of the cloud chamber.

The discussion of the particles emitted from the nuclear event at A has been confined to the 4 particles emitted at angles less than 10° from the direction of (a). In addition, 4 penetrating particles are seen to have emerged from the same event at large angles to the direction of the incident particle (a). Particles (g, h, i) do not remain in the visible region of the cloud chamber for sufficient distances to make an analysis of their secondary interactions possible. The fourth particle (f) is scattered on traversal of the gold plates a number of times before it passes out of view. The measured value of the projected rms scattering angle yields an energy $E=4\times10^8$ ev for a proton, and, for a π-meson, $E=5.5\times10^8$ ev. Making use of these estimates of the energies of some of the individual particles, one can obtain an approximate value of the total energy which is dissipated in the chamber by the nuclear interaction of particle (a). Assuming that a large fraction of the energy of particle (a) was lost in the chamber, this determination, then, should give an approximate value of the total energy of (a). It seems unlikely that a high energy cosmic-ray particle colliding with a gold nucleus can lose only a small fraction of its energy, since the secondary particles produced will make additional collisions with the nucleons present in the gold nucleus. In addition, the secondary particles produced must pass through the material in the cloud chamber which corresponds to a total of two collision mean free paths.

The energies of the individual secondary particles emitted from the event A are given in Table II. It is seen that the total energy of the event shown in Fig. 2 is greater than 3.4×10^{10} ev.

The event of Fig. 2 has a lower energy electron shower than average, and, also, the secondary particles are emitted from the

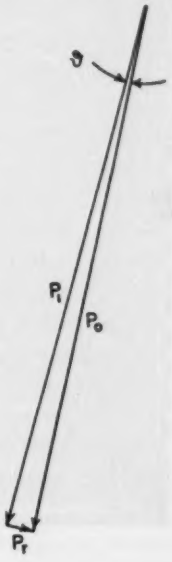

FIG. 4. Simplified momentum vector diagram of the collision of particle (d) at D of Fig. 2.

TABLE II. Energies of particles shown in Fig. 2.

Particle	Estimated energy (ev)
b	$>2\times10^{9}$
c	2×10^{9}
d	2.5×10^{10}
e	$>10^{9}$
f	5×10^{8}
S	10^{9}
3 others	$\sim2\times10^{9}$
Total	$>3.35\times10^{10}$ ev

initial event at wider angles with respect to the incident particle than the average angular divergence of the secondaries of all penetrating showers in this experiment.

(B)

Figure 5 is a photograph of an event (diagrammed in Fig. 6) which shows the presence of a higher energy electron shower than does the event of Fig. 2. A penetrating shower is initiated in the top steel wall of the cloud chamber at (A). An electron cascade starting at (A) develops a broad maximum after penetrating 7 radiation units of gold. Below the sixth plate (20 radiation units), there are 20 ± 5 electrons present in the shower. These figures are in good agreement with the values predicted by the theory for a cascade shower initiated by an electron or photon of about 10^{10} ev energy. Unfortunately, the density of particles in the shower is too high to allow an estimate to be made of the number of particles at the position of its maximum. However, the theory predicts that 200 electrons should be present below the second plate. This number conforms to the appearance of the shower.

The are secondary nuclear interactions occurring at C, D, and E above the counters and at F, G, H, J, and K below the counters. In Fig. 5, it is clear that there may have been other nuclear events which are not seen because of the large number of electrons present in that region of the chamber.

Three penetrating particles are seen in the core of the initial penetrating shower below the counters. Two of them (a and c), cause nuclear disruptions in the eighth plate at F and G. The collision of particle (c) at G gives rise to two particles which penetrate the tenth plate and stop in the eleventh plate. Both the sudden increase in ionization and the large scattering of these two particles on their passage through the tenth plate show that they are mesons.

Particle (a) makes a very remarkable nuclear collision in the eight plate at F. As seen, at least 4 minimum ionization particles are ejected at F. One other particle above the eighth plate may also come from F. In spite of the apparent high energy (5×10^{8} ev) of the star produced by particle (a) in the collision at F, its path is not deviated by more than 3°. By using the same method as was used in the determination of the energy of particle (d) of Fig. 2, the minimum value of the energy of particle (a) is $E=2.2\times10^{10}$ ev for a π-meson and 2.1×10^{10} ev for a proton.

It is remarkable also that particle (a) after traversing two more plates makes another collision with a gold nucleus in the eleventh plate at H. A large number of penetrating particles are seen to emerge from the collision at H, and also a low energy electron shower is present. The short paths of the tertiary particles from event H, occurring in the lower part of the chamber, do not allow a direct estimate of the energy of the event. However, the general appearance of H is rather similar to that at (A) of Fig. 2, hence

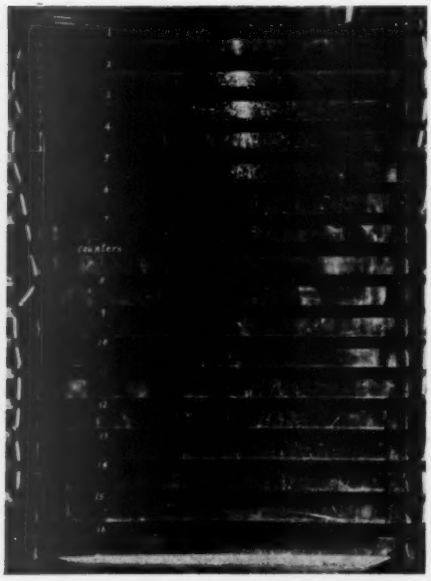

FIG. 5.

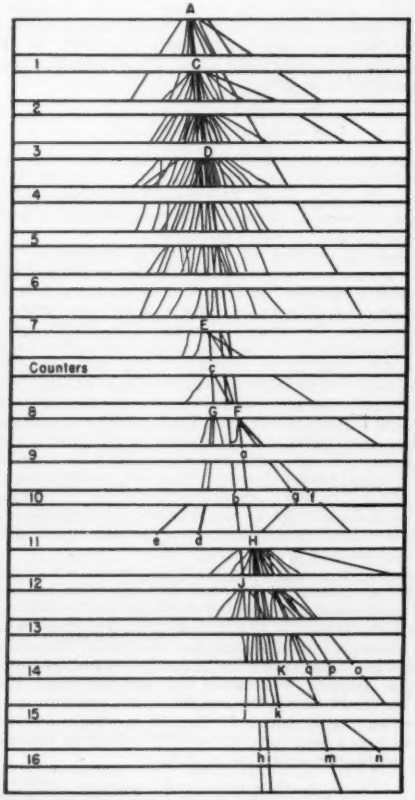

FIG. 6. Diagram of the events of Fig. 5.

it is not unlikely that particle (a) has an energy as high as $E=2\times10^{10}$ ev.

The third of the particles (b) in the core of the initial penetrating shower makes a nuclear collision in the twelfth plate at J with the ejection of at least 4 minimum ionization particles. The energy of (b) must be at least 7×10^{9} ev in order to produce a disruption of this size.

Summing the energy of all particles present, one finds, for the total energy of the event in Fig. 5, $E\geq3\times10^{10}$ ev.

Figure 7 is a photograph of a high energy penetrating shower which traverses the entire height of the cloud chamber and the gold that it contains. This event has 4 or more electron showers associated with the numerous nuclear events produced by the secondary particles of the initial event. There is a penetrating shower produced in the top steel wall of the chamber, and one of the secondary particles from that event produces a nuclear event at (C) in the first gold plate. Seven or more penetrating particles can be extrapolated to the point (C).

There is an electron shower produced in the first plate and another in the second plate. This second shower has an energy of 7×10^{9} ev, as was determined in the manner exemplified in the discussion of Figs. 2 and 5. The determination of the energy of the electron shower produced in the second plate is rendered less accurate than other determinations because of the presence of the shower initiated in the first gold plate.

The central core of the penetrating shower contains at least 5 secondary penetrating particles which can be extrapolated to the point (C). Numerous other particles are present whose origin is less certain. All of these particles are emitted at angles less than 2.5° from the apparent axis of the entire event. This small angular divergence of the penetrating particles in the core of the shower indicates that the energy of the particle which initiated the event occurring at (C) can be estimated be between 5 and 10×10^{10} ev, as will be shown later.

Another indication of the very high energy of the primary particle which produced this event is the large number of secondary nuclear events which are observed in Fig. 7. A few of these are clearly visible in plates 8, 9, 11, and 13. Nuclear collisions in the eighth and ninth plates have given rise to at least two well-separated secondary electron showers. The event of Fig. 7 is direct evidence that more than one of the secondaries of high energy penetrating showers can produce electron showers. Other photographs, similar to that shown in Fig. 7, in which the individual electron showers have been initiated in two or more places by secondary particles present in high energy penetrating showers, have been obtained in this experiment.

V. DETERMINATION OF Λ

In order to determine the value of the mean free path for nuclear collision Λ, 40 pictures of penetrating showers were selected. Each individual shower photograph was chosen for the presence of well-separated and clearly defined penetrating secondary particles. This requirement is more easily met by the lower energy showers than it is by the very high energy showers, because the average angle between any two secondary particles in the core of the shower decreases as the total energy increases. It will be shown that there are two reasons for this fact. (1) The angular divergence of the secondary particles decreases as the total energy of the shower increases. (2) There are more secondary particles ejected from the higher energy nuclear events.

Estimates of the energies of the particles used in the determination of Λ and of the energies of the entire showers observed in this experiment will be discussed in detail in Sec. VI.

FIG. 7.

In the 40 selected pictures taken by the center camera, there were 234 tracks of secondary particles which made traversals of gold plates and fulfilled all requirements in order to be useful in the determination of Λ (Sec. III). These particles traversed 19,400 g/cm² of gold in clear regions of the cloud chamber. Using the notation of formula (4),

$$\rho N dx = 19{,}400 \text{ g/cm}^2.$$

In obtaining this value, corrections have been applied in order to obtain the actual amount of material traversed by each of the 234 tracks which were inclined with respect to the vertical direction as seen in the center camera view. In addition, a small correction totalling 5 percent had to be applied to the value of $\rho N dx$ (1) because of the inclination of the tracks in the vertical plane perpendicular to the plane viewed by the center camera, and (2) because of the tilt of the gold plates near the top and bottom of the cloud chamber (Fig. 1).

By the aid of the four criteria given in Sec. III, a minimum of 69 events were classed as nuclear collisions of the 234 secondary particles as they traversed the 19,400 g/cm² of gold. This value of 69 for the number of nuclear events produced is the minimum value of the number dN [notation of Eq. (4)], and both (1) secondary penetrating showers and small stars and (2) scatterings which are certainly nuclear scatterings have been included. Since the minimum value of dN is the actually observed 69 events, it follows that the maxi-

mum value of the mean free path Λ can be computed from Eq. (4).

$$\Lambda = \rho N dx/dN = 19{,}400/69 = 282 \text{ g/cm}^2.$$

(A) Discussion of Errors in the Determination of Λ

The largest error in this value of Λ is caused by a failure to observe some of the lower energy secondary nuclear events which occurred in the interior of the gold plates, since some of the nuclear fragments which are known to be present in such stars do not carry sufficient energy to emerge from the 1-cm thick gold plates. For example, a proton must have an energy of 7.2×10^7 ev in order to penetrate 0.5 cm of gold; an alpha-particle of the same range must have 2.8×10^8 ev and a π-meson 3.0×10^7 ev. Thus, stars produced by secondary particles are more likely to be missed if the average energy of the ejected star particles is relatively low. Lovati and his co-workers[10] have added 116 percent more nuclear events to the number they actually observed in order to correct for the number of stars not observed because of the absorption of all tertiary particles in the lead plates. Brown and McKay[11] have applied a similar correction of 74 percent for the loss of secondary nuclear events in lead plates 0.5 in. thick. However, since there is strong evidence that the average energy of the secondary particles observed in this experiment is much higher than the average energies of the particles observed in the other two experiments mentioned, it is probably not justified to apply such large corrections to the data used for the determination of the value of Λ in this experiment. In order to determine the correct value of Λ, it is necessary to correct dN for the number of secondary nuclear events which are not observed. This correction was estimated through the use of the curves plotted in Fig. 8. The ordinate of the curve A gives the number of secondary nuclear events observed in this experiment for which the number of tertiary minimum ionization particles observed is greater than or equal to n_s, the abscissa. It is seen that curve A is a straight line except for a break at $n_s=1$. The significance of this break is that only 1 of the 69 secondary nuclear events observed did not show the presence of any minimum ionization prongs other than the particle which produced the event. In addition, only 3 of the 15 secondary events which showed the presence of only one emitted minimum ionization prong produced observable heavily ionizing particles. The remaining 12 of these 15 events were observable as nuclear events because of the occurrence of a large angle scattering of the secondary minimum ionization particle in one of the gold plates; (criterion 4).

The other curves of Fig. 8 represent the minimum ionization prong distribution for stars observed in photographic emulsions at different elevations.

Curve B gives the number of stars observed in photographic emulsions at 95,000 ft, which shows n_s or more minimum ionization prongs.[12]

Curve C gives the number of stars produced in photographic emulsions at 70,000 ft by singly charged relativistic particles from which n_s or more minimum ionization prongs are observed to emerge.[13]

Curve D gives the number of stars produced in photographic emulsions at 11,000 ft by singly charged relativistic particles from which n_s or more minimum ionization prongs are observed to emerge.[14]

Curves B, C, and D have been normalized to curve A at the point corresponding to 68 events and $n_s=1$. The intercepts of the curves B, C, and D with the axis $n_s=0$ give the numbers of nuclear events from which no minimum ionization secondary prongs were observed to emerge in the corresponding experiments. They are as follows: B—110 events; C—114 events; and D—174 events. It will be seen that the slopes of the curves B, C, and D decrease as the altitude at which the data was taken decreases, and also that the curves representing data taken in photographic emulsions show curvature, while the curve A representing nuclear events in gold is a straight line within the accuracy of the data. A combination of factors is responsible for these differences.

(1) A different energy spectrum of the particles initiating the events is present at the different altitudes at which the experiments were performed. It is seen that high multiplicities of minimum ionization particles are more probable at higher altitudes, and, therefore, it can be assumed that the higher average energy of the initiating particles at higher altitudes is partially responsible for this large variation among the three curves B, C, and D. These considerations indicate that curve A represents nuclear events initiated by charged particles of very high average energy.

(2) Curves B, C, and D represent the properties of nuclear events which occurred in photographic emulsions and, hence, of lower average atomic number than gold. There are undoubtedly differences in the multiplicities of minimum ionization secondary

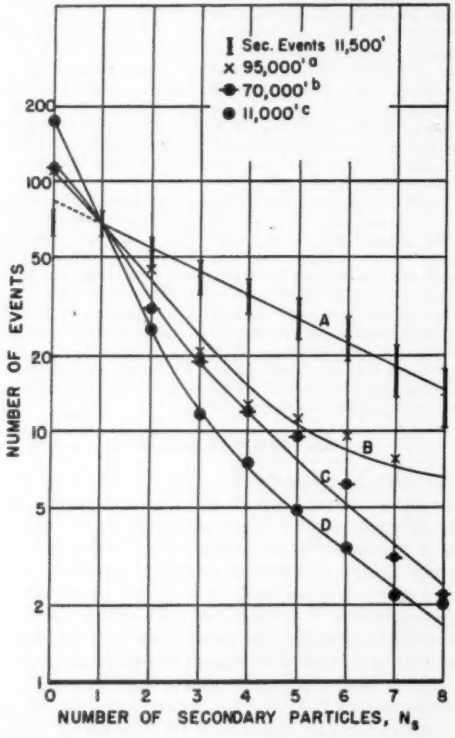

FIG. 8. Number of events emitting n_s or more minimum ionization secondary particles. (*A*) Secondary events produced in gold by penetrating minimum ionization secondary particles in penetrating showers at 11,500 ft. (*B*) Nuclear events produced in photographic emulsions at 95,000 ft. (*C*) Nuclear events produced in photographic emulsions at 70,000 ft by particles of minimum ionization. (*D*) Nuclear events produced in photographic emulsions at 11,000 ft by particles of minimum ionization.

[10] Lovati, Mura, Salvini, and Tagliaferri, Phys. Rev. **77**, 284 (1950).

[11] W. W. Brown and A. S. McKay, Phys. Rev. **77**, 342 (1950).

[12] J. J. Lord, and M. Schein, Phys. Rev. **77**, 19 (1950). These data may include neutron produced events.

[13] Camerini, Coor, Davies, Fowler, Lock, Muirhead, and Tobin, Phil. Mag. **40**, 1073 (1949).

[14] Brown, Camerini, Fowler, Heitler, King, and Powell, Phil. Mag. **40**, 862 (1949).

particles emitted from nuclear collisions with nuclei of different atomic numbers. One reason for such a difference is that secondary particles of sufficiently high energy may make collisions with nucleons in the same nucleus as the one in which they were originally produced. Such "plural production" will increase the number of minimum ionization particles emerging from nuclear events occurring in materials of high atomic number.[16] The curvature shown by curves B, C, and D at small prong numbers can then arise partly from the mixture of nuclei of different atomic numbers present in the photographic emulsions.

(3) Since the nuclear events represented by curve A are all produced by ionizing secondary particles of penetrating showers produced in the neighborhood of the cloud chamber, it must be expected that π-mesons will have produced many of them.[16] On the other hand, the short mean life of the π-mesons[17] will reduce the number of stars produced in photographic emulsions where there is no dense material immediately above the photographic plate. Since curves B, C, and D were obtained under these conditions, it can be assumed safely that almost all stars produced by ionizing particles were produced by protons.

From this discussion of the curves A, B, C, and D it is seen that the minimum number of nuclear events $dN=69$ which were directly observed in this experiment is too small, since some stars were missed in the gold plates. The total number of nuclear events that were present, if the extrapolation of curve B to $n_s=0$ is assumed to be correct, is 110. The corresponding value of $\Lambda=176$ g/cm^2 is probably too small.

The most probably correct number of nuclear events produced by the 234 secondary particles in traversing 19,400 g/cm^2 of gold is obtained by extrapolation curve A to $n_s=0$. This gives, for the total number of nuclear events produced, $dN=84$; the added number of events comprise 22 percent of the number of stars observed. The corresponding most probable value of Λ is 231 g/cm^2. In summary, the value of the mean free path for nuclear collision is found to be

$$\Lambda=230\pm60 \text{ g/cm}^2.$$

The error given is such as to include both the maximum and the minimum values of Λ.

There are other errors present in the determination of Λ which will be discussed very briefly, since they will be shown to be much smaller than the error caused by the omission of nuclear events.

An error may arise through the use of criterion 4 for the classification of secondary collisions as nuclear events, if the scattering angle ϑ of a particle is greater than 2 times the rms scattering angle for that track. Twelve events were classed as nuclear scatterings by the use of this criterion, and there are four cases of scattering of a penetrating particle observed which did not meet this criterion. The sum of the probabilities that each of the observed 16 scatterings is due to multiple scattering is 0.85, and, hence, it is probable that at most one of the 16 should not be classed as a nuclear event. The addition of three more scatterings to the number dN will reduce the values of Λ by 4 percent.

However, the smoothness of curve A of Fig. 8 is an indication that the number of scatterings included in those data is nearly correct. The addition of three scatterings discussed above would introduce a bend in the curve at $n_s=2$ and make it more like the curves B, C, and D of that figure, so that it is not possible to say at the present time which of the alternatives is the more correct.

There are also errors possible because of the chance that two secondary particles will travel too nearly in the same direction to be resolved in the pictures even by the use of the stereoscopic photographs. A careful estimate of the size of this error indicates that it will tend to increase the value of Λ by less than 1 percent, and, hence, no correction has been applied.

(B) Comparison with Other Determinations of Λ

Some values of the mean free path for nuclear collision of the secondary particles of penetrating showers which were obtained by various workers have been compiled by Camerini *et al.*[2] The measurements with cloud chambers of the mean free path in lead can be compared directly with the measurement of the present experiment in gold, since the mean free paths corresponding to the geometrical areas of two nuclei differ by less than 2 percent. The results of some recent experiments follow:

Fretter[18] obtained a value of the collision mean free path $\Lambda=750$ g/cm^2 in lead plates of 0.5-in. thickness. Fretter considered this to be a maximum value of Λ, because no correction was made for the numbers of nuclear events not observed. The result of the present experiment that the maximum value of Λ is 282 g/cm^2 is to be compared with Fretter's value. The important differences between the two experiments which could be responsible for the differences in the measured maximum values of Λ are the following.

(1) Only traversals of plates in clear regions of the cloud chamber were considered in the present experiment, while Fretter applied a less stringent requirement and made use of traversals of 0.5-in. lead plates in regions of his chamber in which the observation of low energy nuclear events may have been more difficult.

(2) The average energy of the penetrating showers observed in the present experiment is higher than the average energy of the showers observed by Fretter. The reasons for this statement will be given in the following section of this paper. The higher average energy of the penetrating showers observed in this experiment will lead to higher average energies of the secondary particles and, therefore, the values of Λ measured in the two experiments can differ, because (1) the actual value of the collision mean free path may vary with energy, and (2) there may be different fractions of π-mesons and protons present in the secondaries observed in the two experiments.

Lovati *et al.*[10] have obtained a value of 300 ± 100 g/cm^2 for the collision mean free path of secondary particles of penetrating showers. These workers used lead plates of 16.5 g/cm^2 and of 1.8 g/cm^2 in thickness and have corrected their results for the number of secondary nuclear events not actually observed because of the absorption of the tertiary particles in the lead plates. This result is to be compared with the value $\Lambda=230\pm60$ g/cm^2 obtained in this experiment. The most important difference between the two experiments is that the average energy of the penetrating showers observed in the present experiment is considerably higher.

Brown and McKay[11] have found the value $\Lambda=316\pm70$ g/cm^2 in an experiment performed with a cloud chamber fitted with lead plates 0.5 in. in thickness. They state that they believe that the average energy of the penetrating showers used in their analysis is lower than the average energy of the showers observed by Fretter, and, hence, it must be lower than the average energy of the penetrating showers used in the present determination.

(C) Nature of the High Energy Secondary Particles Observed

The value of the mean free path obtained in this experiment as well as the values obtained by other workers who used counter controlled cloud chambers can

[15] W. Heitler and L. Jánossy, Proc. Phys. Soc. (London) **A62**, 374 (1949).

[16] P. H. Fowler, Phil. Mag. **41**, 169 (1950); O. Picconi, Phys. Rev. **77**, 1 (1950).

[17] J. R. Richardson, Phys. Rev. **74**, 1720 (1948); E. A. Martinelli, and W. K. H. Panofsky, Phys. Rev. **77**, 465 (1950); Kraushar, Thomas, and Henri, Phys. Rev. **78**, 486 (1950); Chamberlain, Mozley, Steinberger, and Wiegand, Phys. Rev. **79**, 394 (1950).

[18] W. B. Fretter, Phys. Rev. **76**, 511 (1949).

be considered to be an average value for the mixture of mesons and protons which are present in the secondaries of penetrating showers. Fowler[19] has shown that more than 90 percent of the minimum ionization particles emitted from high energy nuclear events produced in photographic emulsions are π-mesons and that the majority of the remaining 10 percent are protons. Reasons were given in the discussion of Fig. 8 for expecting the average energy of the nuclear events observed at 70,000 ft, which were used by Fowler in his measurements, to be lower than the average energy of the events observed and used in the present experiment. However, the fraction of π-mesons among the secondary particles emitted from high energy nuclear events produced in gold may differ from 0.9 because of the small difference between the probabilities of plural production of secondary particles in gold and in the silver of the emulsion.

An estimate of the number of protons present among the secondaries of the penetrating showers observed in this experiment can be made by determining the number of neutrons present, since the number of high energy protons and neutrons produced are expected to be equal at the high energies involved in this experiment. A total of 9 possible stars (2 of which were certain cases[20]) in which a secondary nuclear event was produced by a neutral particle were observed in the 40 photographs of penetrating showers used. These stars occur in regions of each shower in which nuclear disruptions used in the analysis for Λ were observed. It then follows that approximately 9 (13 percent) of the 69 observed secondary nuclear events used were produced by high energy protons. In addition to the estimated 9 proton-produced secondary events, some of the 15 stars added to the actually observed 69 can have been produced by low energy protons. If it is assumed that all of these added unseen nuclear events were produced by protons, then the total maximum fraction of protons among the ionizing secondary particles emitted from the penetrating showers used in the determination of Λ is 28 percent.

On the other hand, since 2 nuclear events in the 40 photographs were certainly neutron produced, it is probable that a minimum of 2.5 percent of the ionizing secondary particles were high energy protons.

In summary, the direct data available in this experiment indicate that the fraction of protons used in the determination of Λ is in agreement with the result of Fowler that less than 10 percent are high energy protons. Therefore, the value of $\Lambda = 230 \pm 60$ g/cm^2 refers to a mixture of ionizing particles of which a majority are π-mesons.

If it is then assumed that 10 percent of the high energy secondary nuclear events are produced by protons with a collision cross section equal to the geometric area of the gold nucleus, the remaining π-mesons have a collision mean free path $\Lambda = 240 \pm 60$ g/cm^2. However, the errors involved in the determination of the mean free path are large, and it cannot be said with certainty whether or not the collision cross section of high energy π-mesons is slightly smaller than the area of the nucleus.

The possibility that many μ-mesons are present among the secondary particles emitted from high energy penetrating showers produced in gold is excluded by the low value of the collision mean free path observed. This is in agreement with a result of Picconi.[21]

TABLE III. Estimates of energies of particles scattered at stars.

Scattering angle (degrees)	Estimated star energy (ev)	Momentum of secondary particle (ev/c)	Energy of secondary meson (ev)	Energy of secondary proton (ev)
3	5×10^{8}	2.1×10^{10}	2.1×10^{10}	2.0×10^{10}
5	5×10^{8}	1.2×10^{10}	1.2×10^{10}	1.1×10^{10}
6	5×10^{8}	1.0×10^{10}	9.9×10^{10}	9.1×10^{9}
10	5×10^{8}	6.3×10^{9}	6.2×10^{9}	5.4×10^{9}
22	5×10^{8}	2.5×10^{9}	2.4×10^{9}	1.6×10^{9}
35	5×10^{9}	1.8×10^{9}	1.7×10^{9}	1.1×10^{9}

VI. ENERGIES OF THE PENETRATING SHOWERS

(A) Energies of Secondary Particles

Estimates of the momenta of secondary particles were made in the analysis of the nuclear events reproduced in Figs. 2 and 5. Additional estimates made by the same method are given in Table III.

As was mentioned in the discussion of the mean free path, an observable star is not always seen at the point at which a penetrating secondary particle is scattered. In such a case an upper limit for the energy of the scattered particle can be estimated by assuming an upper limit for the energy of the star which was not seen. The results of such calculations are given in Table IV. However, it should be pointed out that these momentum estimates will be in error if the scattered particle transmitted its recoil momentum to more than one of the nucleons in the scattering gold nucleus. In view of the fact that 14 percent of the secondary nuclear events are such scattering processes without observable tertiary particles, it would be of interest to know the nature of these processes.

In favorable cases, a lower limit on the momentum of a particle can be found from the upper limit of the rms multiple scattering angle of the track as it traversed the gold plates in the cloud chamber. An example of such an estimate was given in the discussion of Fig. 2. Further examples are given in Table IV.

It is of interest to note that in most cases the momenta given in Tables III and IV lie between 10^9 and 10^{10} ev/c, and there are few cases in which the momenta

[19] P. H. Fowler, Phil. Mag. **41**, 169 (1950).

[20] Seven of the 9 stars observed must be considered to be questionable cases of neutrally produced nuclear events because of the high density of ionizing particles above the gold plates in which they were produced.

[21] O. Picconi, Phys. Rev. **77**, 1 (1950).

TABLE IV. Momentum estimates of particles scattered with no star visible.

Scattering angle (degrees)	Estimated star energy (ev)	Minimum momentum from rms scattering (ev/c)	Maximum momentum from nuclear scattering (ev/c)
3	2×10^8	1.1×10^9	1.2×10^{10}
4	2×10^8	9.3×10^8	9.2×10^9
5	2×10^8	1.1×10^9	7.4×10^9
6	2×10^8	9.3×10^8	6.2×10^9
7	2×10^8	1.3×10^9	5.3×10^9
14	2×10^8	5.2×10^9	2.6×10^9

could be below 10^9 ev/c. In contrast, Butler, Rosser, and Barker[22] have found that the momentum spectrum of secondary particles emitted from penetrating showers, observed at sea level in a cloud chamber placed in a magnetic field, has a maximum near 10^9 ev/c. These authors estimate that the average energy of the showers observed in their experiment is smaller than that observed by Fretter. Since the energies of the showers observed by Fretter are smaller than those in the present experiment, as will be shown in the next section, it is to be expected that the momenta of secondary particles observed here (note values given in Tables III and IV) are considerably higher than the momenta observed by Butler, Rosser, and Barker.

(B) Electronic Cascades Associated with Penetrating Showers

Electron cascades were observed in 88±3 percent of the penetrating showers produced in the chamber in this experiment. Events which were seen to be accompanied by an atmospheric shower were excluded from these data. The remaining fraction of the events may have low energy electron showers present, since such showers with total energies less than 10^8 ev are not always detectable in this apparatus. Although more than one electron shower is often present in the same penetrating shower (Fig. 7), the electron shower with the highest energy is usually produced near the initial encounter, and lower energy showers are found to be initiated near the position of nuclear encounters of secondary particles.

The method by which rough estimates of the energies of electron cascades were obtained is employed in the discussion of Figs. 2 and 5. Again, it should be emphasized that the method used gives an estimate of the highest energy electron shower present and that there may be cascades present of lower energy. This will be the case if several γ-rays were emitted as decay products of neutral mesons produced in the initial nuclear encounter. Therefore, the energies given here represent the lower limits on the total energy of all electron showers present in the event.

Figures 9 and 10 are given to illustrate the appearance of penetrating showers showing the presence of high energy electronic cascades. These events are of high total energy, while the events of Figs. 2, 5, and 7 represent penetrating showers of more nearly the average energy of the events observed in this experiment. Both Figs. 9 and 10 show the presence of numerous penetrating particles, and secondary nuclear events are seen in the cores of the two showers. In each of the two figures the retarding effect of the counter tray on the multiplication of the particles in the shower is clearly visible. The energies of the electron showers in the two events are given in Table V.

Although the fraction of energy of the particle initiating a penetrating shower which is dissipated in the electron cascade produced may vary somewhat, the energies of electronic cascades observed in an experiment of this kind will give an indication of the lower limit to the energies of the penetrating showers observed. This fact makes possible a comparison of the energies observed here with those of Fretter. He gives data from which one can see that 68 percent of the penetrating showers observed in his apparatus showed the presence of electron cascades. The larger fraction of 88 percent of events showing electron showers observed in this experiment under comparable conditions is then definite evidence of the higher average energy of the initiating particles. In addition, it is of interest to note that the average energy of the electron showers as measured from their penetration is definitely higher in this experiment than it is in Fretter's.

The fact that penetrating showers contain electron showers in the large fraction of 88 percent of the events is definite evidence that the cross section for the production of electron showers is very nearly the same as it is for a nuclear collision in which a penetrating shower occurs. Since it has been shown that most of the ionizing particles produced in penetrating showers are π-mesons, this is an indication that these cascades arise from the disintegration into γ-rays of neutral mesons produced in the same collision. A further discussion of the electron cascades associated with high energy penetrating showers will be published later.

VII. THE ANGULAR DISTRIBUTION AND MULTIPLICITY OF MINIMUM IONIZATION SECONDARY PARTICLES

Considerable knowledge of the energies of penetrating showers can be gained from a study of the angular distribution of the emitted secondary particles. The following discussion will refer only to high energy penetrating particles whose paths can be extrapolated to a single point.

In order to compare the angular distribution of secondary particles emitted from penetrating showers of different energies, the energy of the electron shower present was used as an indication of the energy of the initiating particle. Accordingly, the angular distribution of the two following groups of penetrating showers was determined.

[22] Butler, Rosser, and Barker, Proc. Phys. Soc. (London) **A63**, 145 (1950).

(1) Twenty-five events were produced in the chamber or in the top wall of the chamber which did not show the presence of any electron shower or have an electron cascade of energy $E \leq 7 \times 10^9$ ev.

(2) Ten events were produced in the chamber or in the top wall of the chamber which showed the presence of an electron shower with an energy $E > 7 \times 10^9$ ev.

The corresponding distributions of the projected angles of the secondary particles with respect to the axis of each shower are given in Figs. 11 and 12, respectively. It will be seen that, in Fig. 11, the number of particles per degree falls to one-half of its maximum value of an angle $\psi = 5°$. For the events of higher energy represented in Fig. 12, it is seen that $\psi = 2.5°$. In both figures, the number of particles emitted at large angles with respect to the axis of the penetrating shower is very small.

If it is assumed that π-mesons are emitted isotropically in the center-of-mass system of two colliding nucleons, then it is possible to determine the energy of the incident nucleon from the angle ψ by applying relativistic transformations to the momenta of the emitted mesons. If ψ is taken to be its maximum possible value, $\psi = 5°$ for the data of Fig. 11, then it is found that the energy of the incident nucleon must have been 4.4×10^{11} ev. This high value is in direct contradiction with the energies of showers as estimated directly from the interactions of secondary particles in the cloud chamber. For the events whose data are given in Fig. 12, an even higher energy is given by the calculation. If, as the direct estimates show, the average energy of the penetrating showers of Fig. 11 is taken to be 3×10^{10} ev, then ψ must have the high value of 19° provided the angular distribution of the mesons in the center-of-mass system is taken to be isotropic. Although the calculations do not take into account the possibility of successive collisions with nucleons by secondary particles as they traverse the gold nucleus, it is very difficult to see how such plural production could sharpen the angular distribution of secondary particles in the laboratory system.

A possible way of explaining this difficulty has been indicated by Lord, Fainberg, and Schein.[23] These authors point out that in a recent paper by Fermi,[24] it is mentioned that the distribution of mesons in the center-of-mass system can be concentrated in two cones of half-angle θ' centered about the velocities of the two colliding nucleons. The experiments of Lord, Fainberg, and Schein are in good agreement with $\theta' = 30°$ for an incident particle of energy $E = 3 \times 10^{13}$ ev.

In the present case, θ' can be determined from the equation

$$\gamma = 2(\tan^2\tfrac{1}{2}\theta'/\tan^2\theta) - 1, \qquad (6)$$

which is a modification for the observed lower energies of this experiment of an equation given by Lord,

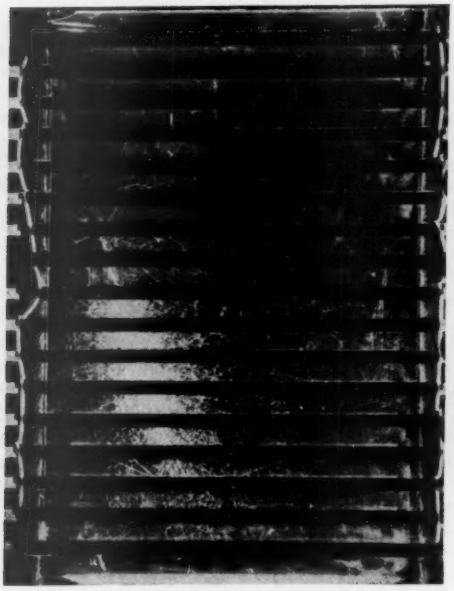

FIG. 9.

FIG. 10.

[23] Lord, Fainberg, and Schein, Phys. Rev. **80**, 970 (1950).
[24] E. Fermi, Prog. Theor. Phys. **5**, 570 (1950); Phys. Rev. **81**, 683 (1951).

TABLE V. Electron shower energies of two events.

Figure	Position in radiation units from shower origin	Number of electrons	Estimated total shower energy (ev)
9	30	15±5	2×10^{11}
	12±3	maximum	
10	35	20±5	10^{12}
	13±3	maximum	

Fainberg, and Schein. In Eq. (6), θ is the half-angle of the cone of secondary particles observed in the cloud chamber, and γ is the energy of the colliding nucleon in units of its rest energy. It is difficult to determine the value of θ from Fig. 11, since it includes data taken from many showers, and the half-width of the cone will vary with the energy of the event. However, one can take the average value of $\theta=7°$ from Fig. 11. Assuming $\gamma=32$ corresponding to an energy of 3×10^{10} ev, Eq. (6) yields a value of 50° for θ'.

This value of θ' is somewhat larger than the value given by Lord, Fainberg, and Schein. The much lower energies of events observed in this experiment is most probably responsible for this difference.

The above considerations are based upon the assumption that the secondary particles observed were produced in a nucleon–nucleon collision. Since a number of the secondary minimum ionization particles observed are due to plural production in the gold nucleus, the conclusions regarding the value of θ' must be regarded as tentative. However, it should be pointed out that an expected widening of the angular distribution by plural production can have the effect that the value of θ' is somewhat overestimated.

Figure 12 shows the angular distribution of secondary particles emitted from events showing the presence of electron cascades above 7×10^9 ev. It will be seen that the number of particles observed between 0° and 1° from the axis of the showers is not as much higher than the number observed between 1° and 2°, as would be expected from the trend of the other points of the graph. The reason for this is that secondary particles in the very dense core of the high energy penetrating showers are not all resolvable in this experiment. The estimated number of particles missed between 0° and 1° from the axis of the events is indicated by the dotted line in Fig. 12.

If θ' is assumed not to change greatly in the range of energies of showers observed in this experiment and if $\theta=5°$ for the events represented in Fig. 12, the energy of those events is found from Eq. (6) to be 6×10^{10}.

Some of the important facts regarding the events whose angular distributions are given in Figs. 11 and 12 are presented in Table VI.

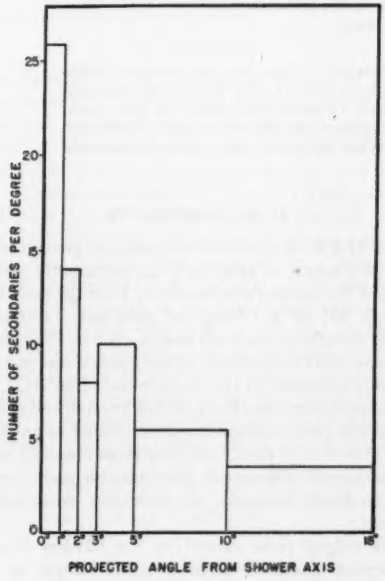

FIG. 11. Projected angular distribution of minimum ionization penetrating secondary particles of events showing either no electron shower or showing electron showers with energies $E\leq7\times10^9$ ev.

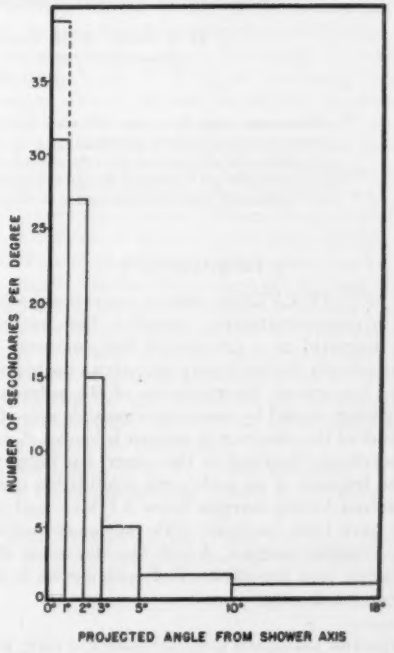

FIG. 12. Projected angular distribution of minimum ionization penetrating secondary particles of events showing electron showers with energies $E>7\times10^9$ ev.

TABLE VI. Comparison of two groups of penetrating showers.

Range of electron shower energies (ev)	Estimated average energy (ev)	Average number of penetrating secondaries per event
$0-7\times10^9$	3×10^{10}	7 ± 1
$>7\times10^9$	6×10^{10}	11 ± 2

Multiplicities of High Energy Secondary Particles

As is seen from Table VI, the multiplicities of minimum ionization penetrating secondary particles originating in the initial nuclear encounter are 7 and 11, respectively, for the lower and the higher energy events. A comparison with the number of π-mesons predicted at each of these energies by Fermi[24] shows that the number of particles observed is approximately 3 times higher than those predicted. The difference is attributable partly to the presence of protons among the penetrating ionizing secondary particles and partly to the plural production of secondary particles. It is felt that the existing uncertainties in the interpretation of the results of this experiment are too large to enable a quantitative comparison to be made.

In accordance with the momenta determined from scatterings (Tables III and IV), if the average energy of the secondary particles is estimated to be 4×10^9 ev, then the multiplicities of 7 and 11 given in Table VI indicate that the energies of the two groups of events are 3×10^{10} and 4×10^{10} ev per shower, respectively. When the energy of the electron showers is added to these values, the agreement with the estimated energies of the initiating particles of the two groups of showers is satisfactory.

The author wishes to express his appreciation to Professor Marcel Schein for his great interest and guidance during the course of this research. The gold plates used in this experiment were kindly supplied by the Office of Naval Research. The author wishes to thank Mr. C. J. Abrams of the Climax Molybdenum Company for his hospitality during the operation of the apparatus at Climax, Colorado.

PHYSICAL REVIEW VOLUME 82, NUMBER 3 MAY 1, 1951

Response of an Anthracene Scintillation Counter to Protons*

H. B. FREY,† W. M. GRIM,† W. M. PRESTON,‡ AND T. S. GRAY†
Massachusetts Institute of Technology, Cambridge, Massachusetts
(Received December 18, 1950)

The proton response of an anthracene scintillation counter below 3.7 Mev has been measured. When combined with previously published data up to 17 Mev, a smooth curve results. An attempt was made to correlate the efficiency of the light output with the ion density by plotting the differential light output as a function of the differential energy absorption for both electrons and protons. The available information is not sufficiently extensive or accurate to determine whether or not the proton and electron data coincide.

I. INTRODUCTION

A SCINTILLATION counter constructed with a hydrogen-containing phosphor has frequently been suggested as a detector of fast neutrons. This device actually detects recoil protons from the hydrogen within the crystal. Interpretation of the pulse-height distribution caused by neutrons is possible only if the response of the phosphor to protons is known. A direct measurement, described in this paper, has been made of the response of an anthracene scintillation counter to protons having energies below 3.7 Mev, and these data have been combined with previously published data at higher energies. A test was also made of the possibility that the efficiency of light output depends only on ion density.

* This work was assisted by a joint program of ONR, Bureau of Ships, and AEC.
† Electrical Engineering Department, M.I.T.
‡ Laboratory for Nuclear Science and Engineering, M.I.T.

II. MEASUREMENTS

The M.I.T. Rockefeller electrostatic generator was used as a source of essentially monoenergetic protons. A few of the protons were scattered from the main beam through 90° by a 1.5-mg/cm² gold leaf. Protons impinged directly on the front face of a 0.5 in. thick, 0.5 in. diameter clear anthracene crystal, which was mounted by canada balsam on the cathode end of an RCA 5819 photomultiplier tube. The gold foil, crystal, and cathode end of the photomultiplier were mounted in an evacuated T section of pipe. Counting rates obtained with a single-channel differential discriminator were normalized to beam intensity, as indicated by a monitor channel.[1]

The output pulse caused by the 624-kev internal-conversion electrons[2] from a small sample of Cs^{137} within the vacuum system was used as a reference level

[1] W. C. Elmore, Nucleonics 2, 16 (1948).
[2] L. M. Langer and R. D. Moffat, Phys. Rev. 78, 74 (1950).

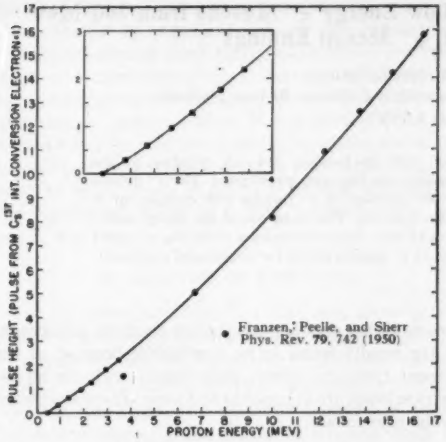

FIG. 1. Light output as a function of proton energy for an anthracene scintillation counter. The insert is an enlarged portion showing the new data below 3.7 Mev. Although 0.4-Mev protons were easily detected, the most probable pulse height could not be separated from dark current with the data taken.

for the proton measurements.[3] Since Cs^{137} emits two beta-particles, in addition to an internal-conversion electron, an approximate beta-curve was subtracted from the total curve of counting rate *vs* differential pulse height[4] to locate more closely the peak of the internal-conversion-electron curve.

III. RESULTS

The insert in Fig. 1, an expanded portion of Fig. 1, shows the relation between the energy of the incident proton and the most probable light-pulse amplitude for the heretofore unreported region below 3.7 Mev. The ordinate of each of the points on the curve represents the pulse amplitude of the peak of a pulse-height distribution curve containing approximately eight points taken for each of the seven proton energies plotted. The energies were measured on a generating voltmeter calibrated with the $Li^7(p,n)$ threshold at 1.882 Mev. The width of the distribution curves is in good agreement with that given by Morton[5] for scintillation counters. A correction of approximately 0.1 Mev has been applied to the initial proton energies to account for the average loss in the gold scattering foil.

When the data mentioned above and those published by Franzen, Peelle, and Sherr are plotted to the same

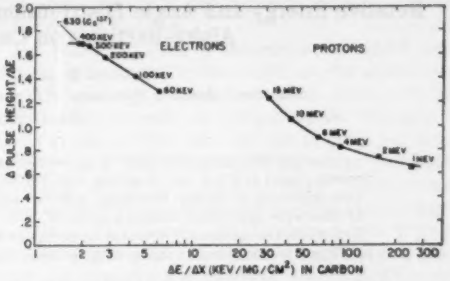

FIG. 2. Differential light output obtained from Fig. 1 as a function of the differential energy loss. The electron and proton data were normalized to the light output caused by the 624-kev Cs^{137} electron.

scale, the smooth curve of Fig. 1 is obtained. Only their point at 3.7 Mev, the exact energy of which they questioned, fails to fall close to the curve.

The fact that protons and alpha-particles produce smaller light pulses than do electrons of equal energy[4] is usually attributed to a saturation effect arising from the much higher specific ionization (at equal energies) of the heavier particles. The slope of curves like Fig. 1 gives the differential light output as a function of energy, dL/dE. The rate of energy loss of electrons[6] and protons,[7] dE/dx, is known. Hence, one can plot curves showing dL/dE as a function of dE/dx for both protons and electrons. Since the specific ionization is nearly proportional to dE/dx and the energy loss per ion formed is about the same for protons and electrons, one might expect that the two curves would coincide roughly if the efficiency of light output in fact depends only on the ion density. Such a plot is shown in Fig. 2. The proton information is taken from Fig. 1 and that for electrons from Hopkins.[8] Because the data available are less reliable at lower than at high energies, the values of the slope, dL/dE, at low energies may be only approximate. The two curves show the expected trend, individually. Their apparent failure to coincide may be due to insufficiently accurate data or to an unknown dependence of light output on factors other than rate of energy loss. Additional information will be required on the differential light output caused by protons at higher energies and electrons at lower energies in order to test further the theory.

We are indebted to Dr. Clark Goodman for his constant encouragement and interest in this work.

[3] Franzen, Peelle, and Sherr, Phys. Rev. **79**, 742 (1950).
[4] W. H. Jordan and P. R. Bell, Nucleonics **5**, 30 (October, 1949).
[5] G. A. Morton, RCA Rev. **X**, 542 (1949).
[6] H. Bethe, *Handbuch der Physik* (1933), Vol. 24-1, p. 519.
[7] J. O. Hirschfelder and J. L. Magee, Phys. Rev. **73**, 207 (1948).
[8] J. I. Hopkins, Phys. Rev. **77**, 406 (1950).

Relative Energy and Angle Distribution of Low Energy π^- Mesons from 390-Mev Alpha-Particles on Carbon. μ^- Meson Endings

STANLEY B. JONES* AND R. STEPHEN WHITE
Radiation Laboratory, Department of Physics,† University of California, Berkeley, California
(Received December 4, 1950)

A part of the energy spectrum of π^- mesons generated with the Berkeley 184-inch cyclotron by the bombardment of 0.1 g/cm² of carbon with 390-Mev alpha-particles has been investigated. The π^- mesons were registered in nuclear emulsions. Relative values for the numbers of π^- mesons with energies up to 14 Mev were determined at angles up to 60° with the beam direction. The maximum of the energy distribution function apparently occurs at an energy greater than 12 Mev. Some information about the μ^- meson endings is obtained from a region of the emulsion forbidden to π^- mesons except for pronounced scattering.

I. INTRODUCTION

A FEW months after mesons were first produced artificially by the 184-inch Berkeley cyclotron by alpha-particle bombardment,[1] an experiment was undertaken to determine the relative energy and angular distribution functions for π^- mesons generated by the 390-Mev alpha-particle beam incident on a carbon target. It was expected that the meson energies would extend up to a maximum of only a few Mev for an alpha-particle energy of 390 Mev. Such an energy spectrum could be studied conveniently with the then available cyclotron air lock. Results of the experiment, concluded some time ago, appear to indicate that the most probable meson energy lies above the part of the spectrum studied. Publication of the results has been withheld because the range-energy curves for emulsion and glass in the pertinent energy region were in question. Recently, these curves have been determined experimentally over the necessary region by Bradner, *et al.*,[2] and, in addition, Aron[3] has recalculated the glass curve. The portions of the energy and angular distribution spectra on which the apparatus supplied data have now been calculated. Although the most probable π^- meson energy was apparently not reached, publication of the results seems to be worthwhile because, at the present time, no meson experiments with the alpha-particle beam are in progress and none are contemplated in the near future.

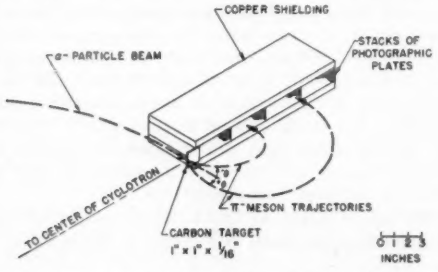

FIG. 1. Schematic view of the exposure arrangement with the plate holder, carbon target, and nuclear emulsions in place.

II. OBSERVATION OF THE MESONS

The π^- mesons were generated in the 184-inch cyclotron by an alpha-particle beam striking a carbon target and were registered in nuclear emulsions. A schematic diagram of the experimental arrangement is presented in Fig. 1. The alpha-particle beam is shown circulating in the clockwise direction and striking a carbon target at a radius of 81 inches, where the beam energy is 390 Mev. Some of the π^- mesons produced leave the target in the plane of the alpha-particle beam, moving in the general direction of the beam, and then are deflected by the magnetic field in a counterclockwise direction into the nuclear emulsions as illustrated. The path of these mesons may make an angle θ with the beam direction at the target from either side of the beam. θ was defined to be negative if the meson initially started inward, and positive otherwise, as shown in Fig. 1.

The carbon target was one inch square and had a thickness of 0.1 g/cm². Most of the alpha-particles were found to hit a region of the target less than $\frac{1}{4}$ inch from the leading edge when the target was monitored with thin polystyrene. The activity of the polystyrene was due to positrons from the C^{11} formed by the reaction $C^{12}(\alpha, \alpha n)C^{11}$.

The nuclear emulsions used were 100-micron thick Ilford C-2 emulsions on one-by-three-inch glass plates. They were placed in stacks of 4 with a blank glass plate on the top and bottom. After exposure in the plate holder, the plates were developed according to standard procedure. A plate from the center of the stack was selected for examination with the aid of a binocular microscope at a magnification of about 600×.

All meson tracks found ending in the emulsion were recorded and labeled either σ (star-forming) or ρ (non-star-forming). Only σ-mesons were used for determining the energy distribution function for the π^- mesons, since there was a possibility that a few π^+ mesons and μ^+ mesons stopped in the emulsions, and since some of

* Now at California Research Corporation, La Habra, California.

† This paper is based on work performed under the auspices of the AEC.

[1] E. Gardner and C. M. G. Lattes, Science **107**, 210 (1948).

[2] Bradner, Smith, Barkas, and Bishop, Phys. Rev. **77**, 462 (1950).

[3] W. Aron, private communication.

the ρ-mesons were certainly μ^- mesons. The σ-meson count should be representative of the number of π^- mesons, since a fixed fraction, 73.2±2.0 percent,[4] of the π^- mesons form stars, μ^+ mesons and π^+ mesons do not form stars, and there is evidence to be discussed later that μ^- mesons seldom if ever initiate stars. As evidence that the selection of negative mesons was much favored by the geometry used, it is worthwhile to point out that in the group of over 600 mesons observed in this experiment, no $\pi-\mu$ ending, indicative of a π^+ meson, was seen.

III. ANALYSIS OF THE DATA

The function $(\Delta N/\Delta\Omega\Delta E)_{rel}$ that was investigated in this experiment represents the relative number of π^- mesons leaving the target per unit meson energy interval per unit solid angle as a function of π^- meson energy E, and angle with the beam direction, θ, when a 390-Mev alpha-particle beam is incident upon a 0.1-g/cm² carbon target. The study was restricted to angles within 60° of the beam direction. The procedure used in finding this function from the data was to correlate a region of the photographic plates with an energy and angle interval for π^- mesons leaving the target. The meson density in the region provided a measure of the desired function.

The positions of all of the mesons observed were plotted, with respect to the target, on the assumption that the plot represented the meson density in the central plane between the cyclotron dees. This plot is shown in Fig. 2. The next step was to mark out areas on the meson plot that corresponded to particular π^- meson energy and angle intervals. First, meson orbits for particular angles and energies at the target were laid out by stepwise graphical construction, since the rapidly falling-off magnetic field in this region very much complicated a mathematical treatment. When the point and angle at which a meson would strike the photographic plates were established, the position where it would end in the emulsion was computed. This was done by taking a group of 100 mesons and observing the fractions of the range traveled in glass and emulsion for each energy. Then the penetration into the plate, neglecting scattering, could be determined from the range energy curves in emulsion and glass.[2,3] Aron's theoretical curve for protons in glass of a composition similar to that used by Ilford is within the probable error of the experimental curve measured by Bradner, *et al.*,[3] and was used in obtaining the ranges in

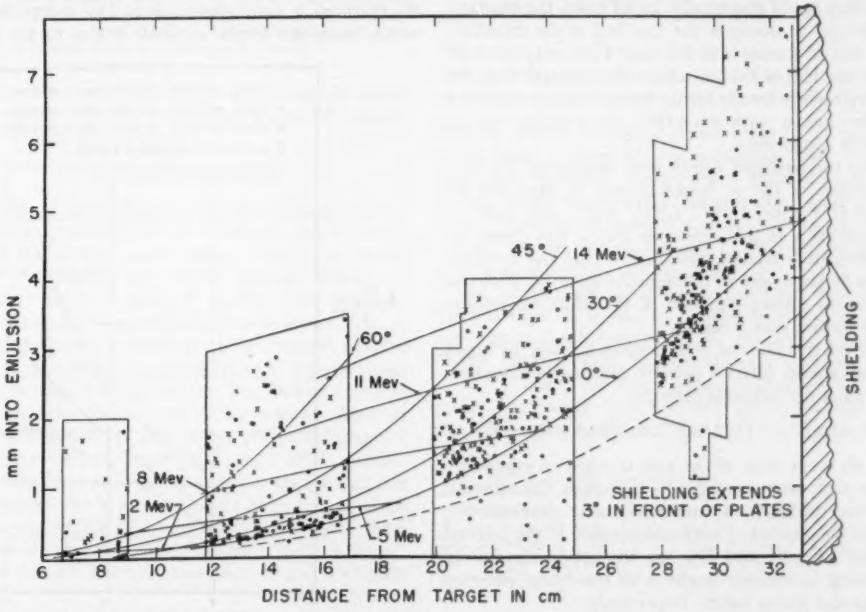

FIG. 2. Plot of meson endings in the photographic emulsions. A cross represents the ending of a σ-meson (star-forming meson) and a dot represents the ending of a ρ-meson (non-star-forming meson). The regions scanned are set off with solid lines. The analysis curves are also indicated with solid lines. Some π^- mesons which are scattered will not penetrate into the emulsion to the $\theta=0°$ analysis curve. The dashed curve was drawn on the basis of the observed density of σ-mesons. The region of the emulsion below this dashed curve contains only those π^- mesons which experienced a large scatter.

[4] F. L. Adelman and S. B. Jones, Science **111**, 226 (1950).

glass. Once the endings for particular energies and angles were established, a chart such as that shown in Fig. 2, denoting the boundaries of particular energy and angle intervals, was constructed. Because mesons leaving the target at angles equal in magnitude but different in sign did not stop at exactly the same position in the photographic plates, the lines representing constant energy and angle values had to be drawn as weighted mean values. A point determining a boundary was taken on the straight line connecting the points for the plus and minus angles. The ratio of its distances from the end points was weighted inversely as the ratio of the numbers of mesons of positive and negative θ that stop in the emulsion. The weighting factor, W, is the product of D, the fraction which survive decay in flight; F, the ratio of the meson density to the meson density that would be obtained if the focusing effect of the horizontal component of the magnetic field were not effective; and $1/S$, the reciprocal of the length of the meson orbit:

$$W=DF/S.$$

D was calculated from the mean-life of the π-meson[5-8] which was taken to be 2.6×10^{-8} sec. The focusing factor, F, representing the familiar focusing effect of the fringing of a cyclotron's magnetic field on a charged beam was found graphically. In all cases, the magnetic field fell off so slowly in the first half of the trajectory that the defocusing was less than 1 percent; however, in the last half of the trajectory, the magnetic field fell off very rapidly for the higher energy mesons; and for a 14-Mev meson with $\theta=+60°$, the focusing was as much as 33 percent.

Once the weighted points were determined for integral values of the π^- meson energy in Mev and for values of θ equal to 0°, ±30°, ±45°, and ±60°, a diagram such as that shown in Fig. 2 was drawn in. The weighting factors combined so that the resultant curves lie very close to the negative θ-curves. This was due to the strong influence of the short trajectories of the mesons with θ negative.

The relative number of π^- mesons leaving the target per unit energy interval per unit solid angle was calculated from the following formula.

$$(\Delta N/\Delta\Omega\Delta E)_{\text{rel}}\propto[1/\Delta\theta\Delta E(\Sigma R_i t_i)](\Delta N_\sigma/W_{\theta^+}+W_{\theta^-}).$$

Here R_i is the ratio of the area scanned on emulsion i to the total area accessible to mesons in this interval; t_i is the thickness of emulsion i after development; ΔN_σ is the number of σ-mesons counted in the interval $\Delta\theta$ and ΔE; W_{θ^+} and W_{θ^-} are the previously defined weighting factors for angles with the beam direction of plus and minus values, respectively.

As only relative distributions were measured, the fractional shrinkage of the emulsion during development was not needed. It was assumed, however, that the fractional shrinkage was constant for all of the emulsions.

IV. RESULTS

In order to obtain acceptable statistics, the values of ΔN_σ were combined into groups. This was done in two ways. One grouping was made such that π^- meson energy distribution functions could be determined. Calculations were made for energy intervals of 2 to 6 Mev, 6 to 10 Mev, and 10 to 14 Mev for ranges of θ of 0°–30°, 30°–60°, and 0°–60°. The other grouping was chosen so that calculations of angular distribution functions could be done. The angular intervals used were 0°–30°, 30°–45°, and 45°–60°, and the energy intervals were taken to be 2 to 8 Mev, 8 to 14 Mev, and 2 to 14 Mev.

The values of $(\Delta N/\Delta E\Delta\Omega)_{\text{rel}}$ are plotted in arbitrary units in Figs. 3 and 4. The energy distribution function is shown in Fig. 3 and the angular distribution function in Fig. 4. One can see from Fig. 3 that a maximum of the energy distribution has probably not been reached at an energy of 12 Mev. Figure 4 indicates that the meson density falls off markedly when θ is increased from 0° to 52.5°. This method of obtaining the angle and energy distributions is most applicable to low energy mesons which leave the target at small angles to the beam

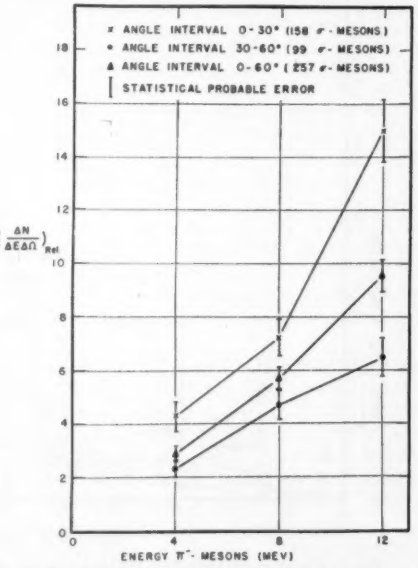

FIG. 3. Relative values of the energy distribution functions measured for π^- mesons produced by 390-Mev alpha-particles bombarding 0.1 g/cm² of carbon. Functions are given for angles of 0°–30°, 30°–60°, and 0°–60° with the beam direction. The ordinate is in arbitrary units. Solid lines were drawn connecting the points.

[5] J. R. Richardson, Phys. Rev. **74**, 1720 (1948).
[6] E. Martinelli and W. Panofsky, Phys. Rev. **74**, 465 (1950).
[7] Chamberlain, Mozley, Steinberger, and Wiegand, Phys. Rev. **79**, 394 (1950).
[8] Kraushaar, Thomas, and Henri, Phys. Rev. **78**, 486 (1950).

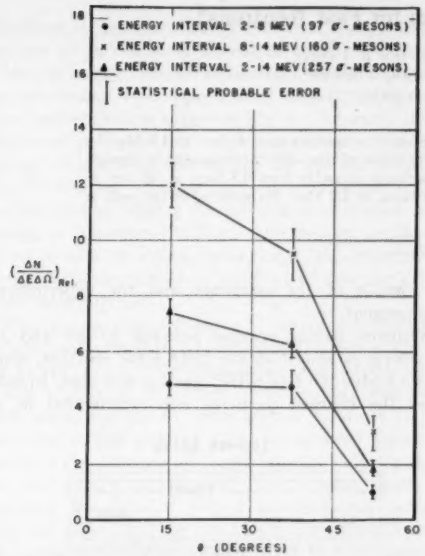

FIG. 4. Relative values of the angular distribution functions measured for π^- mesons produced by 390-Mev alpha-particles bombarding 0.1 g/cm² of carbon. Functions are given for energy ranges of 2–8, 8–14, and 2–14 Mev. The ordinate is in arbitrary units. Solid lines were drawn connecting the points.

direction. The systematic errors, which are not shown on the graphs, increase with larger angles of emission and with larger meson energies.

V. μ^- MESON ENDINGS

Because of scattering in the emulsion and glass, some of the π^- mesons will not penetrate into the emulsion as far as the range-energy calculations would predict. Therefore, the meson endings below the analysis curve for θ equals 0° in Fig. 2 are to be expected. From the observed density of σ-meson endings, one can construct a curve below which there is a region of the emulsion which is inaccessible to π^- mesons unless they experience a large scatter. The dashed curve in Fig. 2 has been constructed in this manner. Most of the mesons ending in this region are presumably μ^- mesons which come from decay in flight of π^- mesons. There were 15 mesons which ended in the part of this lower region which was scanned; only one of these made a star. Of the 14 non-star-forming mesons, there were two which had a "club" at their ends. A "club" has been defined arbitrarily as a group of grains without direction which has a spatial extent in the emulsion of at least twice the width of the meson track near its ending. These are possibly grains caused by recoil of the product nucleus on the ejection of a neutron. Gardner,[9] using a technique similar to that described in this paper, found 13 mesons, one of which formed a star. Two of the non-star-forming mesons formed a "club." He has kindly permitted us to add his statistics to our own. This information is summarized in Table I.

The number of μ^+ mesons that stopped in the region forbidden to π^- mesons is estimated to be <5 percent of the μ^- mesons. This is in part the result of the small value[10] of 0.2, for the ratio of the cross section for production of low energy π^+ mesons to that for π^- mesons, and in part to the geometry which was favorable for registering μ^- mesons rather than μ^+ mesons.

It should be emphasized that this experiment cannot be made entirely free from contamination by π^- mesons as there is a finite probability for large scattering anywhere along a meson's path; therefore, the two star-

TABLE I. Data on μ^- meson endings.

Observer	Mesons ending in μ^- area	No. of σ-mesons	No. of ρ-mesons	No. of mesons having clubs	Fraction of μ^- mesons which form stars	Fraction of μ^- mesons which have clubs
Authors	15	1	14	2		
Gardner	13	1	12	2		
Total	28	2	26	4	$\leq 0.07 \pm 0.03$	$\leq 0.14 \pm 0.05$

forming mesons mentioned above could be π^- mesons which have undergone large scattering. This experiment does, however, put an upper limit of about 10 percent on the fraction of μ^- mesons which form stars. These results are in essential agreement with those of Chang[11] on cosmic-ray mesons. Further study of μ^- mesons is planned at this Laboratory.‡

The authors are indebted to Professor Ernest O. Lawrence for his continued interest in this work. We also wish to thank Professor R. L. Thornton, and Drs. Walter Barkas, Hugh Bradner, Eugene Gardner, and C. M. G. Lattes for much helpful discussion. We are grateful to James Vale and the cyclotron crew for making the bombardments.

[9] E. Gardner, private communication.
[10] W. H. Barkas, Phys. Rev. **75**, 1467 (1949).
[11] W. Y. Chang, Revs. Modern Phys. **21**, 166 (1949).
‡ *Note added in proof:* George and Evans [Proc. Phys. Soc. (London) **64**, Part 2, 193 (1951)], from studies of nuclear emulsions exposed underground, find that 0.055 ± 0.011 of the μ^- mesons which stop in the emulsions produce stars.

Total Cross Section of Helium for Fast Neutrons*

S. BASHKIN,† F. P. MOORING, AND B. PETREE
University of Wisconsin, Madison, Wisconsin
(Received December 19, 1950)

The total neutron cross section of helium has been determined at energies from 40 kev to 4.9 Mev by comparison of the transmission of neutrons through a helium-filled cylinder with the transmission through an identical empty cylinder. The observed cross section increases smoothly from 0.8 barn at 40 kev to 6.7 barns at 1.15 Mev, and then decreases smoothly to 2.3 barns at 4.9 Mev. No splitting of the peak at 1.15 Mev was observed.

I. INTRODUCTION

THE differential cross section for the scattering of neutrons by helium has been studied on several occasions. Staub and Stephens[1] found a resonance for the backward scattering at about 1-Mev neutron energy and attributed it to a p-level in the He^5 nucleus. This resonance was also observed by Gaerttner, *et al.*[2] Further work by Staub and Tatel[3] indicated that the half-width of the resonance was about 0.4 Mev and seemed to show a doublet structure with a splitting of about 0.3 Mev.

Barschall and Kanner,[4] using monochromatic neutrons, obtained the angular distribution of neutrons at energies of 2.5 and 3.1 Mev. Wheeler and Barschall[5] found that those angular distributions could be interpreted as a superposition of outgoing S, $P_{\frac{1}{2}}$, and $P_{\frac{3}{2}}$ waves, with large phase shifts between the $P_{\frac{1}{2}}$ and $P_{\frac{3}{2}}$ waves.

Hall and Koontz[6] obtained angular distributions at several neutron energies between 0.6 and 1.6 Mev. Their data were fitted with parabolas derived on the assumption that only s- and p-waves were important in the scattering. By extrapolating the parabolas to zero scattering angle and determining the areas under the curves, Hall and Koontz obtained a value for the total cross section at each energy. These total cross section values gave a slight indication that the resonance at 1 Mev is split.

II. EXPERIMENTAL

In the present experiment, the total neutron scattering cross section of helium has been determined from 40 kev to 4.9 Mev by measuring the neutron transmission of a helium-filled cylinder. Conditions were such that neutrons scattered through an angle greater than 6° could not enter the detector. This geometry was obtained by compressing purified helium to 8000 psi in a thin-walled steel vessel. Figure 1 shows the details of the container and the experimental arrangement.

Neutrons having energies between 40 kev and 2.1 Mev were produced by the $Li^7(p,n)Be^7$ reaction, while above 3 Mev the $D(d,n)He^3$ reaction was used. In both cases the charged particles were accelerated in an

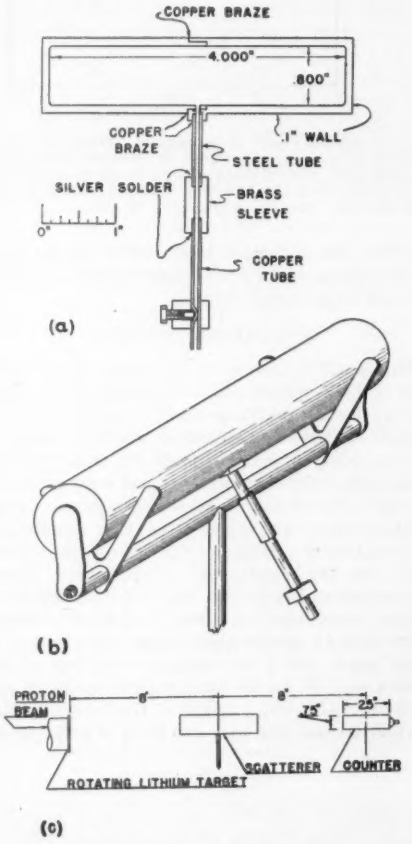

FIG. 1. (a) Helium cylinder. (b) Cylinder mounting. (c) Geometry for scattering experiment.

* This work was supported by the Wisconsin Alumni Research Foundation and the AEC.
† Now at Louisiana State University, Baton Rouge, Louisiana.
[1] H. Staub and W. E. Stephens, Phys. Rev. **55**, 131 (1939).
[2] Gaerttner, Pardue, and Streib, Phys. Rev. **56**, 856A (1939).
[3] H. Staub and H. Tatel, Phys. Rev. **58**, 820 (1940).
[4] H. H. Barschall and M. H. Kanner, Phys. Rev. **58**, 590 (1940).
[5] J. A. Wheeler and H. H. Barschall, Phys. Rev. **58**, 682 (1940).
[6] T. A. Hall and P. G. Koontz, Phys. Rev. **72**, 196 (1947).

electrostatic generator and defined in energy to 0.2 percent by an electrostatic analyzer. For the *d-d* work a deuterium gas chamber, separated from the analyzer's vacuum system by a $\frac{1}{10}$-mil thick nickel foil, replaced the rotating lithium target of Fig. 1. The finite target thickness produced an appreciable neutron energy spread. This spread was 60 kev for the 40-kev point and 30 kev for all other data up to 2.1 Mev. The neutron energy spread for the *d-d* work varied with energy, as is indicated in Fig. 2; the energies designated by the points are average energies weighted according to the variation of neutron yield[7] at 0° over the calculated energy spread.

The neutron detector was a hydrogen recoil proportional counter filled to a pressure of 150 mm of Hg for the 40-kev point and two atmospheres for all other work.

The scattering properties of the helium container were accounted for by inserting an identical empty container in the neutron flux. Background measurements of the neutrons scattered into the detector from the floor, walls, and similar objects were made by replacing the cylinder with a paraffin-boron carbide cone which absorbed the neutrons coming directly from the source towards the detector. If T be the transmission, N_s the number of counts with the sample cylinder in place, N_0 the number with the empty cylinder in place, and B the number of background counts, the cross section, σ, is found from

$$T=(N_s-B)/(N_0-B)=\exp(-n\sigma),$$

where n is the number of scattering centers per cm^2. In this experiment, n was found from the weight of the cylinder when filled and when empty and from the known dimensions of the cylinder.

In order to check against possible systematic errors, the transmission of an identical cylinder containing purified hydrogen at 10,000 psi was measured at several energies so that the cross section thus obtained could be compared with other determinations of the hydrogen cross section.[8,9]

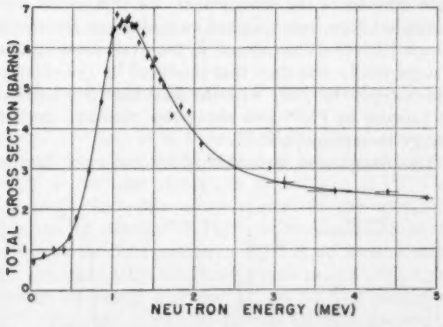

FIG. 2. Total neutron cross section of helium. The vertical bars indicate the statistical uncertainty in cross section. The horizontal bars on the four high energy points indicate the energy spread of the neutrons, which were obtained from the D(d,n)He^3 reaction. At all other energies the neutrons were obtained from the Li^7(p,n)Be^7 reaction, and the spread was 30 kev, except at the 40-kev point, where the spread was 60 kev.

[7] G. T. Hunter and H. T. Richards, Phys. Rev. **76**, 1445 (1949).

III. RESULTS

The results of the measurements are shown in Fig. 2; the vertical bars indicate the statistical uncertainty, and the horizontal bars (on the *d-d* points) the neutron energy spread.

The extrapolated thermal cross section of 0.8 barn disagrees with the 1.25 barns reported by Carroll[10] and the 1.4 barns reported by Harris.[11] This discrepancy is not now understood.

The resonance at 1.15 Mev fails to show any splitting such as Staub and Tatel[3] found in the differential cross section for back scattering. It is believed that the 300-kev splitting of the $P_{\frac{3}{2}}$ and $P_{\frac{1}{2}}$ levels proposed by these authors to fit their data would have been clearly resolved in the present work. From 650 kev to 2.1 Mev the data of Fig. 2 should be corrected to account for the low energy neutrons[12] from the excited state of Be^7. The percentage of low energy neutrons is not well known over this energy range, however, and it was not considered advisable to correct the data at this time. Such a correction would increase the cross section between 650 kev and 1.45 Mev, and decrease it between 1.45 and 2.1 Mev. If one assumes the low energy neutrons to be 10 percent of the main group, this correction will increase the cross-section peak at 1.15 Mev to 7.4 barns, and decrease the cross sections at 1.6 and 2.1 Mev to 4.8 and 3.6 barns. The hydrogen cross sections measured at several neutron energies near 1.1 Mev agree well with the established values.[8]

The cross sections at 3.1, 3.7, 4.4, and 4.9 Mev were obtained with neutrons from the D(d,n)He^3 reaction. It was found, by replacing the deuterium in the target chamber with hydrogen, that about 5 percent of the neutron counts were from reactions other than D(d,n)He^3. The hydrogen cross sections determined at these energies are about 10 percent higher than the values of Bailey, *et al.*[9] who estimate their accuracy at five percent. Thus, it seems likely that the extraneous neutrons were predominantly of low energy. From this fact alone one cannot conclude whether the low energy neutrons increased or decreased the observed cross section of helium, because neutrons of about 1.15 Mev would reduce the observed transmission, whereas neutrons of less than 500-kev energy would increase it.

[8] Lampi, Freier, and Williams, Phys. Rev. **80**, 853 (1950).
[9] Bailey, Bennett, Bergstrahl, Nuckolls, Richards, and Williams, Phys. Rev. **70**, 583 (1946).
[10] H. Carroll, Phys. Rev. **60**, 702 (1941).
[11] S. P. Harris, Phys. Rev. **80**, 20 (1950).
[12] Johnson, Laubenstein, and Richards, Phys. Rev. **77**, 413 (1950).

The effect is small, however, and at worst could cause the observed cross sections to be in error by about 10 percent.

We wish to thank Professor R. J. Roark of the Department of Mechanics, who kindly discussed designs for the high pressure cylinders, and Professor D. J. Mack of the Department of Mining and Metallurgy, who suggested suitable cylinder materials and x-rayed the cylinders for flaws. Professor J. R. Roebuck gave valuable advice concerning the production of high pressures and the properties of materials subjected thereto. We also wish to thank C. H. Johnson, L. J. Koester, D. W. Miller, and R. E. Peterson for help in many phases of this experiment.

PHYSICAL REVIEW VOLUME 82, NUMBER 3 MAY 1, 1951

Neutron Capture γ-Rays from Lead and Bismuth

B. B. KINSEY, G. A. BARTHOLOMEW, AND W. H. WALKER*
Division of Atomic Energy, National Research Council of Canada, Chalk River, Ontario, Canada
(Received November 20, 1950)

Only two strong γ-rays have been detected with a pair spectrometer during the bombardment of lead thermal neutrons. The weaker of the two is due to capture in Pb^{206} and has an energy of 6.734 ± 0.008 Mev, and the stronger is due to capture in Pb^{207} and has an energy of 7.380 ± 0.008 Mev. Apart from a very weak γ-ray with an energy of 6.90 ± 0.05 Mev, no other radiation has been detected. The 6.9-Mev γ-ray may be due to the excitation of a hitherto unknown state in Pb^{208}, or it may be due to an impurity.

Bismuth produces a γ-ray with an energy of 4.170 ± 0.015 Mev. The breadth of the coincidence peak is about 70 kev greater than would be expected for a homogeneous radiation. The γ-rays revealed by the coincidence spectra of lead and bismuth have intensities of about one quantum per capture.

The binding energies of four neutrons in Pb^{210} (RaD) have been calculated using the above experimental data and compared with that computed from the decay of Pb^{210} and its products. The latter exceeds the former by 0.37 ± 0.07 Mev. The origin of this discrepancy is discussed.

The binding energy of Pb^{210} is shown to be less than the energy of disintegration of RaC″, and experiments are described which prove that if neutrons are produced in the decay of the latter, the yield is less than one neutron per two hundred and fifty disintegrations.

No γ-ray with the binding energy of Pb^{205} (6.4 ± 0.2 Mev) was detected. Pb^{205} is shown to be unstable against electron capture to Tl^{205} by about 300 kev. Both Bi^{208} and Bi^{209} are shown to be unstable for α-decay by 3.25 Mev.

I. INTRODUCTION

A PRELIMINARY report on the energies of the γ-rays produced by capture of slow neutrons in lead and bismuth has already been published.[1] The present paper contains details of this work. The method of energy and intensity measurement will be discussed elsewhere.

A sample of the material to be examined is placed in a high neutron flux in a hole which traverses the concrete radiation shield of the pile. Gamma-rays from the pile are prevented from passing down the hole by a block of bismuth 5 in. long. The pair spectrometer is placed outside the concrete shield, and a series of lead collimators limits the γ-radiation reaching the spectrometer to that emitted from the central region of the sample. In this way, unwanted radiations emitted by the lining of the hole are eliminated.

II. RADIATIONS FROM LEAD

The first measurements with lead were made with two samples, one of chemically pure metallic lead, and the other of litharge (PbO) in a Dural container. The spectra obtained are shown in Fig. 1. It will be seen that the two characteristic peaks at 6.7 and 7.4 Mev appear in the same proportion in the spectra of both samples; and, in addition, the 7.7-Mev aluminum capture γ-ray appears in the litharge sample. Now, it is improbable that an impurity which might be responsible for the weaker of the two peaks should be present in both samples to the same extent; for this reason both radiations have been ascribed to lead. Since the energy released by neutron capture in the even mass number isotope will be less than that produced by the adjacent odd isotope, the γ-ray with the least energy is ascribed to capture in Pb^{206} and the γ-ray with the greatest energy to capture in Pb^{207}.

This assignment is confirmed by the more detailed

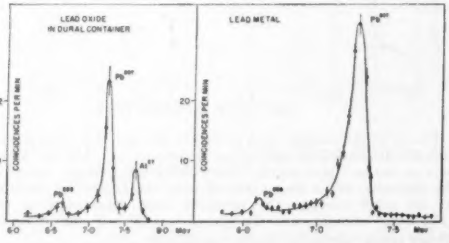

FIG. 1. Coincidence spectra for lead oxide, in a Dural container, and for lead metal, obtained with the pair spectrometer.

* Now at McMaster University, Hamilton, Ontario.
[1] Kinsey, Bartholomew, and Walker, Phys. Rev. 78, 77 (1950).

studies of the lead spectrum shown in Fig. 2, in which the upper curve represents the spectrum obtained with a target of natural lead, and the lower curve, the spectrum obtained with a sample of radiogenic lead,[2] enriched in Pb^{206} and depleted in Pb^{207}. The ordinates of Fig. 2 have been adjusted to correspond to the same pile power, and the peak coincidence counting rates should be in proportion to the isotopic content of the two samples.[3] It will be seen that the 6.7-Mev peak is strongly enhanced in the sample of radiogenic origin, while the 7.4-Mev peak, due to capture in Pb^{207}, is reduced in intensity. The magnitude of the effect is shown in the last row of Table I.

It will be seen that the observed ratio of the peak counting rates of the 7.38-Mev γ-ray (due to Pb^{207}) is in agreement with the value calculated from the ratio of the isotopic contents of the two samples. The ratio

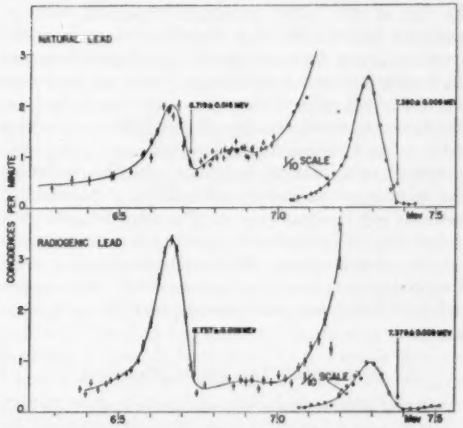

FIG. 2. Coincidence spectra for natural lead and for radiogenic lead, obtained with the pair spectrometer.

of the peak counting rates of the 6.7-Mev γ-ray, however, is much lower than the value expected. The discrepancy may arise from an additional weak γ-ray produced in the natural lead sample with the same energy as that due to capture of neutrons in Pb^{206}. It is possible that this γ-ray is part of the spectrum produced by capture in Pb^{207}; in that event, it must correspond to the creation in Pb^{208} of an excited state with an energy (0.65 Mev) equal to the difference between its energy and that of the binding energy of Pb^{208}, *viz.*, 7.38 Mev. No excited state is known to exist in Pb^{208} with this energy; and, as pointed out below, it is most unlikely that any excited states exist below 2.62 Mev. It is much more probable that the

[2] Prepared from uranium ore by Eldorado Mining and Refining, Ltd. (1944), Port Hope, Ontario.

[3] We are indebted to Dr. Thode of McMaster University for providing the facilities for the isotopic analysis of the radiogenic lead used in this experiment.

TABLE I. Peak coincidence counting rates for the lead γ-rays in relation to isotopic composition.

	Pb^{208}	Pb^{207}	Pb^{206}
Composition (percent):			
Natural lead (*A*)	23.6	22.6	52.3
Radiogenic lead (*B*)	88.2±1.8	8.76±0.17	3.04±0.06
Ratio of peak counting rates:			
Calculated (*B*/*A*)	3.75	0.39	
Observed (Fig. 2)	2.7	0.37	

peak of 6.7 Mev in natural lead is enhanced by a γ-ray due to an impurity.

Figure 2 shows the presence of a very weak γ-ray with an energy of 6.90±0.05 Mev. While this γ-ray is distinct in the upper curve of Fig. 2, its presence is indicated but not definitely established in the lower curve. Evidently, if this γ-ray is produced by lead, it cannot result from the capture of neutrons in Pb^{206} but must be associated with capture by another isotope. This could only be Pb^{207}, because the neutron binding energies in Pb^{205} and Pb^{209} are much lower than the energy of this γ-ray. If it is due to a transition leading to an excited state in Pb^{208}, the energy of this state must be 0.48±0.05 Mev. Now γ-rays with energies of 0.51 and 0.58 Mev are known to occur in the excitation of Pb^{208} produced by the decay of ThC″. These γ-rays are generally supposed to excite the 2.62-Mev level, which is assumed to be the first excited state in Pb^{208}. (See Fig. 6a.) The contrary assumption, that the emission of the 2.62-Mev γ-ray produces an excited state at 0.51 or 0.58 Mev, is inconsistent with the observed end point of the β-spectrum of ThC″ and leads to difficulties in the explanation of the other γ-rays which are emitted. It seems to be more probable that the 6.9-Mev γ-ray is also due to an impurity.

The energies of the two principal γ-rays are given in Fig. 2. The differences between the two sets of results are within the probable statistical errors. The coincidence counting rates produced by the radiogenic lead sample for the 6.7-Mev peak are higher than those of the natural lead sample; and also, as discussed above, the 6.7-Mev peak from natural lead may contain an extraneous component. For these reasons the energy measurement obtained with the radiogenic lead is the more accurate. The weighted mean energies are,

from capture in Pb^{206}: 6.734±0.008 Mev;
from capture in Pb^{207}: 7.380±0.008 Mev.

The residual error given is derived from various systematic errors which may be present in the measurement of the magnetic field of the spectrometer.

Apart from the radiations just described, no other γ-ray between 2.6 and 8 Mev has been detected in a survey of the lead spectrum. No γ-ray has been found with the binding energy of the neutron in Pb^{209} (about 4 Mev); such a γ-ray would not be expected, for the ground-state transition in that nucleus should be highly forbidden. The capture of neutrons in Pb^{207}, however,

might produce the well-known excited state in Pb^{208} at 2.62 Mev. If a transition to this state occurs as often as does the transition to the ground state, it is possible that a γ-ray of this energy might escape detection, because the sensitivity of the pair spectrometer falls by a factor of 40 between 7.38 and 2.62 Mev. The creation of this state could take place as the result of the emission of a γ-ray of 4.76 Mev. A special search was made for a γ-ray of this energy, but none was found. A coincidence peak with one percent of the counting rate of the 7.38-Mev peak would have been detected; such a counting rate would be equivalent to a γ-ray intensity of about 5 percent of that of the ground-state transition.

We have found evidence for such radiations of low energy by comparison of the intensity measured with an ionization chamber with that obtained by counting the recoil electrons produced in an anthracene crystal. The intensity of the soft radiation cannot be very great, however, as it was not shown in a study of the absorption of the capture γ-radiation made with the ionization chamber.

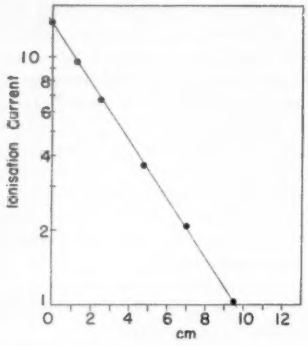

FIG. 3. Absorption of lead capture radiation in brass.

Figure 3 is an absorption curve in brass of the radiation from natural lead. The absorption was measured with the aid of a thick-walled ionization chamber, the small background obtained when the beam of γ-radiation was shut off being subtracted from the ionization current at each point. The logarithmic plot is linear, with an absorption coefficient of 0.271 ± 0.010 cm^{-1}. The measurements were made under exceptionally good geometrical conditions, and the measured absorption coefficient therefore represents the total absorption. The calculated absorption coefficient (0.257 cm^{-1}, which was computed on the basis of the two lead γ-rays with intensities in the ratio of 1:0.093) is in good agreement with this figure.

The linearity of the absorption curve suggests that there is no intense soft γ-radiation. However, the linearity does not prove unequivocally the absence of radiations other than the two γ-rays described above; because the response of a thick-walled ionization chamber is proportional to the energy of the radiation, and the absorption coefficient in most materials does not change much with energy for γ-rays of a million electron volts or more. If the 2.62-Mev γ-ray were present and if the flux of this radiation in photons per unit area per unit time were the same as that of the 7-Mev radiation, it would be only just detectable as a departure from linearity in Fig. 3.

Using an anthracene crystal with a photomultiplier and discriminator circuit, we have computed the total counting rate of recoiling electrons produced by the 7-Mev radiations by extrapolating to zero the curve in which the counting rate obtained is plotted against the bias of the discriminator.[4] The flux of the γ-radiation is readily computed from this counting rate, the number of electrons in the crystal, and the Compton cross section. This method was found to give correct results when applied to the γ-rays produced by a source of Co^{60} of known strength. If no softer γ-rays were present, the flux of the 7-Mev radiations measured with an ionization chamber should be the same as that measured by the counting rate in a crystal. A difference between the results obtained with these two methods should be a sensitive indication of the presence of softer radiations. We have measured the flux of the 7-Mev radiations with a thick-walled ionization chamber, using the figures given by Fowler, Lauritsen, and Lauritsen[5] for the number of ion pairs produced by a thick-walled chamber per incident photon. The flux obtained with the anthracene crystal was found to be twice as great as that obtained with the ionization chamber. The discrepancy indicates the presence of some softer radiation which was not detected with the pair spectrometer.

III. RADIATIONS FROM BISMUTH

Natural bismuth has only one isotope, Bi^{209}. With a bismuth sample a weak broad coincidence peak was found near 4 Mev. In this energy region strong γ-rays from aluminum occur. Aluminum is used in the construction of the pile, and its γ-rays will be superposed on the spectrum to be studied unless precautions are taken to insure that no aluminum lies in the field of view of the spectrometer. Aluminum radiation was successfully eliminated with the aid of extra lead collimators. The effectiveness of these measures was determined readily by setting the spectrometer to count the peak coincidences arising from the strong aluminum γ-ray at 7.72 Mev.

A survey of the γ-rays produced by bismuth showed a coincidence peak near 4 Mev and no evidence for γ-rays at any other energy. A very long and detailed investigation gave the results shown in Fig. 4. The end point of the bismuth spectrum corresponds to an energy of 4.170 ± 0.015 Mev.

[4] The authors are indebted to Dr. W. G. Cross for making these measurements.

[5] Fowler, Lauritsen, and Lauritsen, Revs. Modern Phys. 20, 236 (1948).

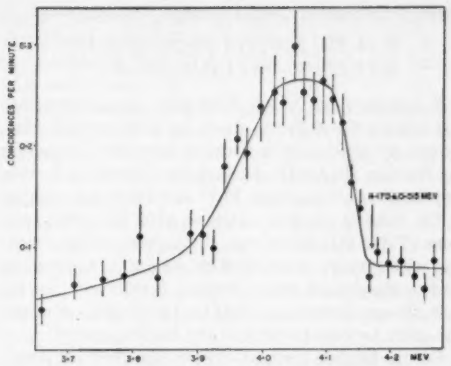

FIG. 4. Coincidence spectrum for bismuth obtained with the pair spectrometer.

Experience has shown that the width (at half-maximum) of the coincidence peak produced by a homogeneous γ-ray is, in energy units, nearly independent of the γ-ray energy. For the particular arrangement of slits which define the aperture of the Geiger counters in the present work, this width is about 130 kev. The width of the bismuth peak, however, is nearly 200 kev. It is certain, therefore, that more than one γ-ray contributes to the spectrum of Fig. 4. Two radiations with an energy difference of 70 kev and of about equal intensity could account for the width observed. This difference is greater than the energy of the highest of the known low-lying states in Bi^{210} (RaE) but much less than the energy of the first excited state produced in the (d,p) reaction.[6] It is possible that the lower energy capture γ-ray is responsible for the production of the isomeric state of RaE recently discussed by Neumann, Howland, and Perlman.[7]

IV. INTENSITIES OF THE LEAD AND BISMUTH γ-RADIATIONS

The simplicity of the γ-ray spectra of lead and bismuth indicates that roughly one photon is emitted per capture. This conclusion has been verified by a comparison of the intensities of these γ-rays with those produced by some light elements which are also responsible for apparently homogeneous radiations.

If is it assumed that the neutron flux is constant throughout the sample material, the peak coincidence counting rate (q_γ) for a γ-ray of energy E_γ is given by:

$$q_\gamma = CN\sigma p_\gamma T_\gamma T_\gamma' \epsilon_\gamma,$$

where C is a constant, N is the number of atoms presented to the field of view of the spectrometer, σ is the capture cross section for thermal neutrons, p_γ is the number of γ-rays produced per capture, T_γ and T_γ' are the fractions of this radiation transmitted through the sample itself and through the boron-paraffin block used to remove neutrons from the beam of radiation, and ϵ_γ is the counting efficiency in the spectrometer (which is a known function of the γ-ray energy).

This expression can be used to compute p_γ, for all other quantities contained in it can be measured or calculated. The constant C will depend on the neutron flux. If the neutron flux is assumed to be the same for different samples when the pile is operated at the same power level, C may be determined from a measurement on the 2.75-Mev γ-ray emitted by Na^{24} generated in a sodium sample. Because when radioactive equilibrium is established between the Na^{24} activity and the neutrons producing it, p is unity for this γ-ray, and the coincidence counting rate will measure the rate of neutron capture.

The number of γ-rays (p) per neutron capture found for lead and bismuth are given in Table II and compared with those obtained for two light elements, *viz.*, Be and C. The capture cross section of lead was taken to be 220 millibarns and that of bismuth 15 millibarns. The results shown in Table II are necessarily inaccurate; there is no significance in the fact that the number of quanta per capture is greater than unity in some cases. The method is subject to a large error (possibly 20 percent) involved in the assumption that the neutron flux in the samples is identical for the same pile power, because, in fact, the neutron flux varies rapidly along the axis of the hole in the pile and quite appreciably in a distance equal to the length of a sample container. In addition, other errors are introduced in the calculation of the counting efficiency of the spectrometer.

The capture cross section due to Pb^{206} has been ignored in the calculation of the yield of the γ-ray produced by Pb^{207}, because the intensity of the Pb^{206} γ-ray is only one-thirteenth of that of the former. It is possible that strong γ-rays of lower energy are produced by capture in Pb^{206} without being detected. Therefore, until the thermal neutron cross section of Pb^{206} has been separately measured, the absolute yield of the Pb^{206} γ-ray cannot be found.

V. CAPTURE OF NEUTRONS BY Pb^{204}

The energy of the ground state γ-ray due to neutron capture in Pb^{204} may be calculated from the disintegration energies of Tl^{204} and Tl^{206} and the data now available on the binding energies of lead and thallium isotopes. The sum of the binding energies of Pb^{205} and Pb^{206} less the sum of the binding energies of Tl^{205} and

TABLE II. Estimated number of quanta produced per capture in a direct transition to the ground state of the product nucleus.

Sample material	Number of quanta per capture
Pb^{207}	1.3
Bi	1.6
Be	1.7
C^{12}	1.0

[6] J. A. Harvey, Phys. Rev. 79, 241(A) (1950).
[7] Neumann, Howland, and Perlman, Phys. Rev. 77, 720 (1950).

Tl^{206} is equal to the difference in the disintegration energies of the two β-emitting bodies, Tl^{206} and Tl^{204}. For the binding energy of Pb^{206} we assume 8.15±0.05 Mev, an average of the results of Harvey and of Palevsky and Hanson (Table III); for that of Tl^{205}, 7.48±0.15 Mev, obtained by Hanson and his collaborators.[8] Our value for the binding energy[9] of Tl^{206} is 6.23±0.05 Mev. Neither Tl^{204} nor Tl^{206} emits γ-radiation[10,11] and the end points of their β-spectra[10–12] are at 0.80±0.03 and 1.63±0.1 Mev.[7] Thus, we obtain a binding energy of 6.4±0.2 Mev for Pb^{205}. No γ-ray has been found in the capture γ-ray spectrum at this energy (Fig. 2).

From these figures it follows that Pb^{205} is unstable against decay to Tl^{205} by 300±130 kev. Therefore, its decay of Tl^{205} is possible only by electron capture. The decay radiations of Pb^{205} have not yet been identified with certainty.

VI. THE NEUTRON BINDING ENERGIES

The experimental values of the neutron binding energies of lead and bismuth are listed in Table III. Harvey's results[13] were obtained from the Q-values of the highest energy groups of protons and tritons observed in (d,p) and (d,t) reactions using a 16-Mev deuteron beam. The results of Palevsky and Hanson[14] and of McElhinney and his collaborators[15] were obtained by the measurement of the thresholds of the (γ,n) reactions.

If $B_n(A,Z)$ is the neutron binding energy of a nucleus of mass A and charge Z and if B_d and B_t are the binding energies of the deuteron and the triton, respectively, the binding energy is related to the Q-values of the particle groups which lead to the ground states of the product nuclei through the equations:

$$B_n(A,Z)=B_d+Q[(A-1,Z)(d,p)(A,Z)]$$
$$B_n(A,Z)=B_t-Q[(A,Z)(d,t)(A-1,Z)].$$

B_d has the value 2.230±0.007 Mev, according to Bell and Elliott;[16] and B_t has the value 6.262±0.023 Mev, a quantity which can be deduced from the Q-value for the reaction $H^2(d,p)H^3$ obtained by Tollestrup, Fowler, and Lauritsen.[17] For both Pb^{207} and Pb^{208}, the equality of the binding energies obtained with these two reactions (Table III) shows that the highest energy proton and triton groups observed must, indeed, be those which lead to the ground states, because if this were not the case, the one expression would lead to a higher value and the other to a lower value of the binding energy.

For the binding energies of Pb^{207} and Pb^{208} our results are in close agreement with those obtained by Harvey. The two stronger γ-rays of Fig. 2 therefore represent the ground state transitions in these isotopes.

The binding energy of Pb^{208} determined by Palevsky and Hanson is in agreement with the other results. Their value for the binding energy of Pb^{207}, however, is about 220 kev too high. While the error in the absolute value of their measurements is rather high, the error in the difference of the binding energies should be much smaller. The difference in the binding energies of Pb^{208} and Pb^{207} is 0.49 Mev. If 7.38 Mev is assumed to be the more accurate value for the binding energy in Pb^{208}, this indicates that the binding energy of Pb^{207} should be 6.89±0.06 Mev. This value is considerably greater than the result of the present measurements; there seems to be no explanation of this discrepancy.

More recently, the thresholds of the (γ,n) reactions in Pb^{208} and Pb^{207} have been measured by Parsons, Lees, and Collie.[18] For Pb^{208} they find a binding energy of 8.1±0.3 Mev and for Pb^{207} a value 1 Mev less. Their results do not agree with any of those listed in Table II, although they were obtained with a method similar to that used by Palevsky and Hanson.

The binding energy of a neutron in Pb^{210} can be calculated from that of Bi^{210} using the disintegration energies of Pb^{209} (0.70 Mev)[10,19] and of Pb^{210} (RaD). There are difficulties in the interpretation of the γ-rays produced by RaD, but the total disintegration energy is not likely to differ much[20] from 0.06 Mev. With these figures, the binding energy of a neutron in Pb^{210} becomes 4.81±0.03 Mev.

TABLE III. Experimental values of neutron binding energies in Pb and Bi (in Mev).

Nucleus	Present work	Harvey[a] (d,p)	Harvey[a] (d,t)	Palevsky and Hanson[b]	McElhinney, *et al.*[c]
Pb^{208}			8.10±0.10	8.25±0.10	
Pb^{207}	6.734±0.008	6.71±0.03	6.70±0.05	6.95±0.10	
Pb^{206}	7.380±0.008	7.37±0.03	7.37±0.05	7.44±0.10	
Pb^{205}		3.87±0.05			
Bi^{209}			7.44±0.05		7.45±0.20
Bi^{210}	4.170±0.015	4.14±0.03			

[a] Reference 13. [b] Reference 14. [c] Reference 15.

VII. COMPARISON WITH DATA OF RADIOACTIVITY

The binding energy of four neutrons in Pb^{210} can be obtained in two ways: (1) by the addition of the experi-

[8] Hanson, Duffield, Knight, Diven, and Palevsky, Phys. Rev. **76**, 578 (1949).

[9] We are indebted to Dr. J. A. Harvey for the communication of his result for the binding energy of Tl^{206}, *viz.*, 6.16±0.15 Mev. We have found a strong γ-ray produced by capture of neutrons in thallium at 6.23±0.05 Mev which may be identified with the binding energy.

[10] K. Fajans and A. F. Voigt, Phys. Rev. **60**, 619 (1941).

[11] K. Fajans and A. F. Voigt, Phys. Rev. **58**, 177 (1940).

[12] R. S. Krishnan and E. A. Nahum, Proc. Camb. Phil. Soc. **36**, 490 (1940).

[13] Private communication. We are indebted to Dr. J. A. Harvey for the privilege of using these results before publication.

[14] H. Palevsky and A. O. Hanson, Phys. Rev. **79**, 242A (1950).

[15] McElhinney, Hanson, Becker, Duffield, and Diven, Phys. Rev. **75**, 542 (1949).

[16] R. E. Bell and L. G. Elliott, Phys. Rev. **79**, 282 (1950).

[17] Tollestrup, Fowler, and Lauritsen, Phys. Rev. **78**, 372 (1950).

[18] Parsons, Lees, and Collie, Proc. Phys. Soc. (London) **A63**, 915 (1950).

[19] W. Rall and R. G. Wilkinson, Phys. Rev. **71**, 321 (1947).

[20] H. O. W. Richardson and A. Leigh-Smith, Proc. Roy. Soc. (London) **A160**, 454 (1937).

mental binding energies listed in Table III, together with that calculated for Pb^{210} and referred to in the last paragraph, and (2) from the radioactivity data of RaD and its products.

(1) The results of the present γ-ray measurements are probably the most accurate values for the binding energies of Pb^{207} and Pb^{208}. For the binding energy of Pb^{209}, we use that obtained by Harvey and for the binding energy of Pb^{210}, the value 4.81±0.03 Mev. The sum of these four quantities is 22.79±0.05 Mev.

(2) The binding energy of four neutrons in Pb^{210} is equal to the energy equivalent of the difference in mass between four neutrons and the α-particle, less the total energy set free in the consecutive disintegrations between Pb^{210} and Pb^{206} (Fig. 5). Using the data recently compiled by Tollestrup, Fowler, and Lauritsen,[17] the mass difference $(4n-\alpha)$ is equivalent to 29.79±0.04 Mev (1 mMU is equivalent to 0.93104 Mev).[21] For the disintegration of RaD, we assume[20] 0.06 Mev; for RaE, 1.17 Mev;[22–24] and for Po^{210}, 5.40 Mev.[25] The binding energy of four neutrons in Pb^{210} is therefore 23.16±0.05 Mev. This quantity exceeds that obtained by method (1) by 0.37 Mev.

This discrepancy is difficult to explain. For the reasons given in a previous paragraph, there seems to be no doubt that the energies of the two principal γ-rays of Fig. 2 are indeed the binding energies of Pb^{207} and Pb^{208}. It is most improbable that the discrepancy can arise from errors contained in the disintegration energies of RaD, RaE, or Po and most unlikely that individual errors in these quantities could accumulate to this difference. Furthermore, the calculated binding energy of a neutron in Pb^{210} contains only the neutron binding energy of Bi^{210} and the β-disintegration energies of RaD and Pb^{209}; of the latter energies, the β-disintegration energy of RaD is unlikely to be in error by as much as 0.02 Mev, and the β-decay of Pb^{209}, which has been accurately measured, is not followed by the emission of γ-radiation. Therefore, either one or both of the neutron binding energies of Pb^{209} and Bi^{210} have been underestimated. We must conclude that the bismuth γ-ray or the higher energy proton group formed in the $Pb^{208}(d,p)Pb^{209}$ reaction, or both, do not represent the direct transitions to the ground states of the product nuclei.

A similar conclusion has been obtained independently by Huizenga, Magnusson, Simpson, and Winslow.[26] These authors suggest that the binding energy of Pb^{209} is given correctly by the energy balance in Harvey's experiments on the reaction $Pb^{208}(d,p)Pb^{209}$ and that the experimental value for the binding energy of Bi^{210} is deficient. Their argument is based in part on the normal position of Pb^{209} and the anomalous position of Bi^{210} in relation to the alternation of binding energies in a sequence of isotopes if these binding energies are correctly given in Table III. This is indeed a cogent argument if applied to a succession of isotopes of the same element for which no discontinuity in the binding energy is known to exist. However, some irregularity in the binding energy alternation might be expected at the commencement of the new shell which is created in the addition of the 127th neutron and the 83rd proton. For this shell is unique in that the addition of these nucleons halves the neutron and proton binding energy which obtained at the closure of the previous shell at the Pb^{208} nucleus. Huizenga and his associates also point out that if the true binding energy of Pb^{209} is greater than the experimental value by the whole of the deficiency, the binding energy of that isotope would be greater than that of the odd-odd nucleus Bi^{210}, which, on account of the interaction of the unpaired neutron and proton, would be expected to be more tightly bound. This argument, which is more convincing, suggests that the energy deficiency should be ascribed to Bi^{210}. It is supported by the fact that the last neutron or proton, respectively, in the even-even nuclei Pb^{210} and Po^{210} has higher binding energy than the odd neutron in Pb^{209}.

It is difficult to understand why the ground state of Pb^{209} or Bi^{210} should not be obtained as a product of the (d,p) reactions. The critical orbital angular momentum of the 16-Mev deuterons used in Harvey's experiments is about $10\hbar$. This is quite sufficient to produce the ground state of Pb^{209}, which according to Feather and Richardson[27] has a spin of 11/2. The spin of Bi^{210} is probably 2 units, and its ground state should be no more difficult to produce directly even if, as would seem very probable, it is compounded of a closed core together with a neutron and a proton in states of the same orbital angular momentum.

Too little is known about the mechanism which determines the intensity of γ-radiation to decide

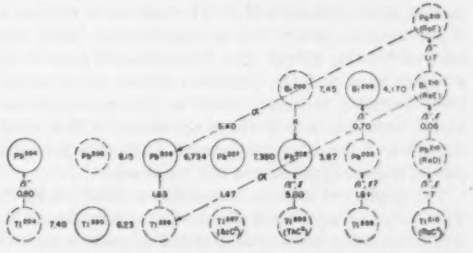

FIG. 5. Relations between certain isotopes of Tl, Pb, Bi, and Po. Experimental neutron binding energies are written between the symbols for the isotopes, and the decay energies between those for the isobars.

[21] J. W. M. DuMond and E. R. Cohen, Revs. Modern Phys. **21**, 651 (1949).
[22] L. M. Langer and M. D. Whitaker, Phys. Rev. **51**, 713 (1937).
[23] A. Flammersfeld, Z. Physik **112**, 727 (1939).
[24] G. J. Neary, Proc. Roy. Soc. (London) **A175**, 71 (1940).
[25] Perlman, Ghiorso, and Seaborg, Phys. Rev. **77**, 26 (1950).
[26] Huizenga, Magnusson, Simpson, and Winslow, Phys. Rev. **79**, 908 (1950).
[27] N. Feather and H. O. W. Richardson, Proc. Phys. Soc. (London) **61**, 452 (1948).

whether the radiative capture of a neutron by Bi^{209} should lead directly to the ground state of Bi^{210}. The spin of Bi^{209} (9/2) and its magnetic moment suggest that the odd proton in this nucleus has an orbital angular momentum of 5 units. If its parity is odd, the radiative transition to the ground state, which would result from the capture of a slow neutron, would produce a change of parity. This follows because the β-disintegration of Bi^{210} is second forbidden and produces no change in parity. The parity of the ground state of Bi^{210} is, therefore, that of the even-even nucleus Po^{210}, which is probably even, for it differs from the closed shell nucleus Pb^{208} only by the possession of the two extra protons. Since the spin of Bi^{210} is probably 2 units, the minimum spin radiated will be 2 units and the γ-ray will be magnetic quadrupole in type. Theoretically, such a third-order γ-ray should be forbidden as compared with first- and second-order radiations. Experimental evidence does not support this conclusion, however, for, as pointed out in another communication,[28] there seem to be instances (e.g., K^{40}) in which magnetic quadrupole radiation emitted in a transition directly to a ground state can compete successfully with γ-rays emitted in transitions to a variety of excited states.

VIII. THE DISINTEGRATION OF RaC″

The neutron binding energy of Pb^{210} (RaD) of 4.81 Mev is lower than the energy produced in the disintegration of its parent, Tl^{210} (RaC″). This fact suggests the possibility that neutrons may be emitted in the disintegration of RaC″. Inasmuch as the binding energy of Pb^{210} is calculated from that of Bi^{210}, this possibility still exists if the neutron binding energy of Bi^{210} is greater than the energy of the capture γ-ray from Bi^{209} by 0.37 Mev, the full amount of the energy discrepancy previously discussed.

Now the neutrons emitted in the disintegration of N^{17} are easily detected because the β-transition between the ground state of that nucleus and its product is forbidden; and, therefore, most of the transitions lead to neutron emission. However, the β-disintegration of RaC″ is of the allowed type and produces RaD in an excited state at about 4 Mev. The position of this state is not known exactly, but it certainly lies below the neutron binding energy. If a β-transition is possible to a higher level of RaD, neutron emission could occur; these neutrons, however, would be produced in measurable numbers only if the β-transition to that level were also of the allowed type and if the energy of the partial β-disintegration was not too small.

The product of neutron emission from RaC″ is Pb^{209}. This body has a period of about 3 hr; and its β-activity would probably remain undetected when a source of RaC″ (prepared by recoil) had decayed to a few tenths of a percent of its original strength, for such sources invariably contain an appreciable contamination of RaC introduced by the process of aggregate recoil. No

[28] Kinsey, Bartholomew, and Walker, Phys. Rev. 78, 481 (1950).

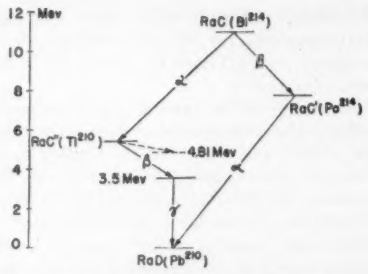

FIG. 6. The disintegration of RaC and its immediate products drawn on the assumption that the most energetic β-particles of RaC produce the ground state of RaC′.

residual activity ascribable to Pb^{209} can be discerned in the decay curves of RaC″ obtained by Fajans.[29] If neutrons are emitted, their presence, therefore, is likely to be established only by direct measurement.

RaC″ is produced by the α-decay of RaC only to the extent of one atom in 4000 disintegrations of that nucleus (Fig. 6). The remainder decay by β-emission to RaC′ and thence to RaD by α-disintegration. Owing to the small extent to which it is produced in the decay of RaC and owing to its short life of 1.32 min, the total disintegration energy of RaC″ has not been measured accurately by a direct method. The end point of the β-spectrum was found to be 1.7 Mev by Goldstein and Lecoin[30] and 1.95 Mev by Devons and Neary.[31] The latter experimenters found that the γ-ray energy emitted per disintegration was about 5 ± 1 Mev. The total disintegration energy is therefore about 7 ± 1 Mev.

In principle the total energy of disintegration of RaC″ can be found much more exactly by subtracting from the total energy set free in the branch RaC–C′–D, the energy of the most energetic group of α-particles due to the branch RaC–C″ (Fig. 6). At present this method is subject to some doubt because of an uncertainty in the energy of the disintegration of RaC. According to the scheme drawn up by Ellis,[32] the highest energy group of β-particles produces an excited state in RaC′ at 606 kev, and recently Feather and Richardson[27] have given theoretical reasons to show that the disintegration should follow this course. However, Bothe and Maier-Leibnitz[33] failed to find coincidences between the highest energy β-group and the 606-kev γ-ray. This indicates that the most energetic β-group leads directly to the ground state of RaC′. According to Constantinov and Latyshev,[34] the energy of this group is 3.17 Mev. Until further measurements are made on the disintegra-

[29] K. Fajans, Physik. Z. 12, 369 (1911).
[30] L. Goldstein and M. Lecoin, Compt. rend. 202, 1169 (1936).
[31] S. Devons and G. J. Neary, Proc. Cambridge Phil. Soc. 33, 154 (1937).
[32] C. D. Ellis, International Conference on Physics, London (1934).
[33] W. Bothe and H. Maier-Leibnitz, Z. Physik 104, 604 (1937).
[34] A. A. Constantinov and G. D. Latyshev, J. Phys. (U.S.S.R.) 5, 249 (1941).

tion of RaC, the total disintegration energy must be considered to be uncertain: its value may be 3.17 or 3.78 Mev. Using the α-particle energy measurements of Lewis and Bowden,[35] it follows that the total disintegration energy of RaC″ is 5.39 or 6.00 Mev. The latter figure, which corresponds to the direct production of the 606-kev level in RaC′ by the most energetic β-particles of RaC, is in better agreement with the results of Devons and Neary than is the former figure. The total disintegration energy of RaC″, as mentioned at the beginning of this section, therefore is greater than the neutron binding energy of Pb^{210}.

In collaboration with Dr. C. H. Millar of this laboratory we have measured the total neutron emission from commercial sources of radium and radiothorium in equilibrium with their products, using specially sensitive boron trifluoride counters. While the neutron emission from radium was found to be about one neutron per million disintegrations of radium, that from the radiothorium source was considerably higher. Now no possibility exists for the emission of delayed neutrons in the thorium series, and so it is clear that the greater part of the neutrons observed from both sources are due to the disintegration of light elements in the container or in chemical combination with the active element. Since the fraction of atoms of RaC which disintegrate along the RaC″ branch is only 2.5×10^{-4}, the present measurement shows that the neutron yield is not more than 1 in 250 disintegrations of RaC″. If an excited state in RaD exists just above the neutron binding energy (which is assumed to be 4.81 Mev: the dotted line in Fig. 6), it would be excited in an allowed transition twenty times or twice per hundred disintegrations, according to whether the disintegration energy of RaC″ is 6.00 or 5.39 Mev. This calculated yield is much greater than that observed, and the low value of the latter indicates a low density of levels in RaD at 5 Mev with the spin and parity appropriate for an allowed β-transition from RaC″.

IX. INSTABILITY OF BISMUTH

The α-disintegration energy of Bi^{209} can be calculated from the neutron binding energies of Table III and certain disintegration energies. The α-disintegration energy is equal to the binding energy of the α-particle less the sum of the binding energies of the two neutrons and two protons which, when removed separately, create the product nucleus. The proton binding energy of Bi^{209} can be calculated from Harvey's value of the neutron binding energy of Pb^{209} and the β-disintegration energy of Pb^{209}. Assuming that the latter is 0.70 Mev, this proton binding energy is 3.79 Mev.[36] For the two neutron binding energies, the energies of the two lead γ-rays are used; finally, the proton binding energy of Pb^{208} is found to be 7.08 Mev. These figures lead to an α-disintegration energy of 3.25 Mev in Bi^{209}. In view of the discrepancy in the binding energies of four neutrons in Pb^{210}, discussed above, this result may be too high by 0.36 Mev.

The half-life of Bi^{209} can be calculated from this disintegration energy. The result obtained by using the Bethe formula,[37] corrected by a factor of a hundred to allow for the forbidden nature of α-emission from bismuth isotopes,[38] is about 10^{16} years. This value is of the same order as that obtained by Jenkner and Broda,[39] who, using a specially sensitive photographic method, have shown that the half-life must be greater than 3×10^{18} years. The calculated result, however, is a lower limit for the lifetime; if we use the lower value of the disintegration energy, *viz.*, 2.89 Mev, the half-life is of the order of 10^{18} years.

The range of the Bi^{209} α-particle should lie between 1.65 and 1.9 cm of air. This range is very close to the value equivalent to the radius of the unidentified *K* ring in pleochroic halos (1.74 cm of air).[40] It does not seem possible, however, to identify this halo with Bi^{209}, as has been suggested,[39] for the disintegration rate is probably insufficient to produce the effect.

The difference between the α-disintegration energy of Bi^{208} and that of Bi^{209} is equal to the difference in the neutron binding energies of Bi^{209} and Tl^{205}, and these are equal within the limits of experimental error. Therefore, the α-disintegration energy of Bi^{208} is equal to that of Bi^{209}. This energy is too low to identify Bi^{208} with the long lived α-emitter produced by neutron bombardment of bismuth which according to Neumann, Howland, and Perlman[7] has a disintegration energy of 5.12 Mev. The present results therefore confirm their conclusion that that body is an isomer of Bi^{210} and does not arise from the production of Bi^{208} by an $(n,2n)$ process.

X. SIMPLICITY OF THE LEAD AND BISMUTH γ-RAY SPECTRA

The simplicity of the γ-ray spectra produced by lead and bismuth is their most remarkable feature. It is quite unique among the heavy elements. In this respect, these nuclides resemble the lightest elements. The latter produce single homogeneous γ-rays because no excited states exist between the ground state and the neutron binding energy or because the probability of radiation to one of these states is greatly reduced by the small energy difference available. The latter explanation is probably sufficient to account for the simplicity of the γ-radiation produced by capture in bismuth. For the neutron binding energy is very low and, with the exception of the multiplicity of low-lying levels

[35] W. B. Lewis and B. V. Bowden, Proc. Roy. Soc. (London) **A145**, 235 (1934).

[36] It is significant that the energy required to remove the 83rd proton from Bi^{209} is so close to that required to remove the 127th neutron from Pb^{209}. This equality is also revealed by the close similarity of the disintegration energy of Pb^{209} with the energy equivalent of the mass difference between the neutron and the hydrogen atom.

[37] I. Perlman and T. J. Ypsilantis, Phys. Rev. **79**, 30 (1950).

[38] H. M. Neumann and I. Perlman, Phys. Rev. **78**, 191 (1950).

[39] K. Jenkner and E. Broda, Nature **164**, 412 (1949).

[40] G. H. Henderson and L. G. Turnbull, Proc. Roy. Soc. (London) **A145**, 582 (1934).

which have been revealed in the decay RaD, only three excited states are known to exist between the ground state of Bi^{210} and its neutron binding energy.[6] However, some different explanation is required for lead, because the energy levels available for excitation in Pb^{208} are more numerous. Clearly, the homogeneity of the lead radiations must be associated in some way with the closing of the nuclear shell at Pb^{208}. It will be shown below that the transitions which can arise between the neutron capturing state and the known excited states of Pb^{208} would produce, with one exception, γ-radiations of a high order of multipolarity; and this may be an explanation of the high probability of the direct transition to the ground state.

The system of levels in Pb^{208} which is excited in the decay of ThC″ is shown in Fig. 7(a). According to Martin and Richardson,[41] the spin of the 2.62-Mev level is 1, that of the higher levels 3 or 4, and all have the same parity as that of the ground state. Now a consideration of the magnetic moment of Pb^{207} suggests that its ground state has odd parity. If we take the parity of the closed shell nucleus, Pb^{208}, to be even, the direct transition to the ground state which follows the capture of a thermal neutron by Pb^{207} must produce a change of parity. It follows from the spin of Pb^{207} (1/2) that this γ-ray is of the electric dipole type. Likewise, direct transitions from the neutron capturing state of Pb^{208} to any of the levels of Fig. 7a must also produce a change of parity. Therefore, with the exception of the transition to the ground state or to the 2.62-Mev level, these transitions must produce γ-rays of the third multipole order or higher. In a previous paragraph we have shown that magnetic quadrupole radiation generally may not be a forbidden type. However, in the present instance, third-order radiations may well be forbidden by comparison with electric dipole radiation. It is very curious that there is no transition to the 2.62-Mev state, because there is no known selection rule which forbids this transition.

The assignment of spins to the excited states of Pb^{208} discussed by Martin and Richardson has been rendered doubtful by recent measurements of the angular correlation of the 2.62-Mev with the 0.58-Mev γ-rays.

[41] D. G. E. Martin and H. O. W. Richardson, Proc. Phys. Soc. (London) **63**, 223 (1950).

FIG. 7. The energy levels of Pb^{208}: (a) as found from the decay of ThC″ and (b) as revealed by the $Pb^{208}(d,p)Pb^{209}$ reaction.

These new results are compatible only with a spin of 2 units for the 2.62-Mev state and 4 units for the 3.2-Mev state.[42] If this is the correct assignment, there is still no explanation of the absence of the γ-ray leading to the 2.62-Mev state although the remaining γ-rays may be forbidden to the same degree.

A curious feature of the excitation of the Pb^{208} nucleus by the (d,p) reaction (Fig. 7b) is the absence of the excitation of the 2.62- and 3.20-Mev states. The first state to be excited in this reaction has an energy of about 3.5 Mev, but the accuracy of measurement is hardly sufficient to identify this level with any of those displayed in the decay of ThC″. Such a level, if it had a low spin, 0 or 1, would not be accessible to the β-decay of ThC″, for which the spin is at least 4 units. Now we have found a general correspondence between the excitation of nuclear levels by the (n,γ) and (d,p) reactions which would lead one to expect that a failure to excite the 2.62-Mev level in the (n,γ) reaction would have its counterpart in a similar failure to excite this state in the (d,p) reaction. On the other hand, the (d,p) reaction produces an excited state at 3.5 Mev in Pb^{208}; one would expect to find a γ-ray with this energy or with 3.9 Mev, the difference between it and the binding energy. These γ-rays have not been detected.

[42] We are indebted to Dr. M. Johns for the privilege of seeing his results before publication.

A Note on Dirac Central Field Wave Functions*

M. E. Rose
Oak Ridge National Laboratory, Oak Ridge, Tennessee
(Received November 16, 1950)

A systematic treatment is developed for the discussion of the solution of the Dirac wave equation for a central field for the purposes of theories involving the finite size of the nucleus.

I. INTRODUCTION

THERE are a number of problems for which the effect of the finite size of the nucleus is of interest.[1] In an attempt to systematize the treatment of some of these problems certain procedures for the calculation of wave functions have been developed which the author has found to be particularly useful. In view of the possible application of these procedures to other problems, it is felt to be worth while to present the following discussion.

II. THEORY

In the representation[2] in which j^2 and j_z are diagonal, the "small" and "large" radial functions, u_1/r and u_2/r, respectively, are given in terms of the solutions of the differential equations,

$$du_i/dr=\alpha_{ij}u_j; \quad i,j=1,2, \tag{1}$$

sum over repeated indices implied, and

$$[\alpha_{ij}]=\begin{bmatrix}\kappa/r & -(W-1-V)\\ W+1-V & -\kappa/r\end{bmatrix}. \tag{2}$$

In Eq. (2), W and V are the total energy and scalar potential, respectively, and

$$\kappa=\pm(j+\tfrac{1}{2}) \quad \text{for} \quad j=l\mp\tfrac{1}{2} \tag{3}$$

is a nonvanishing integer. Throughout, we use

$$\hbar=m=c=1.$$

(A) Quadrature Solution

For an investigation of the effect of the finite size of the nucleus, it is necessary to obtain wave functions in the smeared-out nuclear charge distribution. While these are easily obtained for all of the simple models customarily used, there are certain advantages to be derived from the following more general procedure. A formal integration of (1) gives

$$u_1=r^{\kappa}\left(C_1+\int_0^r r^{-\kappa}\alpha_{12}u_2dr\right), \tag{4a}$$

$$u_2=r^{-\kappa}\left(C_2+\int_0^r r^{\kappa}\alpha_{21}u_1dr\right), \tag{4b}$$

where C_i are integration constants. For $\kappa<0$, and $|\kappa|=k$, we have $C_1=0$ for the regular solution and we write (4) in the form

$$u_1=\omega_1u_2, \quad u_2=u_2^{(0)}+\omega_2u_1, \tag{4c}$$

where $u_2^{(0)}=C_2r^k$, and (4) defines the integral operators ω_i. The solution of (4c), obtained by iteration, is

$$u_2=\sum_0^{\infty}(\omega_2\omega_1)^nu_2^{(0)}, \tag{5}$$

and u_1 is obtained from the first of (4c) or from (1). For any function $f(r)$,

$$\omega_2\omega_1f(r)=r^k\int_0^r y^k\alpha_{12}(y)\zeta(r,y)f(y)dy, \tag{5a}$$

where

$$\zeta(r,y)=\int_y^r x^{-2k}\alpha_{21}(x)dx \tag{5b}$$

is a given function once V is specified.

For $\kappa>0$ we replace $\omega_2\omega_1$ by $\omega_1\omega_2$, which (with $\kappa=k$) is equivalent to interchanging[3] α_{12} and α_{21}.

The solution (5) and the corresponding one for $\kappa>0$ may be applied only in those cases for which the integrals exist. In the form given, (5) is an expansion around the origin and we must make the restriction $\lim rV=0$ as $r\to 0$. However, for a finite size nucleus this condition will always be fulfilled. The fact that (5) does constitute an expansion around the origin is evident if we use

$$\int_0^r f(r)dr=O(rf(r)),$$

* This paper is based on work performed for the AEC at the Oak Ridge National Laboratory.

[1] Forbidden (zero-zero) transitions, S. D. Drell, Phys. Rev. **81**, 656A (1951); Isotope shift, G. Breit, Phys. Rev. **42**, 348 (1932); Hyperfine structure, A. Bohr and V. F. Weisskopf, Phys. Rev. **77**, 94 (1950); Electron scattering, M. E. Rose, Phys. Rev. **73**, 279 (1948); L. Acheson, Ph.D. dissertation (M.I.T.); L. R. B. Elton, Phys. Rev. **79**, 412 (1950); Effect in β-decay, M. E. Rose and D. K. Holmes (in preparation).

[2] M. E. Rose, Phys. Rev. **51**, 484 (1937).

[3] This is an example of the general result that changing the sign of κ is equivalent to changing the sign of W and V and interchanging u_1 and u_2, as can be verified directly from (1). If we denote these operations by the operators Ω_κ, Ω_W, Ω_V, and Ω_{12}, respectively, acting on the 2-spinor (u_1, u_2), then

$$\Omega_\kappa\Omega_W\Omega_V\Omega_{12}=1,$$

since for each operator $\Omega^2=1$, $\Omega=\Omega^{-1}$, and all of these operators commute.

where O means "of order of," which will always be valid for the quadratures appearing in (5). It is now clear that the ratio of the $(n+1)$st to the nth term is $O(r^2)$. The convergence domain of (5) is easily established. For example, if V is bounded, (5) converges as well as in the case $V=$const, and in this latter case (5) gives the power series for r times the spherical bessel functions, which are the well-known solutions in this case.

Where the solutions are obtainable in the form of a power series in r, (5) will generate the same series but with a reordering of the terms so that each term is a polynomial with the sum of the first m terms of (5) containing at least the sum of the first m terms of the power series. A particularly useful feature of the series (5) is the fact that an upper limit on the error incurred in terminating the series can be obtained in almost all cases. Usually V will be negative-definite, and this will almost certainly be the case over the region where (5) would be used. In that case, for the electron continuum, $(W>1)$, α_{12} and α_{21} are negative-definite and positive-definite, respectively. The series (5) is therefore alternating and, over a large domain, the absolute value of the term is monotonic decreasing so that the error is less than the first term neglected. For bound states there will always be a turning point ($\alpha_{12}=0$), but $\alpha_{12}<0$ for smaller values of r. In any practical case the turning point will be beyond the nuclear radius and usually far beyond it, so that the alternating character of the series (5) is retained for bound states also.

The general form of the solution (5) permits a simple examination of the effect of a coulomb field deviation on the small distance behavior of the wave functions. For the leading terms we have ($\kappa<0$)

$$u_2=C_2r^k,$$

$$u_1=-C_2r^{-k}\int_0^r(W-1-V)r'^{2k}dr'.$$

Since $|V|\gg W$, usually, we write u_1 in the form

$$u_1\approx C_2r^{-k}\int_0^r Vr'^{2k}dr'=\frac{C_2r^{j+1}}{2j+2}\int_0^1 Vw(x)dx, \quad (6a)$$

where we have introduced $x=r'/r$ and the normalized weight factor $w(x)=(2j+2)x^{2j+1}$, $(0\leqslant x\leqslant 1)$. Similarly, for $\kappa>0$,

$$u_1=C_1r^k,$$

$$u_2=-\frac{C_1r^{j+1}}{2j+2}\int_0^1 Vw(x)dx. \quad (6b)$$

Therefore, of the four radial functions for given j, two, namely, $u_1(\kappa<0)$ and $u_2(\kappa>0)$ are sensitive at small r to coulomb field deviations. For the other pair, the indicial, behavior is chiefly determined by the angular momentum and not by the field V. Calculations of the effect of finite nuclear size in β-decay exhibit this effect rather strikingly.[1] From (6) it is clear that the short-range coulomb field deviation is important only for low angular momenta, as expected. This follows, since, for large j, $w\to\delta(1-x)$ and the details of the field V at small r become unimportant.

(B) Normalization

For the continuum, the normalization constants C_i in (5) can be determined only if (5) can be joined to the asymptotic solutions. In the case of the finite nucleus, where V is a coulomb field for $r>R$ (the nuclear radius), the joining is very simple. Actually, all that is needed in this case is the ratio $\rho=u_1/u_2$ at $r=R$, and then the constants C_i drop out. For bound states, the joining condition at $r=R$ fixes the eigenvalue W, and the normalized solutions are determined as follows. Consider two stationary-state time-dependent wave functions Ψ_j and Ψ_k corresponding to energies W_j and W_k, respectively. Then

$$\operatorname{div}(\Psi_j^*\boldsymbol{\alpha}\Psi_k)+\partial(\Psi_j^*\Psi_k)/\partial t=0, \quad (7)$$

where $\boldsymbol{\alpha}$ is the usual Dirac matrix vector. Carrying out the time differentiation and inserting the time independent wave functions ψ_j and ψ_k, we then integrate over a closed volume and obtain

$$\int\psi_j^*\alpha_n\psi_k dS=i(W_k-W_j)\int\psi_j^*\psi_k d\tau, \quad (8)$$

where α_n is component of $\boldsymbol{\alpha}$ along the outward normal, and dS is an area element of the bounding surface. Now let $W_j=W_k+dW$ so that

$$\int\psi^*\psi d\tau=i\int(\partial\psi^*/\partial W)\alpha_n\psi dS. \quad (9)$$

On specializing to the representation used above and applying (9) to a spherical shell of radii r_1 and r_2, we get

$$\left[u_1\frac{\partial u_2}{\partial W}-u_2\frac{\partial u_1}{\partial W}\right]_{r_1}^{r_2}=\int_{r_1}^{r_2}(u_1^2+u_2^2)dr, \quad (10)$$

which can be obtained directly from (1). If we consider a solution regular at the origin (but not necessarily so at ∞) and take $r_1=0$, $r_2=r$, we obtain

$$u_2^2\partial\rho_L/\partial W=-\int_0^r(u_1^2+u_2^2)dr, \quad (11)$$

where $\rho=u_1/u_2$ and the subscript L indicates regularity at the left end of the interval $(0, \infty)$. The left side of (11) is evaluated at r, and on the right side, L solutions are to be understood. Next, consider a solution regular at ∞ (but not necessarily so at $r=0$) and take $r_1=r$, $r_2=\infty$. Then,

$$u_2^2\partial\rho_R/\partial W=\int_r^\infty(u_1^2+u_2^2)dr, \quad (12)$$

and again R implies regularity at ∞, the left side of (12) is evaluated at r, and on the right side, R solutions are to be understood. If W is set equal to an eigenvalue W_n, u_1 and u_2 (with phases suitably chosen) are continuous at r (but $\partial\rho_L/\partial W \neq \partial\rho_R/\partial W$), and for the normalized solution, we obtain

$$u_2^2(r)=\{[(\partial\rho_R/\partial W)-(\partial\rho_L/\partial W)]_{r,W_n}\}^{-1}, \quad (13a)$$

$$u_1^2(r)=\rho^2 u_2^2(r). \quad (13b)$$

By means of (5) and (4c) one can evaluate ρ_L. If an analytic solution is known for points beyond r (a coulomb field solution, for example) giving ρ_R, the result (13) provides a relatively simple procedure for normalization and avoids the use of indefinite integrals, which often cannot be evaluated analytically. This result is also rather convenient in a simpler field V (such as a coulomb field). In this case, if a solution regular at the origin is known for all W, the normalization integral is given by (11), with $r=\infty$ in terms of the asymptotic behavior at ∞, and, if a solution properly behaved at ∞ can be represented in analytical form for all W, the result (12) with $r=0$ gives the normalization in terms of the behavior of the solutions around the origin.[4]

(C) Phase Shifts

We again consider the situation in which $V=V_0(r)$ (a coulomb field, say) for $r>R$ and $V=V_1(r)$ for $r<R$. Then, of course, the wave functions for $r>R$ are completely determined in terms of the phase shifts for each partial wave (labeled by κ). The regular and irregular solutions of (1) for $V=V_0$ are denoted by v_i and $\bar{v}_i$, respectively. Then the integral equation obtained by use of the Green function for (1) is, with $P(r)=V-V_0$,

$$u_i=v_i\left[1-\int_r^\infty \bar{v}_j(r')u_j(r')P(r')dr\right] -\bar{v}_i\int_0^r v_j(r')u_j(r')P(r')dr'$$

$$=v_i-\int_0^\infty G_{ij}(r,r')u_j(r')P(r')dr' \quad (14)$$

subject to the normalization condition

$$v_1\bar{v}_2-v_2\bar{v}_1\equiv 1. \quad (15)$$

In (14), the Green function (matrix) is

$$G_{ij}(r,r')=v_i(r)\bar{v}_j(r'), \quad r'>r$$
$$=\bar{v}_i(r)v_j(r'), \quad r>r'. \quad (16)$$

The properly normalized solutions v_i and $\bar{v}_i$ have the asymptotic behavior

$$v_1\to[(W-1)/p]^{\frac{1}{2}}\sin\xi, \qquad \bar{v}_1\to[(W-1)/p]^{\frac{1}{2}}\cos\xi,$$
$$v_2\to-[p/(W-1)]^{\frac{1}{2}}\cos\xi, \quad \bar{v}_2\to[p/(W-1)]^{\frac{1}{2}}\sin\xi, \quad (17)$$

where $p=(W^2-1)^{\frac{1}{2}}$ is the electron momentum and ξ is the total phase.[5] For u_i, the asymptotic behavior is taken to be

$$u_1\to[(W-1)/p]^{\frac{1}{2}}(\sin\xi+\tan\delta\cos\xi),$$
$$u_2\to-[p/(W-1)]^{\frac{1}{2}}(\cos\xi-\tan\delta\sin\xi). \quad (18)$$

It follows from (14), (17), and (18) that[6]

$$\tan\delta=-\int_0^\infty v_j(r')u_j(r')P(r')dr'. \quad (19)$$

In this form the phase shift, δ, is not stationary with respect to variations δu_i. To obtain the phase shift from a variation principle, we proceed in complete analogy with Schwinger's derivation of the corresponding nonrelativistic phase shift.[7] The final result for the relativistic generalization of Schwinger's variation principle is

$$-\cot\delta=\frac{\int_0^\infty drP(r)u_j(r)u_j(r)+\int_0^\infty dr\int_0^\infty dr'P(r)u_i(r)G_{ij}(r,r')u_j(r')P(r')}{\left[\int_0^\infty drP(r)u_j(r)v_j(r)\right]^2}. \quad (20)$$

A more convenient form of variation principle is obtained by putting (1) in hamiltonian form. Then, with the normalization (18) and the regularity condition $u_i(0)=0$, we find that

$$F[u]=\tan\delta-\int_0^\infty u_i\gamma_{ij}[(du_j/dr)-\alpha_{jk}u_k]dr \quad (21)$$

is stationary for the correct wave function. In (21)

$$(\gamma_{ij})=\begin{pmatrix}0 & -1\\ 1 & 0\end{pmatrix}.$$

More specific results can be obtained in analogy with the treatment of corresponding nonrelativistic problems.[8]

[4] A corresponding result for the nonrelativistic case has been given by W. Furry, Phys. Rev. **71**, 360 (1937).

[5] Defined for coulomb fields in reference 2.

[6] A similar result has been obtained by G. Parzen, Phys. Rev. **80**, 261 (1950).

[7] J. M. Blatt and J. D. Jackson, Phys. Rev. **76**, 18 (1949). The difference between our result (20) and their result (2.11) arises from the different definitions of the Green function.

[8] T. Kato, Phys. Rev. **80**, 475 (1950).

Effect of Short Wavelength Interference on Neuteron Scattering by Dense Systems of Heavy Nuclei*

G. PLACZEK, B. R. A. NIJBOER,† AND L. VAN HOVE‡
Institute for Advanced Study, Princeton, New Jersey
(Received October 13, 1950)

The interference term in the expression for the total cross section for scattering of neutrons by dense systems of heavy nuclei is investigated in the region of small wavelength. Asymptotically, this term has the form $\delta\sigma/\sigma=-(\lambda^3\rho^{\frac{1}{2}}/8\pi)I$, where λ is the neutron wavelength and ρ the number of particles per unit volume. The discussion of the coefficient, I, and its evaluation for various systems is the main object of the paper. It is based on an extension to general systems of particles of Ewald's method for the calculation of lattice sums. For any system, I is found to be smaller than 3. It remains very near to this value for all systems not too far removed from conditions of close packing. The cases of ideal lattices, real crystals with thermal disorder, and liquids are treated in detail.

I. INTRODUCTION

IT has been shown previously[1] that the scattering of neutrons by a system of heavy nuclei may, for neutron energies that are large compared with the level separation of the system, be described in terms of averages of simple two-particle operators over the initial state. The relevant level separation in the case of crystals and liquids is of the order of the Debye temperature. In this theory the angular and energy dependence of the cross section is given in the form of an expansion in powers of the ratio of neutron to nuclear mass. The first term of this expansion, which is independent of the mass ratio, corresponds to the familiar classical interference theory and thus consists of the cross sections of the bound nuclei and of an interference term.

We shall evaluate this interference term in the expression for the total scattering cross section in the case of small neutron wavelength and dense systems. While the effects depending on the mass ratio, the most important of which is the Doppler effect, are frequently of the same order as the classical interference term, they can be treated separately and will not be discussed here. In the following, we assume the mass ratio to be zero.

The problem treated here may be considered to be of some theoretical interest as a rather general problem in the theory of interference phenomena. The investigation of certain of its aspects has also a direct bearing on the interpretation of recent neutron scattering experiments by Rainwater, Rabi, and Havens[2] carried out with the purpose of detection and measurement of a nonmagnetic interaction between neutrons and electrons, which may be expected to cause an energy dependence of the total scattering cross section in the region where the atomic form factor varies. The experiments measured the variation with wavelength of the transmission through liquid bismuth of neutrons of rather small wavelength (0.3 to 1.3A), which is found to be of the order of magnitude of about 3 percent. Consequently, their discussion requires a careful investigation of the energy dependence of the nuclear scattering, part of which is due to the interference term dealt with in the following.

II. GENERAL FORMULA FOR THE TOTAL CROSS SECTION

We consider a system containing an infinite number of nuclei of a single type and assume the scattering cross section of the isolated nucleus to be independent of scattering angle, neutron energy, and relative orientation of neutron and nuclear spin. As has been already mentioned, we assume the ratio of neutron to nuclear mass to be zero. Using as unit of cross section the differential cross section of the isolated nucleus and as unit of length the cube root of the atomic volume, we have for the differential cross section per nucleus

$$\sigma(\mathbf{h})=1+\int w(\mathbf{r})\exp(2\pi i\mathbf{h}\cdot\mathbf{r})d\mathbf{r}-\delta(\mathbf{h}). \quad (2.1)$$

The vector $\mathbf{h}$ is given by

$$\mathbf{h}=(\mathbf{k}-\mathbf{k}')/2\pi$$

($\mathbf{k}$ and $\mathbf{k}'$ the wave vectors of the incident and scattered neutrons), its magnitude h by

$$h=(2\sin\tfrac{1}{2}\theta)/\lambda=[2(1-\cos\theta)]^{\frac{1}{2}}/\lambda \quad (2.2)$$

(λ is the wavelength and θ is the scattering angle). $\mathbf{h}$ can be interpreted as the radius vector in fourier space. $w(\mathbf{r})$ is the density at the distance $\mathbf{r}$ from a given nucleus; it is identical with the well-known pair distribution function divided by the number of particles per unit volume.[3]

The first term in (2.1) represents the scattering of the isolated nucleus, the second term the interference

* This work was supported by grants-in-aid from the Institute for Advanced Study, in the case of one of the authors (G.P.) out of AEC funds, by the ONR, which made available computing help for the numerical calculations, and by the Board of Foreign Scholarships which awarded travel grants under the Fulbright act to two of the authors (B.R.A.N. and L.V.H.).
† Present address: University of Utrecht, Holland.
‡ Present address: Université Libre, Bruxelles, Belgium.
[1] G. Placzek, Phys. Rev. **75**, 1295 (1949).
[2] Rainwater, Rabi, and Havens, Phys. Rev. **75**, 1295 (1949).
[3] J. de Boer, Reports on Progress of Physics **12**, 305 (1948–49).

effect. This term contains a singularity $\delta(\mathbf{h})$. Since this type of singular scattering in the forward direction is equivalent to undisturbed propagation of the incident wave, $\delta(\mathbf{h})$ has to be subtracted. Combining the second and third term in (2.1), we have

$$1-\sigma(\mathbf{h})=\int\{1-w(\mathbf{r})\}\exp(2\pi i\mathbf{h}\cdot\mathbf{r})d\mathbf{r} \quad (2.3a)$$

and conversely,

$$1-w(\mathbf{r})=\int\{1-\sigma(\mathbf{h})\}\exp(-2\pi i\mathbf{h}\cdot\mathbf{r})d\mathbf{r}. \quad (2.3b)$$

We now wish to determine the total scattering cross section of a randomly oriented system. For this purpose we must average over all directions of $\mathbf{h}$ and integrate over all scattering angles. If we measure the total cross section in units of the total rather than the differential cross section of the isolated nucleus, the second integration must also be replaced by an average. It is convenient to carry out both averaging processes together. We have thus

$$\sigma_{\text{tot}}=\int_{-1}^{+1}\tfrac{1}{2}d(\cos\theta)\int\sigma(\mathbf{h})d\Omega_h/4\pi.$$

From (2.2) we have

$$d(\cos\theta)=-\lambda^2hdh$$

and thus

$$\sigma_{\text{tot}}=(\lambda^2/8\pi)\int_0^{2/\lambda}hdh\int\sigma(\mathbf{h})d\Omega_h$$

or, with

$$d\mathbf{h}=h^2dhd\Omega_h,$$

$$\sigma_{\text{tot}}=(\lambda^2/8\pi)\int\sigma(\mathbf{h})d\mathbf{h}/h=\frac{\int_S\sigma(\mathbf{h})d\mathbf{h}/h}{\int_S d\mathbf{h}/h}, \quad (2.4)$$

where the integrals are to be extended over a sphere of radius $2/\lambda$, which we indicate by the suffix S. The combined averages over orientation and scattering angles correspond thus to the average over a sphere of radius $2/\lambda$ in fourier space, weighted with the inverse distance in this space. We can also write (2.4) as

$$\sigma_{\text{tot}}=1-(\lambda^2/8\pi)\int_S\{1-\sigma(\mathbf{h})\}d\mathbf{h}/h. \quad (2.5)$$

For large h [i.e., $\lambda/2\sin(\theta/2)$ small compared with atomic distances] interference effects become negligible and $\sigma(\mathbf{h})$ tends to unity.[4] For short wavelengths, the integration in (2.5) can thus be extended over the whole of fourier space and we have for the asymptotic total cross section

$$(\sigma_{\text{tot}})_{As}=1-(\lambda^2/8\pi)I, \quad (2.6)$$

$$I=\int\{1-\sigma(\mathbf{h})\}d\mathbf{h}/h. \quad (2.7a)$$

Since the integral of a product of two functions over all space is equal to the integral of their fourier transforms, we obtain,[5] with (2.3b) and (A.5), an equivalent for I as an integral in ordinary space:

$$I=\int\{1-w(\mathbf{r})\}d\mathbf{r}/\pi r^2. \quad (2.7b)$$

Equation (2.6) gives the dependence of the total scattering cross section on neutron energy for small wavelength. Our concern will now be the discussion and evaluation of the coefficient I for various dense systems. The expressions (2.7a) and (2.7b) do not seem convenient for that purpose. The introduction of theoretical functions for $w(\mathbf{r})$ and $\sigma(\mathbf{h})$ for crystals or liquids leads to complicated calculations and rather inaccurate results. For liquids the evaluation of (2.7a) from x-ray scattering data is extremely deceptive, since a small change in $\sigma(\mathbf{h})$ will lead to a large change in I. This situation is hardly improved if (2.7b) rather than (2.7a) is used, since the process of using derived data ($w(\mathbf{r})$) instead of the original $\sigma(\mathbf{h})$ only introduces further uncertainties. Accordingly, we have attempted to obtain some orientation concerning the behavior of I for liquids by estimating in various ways, either from (2.7a) or (2.7b), its value for ideal or schematically distorted lattices. In particular, it has been pointed out by Rainwater, Rabi, and Havens[5a] that the value of I for various lattice types does not appear to vary very much. While such considerations are instructive, they are based on estimates obtained by procedures which remain to be justified; and above all they do not answer the question to what extent results obtained for lattices can be applied to liquids.

In the next paragraph we therefore attempt to approach the problem in a somewhat different manner.

III. AN UPPER BOUND FOR I AND A METHOD FOR THE ACCURATE DETERMINATION OF I FOR CONDENSED SYSTEMS

Starting from the expression (2.7b), we split the integral I into two parts:

$$I=I_1+I_2,$$

$$I_1=\int\{1-w(\mathbf{r})\}\{[\exp(-\pi r^2)]/\pi r^2\}d\mathbf{r}, \quad (3.1)$$

$$I_2=\int\{1-w(\mathbf{r})\}\{[1-\exp(-\pi r^2)]/\pi r^2\}d\mathbf{r}.$$

[4] For crystals, this statement must be qualified, see Secs. IV and V.

[5] Numbers preceded by the letter A refer to the table of fourier transforms in the Appendix.

[5a] This result was stated in the oral presentation of the paper quoted in reference 2.

Transforming I_2 into fourier space, we have, with (2.3a) and (A.7),

$$I_2=\int\{1-\sigma(\mathbf{h})\}\{[\phi(\pi^{\frac{1}{2}}h)]/h\}d\mathbf{h},$$

$$\phi(x)=2\pi^{-\frac{1}{2}}\int_x^\infty \exp(-t^2)dt$$

and thus

$$I=\int\{1-w(\mathbf{r})\}\{[\exp(-\pi r^2)]/\pi r^2\}d\mathbf{r}$$

$$+\int\{1-\sigma(\mathbf{h})\}\{[\phi(\pi^{\frac{1}{2}}h)]/h\}d\mathbf{h}. \quad (3.2)$$

The integral I is now expressed by the sum of an integral in ordinary and an integral in fourier space. Both integrals contain weight factors which decrease rapidly with increasing distance from the origin. It should be noted that for large values of h the two weight factors become symmetric, since, from the asymptotic representation of the error function,

$$\phi(\pi^{\frac{1}{2}}h)/h=[\exp(-\pi h^2)]/\pi h^2 \text{ for } h\gg 1.$$

This procedure is a straightforward generalization of Ewald's method for the evaluation of lattice sums by the use of the transformation properties of 3-dimensional theta-functions.[6]

It is now important to note that, while in Eqs. (2.7a) and (2.7b) the integrals over $w(\mathbf{r})$ and 1, and similarly over $\sigma(\mathbf{h})$ and 1, are divergent if taken separately, this is no longer the case in Eq. (3.2), since

$$\int\frac{\exp(-\pi r^2)}{\pi r^2}d\mathbf{r}=\lim_{h\to 0}\frac{1-\phi(\pi^{\frac{1}{2}}h)}{h}=2,$$

and

$$\int[\phi(\pi^{\frac{1}{2}}h)/h]d\mathbf{h}=\lim_{r\to 0}\frac{1-\exp(-\pi r^2)}{\pi r^2}=1.$$

Hence, we can write (3.2) as

$$I=3-S-R,$$

$$S=\int w(\mathbf{r})\{[\exp(-\pi r)]/\pi r^2\}d\mathbf{r}, \quad (3.3)$$

$$R=\int\sigma(\mathbf{h})\{[\phi(\pi^{\frac{1}{2}}h)]/h\}d\mathbf{h}.$$

Since $w(\mathbf{r})$ and $\sigma(\mathbf{h})$ are non-negative, (3.3) gives immediately an upper bound for I:

$$I<3. \quad (3.4)$$

For liquids, $w(\mathbf{r})$ and $\sigma(\mathbf{h})$ depend only on the magnitudes of $\mathbf{r}$ and $\mathbf{h}$; we can then write (3.3)

$$S=4\int_0^\infty w(r)\exp(-\pi r^2)dr,$$

$$R=4\pi\int_0^\infty\sigma(h)\phi(\pi^{\frac{1}{2}}h)hdh. \quad (3.5)$$

Equation (3.5) can also be used for crystals if we define $w(r)$ as the radial distribution function,

$$w(r)=\int w(\mathbf{r})d\Omega_r/4\pi,$$

and $\sigma(h)$ as the cross section averaged over all orientations of the crystal:

$$\sigma(h)=\int\sigma(\mathbf{h})d\Omega_h/4\pi.$$

For most purposes, however, it will be more convenient in the case of crystals to use (3.3) rather than (3.5).

Both integrals in (3.3) or (3.5) are small compared with 3, if the system is not too far removed from conditions of close packing and small compressibility. This can be seen as follows. The function $w(\mathbf{r})$ is 0 for $r<a$, where a is the distance of closest approach. For systems near close packing, a is of the order of the average interatomic distance, and thus in our units is of the order of unity, so that the whole function lies in a region where the weight factor is small. To estimate the integral in fourier space, we note that $\sigma(0)$ is equal to the average square fluctuation of the number of particles per unit volume,[7] and thus to the relative compressibility (isothermal compressibility of system divided by isothermal compressibility of ideal gas of same density). If this quantity is small, similar, although less sharp, considerations hold as in ordinary space. This point will be substantiated in the following paragraphs.

It is important to note, however, that for dilute systems the two integrals will be of order 3 or even larger. For the ideal gas we have $\sigma(h)=w(r)=1$ and $I=0$. Under conditions where the influence of attractive forces on $w(r)$ is important, in particular in the neighborhood of critical conditions, the sum of the integrals is larger than 3 and I becomes strongly negative. In these cases Eqs. (3.3) and (3.5) lose their usefulness entirely and one must revert to (2.7a) or (2.7b).

We now determine the value of I for special systems.

IV. IDEAL LATTICES

For ideal lattices the transition from (2.5) to (2.6) is not legitimate, since the function $\sigma(h)$ will have a peak at each point of the reciprocal lattice, the height of which does not decrease with increasing h [see Eq. (4.3)

[6] P. P. Ewald, Ann. Physik **64**, 253 (1921); Z. Krist. **56**, 129 (1921); see also M. Born and R. D. Misra, Proc. Cambridge Phil. Soc. **36**, 466 (1940).

[7] This relation between the integral $\int\{w(\mathbf{r})-1\}d\mathbf{r}$ and the density fluctuations were first derived by L. S. Ornstein and F. Zernike, Proc. Koninkl. Akad. Wetenschap. Amsterdam **17**, 793 (1914). See also reference 3.

below]. Consequently, the total cross section as function of the wavelength will exhibit a jump every time the sphere of reflection of radius $2/\lambda$ [see Eq. (2.5)] passes through a lattice point. For symmetric lattices, the sphere of reflection passes through many lattice points at the same time. The number of equivalent points (multiplicity) increases with increasing h, and from this it can be shown that the jumps in the total cross section do not generally decrease with decreasing wavelength. Only the average of $\sigma(h)$ taken over a region containing a large number of non-equivalent lattice points tends to unity for large values of h, and the asymptotic expression (2.6) for the total cross section will be valid only when (2.5) is averaged over an appropriate wavelength region. Accordingly, the integral (2.7a) can be given meaning only if defined by means of this averaging process.

For real crystals, however, when the motion of the particles is taken into account, it will be shown later that Eqs. (2.6) and (2.7a) are strictly correct. The quantity I will be expressed as a difference of two terms;

$$I=I_0-I_d,$$

where I_0 is obtained from Eq. (3.3) when applied to the ideal lattice, whereas I_d is a small positive correction term due to the displacements of the particles.

Let us consider an ideal lattice in which all particles occupy equivalent positions. Placing one particle at the origin of the elementary cell, we have for the pair distribution function[7a]

$$w(\mathbf{r})=\sum_{[s]}\sum_{[l]}\delta(\mathbf{r}-\mathbf{s}-\mathbf{l})-\delta(\mathbf{r}), \qquad (4.1)$$

where $\mathbf{s}$ is a lattice vector and $\mathbf{l}$ gives the coordinates of the particles in the elementary cell. In our units, the volume of the cell is equal to Z, the number of particles in the elementary cell. Then, making use of the well-known relation

$$\sum_{[s]}\exp(2\pi i\mathbf{h}\cdot\mathbf{s})=(1/Z)\sum_{[h_0]}\delta(\mathbf{h}-\mathbf{h}_0), \qquad (4.2)$$

it follows from (2.1) and (4.1) that

$$\sigma(\mathbf{h})=\sum'_{[h_0]}\delta(\mathbf{h}-\mathbf{h}_0)F(\mathbf{h})/Z.$$

Here h_0 stands for the lattice vectors in the reciprocal lattice, the sum $\sum'$ excludes the zero vector, and

$$F(\mathbf{h})=\sum_{[l]}\exp(2\pi i\mathbf{h}\cdot\mathbf{l})$$

is the structure factor. All particles having equivalent positions, we can average over the particles in the elementary cell. We then obtain

$$\sigma(\mathbf{h})=\sum'_{[h_0]}(|F(\mathbf{h})|/Z)^2\delta(\mathbf{h}-\mathbf{h}_0). \qquad (4.3)$$

Introducing (4.1) and (4.3) into the integrals S and R in (3.3), we have with $\mathbf{s}+\mathbf{l}=\mathbf{r}_0$

$$I_0=3-S_0-R_0, \qquad (4.4)$$

$$S_0=\sum'_{r_0}g(r_0)\exp(-\pi r_0^2)/\pi r_0^2, \qquad (4.5)$$

$$R_0=Z^{-2}\sum'_{h_0}\bar{g}(h_0)|F(h_0)|^2[\phi(\pi^{\frac{1}{2}}h_0)]/h_0. \qquad (4.6)$$

[7a] The symbol $\Sigma_{[s]}$ indicates summation over the vectors $\mathbf{s}$.

The factors $g(r_0)$ and $\bar{g}(h_0)$ indicate the multiplicity of distances between an arbitrary lattice point and all others in ordinary and fourier space, respectively. The series (4.5) and (4.6) are rapidly convergent and lend themselves easily to computation.

Table I gives in six decimal places the values of S_0, R_0, and I_0 as well as the closest distances in ordinary and fourier space for some familiar lattices. To illustrate the procedure in a little greater detail, we give in Tables II and III, for the two closed-packed structures, the contribution of all relevant terms of S_0 and R_0.

The main contribution to S_0 and R_0 comes usually from the closest point, except in the case of R_0 for the hexagonal close-packed structure, where the third closest point because of its high multiplicity gives the largest contribution. In Table I, the lattices are arranged in the order of decreasing closest distance (for unit volume per particle); i.e., decreasing closeness of packing. The contribution of S_0+R_0 to I_0 varies from 3.9 percent for the face-centered cubic to 11.4 percent for the diamond lattice. For any structure, the closeness of packing can be measured when using our unit of length by the quantity $(r_{0,\min})^3/\sqrt{2}=\gamma$, which has the following interpretation: the particles are supposed to be hard spheres with diameter equal to the closest distance $r_{0,\min}$; γ is then the ratio of the actual density to the density for close packing of these hard spheres, where, of course, both densities must now be measured with the same unit.

Table I gave the values of I_0 for a few structures with decreasing values of γ. Only for $\gamma=1$ (close-packed structures) had we two lattices; their values of I_0 differed very slightly. In order to investigate the variation of I_0 with structure for smaller γ, we consider a lattice with variable parameter, namely, the tetragonal face-centered. The mutually orthogonal axes of the tetragonal cell having lengths a,a, and c, the ratio a/c is varied. Each value of γ can be obtained twice, for $a<c$ (series I) and for $a>c$ (series II). Considering again the particles as hard spheres of diameter $r_{0,\min}$, the lattices of series I can be visualized as consisting of layers in which each sphere touches its 4 neighbors, whereas spheres in different layers are not in contact. In series II, for $c<a<c\sqrt{3}$, i.e., $0.918559<\gamma<1$, the lattices are packings of spheres, each sphere being touched by its 8 neighbors. For $a>c\sqrt{3}$, i.e., $\gamma<0.918559$, the lattices are composed of fibers of spheres in contact, spheres in different fibers not touching each other. The two lattices considered for every value of γ will therefore represent rather extreme types of configuration. The face-centered cubic structure is obtained for $a=c$, the body-centered for $a/c=\sqrt{2}$ in series II. In Table IV the values of S_0, R_0, and I_0 are given for values of γ ranging from 1 to 0.459279 (i.e., the value of γ for diamond), including the data relative to the lattices of Table I. The results indicate that, while in every series I_0 decreases regularly with γ, the variation of I_0 between different structures of same γ, negligible for γ close to 1, increases

TABLE I. The coefficient I_0 for various lattices.

Lattice	$r_{0,\min}$	$h_{0,\min}$	S_0	R_0	S_0+R_0	I_0
Cubic face-centered	1.122462	1.091124	0.058191	0.053347	0.111538	2.888462
Hexag. close-packed	1.122462	1.028721	0.058193	0.053430	0.111623	2.888377
Cubic body-centered	1.091124	1.122462	0.059668	0.052650	0.111718	2.888282
Mercury type*	1.051289	1.042001	0.066597	0.060632	0.127229	2.872771
Simple cubic	1.000000	1.000000	0.086169	0.076533	0.162702	2.837298
Diamond	0.866025	0.866025	0.164718	0.141882	0.306600	2.693400

* Rhomboedric axes, $Z=1$, cosine of angle between axes $=\frac{1}{3}$.

TABLE II. Face-centered cubic lattice.

r_0	$r_0/r_{0,\min}$	$g(r_0)$	$\exp(-\pi r_0^2)/\pi r_0^2$	$g(r_0)\exp(-\pi r_0^2)/\pi r_0^2$
1.122462	1.000000	12	0.004825	0.057900
1.587401	1.414214	6	0.00046	0.000276
1.944161	1.732051	24	0.000001	0.000014
2.244924	2.000000	12	——	——
				$S_0=0.058191$

h_0	$h_0/h_{0,\min}$	$\tilde{g}(h_0)$	$\lvert F(h_0)\rvert^2/Z^2$	$\frac{\phi(\pi^{\frac{1}{2}}\cdot h_0)}{h_0}$	$\tilde{g}(h_0)\frac{\lvert F(h_0)\rvert^2}{Z^2}\frac{\phi(\pi^{\frac{1}{2}}h_0)}{h_0}$
1.091124	1.000000	8	1	0.005716	0.045730
1.259921	1.154701	6	1	0.001260	0.007561
1.781797	1.632993	12	1	0.000004	0.000054
2.089343	1.914854	24	1	——	0.000002
2.182247	2.000000	8	1	——	——
					$R_0=0.053347$

$S_0+R_0=0.111538$
$I_0=2.888462$

TABLE III. Hexagonal close packing.

r_0	$r_0/r_{0,\min}$	$g(r_0)$	$\exp(-\pi r_0^2)/\pi r_0^2$	$g(r_0)\exp(-\pi r_0^2)/\pi r_0^2$
1.122462	1.000000	12	0.004825	0.057900
1.587401	1.414214	6	0.000046	0.000276
1.832973	1.632993	2	0.000002	0.000005
1.944161	1.732051	18	0.000006	0.000011
2.149351	1.914854	12	——	——
2.244924	2.000000	6	——	——
				$S_0=0.058193$

h_0	$h_0/h_{0,\min}$	$\tilde{g}(h_0)$	$\lvert F(h_0)\rvert^2/Z^2$	$\frac{\phi(\pi^{\frac{1}{2}}\cdot h_0)}{h_0}$	$\tilde{g}(h_0)\frac{\lvert F(h_0)\rvert^2}{Z^2}\frac{\phi(\pi^{\frac{1}{2}}h_0)}{h_0}$
1.028721	1.000000	6	$\frac{1}{4}$	0.009643	0.014464
1.091124	1.060660	2	1	0.005716	0.011433
1.164433	1.131923	12	$\frac{3}{4}$	0.003018	0.027158
1.499606	1.457738	12	$\frac{1}{4}$	0.000114	0.000341
1.781797	1.732051	6	1	0.000004	0.000027
1.933134	1.879162	12	$\frac{3}{4}$	0.000001	0.000006
2.057442	2.000000	6	$\frac{1}{4}$	——	——
2.089343	2.031010	12	1	——	0.000001
					$R_0=0.053430$

$S_0+R_0=0.111623$
$I_0=2.888377$

rapidly when γ decreases. One should notice, however, that the relative variation of I_0 over the range considered does not exceed 8.4 percent. This approximate insensitivity of I_0 to changes of structure and closeness of packing for dense lattices is the main conclusion of the foregoing discussion.

V. REAL CRYSTALS

In order to evaluate I for real crystals, we first give the expressions for the functions $w(\mathbf{r})$ and $\sigma(\mathbf{h})$. For simplicity, we restrict ourselves to the case of a Bravais lattice (one particle per cell). The equilibrium positions of the particles are defined by the lattice vectors $\mathbf{s}$, their displacements from the equilibrium positions by the displacement vectors $\mathbf{u}(\mathbf{s})$. We introduce the relative displacements $\mathbf{U}(\mathbf{s})$ with respect to an arbitrary particle which we take to have its equilibrium position in the zero cell,

$$\mathbf{U}(\mathbf{s})=\mathbf{u}(\mathbf{s})-\mathbf{u}(0). \tag{5.1}$$

The displacement vectors $\mathbf{u}(\mathbf{s})$, as well as the relative displacements $\mathbf{U}(\mathbf{s})$, are linear functions of the normal coordinates of the crystal. It has been shown by Bloch[8] that the probability distribution of the coordinate ξ of a harmonic oscillator at a given temperature, T, is a gaussian function given by

$$P(\xi)d\xi=[2\pi(\xi^2)_{kl}]^{-\frac{1}{2}}\exp[-\xi^2/2(\xi^2)_{kl}]\cdot d\xi, \quad (5.2')$$

where

$$(\xi^2)_{kl}=(E)_{kl}/\omega^2=(\hbar/2\omega)\coth(\hbar\omega/2kT). \quad (5.2'')$$

Since the normal coordinates are independent, any linear function of them will also have a gaussian distribution. This holds in particular for the vectors $\mathbf{U}(\mathbf{s})$, the distribution function of which will have the form

$$F(\mathbf{U})d\mathbf{U}=C(\mathbf{s})\exp[-Q(\mathbf{U},\mathbf{s})]d\mathbf{U}, \quad (5.3)$$

where $Q(\mathbf{U},\mathbf{s})$ is a quadratic form in the components of the vector $\mathbf{U}(\mathbf{s})$, and $C(\mathbf{s})$ is a normalizing constant. The corresponding distribution function for the absolute displacements, $\mathbf{u}(\mathbf{s})$, reduces to an isotropic gaussian distribution if both the crystal symmetry and the proper symmetry of the special positions of the atoms are cubic. This is not the case, however, for the distribution function of the relative displacements.

While the calculation of I with the anisotropic gaussian distribution (5.3) presents no difficulties, the relevant points are obscured somewhat by purely formal complications connected with the treatment of anisotropy, without any essential gain. We shall assume in the following, therefore, that the velocity of sound is independent of polarization and of direction of propagation,[9] in which case, (5.3) becomes isotropic, so that

$$w(\mathbf{r})=\textstyle\sum_{(s)}(2\pi\alpha_s)^{-\frac{1}{2}}\exp[-|\mathbf{r}-\mathbf{s}|^2/2\alpha_s], \quad (5.4)$$

where α_s is the average square of any component of $\mathbf{U}(\mathbf{s})$, or

$$\begin{aligned}\alpha_s&=\langle(U_x(\mathbf{s}))^2\rangle_{kl}\\&=\langle(u_x(0))^2\rangle_{kl}+\langle(u_x(\mathbf{s}))^2\rangle_{kl}-2\langle u_x(0)u_x(\mathbf{s})\rangle_{kl}\\&=2\{\langle(u_x(0))^2\rangle_{kl}-\langle u_x(0)u_x(\mathbf{s})\rangle_{kl}\}.\end{aligned} \quad (5.5)$$

On expressing the displacements in terms of the normal coordinates, we find that

$$\langle(u_x(0))^2\rangle_{kl}=\int[(E)_{kl}/m\omega^2]d\mathbf{q} \quad (5.6)$$

and

$$\langle u_x(0)u_x(\mathbf{s})\rangle_{kl}=\int[(E)_{kl}/m\omega^2]\cos(2\pi\mathbf{q}\cdot\mathbf{s})d\mathbf{q}. \quad (5.7)$$

Here $2\pi\mathbf{q}$ is the wave vector of the elastic waves, ω is the corresponding frequency, and $(E)_{kl}$ is the corresponding average energy as defined by (5.2). The mass of the particles is denoted by m. The integration is to be extended over all elastic waves; i.e., over a full Brillouin zone.

TABLE IV. Dependence of I_0 on the ratio γ of density for close-packed density.

γ	Lattice	S_0	R_0	S_0+R_0	I_0
1.000000	f.c. cubic (I, II, $a/c=1$)	0.058191	0.053347	0.111538	2.888462
	hexag. close-packed	0.058193	0.053430	0.111623	2.888377
0.918559	I, $a/c=0.918559$	0.058630	0.054256	0.112886	2.887114
	b.c. cubic (II, $a/c=1.414214$)	0.059668	0.052650	0.111718	2.888282
0.821584	I, $a/c=0.821584$	0.061351	0.054799	0.116150	2.883850
	II, $a/c=1.855439$	0.063534	0.058634	0.122167	2.877833
	mercury lattice	0.066597	0.060632	0.127229	2.872771
0.760000	I, $a/c=0.760000$	0.065484	0.057386	0.122870	2.877130
	II, $a/c=1.929149$	0.065957	0.061092	0.127049	2.872951
0.707107	I, $a/c=0.707107$	0.071488	0.061867	0.133355	2.866645
	II, $a/c=2.000000$	0.068937	0.063875	0.132812	2.867188
	simple cubic	0.086169	0.076533	0.162702	2.837298
0.650000	I, $a/c=0.650000$	0.081670	0.070664	0.152334	2.847666
	II, $a/c=2.086007$	0.073484	0.067793	1.141277	2.858723
0.600000	I, $a/c=0.600000$	0.094981	0.083738	0.178719	2.821281
	II, $a/c=2.171185$	0.079054	0.072237	0.151291	2.848709
0.550000	I, $a/c=0.550000$	0.114013	0.097482	0.211495	2.788505
	II, $a/c=2.267729$	0.086716	0.077916	0.164632	2.835368
0.500000	I, $a/c=0.500000$	0.140574	0.137124	0.277698	2.722302
	II, $a/c=2.378414$	0.097325	0.085211	0.182536	2.817464
0.459279	I, $a/c=0.459279$	0.169950	0.176347	0.346297	2.653703
	II, $a/c=2.481613$	0.108938	0.092707	0.201645	2.798355
	diamond lattice	0.164718	0.141882	0.306600	2.693400

[8] F. Bloch, Z. Physik **74**, 295 (1932).

[9] The second assumption is not necessary at this stage but will play a role in the derivation of (5.9).

The correlation $\langle u_x(0)u_x(\mathbf{s})\rangle_{kT}$ will vanish as the distance, $\mathbf{s}$, goes to infinity. The asymptotic behavior of this quantity for large distances can be found by an examination of the singularity of the integrand in (5.7) at $q=0$. In the limit $q\to 0$, we have

$$\omega = 2\pi q v, \tag{5.8}$$

where v is the velocity of sound for infinite wavelength, and $(E)_{kT}=kT$ for any finite temperature. Hence,

$$(E)_{kT}/m\omega^2=(kT/mv^2)/4\pi^2q^2,$$

and [see (A.5)]

$$\langle u_x(0)u_x(\mathbf{s})\rangle_{kT}=[(kT/mv^2)/2\pi s]+O(1/s^2), \quad s\gg 1. \tag{5.9}$$

For large distances the correlation thus vanishes as the reciprocal of the distance and α_s tends to

$$\alpha_\infty = 2\langle (u_x(0))^2\rangle_{kT}.$$

We note also that $\alpha_0=0$.

Introduction of (5.4) into (2.1) leads, with the help of (A.6), to the differential cross section

$$\sigma(\mathbf{h})=\sum_{[s]}\exp(2\pi i\mathbf{h}\cdot\mathbf{s}-2\pi^2h^2\alpha_s)-\delta(\mathbf{h}),$$

which, using (4.2) for $Z=1$, may also be written

$$\sigma(\mathbf{h})=[\exp(-2\pi^2h^2\alpha_\infty)]\sum'_{[h_0]}\delta(\mathbf{h}-\mathbf{h}_0) + \sum_{[s]}[\exp(2\pi i\mathbf{h}\cdot\mathbf{s})] \times[\exp(-2\pi^2h^2\alpha_s)-\exp(-2\pi^2h^2\alpha_\infty)]. \tag{5.10}$$

The first term, where $\mathbf{h}_0$ denotes the vectors of the reciprocal lattice, corresponds to the Laue-Bragg scattering, the second term to the diffuse scattering. Both terms have singularities at the reciprocal lattice points. For the Laue-Bragg scattering, they are of the δ-type with an exponentially decreasing factor $\exp(-2\pi^2h^2\alpha_\infty)$ (Debye-Waller factor). Near each Laue spot the diffuse scattering cross section, which has also an exponential factor of the same order, behaves as $1/|\mathbf{h}-\mathbf{h}_0|^2$. This follows from the asymptotic behavior (5.9)

$$\exp(-2\pi^2h^2\alpha_s)-\exp(-2\pi^2h^2\alpha_\infty) \sim 2\pi^2h^2[\exp(-2\pi^2h^2\alpha_\infty)](\alpha_\infty-\alpha_s) \sim 2\pi^2h^2[\exp(-2\pi^2h^2\alpha_\infty)](kT/mv^2)\cdot(1/\pi s)$$

by fourier transform.[10]

[10] If the dependence of the velocity of sound on the direction of the wave vector and on polarization is taken into account, the correlation will still decrease $1/s$, but the coefficient of $1/s$ in (5.9) will depend on the direction of $\mathbf{s}$ and the component of the relative displacement considered, in a way which can be derived from the macroscopic elastic constants of the crystal. As a consequence of this, the singularity $|h-h_0|^{-2}$ in the cross section for the diffuse scattering is multiplied by a factor depending on $\mathbf{h}_0$ and on the direction of $\mathbf{h}-\mathbf{h}_0$. For details, see work on the theory of the diffuse scattering of x-rays, e.g., M. Born, Reports on Progress in Physics 9, 294 (1943), and W. Zachariasen, *Theory of X-ray Diffraction in Crystals* (1945). This theory has been worked out only for the case of wavelength that is large compared with the average displacement of the particles, while we deal here with the opposite case.

From these properties of $\sigma(\mathbf{h})$ it can now be concluded that the transition from (2.5) to (2.6) is legitimate for real crystals, and the asymptotic expression (2.6) for the cross section will be valid for wavelengths $\lambda\ll 4\pi[u_x(0)]_{\text{rms}}$, where $[u_x(0)]_{\text{rms}}$ is the root-mean-square displacement in any direction.

The evaluation of I could now be done either by (2.7a) or by (2.7b). Both procedures, when applied with some care, lead to the correct result; but the fact that $w(\mathbf{r})$ and $\sigma(\mathbf{h})$ are given by slowly convergent series makes a justification of the various steps difficult. When starting from Eq. (3.3), on the contrary, the occurrence of quickly decreasing weight factors in both integrals enables one to make the derivation more rigorous.

According to (5.4), the integral in ordinary space is

$$S=\int w(\mathbf{r})\exp-(\pi r^2)d\mathbf{r}/\pi r^2 = \sum'_{[s]}(2\pi\alpha_s)^{-\frac{1}{2}}\int[\exp(-u^2/2\alpha_s)] \times[\{\exp(-\pi|\mathbf{s}+\mathbf{u}|^2)\}/\pi|\mathbf{s}+\mathbf{u}|^2]d\mathbf{u}.$$

Because of the presence of the gaussian factor $\exp(-u^2/2\alpha_s)$, we can expand $[\exp(-\pi|\mathbf{s}+\mathbf{u}|^2)]/\pi|\mathbf{s}+\mathbf{u}|^2$ in powers of $\mathbf{u}$. Integrating, we obtain for S an asymptotic expansion in powers of α_s, i.e., essentially in powers of the ratio of the average square displacement to the square of the lattice constant. The result proves to be

$$S=\sum'_{[s]}\frac{\exp(-\pi s^2)}{\pi s^2}+\tfrac{1}{2}\sum'_{[s]}\left(\Delta\frac{\exp(-\pi r^2)}{\pi r^2}\right)_{r=s} +\tfrac{1}{8}\sum'_{[s]}\alpha_s^2\left(\Delta^2\frac{\exp(-\pi r^2)}{\pi r^2}\right)_{r=s}+\cdots, \tag{5.11}$$

where Δ denotes the laplacian. On the other hand, with (5.10), the integral in fourier space can be written

$$R=\int\sigma(\mathbf{h})\{[\phi(\pi^{\frac{1}{2}}h)]/h\}d\mathbf{h} =\sum'_{[h_0]}\{\phi(\pi^{\frac{1}{2}}h_0)/h_0\}\exp(-2\pi^2h_0^2\alpha_\infty) -\int\sum'_{[s]}[\exp(2\pi i\mathbf{h}\cdot\mathbf{s})][1-\exp(-2\pi^2h^2\alpha_s)] \times\{[\phi(\pi^{\frac{1}{2}}h)]/h\}d\mathbf{h}+\int\sum_{[s]}[\exp(2\pi i\mathbf{h}\cdot\mathbf{s})] \times[1-\exp(-2\pi^2h^2\alpha_\infty)]\{[\phi(\pi^{\frac{1}{2}}h)]/h\}d\mathbf{h}.$$

Using, in the last integral, Eq. (4.2) for $Z=1$, we simply get[11]

[11] The interchange of summation and integration can be shown to be permissible just because of the presence of the weight factor $\phi(\pi^{\frac{1}{2}}h)$.

$$R=\sum'_{[h_0]}[\phi(\pi^{\frac{1}{2}}h_0)]/h_0-\int\sum'_{[s]}[\exp(2\pi i\mathbf{h}\cdot\mathbf{s})]$$

$$\times[1-\exp(-2\pi^2h^2\alpha_s)]\{[\phi(\pi^{\frac{1}{2}}h)]/h\}d\mathbf{h}.$$

The weight factor $\phi(\pi^{\frac{1}{2}}h)$ suppresses the contribution of the integrand for large values of h. We may therefore expand $1-\exp(-2\pi^2h^2\alpha_s)$ and again obtain an asymptotic expansion in powers of α_s.

$$R=\sum'_{[h_0]}[\phi(\pi^{\frac{1}{2}}h_0)]/h_0$$

$$+2\pi^2\sum'_{[s]}\alpha_s\int h^2[\exp(2\pi i\mathbf{h}\cdot\mathbf{s})]\{[\phi(\pi^{\frac{1}{2}}h)]/h\}d\mathbf{h}$$

$$+2\pi^4\sum'_{[s]}\alpha_s^2\int h^4[\exp(2\pi i\mathbf{h}\cdot\mathbf{s})]\{[\phi(\pi^{\frac{1}{2}}h)]/h\}d\mathbf{h}.$$

By Eq. (A.7), the result becomes

$$R=\sum'_{[h_0]}\frac{\phi(\pi^{\frac{1}{2}}h_0)}{h_0}+\tfrac{1}{2}\sum'_{[s]}\alpha_s\left(\Delta\frac{1-\exp(-\pi r^2)}{\pi r^2}\right)_{r=s}$$

$$+\tfrac{1}{8}\sum'_{[s]}\alpha_s^2\left(\Delta^2\frac{1-\exp(-\pi r^2)}{\pi r^2}\right)_{r=s}+\cdots. \quad (5.12)$$

Equations (5.11) and (5.12) can be combined to give

$$I=I_0-I_d,$$

where I_0 is the quantity defined in (4.6) for the ideal lattice, and I_d is the correction term due to the displacements

$$I_d=(2\pi)^{-1}\sum'_{[s]}\alpha_s(\Delta r^{-2})_{r=s}$$

$$+(8\pi)^{-1}\sum'_{[s]}(\Delta^2r^{-2})_{r=s}+\cdots$$

or

$$I_d=(1/\pi)\sum'_{[s]}\alpha_s s^{-4}+(3/\pi)\sum'_{[s]}\alpha_s^2 s^{-6}+\cdots. \quad (5.13)$$

One should notice that I_d is essentially positive, and therefore, that the motion of the particles in the crystal gives rise to a slight decrease of I. To calculate the value of I_d under simplifying assumptions, we now take for our crystal the Debye model; i.e., we assume the velocity of sound to be independent of the wavelength. Introducing this assumption into (5.6) and (5.7), one finds in the usual way, for temperatures higher than Debye temperature,

$$\langle(u_s(0))^2\rangle_{h\nu}=(3/4\pi^4)^{\frac{1}{2}}(kT/mv^2)=(3/4\pi^4)^{\frac{1}{2}}c, \quad (5.14)$$

where $c=kT/mv^2$ is the relative compressibility, and

$$\langle u_s(0)u_s(\mathbf{s})\rangle_{h\nu}=\langle(u_s(0))^2\rangle_{h\nu}$$

$$\times\{(Si[(6\pi^2)^{\frac{1}{2}}s])/[(6\pi^2)^{\frac{1}{2}}s]\}, \quad (5.15)$$

where

$$Si(x)=\int_0^x \sin t dt/t=(\pi/2)+si(x). \quad (5.16)$$

We note that for large values of s, (5.15) reduces to the general asymptotic expression (5.9). Introducing (5.14) and (5.15) into (5.5), we have

$$\alpha_\infty=(6\pi^{-4})^{\frac{1}{2}}c, \quad (5.17)$$

and

$$\alpha_s=\alpha_\infty\{1-[(\pi/6)^{\frac{1}{2}}/2s]$$

$$-(si[(6\pi^2)^{\frac{1}{2}}s]/[(6\pi^2)^{\frac{1}{2}}s])\}. \quad (5.18)$$

From (5.13), (5.17), and (5.18), we now find to the first order in c

$$I_d=\beta c,$$

where

$$\pi^3\beta=(6\pi^2)^{\frac{1}{2}}\sum'_{[s]}s^{-4}-(\pi/2)\sum'_{[s]}s^{-5}$$

$$-\sum'_{[s]}s^{-3}si[(6\pi^2)^{\frac{1}{2}}s]. \quad (5.19)$$

The lattice sums $\sum'(1/s^4)$ and $\sum'(1/s^5)$ have been calculated by Jones and Ingham for simple, face-centered, and body-centered cubic lattices.[12] The last sum in (5.19) has been evaluated numerically. It represents only a small contribution. From Table V, which gives the results for the three lattice types, it may be seen that in all three cases β is about 1.5.

The relative compressibility of crystals is of the order of magnitude of the ratio of the average square displacement to the square of the lattice constant. For crystals composed of heavy particles, this is a very small quantity. At room temperature, c for Pb, Bi, Au, and W is about 0.0030, 0.0034, 0.0013, and 0.0007, respectively. Therefore, the term I_d introduces only a small correction to the value I_0 corresponding to the ideal lattice.

VI. LIQUIDS

A liquid under conditions near close packing may be compared to a distorted crystal only as far as the im-

TABLE V. Data on the influence of thermal motion on the coefficient I.

Lattice	$(6/\pi^2)^{\frac{1}{2}}\Sigma's^{-4}$	$(1/2\pi^2)\Sigma's^{-5}$	$\pi^{-3}\Sigma's^{-3}si[(6\pi^2)^{\frac{1}{2}}s]$	β
Simple cubic	2.078	0.526	0.032	1.521
Cubic face-centered	2.007	0.482	0.021	1.504
Cubic body-centered	2.008	0.483	0.021	1.504

[12] Jones and Ingham, Proc. Roy. Soc. (London) **A107**, 636 (1925). It may be remarked that lattice sums of the type $\Sigma'(1/s^n)$, $n\geq 4$, can also be conveniently calculated by applying the general procedure which led us to Eq. (3.3). See also R. D. Misra, Proc. Cambridge Phil. Soc. **36**, 173 (1940).

mediate neighborhood of an atom is concerned. It is this region which determines the value of the integral S in (3.5), which can thus be expected to be of the same order as in a crystal near close packing. The absence of long-range order will make itself felt in the integral R. The region of importance for this integral will be the region between $h=0$ and the value of h beyond the first peak in the $\sigma(h)$-curve. While $\sigma(0)$, which is given by the relative compressibility, may not be very different in a crystal and in a molten metal (for liquid mercury, c is about 0.006 and along the melting curve only about 10 percent different from the value in the crystal), the further behavior of the $\sigma(h)$-curve will rather differ in crystal and liquid. While the first peak of the $w(r)$-curve in a liquid near close packing is not much broader than in a distorted crystal, the first peak in the $\sigma(h)$-curve will be of very different structure in crystal and liquid. In the crystal, the first peak consists of an infinitely sharp maximum at $h=h_{0,\min}$. The disorder does not broaden the peak but only reduces its intensity by a small amount. In the neighborhood of the peak, the $\sigma(h)$-curve has a logarithmic singularity and its integral corresponds approximately to the amount by which the sharp peak is diminished by the disorder. In the liquid, the first peak has considerable width, since it arises essentially from the interference of waves scattered from the central atom and its neighbors. This will appreciably modify the value of R without changing its order of magnitude.

In order to illustrate these considerations, we have evaluated I for liquid mercury by using x-ray scattering data obtained by Hendus.[13] As has been pointed out before, an attempt to evaluate I from (2.7a) or (2.7b) by using experimental data would be entirely hopeless. With our method, on the other hand, only the integrals S and R need be evaluated. Even so, most of the experimental data, in particular those for bismuth[14, 15] did not appear to us to be sufficiently precise to warrant their use. Mercury was chosen because of the data for this frequently investigated substance appeared to be the least inaccurate available.

The $w(r)$-curve derived from his data by Hendus presents no particular problem and gives for the integral S the value 0.08 as compared to 0.067 in the case of the ideal crystal. Figure 1 shows the $\sigma(h)$-curve, corrected for form factor, and, on scale multiplied by 100, the integrand of

$$R=4\pi\int_0^\infty \sigma(h)\phi(\pi^{\frac{1}{2}}h)hdh.$$

The first peak in the $\sigma(h)$-curve is broad and contains two crystal reflections, the position of which is indicated at the bottom of the graph.

For $h\gtrsim 1.6$, $\sigma(h)$ has at least three other distinct maxima which are not included in the graph, because their contribution to R is negligible on account of the weight factor $\phi(\pi^{\frac{1}{2}}h)$. The first maximum of the dotted curve $\sigma(h)h\phi(\pi^{\frac{1}{2}}h)$ is due to the fact that the factor $h\phi(\pi^{\frac{1}{2}}h)$ has a maximum; the second maximum corresponds to the peak in the $\sigma(h)$-curve which is shifted to smaller values of h because of the considerable variation of the factor $h\phi(\pi^{\frac{1}{2}}h)$ over the width. It is important to note that the region in the $\sigma(h)$-curve between $h=0$ and $h=0.86$ appears to have been interpolated by Hendus in an arbitrary way. This makes the equivalent part in the dotted curve correspondingly uncertain. Integrating the dotted curve as it stands, one obtains for R about 0.10 as compared to 0.061 in the ideal crystal, which would give for $S+R$ about 0.18 as compared to 0.127 in the ideal crystal. If we conservatively assume that $S+R$ could be in error by as much as 100 percent, this would correspond to an error of only 6 percent in I. In the case of liquid bismuth, $S+R$ may be somewhat larger than in the case of mercury, since this substance is probably slightly further from close packing than mercury. But this is not likely to change the qualitative nature of the result.

From the above treatment of crystals and liquids we have obtained some insight into the values of I for dense systems; in particular, the consideration of various lattices gave an idea about the density de-

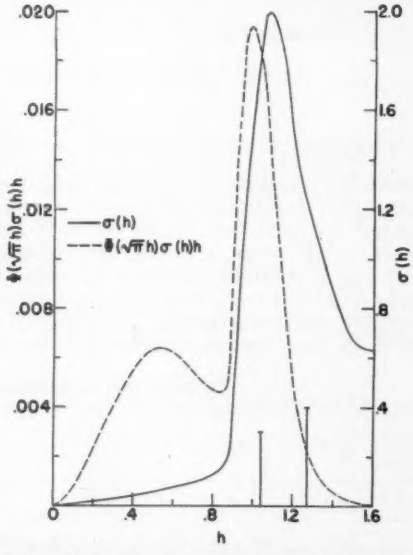

FIG. 1. Angular dependence of differential scattering cross section and of integrand in Eq. (8.1) for liquid mercury.

[13] H. Hendus, Z. Naturforsch. **3A**, 416 (1948). We are obliged to Dr. Hendus for making his complete observational data on Hg available to us.

[14] H. Hendus, Z. Naturforsch. **2A**, 505 (1947).

[15] O. Chamberlain, Phys. Rev. **77**, 305 (1950). These data were obtained with neutrons. Apart from their insufficient accuracy they are not suited for our purposes since they are obtained with long wavelengths for which the validity of the theory of neutron scattering used by us is in doubt. In addition, they contain the effect of the neutron scattering by electrons.

pendence of I under conditions not too far removed from close packing. As was already pointed out, our procedure is not suitable in the case of smaller densities; for the special case of hard spheres without attractive forces, however, it is not difficult to obtain general orientation about the behavior of I for all densities. In this case, I is positive throughout. In the limit of zero density,

$$w(r)=\begin{cases}0 \text{ for } r<a\\ 1 \text{ for } r>a,\end{cases} \tag{6.1}$$

where a is the diameter of the hard spheres, and thus we have from (2.7b)

$$I=4a. \tag{6.2}$$

Reverting now to absolute units of length we may write (2.6)

$$(\sigma_{\text{tot}})_{hr}=1-(\lambda^2/2\pi)a\rho K=1-(\lambda^2\gamma K)/\sqrt{2}\pi a^2, \tag{6.3}$$

where ρ is the density (number of particles per unit volume), a the diameter of the spheres expressed now in absolute units, $\gamma=\rho a^3/\sqrt{2}$ the ratio of the density ρ to the density for close packing as used in Sec. IV, and K is a dimensionless quantity defined by

$$K=I/4a\rho^{1/3}=I/4.2^{1/6}\gamma^{1/3}=(1/a)\int\{1-w(r)\}dr. \tag{6.4}$$

For $\gamma\ll 1$ we have from (6.2),

$$K=1, \quad \gamma\ll 1. \tag{6.5}$$

On the other hand, for close packing,[16]

$$K=2.888/4\cdot 2^{1/6}=0.643, \quad \gamma=1. \tag{6.6}$$

The behavior of K for intermediate values of γ may be obtained from the expansion of $w(r)$ in powers of γ:

$$w(r)=\sum_{n\geq 0} w_n(r)\gamma^n.$$

$w_0(r)$ is given by (6.1); $w_1(r)$ has been calculated by Kirkwood[17] with the result

$$w_1(r)=\begin{cases}0 & \text{for } r<a \text{ and } r>2a\\ (4\pi/3)\sqrt{2}\left\{1-\dfrac{3r}{4a}+\dfrac{r^3}{16a^3}\right\} & \text{for } a<r<2a\end{cases} \tag{6.7}$$

from which

$$K=1-(7\pi\sqrt{2}/48)\gamma+\cdots=1-0.648\gamma+\cdots. \tag{6.8}$$

Equation (6.8) joins smoothly the region of high density in which I is approximately constant so that K will there be approximately represented by

$$K\approx 0.64\cdot\gamma^{-1}.$$

[16] For the two regular close-packed arrangements I is 2.888; for irregular close packing, I has not been calculated but may be assumed to lie in the immediate neighborhood of this value.

[17] J. G. Kirkwood, J. Chem. Phys. 3, 300 (1935).

Returning to Eq. (6.3), it now appears that for large variations of the density the coefficient of λ^2 in this model is grossly proportional to the density, the constant of proportionality decreasing somewhat with increasing density. In the small region near close packing, where I is approximately constant, the coefficient of λ^2 will vary more nearly like $\gamma^{\frac{1}{2}}$ rather than like γ.

VII. A REMARK ON THE MAXIMUM VALUE OF I

It was proved in Sec. III that for any system of particles, the coefficient

$$I=\int\{1-w(\mathbf{r})\}d\mathbf{r}/\pi r^2$$

is smaller than 3 (the unit of length is here again the cube root of the volume per particle). The proof made use only of the following properties of $w(\mathbf{r})$: $w(\mathbf{r})$ is a non-negative function, and $w(\mathbf{r})-1$ has a fourier transform $\sigma(h)-1$ with non-negative $\sigma(h)$. On the other hand, in the evaluation of I for various special systems, the largest value obtained was 2.888462 in the case of the face-centered cubic lattice, one of the two regular close-packed structures. In this connection the question, "Which would be the true maximum value of I and for what system will it be reached?" arises. In investigating this question, one must keep in mind that $w(\mathbf{r})$ cannot be chosen arbitrarily but must satisfy a number of properties which follow from its statistical nature and from which, in particular, the non-negativity of $\sigma(h)$ arises. We do not wish to enter here into a detailed discussion of this problem, since we have not succeeded in solving it so far. We believe, however, that the true maximum of I will lie very close to 2.888462, and we think it rather plausible that the maximum is actually attained by the ideal face-centered cubic lattice with the above value. The way to prove this conjecture does not seem to us to lie in a modification of the weight factors in (3.3) with the aim of depressing the upper bound, but rather in using the characteristic properties of $w(\mathbf{r})$ for the purpose of showing that the sum of the integrals S and R cannot be smaller than a certain minimum value. Indeed, it can be shown easily that the weight factors used in (3.3) are the most favorable ones among a wide class of functions satisfying the requisite conditions.

Let us replace the quantity $\exp(-\pi r^2)/\pi r^2$ in (3.3) by

$$F(r)=\int_0^\infty f(y)\exp(-\pi r^2 y)dy.$$

Denoting by $\Psi(h)$ the fourier transform of $(1/\pi r^2)-F(r)$, we have

$$\Psi(h)=\int_1^\infty y^{-1}\{1-f(1/y)\}\exp(-\pi h^2 y)dy.$$

We may now write

$$I=\int\{1-w(\mathbf{r})\}F(r)d\mathbf{r}+\int\{1-\sigma(\mathbf{h})\}\psi(h)d\mathbf{h}$$

$$=J-\int w(\mathbf{r})F(r)d\mathbf{r}-\int\sigma(\mathbf{h})\psi(h)d\mathbf{h},$$

with

$$J=3+\int_0^1\{f(y)+y^{-1}[1-f(1/y)]\}\{y^{-1}-1\}dy. \quad (7.1)$$

As soon as the functions $F(r)$ and $\Psi(h)$ are non-negative, J is an upper bound for I. The most immediate way to satisfy this requirement is to impose upon $f(y)$ the condition

$$0\leqslant f(y)\leqslant 1. \quad (7.2)$$

As seen easily from (7.1), the upper bound J is then never smaller than 3 and reaches the value 3 for

$$f(y)=\begin{cases}0, & 0\leqslant y\leqslant 1,\\ 1, & y>1,\end{cases}$$

which corresponds to our original choice of weight factors. This conclusion can be shown to hold unchanged when (7.2) is replaced by the less restrictive condition

$$\int_0^y dy_1\int_0^{y_1}dy_2\cdots\int_0^{y_{n-1}}f(y_n)dy_n\geqslant 0,\quad f(y)\leqslant 1,$$

where the first inequality must be satisfied for some value of n.

VIII. DISCUSSION OF VALIDITY OF THE ASYMPTOTIC CROSS-SECTION FORMULA

Let us return for a moment to the asymptotic expression (2.6) for the total scattering cross section and consider the question in what wavelength region it will be valid. First of all, according to (2.5), the contribution of the region $h>2/\lambda$ to the integral over fourier space

$$\int\{1-\sigma(\mathbf{h})\}d\mathbf{h}/h$$

must be negligible. This condition is not extremely restrictive. For liquids, for mercury at room temperature, for instance, as may be seen from the x-ray data of Hendus referred to above, it will be satisfied with a good approximation as soon as λ is smaller than about 1.2A (neutron energy >0.06 ev). The x-ray data on bismuth indicate a similar limiting value for λ.[14] The transmission experiments of Rainwater, Rabi, and Havens mentioned in Sec. I cover an appreciable region where (2.6) is valid.

For crystals, the asymptotic formula will become valid only for somewhat smaller wavelength. It was pointed out in Sec. V that the condition here becomes $\lambda\ll 4\pi[u_x(0)]_{\rm rms}$. From the data on relative compressibilities given in Sec. V it follows that the limiting wavelength $\lambda_0=4\pi[u_x(0)]_{\rm rms}$ in the case of Pb and Bi at room temperature is about 1A. The asymptotic expression neglects fluctuating terms of the order $\exp[-(\lambda_0/\lambda)^2]$ and will therefore be a reasonable approximation if $\lambda<\lambda_0/2.5$. It will be noticed that, even in the case of liquids, the neutron energy in the wavelength region just specified is larger than the Debye temperature, which was the condition of applicability of the general theory of neutron scattering stated in Sec. I.

For values of the wavelength for which the asymptotic expression (2.6) of the cross section is not applicable, one must return to the formula (2.5). In the latter, the coefficient of the λ^2-term can be written

$$\int_S\{1-\sigma(h)\}d\mathbf{h}/h=\int\{1-w(\mathbf{r})\}\{1-\cos(4\pi r/\lambda)\}d\mathbf{r}/\pi r^2$$

$$=I+\int\{w(\mathbf{r})-1\}\cos(4\pi r/\lambda)d\mathbf{r}/\pi r^2.$$

It may be worth mentioning that the correction term due to finite λ can also be written as the sum of an integral in ordinary and an integral in fourier space:

$$\int\{w(\mathbf{r})-1\}\cos(4\pi r/\lambda)d\mathbf{r}/\pi r^2=-2\exp(-4\pi/\lambda^2)$$

$$+\int w(\mathbf{r})[\exp(-\pi r^2)]\cos(4\pi r/\lambda)d\mathbf{r}/\pi r^2$$

$$+\tfrac{1}{2}\int\{\sigma(\mathbf{h})-1\}\{\phi[(h+2/\lambda)\pi^{\frac{1}{2}}]\pm$$

$$\phi[|h-2/\lambda|\pi^{\frac{1}{2}}]\}d\mathbf{h}/h,$$

$$\phi(x)=2\pi^{-\frac{1}{2}}\int_x^\infty[\exp(-t^2)]dt, \quad (8.1)$$

where the plus sign must be taken when $h>2/\lambda$, the minus sign when $h<2/\lambda$. The advantage of the weight factors is here again to restrict the ranges of integration to small domains. While in ordinary space the relevant domain of integration is again the region of small r, where $w(\mathbf{r})$ is small, in fourier space the integration is now restricted to the neighborhood of the spherical surface $h=2/\lambda$. The correction (8.1) depends, of course, on the wavelength and will show fluctuations, which in the case of crystals increase rapidly with increasing wavelength.

In conclusion, one of the authors (G.P.) wishes to thank Professor I. I. Rabi for many stimulating con-

versations and Professors H. A. Bethe and J. G. Kirkwood for several helpful discussions.

APPENDIX.

TABLE OF FOURIER TRANSFORMS IN THREE-DIMENSIONAL SPACE

$F(\mathbf{r})$	$G(\mathbf{h})$	
$F(\mathbf{r})$	$\int F(\mathbf{r})\exp(2\pi i\,\mathbf{h}\cdot\mathbf{r})d\tau$	(1)
$\int G(\mathbf{h})\exp(-2\pi i\mathbf{h}\cdot\mathbf{r})d\mathbf{h}$	$G(\mathbf{h})$	(2)
$\delta(\mathbf{r})$	1	(3)
1	$\delta(\mathbf{h})$	(4)
$1/r^2$	π/h	(5)
$\exp(-\pi\alpha^2r^2)$	$\alpha^{-3}\exp(-\pi h^2/\alpha^2)$	(6)
$[1-\exp(-\pi\beta^2r^2)]/\pi r^2$	$(1/h)\phi(\pi^{\frac{1}{2}}h/\beta)$	(7)
$1-w(\mathbf{r})$	$1-\sigma(\mathbf{h})$	(8)

$$\phi(x)=2\pi^{-\frac{1}{2}}\int_x^\infty \exp(-t^2)dt$$

PHYSICAL REVIEW VOLUME 82, NUMBER 3 MAY 1, 1951

Interaction between the *d*-Shells in the Transition Metals. II. Ferromagnetic Compounds of Manganese with Perovskite Structure

CLARENCE ZENER
Institute for the Study of Metals, University of Chicago, Chicago, Illinois
(Received January 5, 1951)

Recently, Jonker and Van Santen have found an empirical correlation between electrical conduction and ferromagnetism in certain compounds of manganese with perovskite structure. This observed correlation is herein interpreted in terms of those principles governing the interaction of the *d*-shells of the transition metals which were enunciated in the first paper of this series. Both electrical conduction and ferromagnetic coupling in these compounds are found to arise from a double exchange process, and a quantitative relation is developed between electrical conductivity and the ferromagnetic Curie temperature.

I. INTRODUCTION

IN a recent paper,[1] the author has interpreted ferromagnetism as arising from the indirect coupling of incomplete *d*-shells via the conducting electrons. According to the viewpoint therein adopted, all unpaired electrons within each atom or ion strive to attain the configuration of lowest energy, in which, according to Hund's rule, all spins are parallel to one another. Since the conduction electrons carry along their own spins unchanged as they wander from atom to atom, they are able to move within an environment of parallel spins only if the spins of all the incomplete *d*-shells are pointing in the same direction. This indirect coupling via the conduction electrons will therefore lower the energy of the system when the spins of the *d*-shells are all parallel. In that paper it was further assumed that the direct coupling between incomplete *d*-shells always tends to align their spins in an antiparallel manner. It was thereby predicted that ferromagnetism would never occur in the absence of conduction electrons or of some other indirect coupling. As an example of the dependence of ferromagnetism on conduction electrons, the author mentioned the difference in the behavior of manganese atoms in the Heusler alloys and in $MnFl_2$. In both substances the Mn atoms are at least 40 percent further apart than in metallic manganese. The Heusler alloys are both conducting and ferromagnetic, while $MnFl_2$ is nonconducting and antiferromagnetic. An even more striking correlation between conductivity and ferromagnetism may be found in the recent work of Jonker and Van Santen[2,3] on compounds of manganese with a perovskite structure. It is the purpose of the present paper to discuss this correlation. After a brief review of the experimental data (Sec. II), a theory (Sec. III) is developed of the conductivity and ferromagnetism of these compounds. Here conductivity and ferromagnetism are found to be so closely connected that a relation [Eq. (9)] is established between the electrical conductivity, σ, and the Curie temperature, T_C.

II. REVIEW OF EXPERIMENTAL DATA

The perovskite structure is illustrated in Fig. 1. Small metal ions, in our case manganese ions, form a simple cubic lattice. Oxygen ions are at the centers of the cube edges. Large metal ions, such as La, Sr, Ca, Ba are at the center of each unit cube.

The compounds studied by Jonker and Van Santen[2,3] have the composition $(La_{1-x}A_x)MnO_3$, where A represents Ca, Sr, or Ba. Compounds having the extreme values $x=0$, 1 were neither ferromagnetic nor good electrical conductors, being in fact semiconductors. Only compounds with intermediate values of x were ferromagnetic, the strongest ferromagnetism occurring

[1] C. Zener, Phys. Rev. 81, 440 (1951).

[2] G. H. Jonker and J. H. Van Santen, Physica 16, 337 (1950).
[3] J. H. Van Santen and G. H. Jonker, Physica 16, 599 (1950).

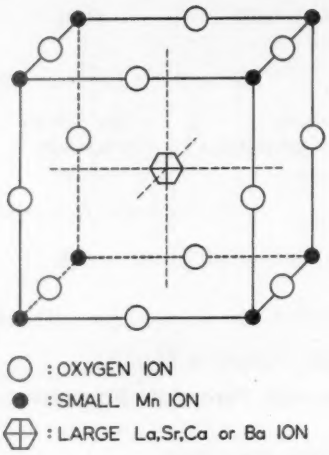

FIG. 1. Structure of manganese compounds with perovskite lattice.

in the range $0.2<x<0.4$. Only within this same range was the electrical conductivity good, the conductivity at 100°K decreasing by a factor of 0.01 as x decreased to 0.1 or increased to 0.6.

From a study of their observations Jonker and Van Santen concluded that the avidity of oxygen atoms for two electrons is sufficiently great to insure that each oxygen atom in the manganese compounds becomes doubly charged, regardless of the nature of atom A and of the value of the parameter x. In the compound of the extreme composition $LaMnO_3$, each metal atom must then become triply charged, the resulting ionic composition being $La^{3+}Mn^{3+}O_3^{2-}$. When, however, one replaces some of the La atoms by atoms having only two electrons outside a closed shell, as Ca, Sr, or Ba, a corresponding number of Mn atoms must become quadruply charged. In support of their viewpoint, Jonker and Van Santen presented the convincing evidence that in the optimum concentration range $0.2<x<0.4$, the saturation value of magnetization, extrapolated to 0°K, corresponds precisely to all the unpaired electrons in the manganese ions having spins pointing in the same direction; Mn^{3+} having 4, Mn^{4+} having 3 Bohr magnetons. They attributed the good electrical conductivity within the range $0.2<x<0.4$ to the transfer of electrons from Mn^{3+} to Mn^{4+} ions.

III. THEORY

The semiconducting property of pure $LaMnO_3$, and of this compound when small amounts, up to 10 percent, of Ca, Sr, or Ba are substituted for La, suggests the inappropriateness of describing the electronic states in terms of the customary band representation. The alternative description is in terms of localized atomic orbitals. The absence of conductivity of $LaMnO_3$ at low temperatures is obtained simply by requiring that each Mn ion have a charge of 3+. The semiconductivity at elevated temperatures then occurs by the thermal ionization of some of the Mn^{3+} ions.

When some of the La^{3+} ions are replaced by, say, Ca^{2+} ions, it is necessary that a corresponding number of Mn^{3+} ions be replaced by Mn^{4+} ions. As suggested by Jonker and Van Santen, it is the migration of these Mn^{4+} ions, accomplished by a Mn^{4+} ion capturing an electron from a neighboring Mn^{3+} ion, that gives rise to electrical conductivity. The precise mechanism whereby such an electron transfer takes place is not trivial, however, since the Mn^{3+} ions are sufficiently far apart as to have no appreciable overlapping. A detailed examination of this mechanism is of value, since we thereby obtain a clue to the relation between electrical conductivity and ferromagnetism.

We first investigate the simpler problem of the transfer of an electron from a Na atom through a closed shell, e.g., through Cl^-, to an adjacent Na^+ ion. The two Na nuclei will be considered sufficiently far apart so that this transfer would not have occurred at an appreciable rate without an intervening Cl^- ion. Towards this end we denote, by ψ_1 and ψ_2, the wave functions representing the configuration of the system before and after the electron transfer as follows:

$$\begin{aligned} \psi_1&: \quad \text{Na } \text{Cl}^-\text{Na}^+, \\ \psi_2&: \quad \text{Na}^+\text{Cl}^-\text{Na} \\ &\quad\ A\ \ B\ \ C. \end{aligned} \tag{1}$$

Since ψ_1 and ψ_2 are degenerate functions, more exact wave functions will be obtained by taking the linear combinations

$$\psi_+=\psi_1+\psi_2, \quad \psi_-=\psi_1-\psi_2. \tag{2}$$

We denote the energy difference of these two linear combinations by 2ϵ. If, initially, we locate the Na valence electron on one nucleus, this valence electron will thereafter oscillate between the two Na nuclei with the frequency

$$\nu=2\epsilon/h. \tag{3}$$

The exchange energy ϵ is given explicitly by the integral

$$\int \psi_1^*(H-\epsilon_0)\psi_2 d\tau, \tag{4}$$

where H is the hamiltonian of the whole system, ϵ_0 is the energy associated with the initial states ψ_1 and ψ_2, and the integral extends over the coordinates and spins of all the electrons. The dominant term in the integrand involves the following product of wave functions:

$$(A|1)^*(B|1)(B|2)^*(C|2). \tag{5}$$

Here $(A|\ )$, $(C|\ )$ are the wave functions of the valence electron on the left and right Na nucleus, respectively, while $(B|\ )$ is that $3p$ wave function of the Cl^- ion which has a zero angular momentum about the common axis. The form of (5) suggests that we visualize the

electron transfer from one Na^+ ion to the adjacent Na^+ ion as the transfer of an electron from the left Na atom to the central Cl^- ion simultaneously with the transfer of an electron from the central Cl^- ion to the right Na^+ ion. Such a transfer we shall call a *double exchange*.

A slight complication arises when we now return to our original problem of two Mn ions separated by an O^{2-} ion. In compliance with Hund's rule, we shall suppose that each Mn ion is in its configuration of highest multiplicity. If we then define ψ_1 and ψ_2 as follows, the integral (4) is nonvanishing only if the spins of the two *d*-shells are parallel.

$$\begin{aligned} \psi_1&: \ Mn^{3+}O^{2-}Mn^{4+}, \\ \psi_2&: \ Mn^{4+}O^{2-}Mn^{3+}. \end{aligned} \tag{6}$$

The lowest energy of our system thus corresponds to a parallel alignment of the spins of the two transition metal ions. This indirect coupling through the oxygen ion by means of a double exchange should not be confused with the indirect coupling introduced by Kramers,[4] and now called "superexchange." In our case, the system is inherently degenerate owing to the presence of Mn ions of two charges. The double exchange thereby introduced leads to a ferromagnetic alignment of spins. In Kramers' case only excited states are degenerate. The superexchange via these excited states leads to an antiferromagnetic alignment of spins.

We have now already encountered one relation between electrical conductivity and magnetism. Namely, we have seen that the lining up of the spins of adjacent incomplete *d*-shells of the Mn ions will be accompanied by an increase in the rate of migration of the Mn^{4+} ions, and hence by an increase in the electrical conductivity. The experiments of Van Santen and Jonker[3] do indeed show a marked increase in conductivity just in that narrow temperature interval in which spontaneous magnetization sets in.

We shall now demonstrate that the mechanism which leads to electrical conduction also insures a coupling which leads to ferromagnetism. Let ψ_1 and ψ_2 be defined by (6). We have then seen that the double exchange represented by the integral (4) is the mechanism for electrical conductivity. We have seen further that this double exchange between a Mn^{3+} and a Mn^{4+} ion occurs only when the spins of their respective *d*-shells point in the same direction. Now a stationary state is represented neither by ψ_1 nor by ψ_2, but by either of the two linear combinations of (2). Depending upon the sign of the exchange integral (4), the double exchange raises the energy associated with ψ_+, lowers the energy associated with ψ_-, or vice versa. Thus, the energy of one of these two stationary states is lowered by the double exchange which takes place when the *d*-shell spins are parallel. At low temperatures, regardless of the sign of the exchange integral, the energy of the system will therefore be lowered by a parallel alignment of spins.

It remains to establish a quantitative relation between electrical conductivity and ferromagnetism. On the one hand the magnitude of the exchange energy, ϵ, determines, through Eq. (3), the rate at which an electron jumps from a Mn^{3+} ion across an intervening O^{2-} ion to an adjacent Mn^{4+} ion. The diffusion coefficient for the Mn^{4+} ion is thus given by

$$D=a^2\epsilon/h,$$

where a is the lattice parameter. From the Einstein relation

$$\sigma=ne^2D/kT$$

between the electrical conductivity, σ, the diffusion coefficient D, and the number of ions (Mn^{4+}) per unit volume n, we obtain

$$\sigma=xe^2\epsilon/ahkT. \tag{7}$$

Here x is that fraction of the Mn ions which have a 4+ charge. On the other hand, the Curie temperature, T_c, is given approximately by

$$kT_c\cong\epsilon. \tag{8}$$

On elimination of the unknown exchange energy ϵ between Eqs. (7) and (8), we obtain

$$\sigma\cong(xe^2/ah)(T_c/T). \tag{9}$$

This relation agrees excellently with the data of Jonker and Van Santen, differing by not more than a factor of 2 from the observations in the center of the range $0.2<x<0.4$ which corresponds to good electrical conductivity and to strong ferromagnetism. In the absence of more detailed published experimental data, a refinement of the above calculations would hardly be significant.

[4] H. A. Kramers, Physica **1**, 191 (1934).

The Spectrum of He^3 I

MARK FRED, FRANK S. TOMKINS, JAMES K. BRODY, AND MORTON HAMERMESH
Argonne National Laboratory, Chicago, Illinois

(Received August 7, 1950)

Helium isotope shift measurements previously reported have been extended and the He^3 hyperfine structure partially resolved. The hfs of the ^3S levels is inverted, indicating a negative nuclear magnetic moment as expected. The splitting of the 2^3S level is 0.221 ± 0.005 cm^{-1}, while higher ^3S levels have a splitting of about 0.216 cm^{-1}, agreeing exactly with the expected values. The observed hfs agrees very well with that calculated by taking into account the perturbations of neighboring fine structure levels. The stronger hfs components of transitions to the ^3P and ^3D levels are not resolved, but the structure must be considered in evaluating the isotope shifts. By including contributions from reduced mass and coupling effects, it is found that the predicted and observed shifts differ by ~0.1 cm^{-1} in the sense that the He^3 ^3S and ^3D terms are higher and the ^1S and ^1D terms lower than expected, with respect to the ^3P and ^1P levels. The differences for S levels show an approximately linear decrease with term value T of $\sim-2.2\times10^{-6}T$. In addition, the trend of the differences for successive D series members indicates an increase in the repulsion of the ^3D and ^1D terms near the crossing at $n=8$ owing to the fact that the He^3 ^3D hfs is larger than the He^4 ^3D fine structure. The results suggest that the Hughes-Eckart coupling terms for the 2^3P and 2^1P levels are too low, by about 12 and 20 percent, respectively, when calculated with one-electron wave functions.

I. INTRODUCTION

ISOTOPE shifts in the spectrum of neutral helium have been reported on fractions of natural helium in which the He^3/He^4 ratio had been increased from the original 10^{-7} to approximately 10^{-2}. Bradley and Kuhn[1] reported $\Delta\nu=-0.83\pm0.03$ cm^{-1} for λ5015A and Andrew and Carter[2] reported $\Delta\nu=-1.045\pm0.010$ cm^{-1} for λ6678. A more favorable source of He^3 became available in this laboratory as the result of the β-decay of tritium (H^3), obtained by neutron irradiation of lithium in a nuclear reactor. Lines of a 1:1 mixture of He^4 and the pure He^3 so obtained could be measured more accurately than those of the above one percent samples, especially triplet lines, for which the shifts are smaller. In addition, each triplet line has a weak He^4 component lying near the main He^3 component, tending to mask it. A preliminary report[3] of shifts for a number of lines showed a small but definite disagreement with shifts calculated according to the standard theory, the shifts being smaller than those expected for lines of the triplet system and larger for the singlets. The agreement became better for successive series members, the difference being approximately proportional to the the square root of the term value of the upper state. Differences in triplet fine structure were also noted for the two isotopes.

The present measurements were undertaken with light sources which gave sharper lines. Shifts were measured for more lines, and the He^3 hyperfine structure was partially resolved and taken into account.

II. EXPERIMENTAL PROCEDURES

The experimental data to be presented were improved successively as each new set of measurements indicated the desirability of still greater accuracy and resolution. Thus, the first isotope shift measurements were made directly with a grating spectrograph, using as light source a discharge tube filled with a mixture of the two isotopes at room temperature and fairly high pressure and operated at high power consumption. The isotope shift measurements so obtained differed from the expected values, described below, by ~0.05 cm^{-1}, which was roughly three times the mean deviation of the individual measurements from the mean shift for each line. Thus, a real discrepancy appeared to be present, but it varied for different lines in a rather irregular manner. Another set of measurements was therefore undertaken with a Fabry-Perot interferometer, using the same discharge tube cooled with liquid nitrogen. These were the values first reported,[3] which established the discrepancies as real, with a systematic decrease for successive series members. It then appeared desirable to investigate the discrepancies more closely by extending the measurements to include more series members and to examine the structure of the He^3 triplet lines, which had been found to be of different width than those of He^4. This was facilitated by modifying the experimental technique so that separate exposures of the pure isotopes could be compared directly, thereby reducing overlapping, and using light sources which produced much sharper lines. In addition, as better observations were obtained, it became necessary to consider the calculated shifts more carefully for interpretation.

(a) Light Sources

The ideal source for the present purpose is the electrodeless discharge, since it will operate at a lower pressure than other sources, thus conserving the sample; there is less contamination or adsorption than with metallic electrodes, and the lines are relatively sharp. However, previous experience with spectrochemical isotopic assay of helium samples revealed a very rapid clean-up, so that tubes filled to only a low pressure

[1] L. C. Bradley and H. Kuhn, Nature **162**, 412 (1948).
[2] A. Andrew and W. W. Carter, Phys. Rev. **74**, 838 (1948).
[3] Fred, Tomkins, and Brody, Phys. Rev. **75**, 1772 (1949).

became inoperative in a matter of minutes. Hence, the first electrodeless discharge tubes used for isotope shift measurements were filled to the relatively high pressure of 5 mm Hg; and since pure He^3 was not available at the time, the He^3/He^4 ratio was adjusted to 1.2 as a matter of convenience in measurement of the shifts.

These discharge tubes were constructed by Pyrex tubing, one inch in diameter by six or eight inches long, with a plane Pyrex window fused on one end. They were excited by inserting them in a coil of about ten turns fed from a 30-Mc/sec oscillator by a tuned transmission line. The actual power dissipated in the tube is difficult to estimate but was probably of the order of 25 watts. Shifts were measured with this source with end-on observation at room temperature with the Baird grating spectrograph and at the temperature of liquid nitrogen with the interferometer and the stigmatic spectrographs.

The considerable width of the helium lines obtained with this source was a severe limitation on the accuracy of the isotope shift measurements. The *Doppler* contribution to the half-width is given by the following expression:

$$\Delta\nu = 0.96 \times 10^{-6} \nu (T/M)^{\frac{1}{2}},$$

where M is the atomic weight and T is expressed in 10^3 °K. For λ5875, for example, $\Delta\nu = 0.026$ cm^{-1} and 0.052 cm^{-1} for 80°K and 300°K, respectively. The observed widths were far larger, indicating that other factors were more important. These include *self-absorption* broadening, owing to the fact that as a line emitted inside a source of appreciable depth diffuses to the exterior by a process of absorption and re-emission, the peak is absorbed more strongly than the wings; *pressure* broadening, to which helium lines are especially sensitive; and *current* broadening, due directly to a fluctuating interatomic Stark effect, as well as produced indirectly by enhancement of pressure (resonance) and self-absorption broadening. These factors are also temperature-dependent, since considerable improvement resulted from operation at liquid nitrogen temperature.

To reduce the line width, as is indicated by the above considerations, the electrodeless discharge tubes finally adopted contained a 5-mm capillary over the central two inches and were viewed side-on in an effort to reduce broadening by self-absorption. It was found to be more convenient to adopt electrostatic (external electrodes) instead of magnetic (coil) excitation because the tuning was much less critical and there was less liquid nitrogen consumption. These tubes were filled with the pure isotopes and sealed off at about 0.3-mm Hg pressure. They were excited at as low a power as would sustain the discharge. The intensity was rather low, requiring exposure times for some lines of many hours, even for the fastest spectrograph. To facilitate taking the long exposures, an automatic liquid nitrogen level control was devised.[4]

[4] M. Fred and E. Rauh, Rev. Sci. Instr. **21**, 258 (1950).

Even these precautions yielded line widths severalfold as large as the Doppler widths, amounting to roughly a tenfold improvement. Further attempts to reduce the line width were unsuccessful. Hollow cathode tubes were found to offer no advantage. Line widths about equal to the Doppler widths were observed in absorption through a feebly excited discharge tube, but this method was applicable only to lines ending on metastable levels. Some consideration was given to the use of an atomic beam source, but this was abandoned as impracticable.

(b) Spectrographs

The first spectrograph used was a Baird 3-meter Eagle mounting used in the 2nd, 3rd, and 4th orders, with reciprocal dispersions of 2.7, 1.7, and 1.2 A/mm, respectively. The stigmatic instruments used with the interferometer were a Bausch and Lomb large Littrow prism spectrograph used with both quartz and glass optics; a Jarrell-Ash 21-foot Wadsworth mounting having a first-order dispersion of 5 A/mm; and a small Zeiss constant deviation spectrograph used with glass optics giving a separation between λ3888 and 10830 of 50 mm. The Bausch and Lomb spectrograph was considered to give interferometer fringes easiest to measure because the large plate tilt gave elliptical ring images which appeared as straight lines instead of arcs over the width of the slit image. The Jarrell-Ash had the largest dispersion, which was sometimes of advantage in interpreting complex interferometer patterns. The Zeiss was much faster than the other spectrographs, a fact which proved to be of importance.

(c) Interferometer

The Fabry-Perot etalon used in the present work was constructed in this laboratory and was modified gradually for increased stability as the desirability of long exposure times became evident. The interferometer was suspended from the lid of a double-walled box which was thermostated by circulating water between the walls. The box was pressure-tight, the interferometer plate adjustment being made by turning fine-pitch worm drives by shafts which extended through Wilson seals in the lid. By this arrangement the final adjustment could be made after putting the interferometer inside the box. The constant temperature bath supplying the circulating water maintained a given temperature to ±0.03°C over approximately a one-minute cycle; the mean temperature over the cycle remained constant for months to much less than 0.01°C. The etalon spacers were of Invar, but the spacer rings as well as the plate mountings were of brass. The control was sufficient to maintain the plate adjustment almost indefinitely, permitting comparison of separate exposures of the individual isotopes.

Etalon spacers of 2.48903, 2.99439, 3.50069, 4.95897, 7.50128, and 12.00721 mm have been used. (An erro-

neous calculation of the 5-mm spacer caused some of the isotope shifts first reported[3] to be too low by 0.8 percent.) The plates were silvered by evaporation from a molybdenum crucible heated by electron bombardment, the residual air pressure being about 10^{-6} mm Hg during the evaporation. The coating thickness could be controlled conveniently by measuring, with an optical pyrometer, the apparent brightness of a tungsten lamp filament observed through one plate. Transmittances at 6500A, ranging from 0.0025 to 0.25, were used.

(d) Comparators

In the absence of an adequate comparator at this laboratory, the first shifts were measured with a Leeds and Northrup recording microphotometer. These plates were later remeasured with the Société Genevoise comparator in the Department of Physics at the University of Chicago. Later plates were measured with a Gaertner comparator acquired by this laboratory. Measurements on the same plates with the three instruments appeared to have comparable precision. (This might not be the case for sharp lines.) However, comparison of microphotometer and comparator measurements of widened triplet lines disagreed by more than would be expected from the mean deviations, apparently owing to a significant difference in judging the center of a fringe on a microphotometer trace and through a comparator.

TABLE I. Isotope effect of pressure shift.

Transition	λ	$\Delta\nu/\Delta P$ He⁴	$\Delta\nu/\Delta P$ He³	$\frac{\partial}{\partial P}\frac{\Delta\nu}{\Delta M}$
2^3P-4^3S	4713	0.0097 ±0.0020 (5)[a]	0.0043 ±0.0012 (5)	+0.0054
5^3S	4120	0.0128 ±0.0013 (5)	0.0122 ±0.0021 (6)	+0.0006
6^3S	3867	0.0106 ±0.0080 (5)	−0.0063 ±0.0051 (4)	+0.0169
2^3P-3^3D	5875	0.6232 ±0.0068 (4)	−0.0285 ±0.0061 (4)	+0.0517
4^3D	4471	0.0072 ±0.0028 (5)	0.0057 ±0.0027 (5)	+0.0015
5^3D	4026	0.0082 ±0.0028 (5)	0.0056 ±0.0034 (6)	+0.0026
6^3D	3819	0.0167 ±0.0041 (5)	0.0165 ±0.0052 (6)	+0.0002
2^1P-4^1S	5047	0.0049 ±0.0038 (3)	0.0117 ±0.0015 (4)	−0.0068
5^1S	4437	0.0091 ±0.0020 (5)	0.0112 ±0.0047 (6)	−0.0021
6^1S	4168	0.0029 ±0.0057 (5)	0.0026 ±0.0048 (5)	+0.0003
2^1P-4^1D	4921	0.0056 ±0.0020 (4)	0.0104 ±0.0026 (4)	−0.0048
5^1D	4387	0.0072 ±0.0013 (5)	0.0115 ±0.0015 (5)	−0.0043
6^1D	4143	0.0065 ±0.0018 (6)	0.0115 ±0.0020 (5)	−0.0050
7^1D	4009	0.0131 ±0.0045 (5)	0.0106 ±0.0026 (6)	+0.0025
2^1S-3^1P	3888	0.0084 ±0.0032 (6)	0.0199 ±0.0045 (5)	−0.0115

[a] (N) indicates N measurements.

III. OBSERVED ISOTOPE SHIFTS

The modifications in the light sources described above reduced the mean deviations of the individual measurements fivefold to tenfold, compared with the original grating shifts, so that the latter are of value chiefly in confirming the interpretation of the interferometer patterns. The most precise data were obtained with the low pressure electrodeless discharge source. The interferometer shifts measured with the cooled high pressure tube showed mean deviations which averaged about 50 percent higher, owing to the greatly increased width. In addition, the magnitudes of the isotope shifts for high and low pressure sources differed by amounts which seemed to be slightly outside the limits of error. An attempt to confirm this phenomenon, constituting an isotope effect of a pressure shift, was made by comparing, directly, ring diameters of successive exposures of different sources taken with the same interferometer adjustment. These data are shown in Table I. In almost every case the frequencies of the various spectrum lines are increased in the high pressure source. The pressure shift of the triplet lines toward higher frequencies is slightly greater for He^4 than for He^3; and, since the He^4 lines are on the high frequency side of the He^3 lines, the frequency separation, i.e., the isotope shift, is increased. For the singlet lines, on the other hand, the pressure shift is greater for the He^3 lines, and they are moved closer to the He^4 lines. It must be emphasized that the data must be regarded as qualitative only. They were taken near the end of the useful life of the high pressure mixture tube when its pressure was no longer very high and it was in the process of cleaning up during these exposures. Consequently, the pressure difference between the two light sources was less for higher series members because they required much longer exposure times than the lower members. Moreover, the wavelength to be assigned to a pressure-broadened line is somewhat arbitrary. Nevertheless, it is believed that the data of Table I are significant in indicating the relative magnitude of the pressure shift for the two isotopes in that the singlet lines behave differently from the triplets, which would not be expected if the measurements reflect merely a difference in pressure broadening. The most reliable isotope shift measurements, the set taken with the low pressure electrodeless discharge sources, are listed, except as noted, in cm^{-1} in Table II. The $\Delta\nu$'s are the mean of several plates and spacers (usually 5 mm and 3 mm).

IV. OBSERVED HYPERFINE STRUCTURE

The observed He^3 hyperfine structure intervals are listed in Table III. These measurements were made using interferometer spacers of 3.0 and 3.5 mm. For such short spacers the wave number separation between successive orders of interference is sufficiently great

TABLE II. Observed isotope shifts of helium lines.

Transition	λ	$-\Delta\nu$	$\epsilon(N)$[a]	Transition	λ	$-\Delta\nu$	$\epsilon(N)$
2^3P-3^3S	7065	−0.006[b]	5(17)	2^1P-3^1S	7281	1.046	5(14)
4	4713	+0.297	5(24)	4	5047	1.333	4(17)
5	4120	0.438	5(35)	5	4437	1.461	4(27)
6	3867	0.508	7(12)	6	4168	1.529	1(15)
7	3732	0.548[c]	11(9)	7	4023		
8	3652	0.586[c]	12(8)	8	3935	1.606[c]	8(8)
2^3P-3^3D	5875	0.123	7(24)	2^1S-3^1D	6678	1.124	4(26)
4	4471	0.360	5(19)	4	4921	1.358	6(21)
5	4026	0.474	4(43)	5	4387	1.462	5(30)
6	3819	0.547	6(38)	6	4143	1.512	4(32)
7	3705	0.592	7(20)	7	4009	1.532	7(25)
8	3634	0.617[c]	16(9)	8	3926	1.543[c]	7(8)
2^3S-2^3P	10830	1.151[b]	3(7)	2^1S-3^1P	5015	0.849	3(34)
3	3888	1.404	9(32)	4	3964	1.165	5(73)
4	3187	1.535[d]	40(6)	5	3613	1.304	4(34)
				6	3447	1.344[c]	13(6)
				7	3354	1.375[c]	14(8)

[a] $\epsilon(N)$ indicates mean deviation in 10^{-3} cm^{-1} of N ring diameter differences on all plates.
[b] Strong He^4 component.
[c] High pressure source.
[d] Grating measurement.

(1.67 and 1.43 cm^{-1}, respectively) that the complete structure of a line is contained within one order. The hfs components are distributed in such a way that longer spacers resulting in overlapping orders could not be used without superposition, so that in addition to the considerable line width, a considerable instrumental width was introduced. It was apparent from the shapes of the fringes that much unresolved structure was present. The He^3 hfs situation is much less favorable than is the case for the He^4 fine structure, for which spacers of 7.5, 12, and 15 mm can be used, producing overlapping of the single weak component by one, two, and three orders of the two strong components, respectively. In addition, the intensity distribution of the He^3 hfs is less favorable than in He^4 in that the weak components are relatively weaker compared with the strong components.

Structures of some typical lines are illustrated in Figs. 1 to 4 as microphotometer traces of one order of interferometer patterns taken with a 3.0 or 3.5 spacer. Also shown are the calculated centers of gravity of hfs groups, as discussed below. Much better resolution for the He^4 lines could be exhibited with longer spacers, as noted above; but since these cannot be used for He^3 lines, the figures show the He^4 fringes as encountered in the isotope shift measurements, for which consecutive exposures of the two isotopes were required

The separations listed in Table III were obtained with both short spacers. To avoid the possible existence of structure completely different from that expected, exposures of λ10830 were taken in the first order of the Jarrell-Ash spectrograph without an interferometer. The grating had 60,000 lines, which were not enough to resolve the two weak components because of the line width; but the greater width of the unresolved pair was evident when compared with the He^4 exposure. No unexpected components showed. Similar exposures were made of λ5875 in the second order to verify its structure.

The microphotometer traces shown, of course, do not provide quantitative intensities without further calibration, the stronger lines tending to be compressed.

V. PREDICTED ISOTOPE SHIFTS OF HELIUM TERMS

The number of factors by which the He^3 spectrum differs from that of He^4 is greater than might at first be appreciated. It should be pointed out that it is especially important for the interpretation of the observations to have calculated values of the shifts because the term shifts cannot be determined uniquely from the observed line shifts by the combination principle, as can the terms themselves.

(a) Reduced Mass Effect

The effect of the finite mass of the nucleus, in atoms with more than one electron, was treated by Hughes and Eckart.[5,6] In this treatment the expression for the kinetic energy of the nucleus of mass M and of the two electrons each of mass m, when transformed from a laboratory to a moving set of coordinates, contains a term describing the motion of the center of mass, which can be ignored here; a term for each electron of the form $p_i^2[(1/m)+1/M]/2$; and a term of the form $\mathbf{p}_1\cdot\mathbf{p}_2/M$, arising from the fact that the relative coordinates are measured from the nucleus and not from the center of mass. Except for the cross-product term, the momentum of each electron is the same in terms of the reduced mass μ as it would be in terms of the electron mass m in the case of an infinite nuclear mass. Hence, from the virial theorem, the energy

TABLE III. Observed He^3 hyperfine structure intervals.

Transitions	λ	Separation from strongest component[a]			$\Delta T(n^3S)$
2^3P-2^3S	10830	−0.191±6(7),	0.192±6(21),	0.907±6(20), 1.128±6(20)	0.221±5(30)
3	7065		−0.186±7(5),	−0.904±5(6), −1.120±5(6)	0.216±4(9)
4	4713		−0.193±6(9),	−0.911±7(12), −1.127±7(12)	0.216±6(22)
5	4120		−0.183±2(2),	−0.920±2(3), −1.142±9(3)	0.222±9(16)
					$\Delta T(n^3D)$
2^3P-3^3D	5875		−0.168±3(7),	−0.886±6(10), −1.092±6(10)	0.206±4(15)
4	4471		−0.161±10(7),	−0.910±2(9), −1.118±6(9)	0.208±6(23)
5	4026			−0.905±3(3), −1.106±9(3)	0.201±9(14)
2^3S-3^3P	3888		0.372±5(3)		

[a] $\Delta\nu\pm\epsilon(N)$: ϵ indicates the mean deviation in 10^{-3} cm^{-1} for N observations.

[5] D. S. Hughes and C. Eckart, Phys. Rev. 36, 694 (1930).
[6] W. H. Keesom, *Helium* (Elsevier, Amsterdam, 1942), Chapter VIII.

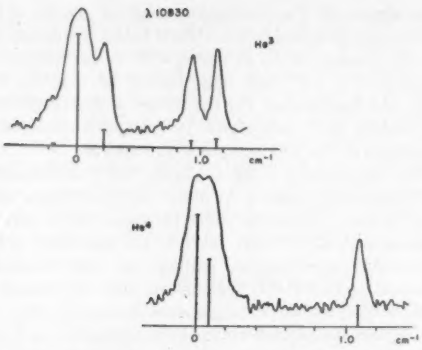

FIG. 1. Structure and isotope shift for λ10830, 2^3S-2^3P. The microphotometer trace covers one order of an interferometer pattern. The vertical lines indicate the calculated incompletely resolved He^3 hfs and the measured He^4 fine structure.

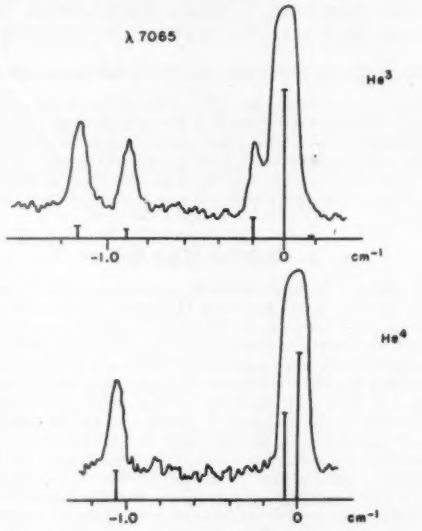

FIG. 2. Structure and isotope shift of λ7065, 2^3P-3^3S.

of any level in the isotopic atom is μ/m times the energy of the atom with $M=\infty$, subject only to the condition that the potential energy contains only terms in $1/r$, i.e., ignoring spin energy and relativity. Each term in the He^3 energy level diagram is therefore raised by

$$\Delta T_1=[(\mu^{(3)}/m)-\mu^{(4)}/m]T=(\Delta\mu/m)T,$$

where T is the He^4 term value.

Using 3.016988 and 4.003860 for the atomic weights of the neutral atoms ($M+2m$), as listed by Mattauch,[7] together with $m=0.00054862$ as given by DuMond and Cohen,[8]

$$\Delta\mu/m=0.99981812-0.99986296=-4.484\times10^{-5}.$$

[7] J. Mattauch, *Nuclear Physics Tables* (Interscience Publishers, Inc., New York, 1946), p. 126.

[8] J. W. M. DuMond and E. R. Cohen, Revs. Modern Phys. **20**, 82 (1948).

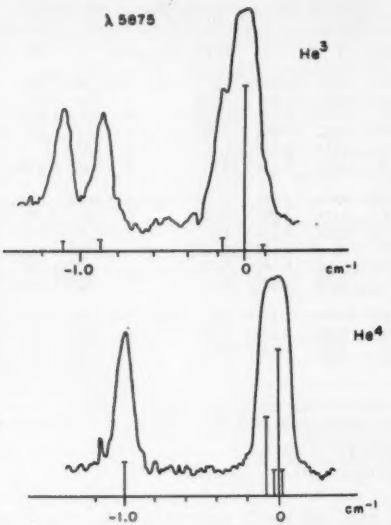

FIG. 3. Structure and isotope shift of λ5875, 2^3P-3^3D.

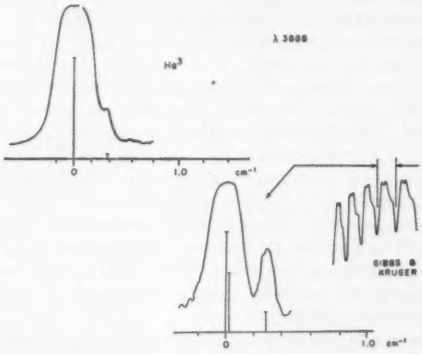

FIG. 4. Structure and isotope shift of λ3888, 2^3S-3^3P. He^4 below.

If integral nuclear masses are used, the calculation of $\Delta\mu/m$ comes out significantly different, namely, $0.99981716-0.99986286=-4.570\times10^{-5}$, owing to the appreciable difference in the mass excess of He^3 as compared with that of He^4. The reduced mass shifts calculated with the former value are given in Table IV. (All term values and term shifts in this paper are expressed in cm^{-1} measured positive downward, with $T=0$ corresponding to the ground state of the ion. In general, ΔT refers to the value of T for He^3 with respect to He^4, i.e., $\Delta T=T^{(3)}-T^{(4)}$, which is negative for the reduced mass shift.)

(b) Coupling Effect

While the reduced mass effect can be calculated immediately, the $\mathbf{p}_1\cdot\mathbf{p}_2/M$ term must be evaluated by a perturbation calculation, for which wave functions are necessary. These are known only approximately for the excited states. Assuming functions which are appropriate linear combinations of products of hydrogenic functions, the only non-zero matrix element of $\mathbf{p}_1\cdot\mathbf{p}_2/M$ is an

exchange integral for P terms which, on evaluation, yields the formula,

$$\Delta T_3 = \pm\frac{m}{M}\frac{128}{3}(Z_1Z_2)^{\frac{1}{2}}\frac{(Z_1n-Z_2)^{2n-4}}{(Z_1n+Z_2)^{2n+4}}n^3(n^2-1)R_\infty,$$

where Z_1 is the effective nuclear charge for the $1s$ electron and Z_2 for the excited electron (all terms observed here have one electron in the $1s$ orbital). The shifts are upward for singlets and downward for triplets. Table IV lists the calculated coupling shifts, with the Z's used as determined independently by the variational procedure by Eckart[9] and Goldberg.[10]

(c) Polarization Effect

While the preceding evaluation of the coupling effect gave zero shift for S and D terms, a more exact calculation by Bethe,[11] using Hylleraas' 6th approximation wave function, gives a ground state shift of -5.2 cm^{-1} for He^4-He^∞. The corresponding He^3-He^4 shift would be $\Delta T_3=-0.43$ cm^{-1}. This indicates that finite shifts for the excited S and D states, and presumably more accurate shifts for the P states, would be obtained using more accurate wave functions. Hamermesh and Eisner[12] have recently calculated He^3-He^4 shifts for the 2^1S and 2^3S states as $\Delta T_3=+0.047$ and $+0.010$ cm^{-1}, respectively, using Hylleraas-type wave functions as determined by Huang.[13] Unfortunately, accurate wave functions for other excited states are not yet available.

TABLE IV. Calculated term isotope shifts.

Term	T	ΔT_1	Z_1	Z_2	ΔT_2	ΔT_3	ΔT
2^3S	38445	−1.724			0	+0.010	−1.714
3	15074	−0.676			0		−0.676
4	8013	−0.359			0		−0.359
5	4964	−0.223			0		−0.223
6	3375	−0.151			0		−0.151
7	2242	−0.101			0		−0.101
8	1849	−0.083			0		−0.083
2^3P	29223	−1.310	1.99	1.09	+0.565		−0.745
3	12746	−0.571	2.00	1.10	+0.175		−0.396
4	7094	−0.318	2.00	1.10	+0.072		−0.246
3^3D	12209	−0.547			0		−0.547
4	6866	−0.308			0		−0.308
5	4394	−0.197			0		−0.197
6	3051	−0.137			0		−0.137
7	2241	−0.100			0		−0.100
8	1716	−0.077			0		−0.077
2^1S	32033	−1.436			0	+0.047	−1.389
3	13446	−0.603			0		−0.603
4	7371	−0.330			0		−0.330
5	4647	−0.208			0		−0.208
6	3196	−0.143			0		−0.143
7	2332	−0.105			0		−0.105
8	1776	−0.080			0		−0.080
2^1P	27176	−1.218	2.003	0.965	−0.372		−1.590
3	12101	−0.543	2.00	1.00	−0.117		−0.660
4	6818	−0.306	2.00	1.00	−0.050		−0.356
5	4368	−0.196	2.00	1.00	−0.026		−0.222
6	3036	−0.136	2.00	1.00	−0.015		−0.151
7	2232	−0.100	2.00	1.00	−0.009		−0.109
3^1D	12206	−0.547			0		−0.547
4	6864	−0.308			0		−0.308
5	4392	−0.197			0		−0.197
6	3050	−0.137			0		−0.137
7	2241	−0.100			0		−0.100
8	1715	−0.077			0		−0.077

(d) Fine Structure

Although the triplet fine structure is fairly satisfactorily described in terms of electron magnetic dipole spin-spin and spin-orbit interactions, which should not depend on nuclear mass, the structure must be considered because it is only partially resolved. The triplet terms are inverted with intervals in the ratio 14:1 instead of 1:2 for ^3P terms and 2:3 for ^3D terms. The fine structure separations are listed in Table V.

It may be of interest to observe that the values obtained by Gibbs and Kruger[14] for the 3^3P intervals are spurious, in the opinion of the authors, being due apparently to self-reversal in the λ3888 transition to the metastable 2^3S level. Gibbs and Kruger included a microphotometer trace of this line showing two strong components of approximately equal intensity just separated (separation 0.165 cm^{-1}) and a weak third component on the shoulder of a strong peak. The present authors obtained traces, as shown in Fig. 5, in which the resolution of the weak component is much better, but the strong peak is much narrower than in the published work, with no trace of doubling. The separation between strong and weak peaks is very near that from Gibbs and Kruger's weak component to the minimum between their two strong peaks. The present finding is in agreement with the experimental results of Houston[15] and with theory.[16]

Most of the observed triplet lines involve the 2^3P level, of which the two strong components are on the limit of resolution, while the third, weak component is usually well resolved. For transitions showing complete resolution, the center of gravity of the strong components must be computed if isotope shifts are to be compared with other lines only partially resolved. Moreover, the center of gravity of the 2^3P term lies 0.067 cm^{-1} above the 2^3P_1 level, 0.145 cm^{-1} above the 2^3P_2 level, or 0.096 cm^{-1} above the center of gravity of the two strong components. It is, of course, the shift of the center of gravity in the case of the triplet terms which was computed in the previous sections; however, each fine structure component will presumably be shifted on the same amount.

TABLE V. He^4 fine structure intervals.

Term	Interval		Theory[a,b]	Literature	Authors[a]
2^3P	$J=2\leftrightarrow J=1$		0.068	0.078[d] 0.071[e] 0.078[f]	0.079±2(4)
	1	0	0.94	0.996[d] 0.992[e] 0.994[f]	0.991±3(13)
3^3P	2	1	0.018		
	1	0	0.218		
	2,1 c.g.	0		0.286[e]	0.287±4(20)
3^3D	3	2	0.0025	0.00–0.01[g]	0.005[h]
	3	1	0.0451	0.047	0.054
4^3D	3	1	0.019	0.016[g]	

[a] See reference 6.
[b] G. Araki, Proc. Phys. Math. Soc. Japan 19, 128 (1937).
[c] $\Delta\nu\pm\epsilon(N)$: ϵ indicates the mean deviation in 10^{-3} cm^{-1} for N observations.
[d] W. F. Meggers and C. J. Humphreys, J. Research Nat. Bur. Stand. 13, 293 (1934).
[e] W. V. Houston, Proc. Nat. Acad. Sci. U. S. 13, 91 (1927).
[f] H. Lowenthal and K. W. Meissner, Master's Thesis, Dept. of Physics, Purdue University, 1946.
[g] G. Hansen, Verhandl deut. physik Ges. 10, 5 (1929).
[h] Using Hansen's $\Delta\nu=0.074\pm3$ percent for λ5875 strong component and the authors' $\Delta T=0.079$ for the ^3P splitting (reference g).

[9] C. Eckart, Phys. Rev. 36, 878 (1930).
[10] L. Goldberg, Phys. Rev. 56, 696 (1939).
[11] H. Bethe, *Handbuch der Physik* (Springer Verlag., Berlin, 1933), Vol. XXIV, 1, p. 374.
[12] M. Hamermesh and E. Eisner, private communication.
[13] Su-Shu Huang, Astrophys. J. 108, 354 (1948).
[14] R. C. Gibbs and P. G. Kruger, Phys. Rev. 37, 1559 (1931).
[15] W. V. Houston, Proc. Nat. Acad. Sci. U. S. 13, 91 (1927).
[16] G. Araki, Proc. Phys.-Math. Soc. Japan 19, 128 (1937).

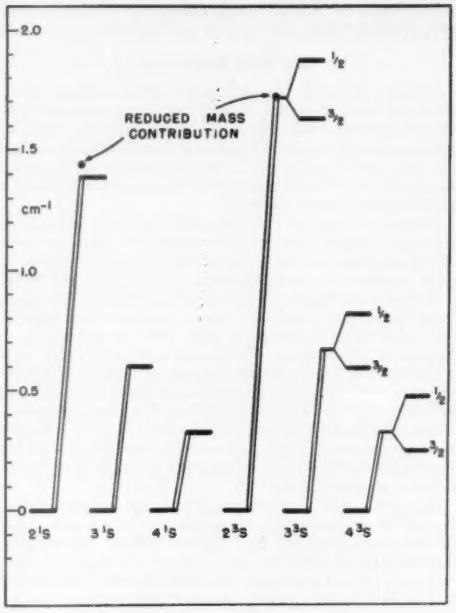

FIG. 5. Calculated isotope shifts and unperturbed He^3 hfs for S terms.

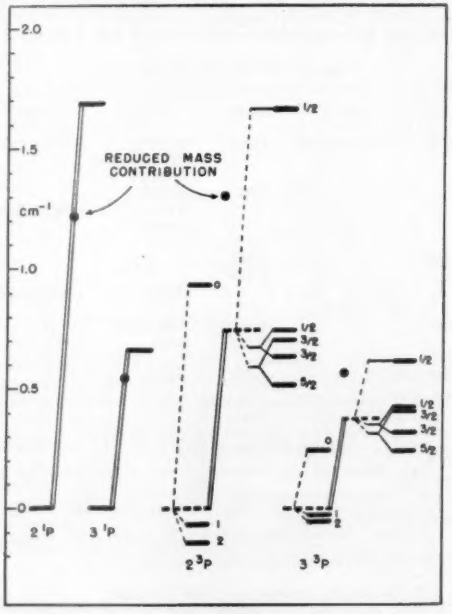

FIG. 6. Calculated isotope shifts and unperturbed He^3 hfs for P terms.

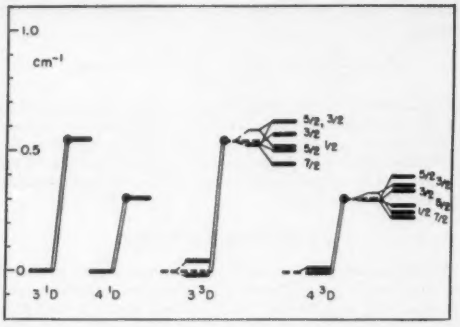

FIG. 7. Calculated isotope shifts and unperturbed He^3 hfs for D terms.

(e) Hyperfine Structure

The He^3 nucleus has a spin[17] of $\frac{1}{2}\hbar$ and a magnetic moment of $(-)2.12815$ nuclear magnetons.[18] The hyperfine structure to be expected in He^3I can be calculated from the usual formulas[19,20] as follows:

$$\Delta T_{I,J}=-\tfrac{1}{2}A[F(F+1)-I(I+1)-J(J+1)],$$
$$A(^3S_1)=\tfrac{1}{2}(a_1+a_2),$$
$$A(^3L_{l+1})\sim a_1/2(l+1),$$
$$A(^3L_l)\sim a_1/2l(l+1),$$
$$A(^3L_{l+1})\sim -a_1/2l,$$
$$A(^1L_l)=0.$$

Here a_1 and a_2 are the hydrogenic splitting factors for the $1s$ and nl electrons, respectively:

$$a_{n0}=(8/3)(R\alpha^2Z^3/n^3)(g_I/1836)$$
$$=-0.0361Z^3/n^3\ \text{cm}^{-1},$$
$$a_1=-0.289\ \text{cm}^{-1}\ (\text{for } Z=2),$$
$$a_{nl}=(R\alpha^2Z^3/n^3)(g_I/1836)/(l+\tfrac{1}{2})l(l+1)$$
$$=-0.107/n^3(l+\tfrac{1}{2})l(l+1)\ \text{cm}^{-1}.$$

The contribution of the excited electron is negligible compared with a_1 except for low ^3S states.

The term structures ΔT_4 predicted from the above formulas are listed in Table VI and are shown in Figs. 5 to 7. No hfs should

TABLE VI. Calculated unperturbed hyperfine structure of He^3 terms.

Term	A	ΔT_4 $F=1/2$	$F=3/2$	$F=5/2$	$F=7/2$	$3/2-1/2$
2^3S_1	−0.162	−0.162	+0.081			0.244
3^3S_1	−0.150	−0.150	+0.075			0.225
4^3S_1	−0.147	−0.147	+0.073			0.220
5^3S_1	−0.146	−0.146	+0.073			0.218
∞^3S_1	−0.144	−0.144	+0.072			0.217
n^3P_0	0	0				
n^3P_1	−0.072	−0.072	+0.036			
n^3P_2	−0.072		−0.108	+0.072		
n^3D_1	+0.072	+0.072	−0.036			
n^3D_2	−0.024		−0.036	+0.024		
n^3D_3	−0.048			−0.096	+0.072	

[17] A. E. Douglas and G. Herzberg, Phys. Rev. **76**, 1529 (1949).
[18] H. L. Anderson, Phys. Rev. **76**, 1460 (1949).
[19] S. Goudsmit and R. F. Bacher, Phys. Rev. **34**, 1501 (1929).
[20] H. Kopfermann, *Kernmomente* (Akademische Verlagsgesellschaft, Leipzig, 1940), p. 31.

TABLE VII. Calculated unperturbed hyperfine structure of some He^3 transitions.

	F	2^3P_0 1/2	2^3P_1 1/2	2^3P_1 3/2	2^3P_2 3/2	2^3P_2 5/2	λ
2^3S_1	1/2	+0.899 5.6	−0.020 7.5	−0.128 3.7	−0.063 55.5	—	10830
	3/2	+1.142 11.1	+0.223 3.7	+0.115 18.5	+0.180 11.1	0.000 100	
3^3S_1	1/2	−0.917 5.6	+0.002 7.5	+0.110 3.7	+0.045 55.5	—	7065
	3/2	−1.142 11.1	−0.223 3.7	−0.115 18.5	−0.180 11.1	0.000 100	
3^3D_1	1/2	−1.088 1.7	−0.169 2.2	−0.061 1.1	−0.126 16.7	—	
	3/2	−0.980 3.3	+0.061 1.1	+0.047 5.6	−0.018 3.3	+0.162 30	
3^3D_2	3/2	—	−0.110 16.7	−0.002 3.3	−0.067 18	+0.113 2	5875
	5/2	—	—	−0.062 30	−0.127 2	+0.053 28	
3^3D_3	5/2	—	—	—	−0.012 70	+0.168 5	
	7/2	—	—	—	—	0.000 100	
	F	3^3P_0 1/2	3^3P_1 1/2	3^3P_1 3/2	3^3P_2 3/2	3^3P_2 5/2	
2^3S_1	1/2	+0.116 5.6	−0.078 7.5	−0.186 3.7	−0.067 55.5	—	3888
	3/2	+0.359 11.1	+0.165 3.7	+0.057 18.5	+0.180 11.1	0.000 100	

occur in singlet terms for strict Russell-Saunders coupling, which is very nearly the case in helium. The splitting constants for the triplet terms have been given a negative sign, corresponding to a negative nuclear magnetic moment expected for an odd-neutron nucleus; but the sign of the moment has not been observed directly.[18] The negative sign would cause the hfs to be inverted, the level with highest F value lying lowest (except for $^3D_1$, $^3F_2$, etc.). However, the closeness of the spacing would make identification of the levels difficult except in the case of the ^3S levels. The structure of the n^3S terms can be observed directly from transitions to the 2^3P_0 level, which is well separated from the other 2^3P levels and not split, giving a series of doublets with separations equal to the various n^3S hfs splittings (0.244, 0.225, $\cdots$, 0.217 cm^{-1} for $n=2, 3, \cdots, \infty$, respectively). The intensity formula for the transitions $J=0$, $F=\frac{1}{2}\rightarrow J=1$, $F=\frac{1}{2}, \frac{3}{2}$ gives an intensity ratio of 2:1, corresponding to the statistical weights $2F+1$ for the two hfs levels. Hence, if the hfs is indeed inverted, the low frequency component of the doublets should be the stronger (except for $n=2$, since 2^3S lies below 2^3P). The identification of the F values of the doublets can also be made by the Zeeman effect.

The predicted hfs's of some representative lines are given in Table VII. The frequencies of the components were calculated from the term splittings of Table VI, combined with the fine structure separations given in the last column of Table V. The intensities were calculated from the usual formulas.[21] The line structures calculated from the term splitting and intensity formulas are shown in Figs. 8 to 11.

[21] See reference 20, p. 52.

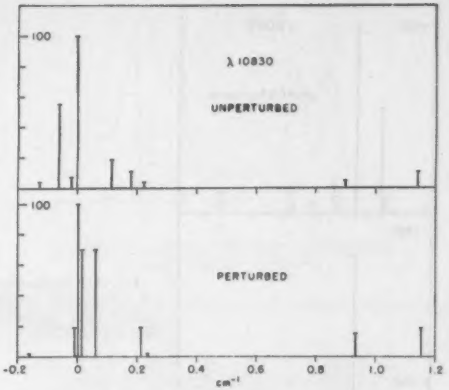

FIG. 8. Comparison of calculated unperturbed and perturbed He^3 hfs for λ10830.

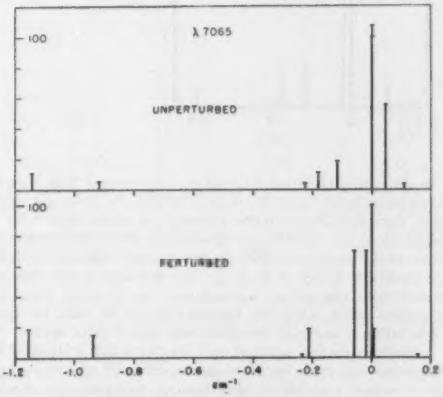

FIG. 9. Comparison of calculated unperturbed and perturbed He^3 hfs for λ7065.

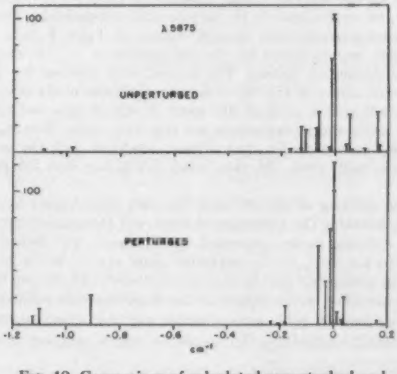

FIG. 10. Comparison of calculated unperturbed and perturbed He^3 hfs for λ5875.

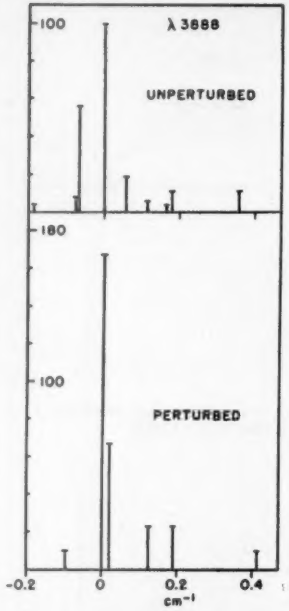

FIG. 11. Comparison of calculated unperturbed and perturbed He^3 hfs for λ3888.

In the case of the ^3P and ^3D states, inspection of Figs. 6 and 7 shows immediately that the usual formulas are really not applicable, since the calculated hfs splittings are of the same order of magnitude as the fine structure separations, while the formulas are based on the assumption that the hfs is small compared with the fine structure. Hence, it is to be expected that levels with the same F value originating from adjacent fine structure levels will be pushed apart, while the formulas should be valid for those levels within a multiplet for which only one F value occurs.

A similar situation is found in Li^7II, for which a detailed hfs calculation was made by Güttinger and Pauli,[22] who treated the fine structure and hfs as simultaneous perturbations. Similar calculations (by M. Hamermesh) based on the Güttinger-Pauli treatment have been carried out for He^3I. The resulting term structures are listed in Table VIII. Zero-term value has been taken as the original, unsplit position of the level of highest J value, for convenience in the isotope shift comparisons. The fine structure intervals from the last column of Table V have been adopted, supplemented by the assumption of a $1/n^3$ decrease where details are lacking. The revised level schemes for a few terms are shown in Fig. 12, with the magnitudes of the perturbations indicated in units of 10^{-3} cm^{-1}. It will be seen that for the close levels the perturbations are relatively large. Whereas the simple formulas predict that adjacent hfs levels with the same F value actually cross, the more exact calculation does not permit this.

The splitting of the 2^3S term has also been revised in Table VIII, following the discussion of Breit and Doermann[23] for LiII. The splitting factor, expressed by Goudsmit and Bacher[19] as $A(^3S)=\frac{1}{2}(a_1+a_2)$, can be evaluated more exactly in the present case by noting that the electron-nuclear moment interaction energy is proportional to the square of the wave function evaluated at the nucleus. A good approximation for the wave function is $N[u(1)v(2)-u(2)v(1)]$, the square of which involves a cross-product term which does not vanish, because the effective nuclear charges are different. Using the Z's which Eckart[9] found minimized, the energy of the 2^3S term, namely, $Z_1=2.01$ and $Z_2=1.53$, the 2^3S splitting calculated from $A(^3S)=\frac{1}{2}(a_1+a_2)$, comes out 0.232 cm^{-1}. Taking into account the cross-product term the splitting is reduced to 0.222 cm^{-1}.

TABLE VIII. Calculated perturbed hyperfine structure of He^3 terms.

Term	$F=1/2$	$F=3/2$	ΔT $F=5/2$	$F=7/2$
2^3S	−0.148	+0.074		
$\infty\,^3S$	−0.144	+0.072		
2^3P_0	−1.081			
2^3P_1	−0.139	−0.163		
2^3P_2		+0.013	+0.072	
3^3P_0	−0.338			
3^3P_1	−0.053	−0.168		
3^3P_2		+0.072	+0.072	
3^3D_1	+0.018	−0.174		
3^3D_2		+0.043	−0.149	
3^3D_3			+0.072	+0.072
4^3D_1	+0.055	−0.152		
4^3D_2		+0.064	−0.143	
4^3D_3			+0.072	+0.072
$\infty\,^3D_1$	+0.072	−0.144		
$\infty\,^3D_2$		+0.072	−0.144	
$\infty\,^3D_3$			+0.072	+0.072

The perturbations of the levels can be expected to have a considerable effect on the intensities of transitions, since the intensity

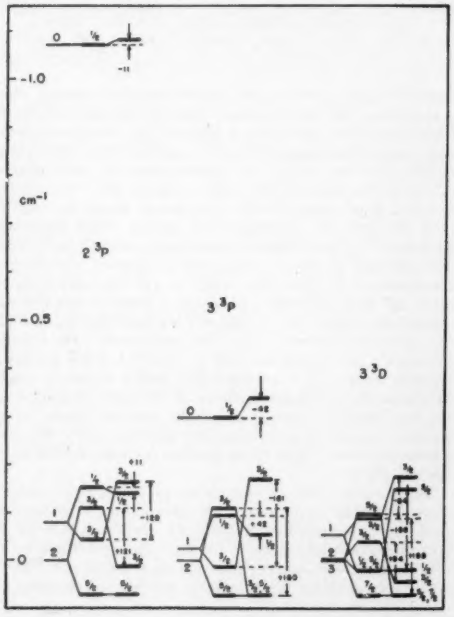

FIG. 12. Calculated perturbations of He^3 term hfs.

[22] P. Güttinger and W. Pauli, Z. Physik. 67, 743 (1931).
[23] G. Breit and F. W. Doermann, Phys. Rev. 36, 1732 (1930).

TABLE IX. Calculated perturbed hyperfine structure of some He^3 transitions.

	F	2^3P_0 1/2	2^3P_1 1/2	2^3P_1 3/2	2^3P_2 3/2	2^3P_2 5/2	λ
2^3S_1	1/2	0.933 15	−0.009 19	0.015 65	−0.161 2	—	10830
	3/2	1.155 19	0.213 19	0.237 2	0.061 65	0.002 100	
3^3S_1	1/2	−0.937 15	0.005 19	−0.019 65	0.157 2	—	7065
	3/2	−1.153 19	−0.211 19	−0.235 2	−0.059 65	0.000 100	
3^3D_1	1/2	−1.099 12	−0.157 9	−0.181 0.6	−0.005 7	—	
	3/2	−0.907 22	0.035 20	0.011 9	—	—	
3^3D_2	3/2	−1.124 6	−0.182 13	−0.206 0.4	−0.030 32	0.029 2.5	5875
	5/2	—	—	−0.014 72	0.162 2.5	—	
3^3D_3	5/2	—	—	−0.235 1.5	−0.059 50	0.000 22	
	7/2	—	—	—	—	0.000 100	
4^3D_1	1/2	−1.136 12	−0.194 9	−0.218 0.6	−0.042 7	—	
	3/2	−0.929 19	0.013 22	−0.011 7	—	—	
4^3D_2	3/2	−1.145 7	−0.203 10	−0.227 0.6	−0.051 31	0.008 2.5	4471
	5/2	—	—	−0.020 72	0.156 2.5	—	
4^3D_3	5/2	—	—	−0.235 1.5	−0.059 50	0.000 22	
	7/2	—	—	—	—	0.000 100	
		3^3P_0	3^3P_1		3^3P_2		
2^3S_1	1/2	0.190 23	−0.095 10	0.020 67	—	—	3888
	3/2	0.412 10	0.127 23		0.002 67	0.002 100	

formulas are given in terms of the quantum numbers J and F; and J becomes no longer well-defined, because the perturbation mixes levels with different J. A Güttinger-Pauli perturbation calculation for intensities has therefore been carried out. The results for typical lines are listed in Table IX, together with the frequencies obtained from term splittings of Table VIII. The calculated perturbed hfs's are likewise shown in Figs. 8 to 11. The calculated line pattern for λ10830 is plotted in Fig. 13 to the same scale as the observed microphotometer trace.

Mottelson[24] has kindly sent us the results of similar calculations he has performed for the ^3P terms, with very good agreement with our calculations for λ10830.

[24] B. Mottelson, private communication.

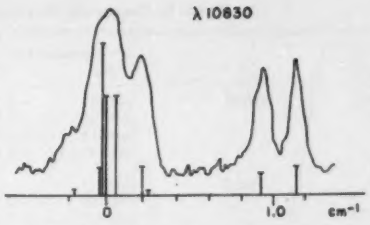

FIG. 13. Comparison of observed and calculated perturbed He^3 hfs of λ10830.

VI. COMPARISON OF CALCULATED AND OBSERVED HYPERFINE STRUCTURE

The observed hfs patterns and those calculated by the perturbation procedure agree remarkably well. For better comparison with the incompletely resolved experimental measurements, centers of gravity were computed for the close groups of calculated components. These calculated positions of partially resolved components are listed in Table X, together with the observed separations from Table III, and are plotted in Figs. 1 to 4. In most cases, the agreement is within the statistical spread of the measurements. It would appear that slightly better agreement might have been obtained for λ10830 and 7065 if the center of gravity of the strong component had been estimated to lie slightly away from the rest of the pattern, but in view of the considerable width of this component such speculations are not significant. It is seen that the splittings of the $^3S_1$ states agree exactly with those expected from the known value of the nuclear moment. The splitting of the $^3D_1$ states is also of similar magnitude, agreeing with the perturbation calculation and amounting to twice that expected from the usual formula. This indicates that a d electron for which the hfs is considerably larger than the fine structure approximates an s electron in interaction with the nuclear moment.

It is evident that the intensity perturbations obtained by the Güttinger-Pauli treatment provide a considerable influence on the agreement of the frequency separations because they affect the computed centers of gravity. A more direct effect is seen for the relative intensities of the weak doublets from the 2^3P_0 level to the split $^3S_1$ levels. As was pointed out above, this intensity ratio would be expected to be 2:1, since the transitions involve one common level and so should depend only on the statistical weights of the $F=1/2$ and $F=3/2$ hfs levels of the ^3S term, according to the usual rules. However, it will be seen from Fig. 12 that the 2^3P_0 level is perturbed by the 2^3P_1 level by one percent in energy, so that its wave function contains 10 percent of the 2^3P_1 wave functions. The relative intensities for the 2^3P_1 part of the 2^3P_0 level are in the

TABLE X. Comparison of calculated and observed hyperfine structure intervals.

Transition	λ	Separation from c.g. of strongest component Calc	Obs[a]	Calc-Obs	$\Delta T(n^3S)$ Calc	Obs	c.g. shift
2^3P-2^3S	10830	−0.181	−0.191±6	+0.010	0.222	0.221±5	+0.020
		+0.195	+0.192±6	+0.012			
		+0.913	+0.907±6	+0.006			
		+1.135	+1.128±6	+0.007			
2^3P-3^3S	7065	+0.177	——	——	0.216	0.216±4	−0.020
		−0.193	−0.186±7	−0.016			
		−0.917	−0.904±5	−0.013			
		−1.133	−1.120±5	−0.013			
					$\Delta T(n^3D)$		
2^3P-3^3D	5875	+0.175	——	——	0.201	0.206±4	−0.013
		−0.166	−0.168±3	+0.002			
		−0.894	−0.886±6	−0.008			
		−1.095	−1.092±6	−0.003			
2^3P-4^3D	4471	+0.175	——	——	0.210	0.208±6	−0.019
		−0.183	−0.161±10	−0.022			
		−0.910	−0.910±2	0.000			
		−1.120	−1.118±6	−0.002			
2^3S-3^3P	3888	+0.386	+0.372±5	+0.014			+0.026

[a] $\Delta\nu\pm\epsilon$: ϵ indicates the mean deviation in 10^{-3} cm^{-1}.

opposite ratio, being twice as strong to the ^3S, $F=1/2$ level as to the ^3S, $F=3/2$ level. When the intensities are calculated rigorously from the matrix elements instead of the J and F quantum numbers, the ratio comes out 19:15, as given in Table IX, instead of 2:1. This result explains why the intensity ratio of the pair of weak components in λ10830 and 7065, while in the right direction to correspond to an inverted ^3S hfs, is so nearly unity instead of 2:1. The experimental difficulty of self-absorption, which is greater for strong lines than weak lines and tends to equalize their intensities, of course contributes to the problem of determining the intensity ratio. On the other hand, intensities calculated rigorously on the assumption that the nuclear moment is positive, leading to normal instead of inverted hfs, change the ratio in the opposite direction to approximately 3:1. In this case, the inner member of the pair would be considerably stronger than the outer, which is definitely not the case. Hence, the intensity ratio of the pair of transitions $2^3P_0-n^3S_1$ provides definite evidence that the nuclear magnetic moment of He^3 is negative.

VII. ZEEMAN EFFECT OF HYPERFINE STRUCTURE

Confirmation of inverted hfs of the ^3S terms was attempted by the Zeeman effect. In a weak magnetic field each hfs level characterized by total angular momentum of F units splits into $2F+1$ levels whose separation from the field-free level is given by[25]

$$\Delta T=4.67\times10^{-5}HM_F g_J \times\frac{F(F+1)+J(J+1)-I(I+1)}{2F(F+1)}\ \text{cm}^{-1},$$

where H is the field strength in gauss, and the other quantities have their usual meaning. For a ^3S term $g_J=2$. For the level with $F=1/2$, the fraction in the above expression is 4/3; and for $F=3/2$, it is equal to 2/3. The Zeeman levels for 3^3S are plotted in Fig. 14, assuming an inverted hfs.

The formula just given is valid only for magnetic fields for which the Zeeman splitting is small compared with the hfs interval. Strong fields give a Paschen-Back effect which is symmetrical about the center of gravity of the ^3S term and gives no direct information about the orientation of the original hfs. Location of the center of gravity of the Paschen-Back pattern with respect to the field-free pattern could be used to identify the component of larger F, but this determination did not appear to be feasible here because of overlapping. Figure 14 shows that a field of about 500 gauss is near the limiting value for undistorted Zeeman effect.

The magnetic field used in the present experiment was obtained by a permanent magnet with adjustable pole pieces. The discharge tube was mounted outside the gap at a point where the field was 550 gauss with negligible variation over the 5-mm capillary, as measured with a General Electric gaussmeter. Observation could thus be made parallel to the field, eliminating the necessity for a polarizer.

Exposures were made of λ10830 and λ7065, the latter giving better resolution of the Zeeman components because of the heavier interferometer coating possible. Figure 15 shows microphotometer traces of the σ components above and of the field-free hfs below. Also shown are the calculated patterns to be expected for a field of 550 gauss, assuming inverted hfs. A more exact calculation of the Zeeman term splittings shows that the 2^3P_0 level, which would normally be expected

[25] See reference 20, p. 32.

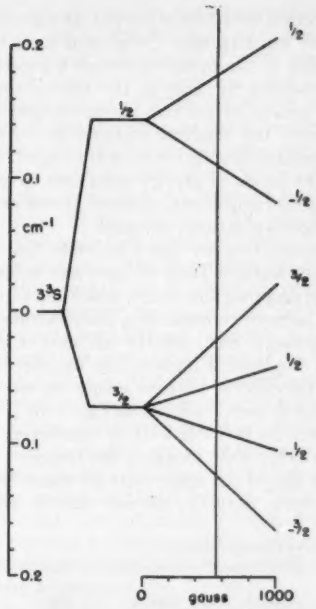

FIG. 14. Zeeman effect of the He^3 3^3S term.

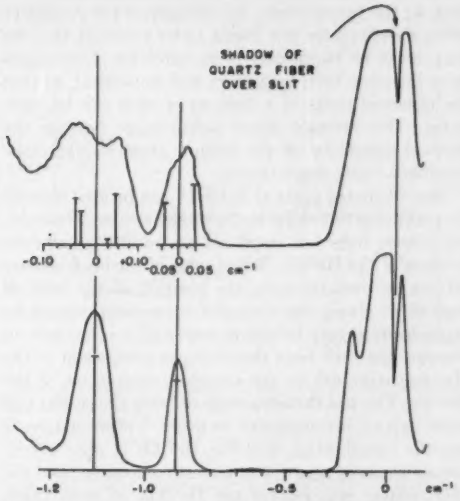

FIG. 15. Comparison of observed and calculated Zeeman effect of λ7065 for a field of 550 gauss (above) and field-free pattern (below).

to remain unsplit by a magnetic field, actually splits into two levels separated by 0.023 cm^{-1}, owing to the 2^3P_1 component in the 2^3P_0 level. Also, a slight interaction for this field was found for the 3^3S levels, those for $M_F=\pm 1/2$ from the $F=1/2$ level each being pushed upward by 0.003 cm^{-1} and those for $M_F=\pm 1/2$ from the $F=3/2$ level each being pushed down the same amount. These slight energy perturbations, however, are sufficient to produce a considerable effect on the intensities of the Zeeman components. The usual Zeeman intensity formulas[26] result in patterns which are symmetrical in intensity, as well as frequency, about the field-free line frequencies. The more exact calculations show a considerable intensity asymmetry caused by the P level splitting and the fact that a field of 550 gauss produces an effect intermediate between a Zeeman effect and a Paschen-Back effect.

The agreement between calculated and observed Zeeman patterns is quite good. The line width prevents complete resolution of the four components of the ^3S, $F=3/2$ transition, so that the F values cannot be determined directly by counting the number of components in each pattern. Unfortunately, further consideration reveals that the agreement of the partially resolved experimental pattern with the calculated pattern is not conclusive evidence for a correct assignment of F values. It might be assumed that normal instead of inverted ^3S hfs would merely exchange the patterns for the two lines, which would put the strong components adjacent instead of on the outside. However, normal 2^3P hfs would change the sign of the perturbations in the P wave functions, and the resulting Zeeman patterns would again have the stronger components on the outside. Hence, it appears that in the present case an incompletely resolved Zeeman pattern cannot provide definite evidence for F value assignment.

[26] See reference 20, p. 56.

VIII. COMPARISON OF CALCULATED AND OBSERVED ISOTOPE SHIFTS

It has been pointed out above that it is not possible to derive term isotope shifts, from the observed spectrum line isotope shifts, since there are more unknowns than observables. If the measured shift of a line does not agree with the predicted shift, it is not known whether it is the lower term or the upper term which has a shift differing from that expected. Since a term near the ionization limit has a small shift compared with that of a deep term, an approximation to the latter can be obtained by assigning to it all of the observed shift of high series members. One can then correct for the contribution of the high term as well as possible. In the case of helium, the reduced mass shift, which can be calculated exactly, should give a good approximation to the shift of the high term, especially for S terms. By comparing the difference between observed and predicted shifts for a series of transitions to a common lower level, a constant value should be obtained if the shifts of the upper states have been calculated correctly. This common difference, then, is a correction to be applied to the calculated shift of the lower term. How-

ever, in the present case, the differences for successive series members are not found to be constant and the data must be considered more carefully. Corrections have therefore been applied as well as possible, so that the observed shifts of a number of lines can be compared. This attempt seems worth while because the unusual simplicity of the helium atom should make possible a fairly exact theory.

The calculated shifts of Table IV can be used directly for predicting line shifts in the singlet system. However, the triplet lines are displaced an additional amount because of the He^3 hfs. While some of the hfs levels are subject to perturbations, the position of the level of highest F, giving the strongest component, should be given fairly closely by the theory; and it seems best to measure the shift from the strongest component of the He^4 fine structure to the strongest component of the He^3 hfs. This has the advantage of being the easiest and most natural measurement to make. Unfortunately, it has the complication that the He^3 hfs is very incompletely resolved near the strongest component, and the short spacer required for the He^3 hfs, in most cases, does not permit resolution of the two strong components of the He^4 fine structure. Corrections have therefore been applied to the measurements of the patterns for lack of resolution by using as He^4 reference point the center of gravity of the two strong components (calculated from the resolved patterns for λ10830 and λ7065, measured directly for other He^4 triplet lines) and for He^3, the center of gravity calculated to exist near the strong hfs components, adjusted as well as possible for the resolution actually attained.

These corrections are listed in Table XI. The calculated term shifts of Table IV have been subtracted to give the appropriate line shifts, which for triplets give the shifts between corresponding fine structure levels in the two isotopes. Since the He^3 hfs level of highest F lies below the level of highest J in the absence of hfs splitting, the effect of hfs is to reduce the term isotope shift, as can be seen readily from Figs. 5 to 7. This has been allowed for in Table VIII by considering that the hfs of the lower state increases the frequency of each line, while that of the upper state decreases the transition frequency. Actually, the net effect is seen to be

TABLE XI. Comparison of calculated and observed isotope shifts.

Transition	λ	Calc $\Delta\nu$ term c.g.	Lower state He^3 hfs	Upper state He^3 hfs	He^4 fine structure c.g.	He^3 hfs c.g.	Calc $\Delta\nu$	Obs $\Delta\nu$	Calc−obs
2^3P-3^3S	7065	−0.069	+0.072	−0.072[a]	+0.030	−0.020	−0.059	+0.036[b]	−0.095
4	4713	−0.386	+0.072	−0.072	+0.030	−0.020	−0.376	−0.297	−0.079
5	4120	−0.522	+0.072	−0.072	+0.030	−0.020	−0.512	−0.438	−0.074
6	3867	−0.594	+0.072	−0.072	+0.030	−0.020	−0.584	−0.508	−0.076
7	3732	−0.644	+0.072	−0.072	+0.030	−0.020	−0.634	−0.548[c]	−0.086
8	3652	−0.662	+0.072	−0.072	+0.030	−0.020	−0.652	−0.586[c]	−0.066
2^3P-3^3D	5875	−0.198	+0.072	−0.072	+0.030	−0.013	−0.181	−0.123	−0.058
4	4471	−0.437	+0.072	−0.072	+0.030	−0.19	−0.426	−0.360	−0.066
5	4026	−0.548	+0.072	−0.072	+0.030	−0.021	−0.539	−0.474	−0.065
6	3819	−0.608	+0.072	−0.072	+0.030	−0.021	−0.599	−0.547	−0.052
7	3705	−0.645	+0.072	−0.072	+0.030	−0.021	−0.636	−0.592	−0.044
8	3634	−0.668	+0.072	−0.072	+0.030	−0.021	−0.659	−0.617[c]	−0.042
2^1P-3^1S	7281	−0.987	0	0	0	0	−0.987	−1.046	+0.059
4	5047	−1.260	0	0	0	0	−1.260	−1.333	+0.073
5	4437	−1.382	0	0	0	0	−1.382	−1.461	+0.079
6	4168	−1.447	0	0	0	0	−1.447	−1.529	+0.082
7	4023	−1.485	0	0	0	0	−1.485	——	——
8	3935	−1.510	0	0	0	0	−1.510	−1.606[c]	+0.096
2^1P-3^1D	6678	−1.043	0	0	0	0	−1.043	−1.124	+0.081
4	4921	−1.282	0	0	0	0	−1.282	−1.358	+0.076
5	4387	−1.393	0	0	0	0	−1.393	−1.462	+0.069
6	4143	−1.453	0	0	0	0	−1.453	−1.512	+0.059
7	4009	−1.490	0	0	0	0	−1.490	−1.532	+0.042
8	3926	−1.513	0	0	0	0	−1.513	−1.543[c]	+0.030
2^3S-2^3P	10830	−0.969	+0.074	−0.072	−0.030	+0.020	−0.977	−1.181[b]	+0.204
3	3888	−1.318	+0.074	−0.072	+0.007	+0.026	−1.283	−1.404	+0.121
4	3187	−1.468	+0.074	−0.072	0.000	+0.028	−1.438	−1.535[d]	+0.097
2^1S-3^1P	5015	−0.729	0	0	0	0	−0.729	−0.849	+0.120
4	3964	−1.033	0	0	0	0	−1.033	−1.165	+0.132
5	3613	−1.167	0	0	0	0	−1.167	−1.304	+0.137
6	3447	−1.238	0	0	0	0	−1.238	−1.344[d]	+0.106
7	3354	−1.280	0	0	0	0	−1.280	−1.375[d]	+0.095

[a] Observed.
[b] Corrected for observed He^4 structure to center of gravity of strong components.
[c] High pressure tube, value omitted in Fig. 16.
[d] Grating.

negligible. The proper sign of the corrections for lack of resolution can be deduced most easily from the calculated patterns of Figs. 8 to 11. The He^3 hfs center of gravity corrections for a few lines are listed in Table X. The algebraic sum of all these corrections is given in the table and should correspond to the measured shifts. The observed shifts are taken to be those measured with the low pressure electrodeless discharge sources, except for a few high series members observed only with the intense source. Finally, Table XI lists the differences between predicted and observed shifts. These differences are plotted in Fig. 16 as a function of the term value of the upper state. If all of the difference is assumed to originate in the upper state, the terms will lie in the energy level diagram as shown in the figure, compared with the predicted location of each term at zero ordinate. That is, the triplet line shifts are smaller than expected, and hence the upper term shifts must be larger than expected in order to be more nearly equal to the 2^3P shift; the reverse applies to the singlets. (Since the 2^3S level lies below 2^3P, the algebraic sign of the difference is reversed for λ10830.) If the 2^3P or 2^1P shift is also different from the expected value, each pair of curves of the same multiplicity will stay the same shape and same distance apart, but the zero will be shifted up or down, accordingly.

It is clear from Fig. 16 that simple corrections to the predicted 2^3P and 2^1P shifts will not produce agreement with the observed line shifts. It is quite possible that P shift corrections should be made, but it is evident that there are other factors contributing to the S and D shifts which are not yet taken into account.

Figure 16 shows that the differences for the S levels are approximately a linear function of the S term value with a slope of about -2.2×10^{-6} cm^{-1}/cm^{-1}. Introducing an empirical correction of $-2.2\times10^{-6}\,T$ to the predicted S term shifts would cause the S difference plots of Fig. 16 to become horizontal lines whose ordinates would presumably correspond to the error in the predicted P term shifts. In attempting to account for the source of this S term correction, it will be recalled that the reduced mass shift is also a linear function of term value, of magnitude $-4.484\times10^{-5}\,T$. Incorporating the hypothetical correction would lower the reduced mass shift to $-4.26\times10^{-5}\,T$. This change implies a change in the relative atomic weights of the two isotopes. That of He^4 is known directly in terms of the fundamental standard by mass spectroscopic measurement of the doublet $(He_2^4)^+/(O^{16})^{++}$ and cannot be much in doubt. The mass of He^3, however, is known at present only through the energies released in various nuclear reactions. If we tentatively assign all of the required change in $\Delta\mu/m$ to He^3, its μ/m is raised from 0.99981812 to 0.99982032, corresponding to a nuclear mass of $M=3.0528$, or an atomic weight of 3.0539, compared with the recent value[27] of 3.016951. This

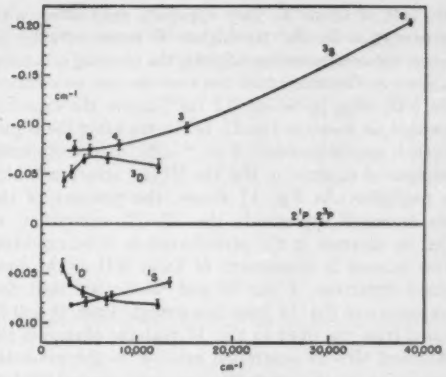

FIG. 16. Comparison of predicted and observed isotope shifts of lines in the series 2^3P-n^3S, 2^3P-n^3D, 2^1P-n^1S, and 2^1P-n^1D. The ordinate is the difference between the predicted and observed line shift; the abscissa is the term value of the upper state.

mass difference corresponds to an energy difference of 34 Mev, which is far beyond the experimental error in measuring nuclear reaction energies. Consequently, it appears necessary to reject the interpretation of the slope of the S term differences of Fig. 16 as a reduced mass correction.

Another possible explanation is a change in the Lamb shift, which amounts to -5.8 cm^{-1} for the ground state of HeI and -4.2 cm^{-1} for the ground state of HeII, according to preliminary calculations of Günther,[28] producing a net decrease in the ionization potential of He^4. If these calculations are correct and if a linear decrease in the shift is assumed for the various excited S states of HeI, this would amount to a variation of $1.6/200{,}000 = 8\times10^{-6}$ cm^{-1}/cm^{-1}. To interpret the present variation of 2.2×10^{-6} cm^{-1}/cm^{-1} as due to an increase in the Lamb shift for He^3 would represent an isotope effect of some 25 percent, which appears to be unreasonable. (Presumably all of the isotope effect of the Lamb shift in helium should occur in HeI, since the hydrogen isotopes show a constant shift.)

A further possibility, also peculiar to S terms, is the nuclear volume effect. This interpretation provides the correct algebraic sign (assuming the He^3 nucleus is the larger) and approximately the correct dependence on n, but the accepted theory[29] predicts much too small an effect.

The trend of the D term differences in Fig. 16 is altogether different from that of the S terms and requires another explanation. The curves somewhat resemble the variation of n^{-3} encountered in perturbed series. Recalling that the ^1D terms actually lie above the ^3D terms in the energy level diagram, it is seen that the curves can be interpreted as a respulsion between the

[27] Tollestrup, Fowler, and Lauritsen, Phys. Rev. **78**, 372 (1950).

[28] M. Günther, Physica **15**, 675 (1949).

[29] Reference 20, p. 73.

two sets of terms as they approach each other with increasing n. In He^4 the higher ^1D terms actually lie below the corresponding triplets, the crossing occurring near $n=8$. The interaction between the two series raises the 8^1D_2 term by about 0.2 cm^{-1} above the expected position, as shown in Fig. 17. In He^3 the hfs of the triplet levels is approximately 0.2 cm^{-1} wide, practically independent of n, while in He^4 the ^3D fine structure width is negligible. As Fig. 17 shows, the presence of the hfs decreases appreciably the $^1D-^3D$ separation, so that an increase in the perturbation is to be expected. The increase is represented in Table XII as the combined departure of the ^1D and ^3D isotope shift discrepancies of Fig. 16 from two straight lines. It will be noted from the inset to Fig. 17 that the change in the observed $^1D-^3D$ separation relative to the predicted separation is approximately inversely proportional to the term separation, as a perturbation should be. The use of He^4 term values for the term separations is, of course, an approximation.

The similarity between a reciprocal and a square root relationship accounts for the preliminary description[3] of the isotope shift discrepancies, now seen to be in error, since better and more extensive measurements have been made.

Since the expected position of the 8^1D term is inside the 8^3D hfs, the structure of transitions to these terms should show large perturbations. Attempts were made to observe these transitions with high resolution but were not successful because of the experimental difficulties. It may be noted that, because of the increased mixing of the ^1D and ^3D wave functions, the intercombination lines $^1D\rightarrow{}^3P$ and $^3D\rightarrow{}^1P$ should be stronger in He^3 than in He^4.

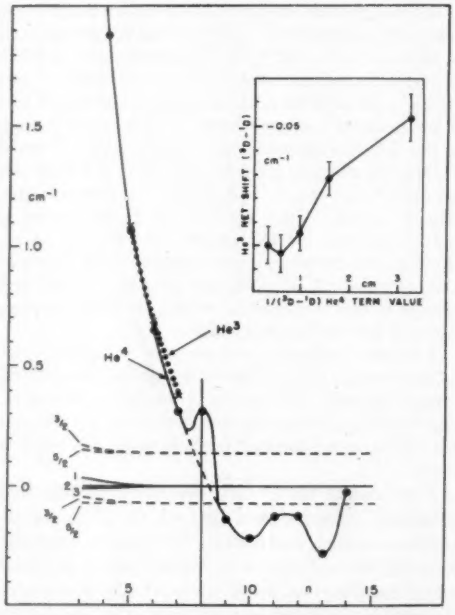

FIG. 17. Separation between ^3D terms (horizontal lines) and ^1D terms as a function of n. Inset: Combined differences between predicted and observed line shifts for 2^3P-n^3D and 2^1P-n^1D series as a function of the reciprocal of the n^3D-n^1D term separation.

It is interesting to note that in Fig. 16 the limiting values for the S term shift as $T\rightarrow 0$ bear approximately the same relationship to the predicted shifts as the D terms for low n before the perturbation becomes large. This suggests that zero ordinate in Fig. 16 should be near the present value of -0.070 cm^{-1} for the triplets and $+0.080$ cm^{-1} for the singlets, implying that the 2^3P and 2^1P shifts should be approximately -0.675 and -1.670 cm^{-1}, respectively. These changes correspond to approximately 12 and 20 percent increases in the Hughes-Eckart coupling term for the 2^3P and 2^1P terms, respectively. In view of the appreciable coupling effect for the 2^1S and 2^3S found by Hamermesh and Eisner using more exact wave functions, the above error does not appear unreasonable for a formula based on one-electron wave functions.

Recently, Hamermesh and Eisner[30] have attempted a more exact calculation of the 2^3P and 2^1P coupling terms using wave functions of the type described by Breit[31] which include the interelectron distance explicitly. They find for $\Delta T_2+\Delta T_3$, defined as in Table IV, $+0.558-0.032$ and $-0.368-0.020$ cm^{-1}, for 2^3P and 2^1P, respectively. The change is thus much too small, and in the case of 2^3P, it is even of the wrong sign to explain the present results. However, Hamermesh and Eisner express the opinion that these calculated isotope shifts are not very reliable, because of the uncertainty in the accuracy of the wave functions. They find that introduction of the extra terms has practically no effect on the energy calculated for the $2P$ states for wide variations in the r_{12} terms with consequent wide variations in the Hughes-Eckart coupling terms. There seems to be no way at present to make a definitive calculation of the P isotope shifts.

An estimation can be made for the 3^3P isotope shift discrepancy, combining the above conclusions concerning the 2^3S and 2^3P shifts with the observed shift for $\lambda 3888$. If the 2^3P shift is decreased by 0.070 cm^{-1}, the 2^3S shift must be increased by 0.134 cm^{-1} to account for the observed $\lambda 10830$ shift. Increasing the calculated $\lambda 3888$ shift by 0.134 cm^{-1} brings it to 1.417 cm^{-1}. Since the observed shift is 1.404 ± 0.009 cm^{-1}, no appreciable 3^3P discrepancy is obtained with this interpretation. This result is reasonable if the 2^3P discrepancy indeed arises from an inadequate wave function, since the 3^3P wave function should be relatively more satisfactory.

Extension of these considerations to the 4^3P term

[30] M. Hamermesh and E. Eisner, private communication.
[31] G. Breit, Phys. Rev. 36, 383 (1930).

TABLE XII. Perturbations of D terms.

	He^4 term values[a]				Calculated minus observed isotope shifts			
n	^3D	^1D	Difference Δ	$1/\Delta$	^3D	^1D	Difference	Net change
3	12209.10	12205.78	3.32	0.301	−0.058	+0.081	0.139	0
4	6866.17	6864.29	1.88	0.532	−0.066	+0.076	0.142	+0.003
5	4393.52	4392.46	1.06	0.944	−0.065	+0.069	0.134	−0.005
6	3050.63	3049.98	0.65	1.54	−0.052	+0.059	0.111	−0.028
7	2241.00	2240.69	0.31	3.23	−0.044	+0.042	0.086	−0.053
8	1715.58	1715.27	0.31	3.23				
9	1355.37	1355.51	−0.14	−7.1				
10	1097.70	1097.92	−0.22	−4.6				
11	907.25	907.38	−0.13	−7.7				
12	762.33	762.46	−0.13	−7.7				
13	649.53	649.81	−0.28	−3.6				
14	560.06	560.08	−0.02	−50				

[a] Charlotte E. Moore, *Atomic Energy Levels* (Natl. Bur. Standards, Washington, D. C., 1949), Circular 467.

leads to a similar conclusion within the large experimental error for λ3187. In the case of the higher ^1P terms, the corresponding treatment cannot be followed exactly, because the transition 2^1S-2^1P is photographically inaccessible at λ20581. However, it is interesting to note that the series 2^1S-n^1P shows a limiting isotope shift discrepancy of about 0.135 cm^{-1} (ignoring the grating measurements on the high pressure tube), indicating that the 2^1S shift is larger by this amount on the assumption of accurately calculated high ^1P shifts. Since this value for the extra 2^1S shift agrees with that for the 2^3S term, the ^1S and ^3S curves of Fig. 16 evidently remain parallel. If the same trend continues as far as the 1^1S term, an additional shift of about 0.5 cm^{-1} is obtained, lowering the ionization potential further by this amount; but there is, of course, no basis whatever to justify such an extrapolation.

If it is assumed that the 2^1S term has an isotope shift larger, by 0.135 cm^{-1}, than expected, the discrepancy for λ5015 of 0.120 cm^{-1} would indicate that the shift of the 3^1P term is larger than expected by about 0.015 cm^{-1}, which is of the same magnitude as found for the 3^3P term but opposite in sign.

IX. CONCLUSIONS

The present investigation of the He^3 spectrum has revealed the following points:

(1) The fine structure of the 3^3P term in He^4 has been found to correspond more closely to that of the 2^3P term than at present accepted.

(2) Accurate helium wavelength measurements are difficult to make because of the considerable pressure broadening and shift. It has been found that the pressure shifts, in general toward higher frequencies, are not the same for the two isotopes, being greater in He^4 than in He^3 for triplet lines, and less for singlets.

(3) The line width problem is especially difficult in the He^3 triplet system because of the presence of appreciable hfs which can be only partially resolved. The structure appears to conform to that expected for a nuclear spin of $\frac{1}{2}h$ and nuclear moment of -2.128 nm, using the usual formulas. The ^3S levels are inverted, confirming the negative sign of the moment. The splitting of the 2^3S term is 0.221 cm^{-1} and is 0.216 cm^{-1} for higher ^3S terms, agreeing exactly with splittings calculated in the proper way. The hfs splittings of the ^3P and ^3D terms also agree remarkably well with centers of gravity of hfs calculated by taking into account the perturbations of neighboring fine structure levels. The perturbations are large.

(4) The isotope shifts of triplet lines are smaller and those of singlets greater than those expected from term shifts calculated from the reduced mass effect and the Hughes-Eckart formula for the coupling terms for P levels. The differences between predicted and observed isotope shifts for S levels show an approximately linear decrease with term value of about -2.2×10^{-6} cm^{-1}/cm^{-1}. This slope is too large to be accounted for by an acceptable change in the reduced mass factor. The differences for the D terms indicate a repulsion between ^3D and ^1D with increasing n, which is explained as an increase in the repulsion over that present in He^4 near the crossing of ^1D and ^3D near $n=8$. If these descriptions for the S and D terms are accepted, the remaining differences may be ascribed to errors in calculating the Hughes-Eckart coupling terms for the P levels.

We are indebted to Mr. J. C. McGuire for the initial preparation of the He^3 samples. We are indebted to the Department of Physics of the University of Chicago for permission to use its comparator and for the use of the Zeiss spectrograph. The advice of Professor K. W. Meissner of Purdue University is gratefully acknowledged. We should like to thank Mr. B. Mottelson for communicating to us his perturbation calculations on the 2^3P hfs.

Lattice Defects in Silver Bromide*

CHESTER R. BERRY
Eastman Kodak Company, Rochester, New York
(Received January 4, 1951)

Measurements have been made of the lattice parameter of silver bromide at room temperature and in the range from about 350 to 420°C. The results are compared with the values obtained on the basis of two contrary assumptions: first, that the lattice expansion is identical with the external expansion measured by Strelkow; and second, that some of the external increase in volume is caused by formation of vacancies, the resultant parameter being that estimated by Lawson. Within experimental error, the measured curve agrees with the first assumption, which is equivalent to the assumption that no Schottky defects have formed. Since it is known from ionic conductivity measurements that there are about 2 percent of defects at temperatures near 420°C, it is concluded that these are Frenkel defects. However, the magnitude of the errors involved in the measurements is such that the existence of a small number (about 10 percent of the total) of Schottky defects cannot be entirely precluded.

I. INTRODUCTION

SOME doubt exists concerning the nature of the defect structure of silver bromide. In the latent-image theory proposed by Gurney and Mott,[1] it was assumed that only Frenkel defects, consisting of interstitial silver ions and vacant silver ion sites, are present. However, a latent-image theory recently proposed by Mitchell[2] assumes that only Schottky defects, consisting of equal numbers of vacant silver ion and bromide ion sites, are important.

Much experimental and theoretical evidence has been presented to support the existence of one or the other type of defect structure. A few examples of this evidence will be given here.

Experiments on ionic conductivity of silver bromide at elevated temperatures reviewed by Tubandt[3] favor the existence of Frenkel defects. Also, Wagner and Beyer[4] report measurements of the x-ray lattice constant and the density of silver bromide near the melting point which indicate the existence of Frenkel defects.

On the other hand, an analysis by Lawson[5] of the data given by Strelkow[6] on the coefficient of expansion of silver bromide leads, with certain assumptions, to the conclusion that Schottky defects predominate near the melting point. Still other experiments on the orientations of silver produced in silver bromide by photolysis[7] indicate the existence of Frenkel defects in the pure crystals and the production of surface vacant anion sites during photolysis.

The present experiments were initiated to determine whether the two types of lattice defects could be distinguished at high temperatures by using the results of measurements of the lattice constant of silver bromide to check the value of lattice constant reported by Wagner and Beyer,[4] and to test the assumption of Lawson[5] that the coefficient of expansion of silver bromide near the melting point is abnormal in the sense that the increase in volume of the crystals is caused partly by the production of lattice defects. The rather large number of defects[8] (≈ 2 percent) present in silver bromide at temperatures near the melting point makes this a simple region to study by x-ray diffraction.

II. EXPERIMENTAL PROCEDURES

Specimens of silver bromide were formed as thin surface layers on silver rods of about 0.8 mm diameter by reaction of the rods in bromine. The lattice parameters of silver and of silver bromide were determined at various temperatures. Because of the high absorption of copper K-α radiation in both silver and silver bromide, only a thin surface layer is effective in producing the diffraction patterns, the total effective thickness of silver bromide and silver being only about 10μ. Since this distance is so small, the reflections from the silver rod can be used to give an accurate calibration of the recording film and temperature determination of the silver bromide.

The temperature of the silver rod relative to 25°C was determined by comparing the lattice-constant change with the data on the expansion of silver given by Scheel,[9] assuming the number of vacant silver lattice sites at these temperatures to be negligible. That this assumption is valid can be seen by an examination of the defect structure of copper, which is similar to that of silver and whose melting point and activation energy for self-diffusion are near those of silver. The detailed calculations of Huntington[10] give an activation energy for vacancy formation in copper of 1.5 to 1.8 ev. Even if the activation energy for vacancy formation in silver were as low as 0.7 ev, the fraction of vacancies would be less than 10^{-5} at 425°C.

* Communication No. 1387 from the Kodak Research Laboratories.
[1] R. W. Gurney and N. F. Mott, Proc. Roy. Soc. (London) **A164**, 151 (1938).
[2] J. W. Mitchell, Phil. Mag. **40**, 249 (1949).
[3] C. Tubandt, *Wien-Harms Handbuch der Experimentalphysik* (Akademische Verlagsgesellschaft m. b. H., Leipzig, 1932), Bd. 1, 12, Teil I, p. 384.
[4] C. Wagner and J. Beyer, Z. physik. Chem. **B32**, 113 (1936).
[5] A. W. Lawson, Phys. Rev. **78**, 185 (1950).
[6] P. G. Strelkow, Physik. Z. Sowjetunion **12**, 73 (1937).
[7] C. R. Berry and R. L. Griffith, Acta Crys. **3**, 219 (1950).
[8] F. Seitz, Phys. Rev. **56**, 1063 (1939).
[9] K. Scheel, Z. Physik **5**, 167 (1921).
[10] H. B. Huntington, Phys. Rev. **61**, 325 (1942).

At room temperature, the lattice parameters of silver and of silver bromide were found, correction for film shrinkage being made by the method of Straumanis and Mellis.[11] Many other types of errors were minimized by obtaining the values of the parameter extrapolated to $\theta=90°$, using the graphical scheme of Nelson and Riley.[12] The same scheme was used at high temperatures for determining the silver lattice parameter, but the back-reflection lines of the silver bromide disappeared because of strong atomic vibrations. For this reason, the forward-reflection silver bromide lines were used, and such corrections were applied to the measured lattice parameters as were shown to be necessary from measurements of neighboring silver reflections.

III. DISCUSSION OF EXPERIMENTAL RESULTS

The lattice constants of the silver and of silver bromide, corrected for refraction and to a temperature of 25°C, were 4.0860±0.0004 and 5.7745±0.0004A, respectively. The lattice constant of pure silver under similar conditions was given by Jette and Foote[13] at 4.08611±0.00008A, and values of the lattice constant of carefully prepared precipitates of pure silver bromide were found to be 5.7743±0.0004A. In view of this agreement, it was assumed that impurities or lack of stoichiometric composition would have no significant effects on the lattice parameters measured at high temperatures.

In Fig. 1 the experimentally determined values of the silver bromide lattice constant at high temperatures have been plotted as a function of temperature, and a smooth curve has been drawn. The temperature of the specimen was determined from the increase in the silver lattice parameter from 4.0861 at 25°C. An error of 0.0001A in the lattice constant gives a temperature error of about 1°C. Since the parameter of silver at high temperatures may be in error by about 0.004A, the temperature uncertainty is ±4°C.

Errors in the lattice parameters of silver bromide are much larger because of the lack of back-reflection lines. In general, the higher the temperature the greater is the error because fewer and less smooth lines appear. The

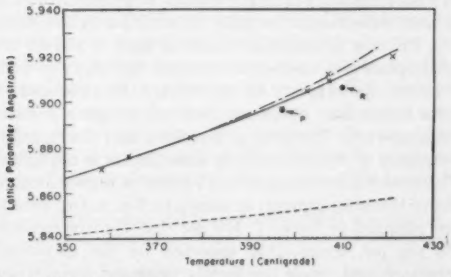

FIG. 1. Silver bromide lattice parameter. ———, experimental; — — — —, crystals having no defects; – – –, assumed by Lawson.

[11] M. Straumanis and O. Mellis, Z. Physik **94**, 184 (1935).
[12] J. B. Nelson and D. P. Riley, Proc. Phys. Soc. (London) **57**, 160 (1945).
[13] E. R. Jette and F. Foote, J. Chem. Phys. **3**, 605 (1935).

effect is to give errors of about ±0.002A at 360°C and ±0.005A above 400°C.

The point, *P*, obtained from the x-ray measurements of Wagner and Beyer,[4] is in good agreement with present results. The uncertainty in the position of this point has not been given.

On the same diagram is plotted the curve obtained from Strelkow's[6] values of the coefficient of expansion of silver bromide, if it is assumed that the silver bromide lattice constant changes in the same way as does the exterior dimension. Otherwise stated, this would be the lattice constant of a specimen having no lattice defects; and in addition, to at least a first approximation, it would represent a crystal with Frenkel defects. From examinations of the random variations in Strelkow's data, it appears unlikely that the curve drawn here could be in error by more than ±0.002A. For comparison with Strelkow's data, the point, *R*, can be obtained from the observation of Wagner and Beyer[4] that the density of silver bromide is 6.049 g/cm³ at 410°C, compared with 6.476 g/cm³ at 20°C. If the value 5.7743A is used for the lattice parameter at 25°C, a perfect crystal should have a parameter corresponding to the point, *R*. The average errors in the mean values of densities given by Wagner and Beyer would give an error of only ±0.002A in the lattice parameter. This discrepancy between the results of Strelkow and of Wagner and Beyer is apparently larger than would be expected on the basis of random errors, but its cause is not known.

The lowest curve is obtained from the coefficient of lattice expansion assumed by Lawson[8] to apply to a silver bromide crystal having no defects. According to Lawson's scheme, the production of Schottky defects should reduce the measured lattice constant still further.

Within the limit of possible experimental errors, the experimental curve is in agreement with the curve for a crystal having no defects or only Frenkel defects, and with the points, *P* and *R*; but it is completely at variance with the assumption made by Lawson. It is possible that all of the defects in silver bromide are Frenkel defects; but if the separation of the uppermost two curves were a real effect, it would correspond to a small concentration of Schottky defects. In this case, the fraction of vacant sites can be determined directly from the separation of the two curves, and is given by the relation: $f=3\Delta a/a$. At 415°C, Δa is about 0.004A, and this corresponds to a fraction of vacancies, $f=0.2$ percent, compared with the number of defects that are known from the relation,[8] $f=29\exp(-5050/T)$, to be about 2 percent. It may be that Schottky defects are present to the extent of 10 percent of the total, but certainly Frenkel defects predominate.

The question of whether Schottky defects, or just vacant bromide ion sites, can be built into the crystal by artificial means, such as sulfur sensitization[3] or by photolysis,[7] is not answered by the present experiments.

On the Absorption of Penetrating Showers

H. A. MEYER, G. SCHWACHHEIM, AND A. WATAGHIN
Departamento de Fisica, Universidade de São Paulo, São Paulo, Brazil
(Received October 16, 1950)

Several experiments on the absorption in lead of the particles of penetrating showers have been performed under different geometrical conditions. The penetrating showers produced in air are shown to have a high penetrating power, whereas those produced locally are strongly absorbed. An interpretation is given by the study of the selection of the penetrating showers by our apparatus. The cross section for nuclear absorption of the π-mesons of the locally produced penetrating showers was measured and shown to be smaller than half the geometrical one. Some data on the structure of the penetrating showers and on the presence of photons were obtained.

I. INTRODUCTION

A SERIES of experiments has been performed to study the absorption of the ionizing particles of penetrating showers (PS). We studied the absorption in lead of the particles of the PS produced in the air as well as those produced in a material located above the arrangement. We call the former atmospheric PS and the latter local PS. The frequency of atmospheric PS is given by the recorded frequency without the producing material (background), since accidental coincidences and coincidences due to mesons and their knock-on secondaries are negligible.[1] Moreover, the lead shields are thick enough to absorb soft showers (a point that is checked in each experiment), and the position of these shields is such that the registration of a PS produced in them would be very improbable. As we observed that the absorption of the atmospheric PS is very small, in general, their absorption in the producing material will be small, and the frequency of local PS will be given by the difference between the frequencies with and without the producing material.

Experiment I was performed in Campos do Jordão (844 g/cm²) during the last months of 1949. The others were performed in São Paulo (950 g/cm²) in 1950. The G-M counters used in our experiments, with sensitive area of 2.9 cm×45 cm=130 cm², had glass walls with an external cathode of conducting paper. All statistical errors given below are standard deviations.

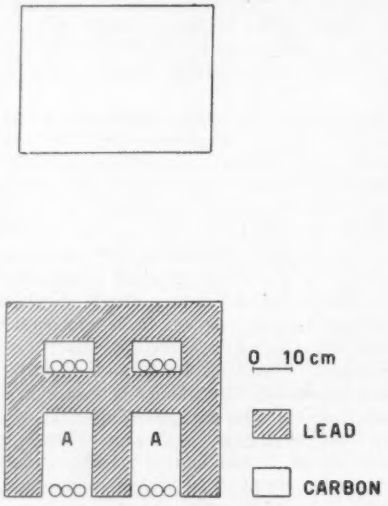

FIG. 1. Arrangement used in Experiment I. The PS were absorbed placing different thicknesses of lead in the cavities A.

II. EXPERIMENT I

Experiment I is a refinement of an experiment described earlier.[2] We recorded coincidences between four trays of counters (Fig. 1). Each tray consisted of three counters in parallel. Figure 1 shows that at least two particles with sufficient energy to penetrate 19 cm of lead were needed in order to record a coincidence. The PS were absorbed in layers of lead, 5 and 10 cm thick, placed in position A between the trays of each telescope. In order to be recorded, a PS produced in these layers must contain at least one energetic particle going upwards. We believe, therefore, that the recorded frequency of PS produced in these layers is negligible. The local PS are produced in 29 g/cm² of carbon located above the arrangement, as shown in Fig. 1. Our results are collected in Table I. We see that the atmospheric PS are not appreciably absorbed by the additional layers of lead, while the locally produced showers are strongly absorbed in 5 cm of lead. These results are in agreement with those of the earlier experiment.[2] In the

TABLE I. Experiment I: Hourly rate of fourfold coincidences.

Lead thickness in position A	Background (atmospheric PS)	With carbon	Production in carbon
0 cm	1.79±0.16	2.21±0.15	+0.42±0.22
5 cm	1.70±0.13	1.53±0.13	−0.17±0.18
10 cm	1.39±0.10	1.50±0.10	+0.11±0.14

[1] Cicchini, Meyer, Schwachheim, and Wataghin, Comm. Ass. Fis. Arg. 23 (May 1949).

[2] Meyer, Schwachheim, Wataghin, and Wataghin, Phys. Rev. 75, 908 (1949).

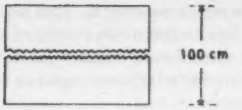

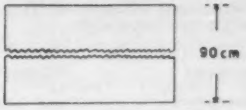

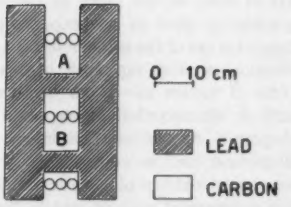

FIG. 2. Arrangement used in Experiment II. The small angle PS were absorbed by lead placed in positions A and B.

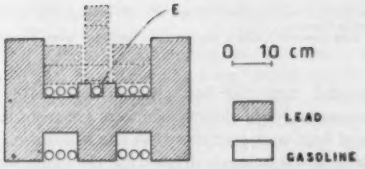

FIG. 3. Arrangement used in Experiment III. The two telescopes selected the PS, and a counter E located between them detected associated particles. The dotted rectangles represent the various lead absorbers.

present experiment we use carbon as the producing material because the atomic weight of carbon is close to the mean atomic weight of the air. The similarity of the results of this experiment and of the earlier one, in which we used gasoline instead of carbon, justifies the indiscriminate use of both materials in our experiments.

III. EXPERIMENT II

The purpose of this experiment is to repeat Experiment I under different geometrical conditions; we wanted to study the absorption of local PS with an appreciably smaller angular aperture.

The PS were selected by three trays of three counters each (Fig. 2). The two outer counters in each tray were connected in parallel. We recorded sixfold coincidences. For a coincidence to be recorded there had to be at least two particles able to penetrate 10 cm of lead. The local PS were produced in carbon. In the cavities A and B, we placed different thicknesses of lead absorbers. Our results are collected in Table II.

The high background counting rate without absorber is due to the fact that electron showers are still recorded. From 2.5 cm to 10 cm of lead the background rate shows only a slight variation. This arises from a small absorption of the atmospheric PS. The locally produced PS are strongly absorbed, however, as in Experiment I.

TABLE II. Experiment II: Hourly rate of sixfold coincidences.

Thickness of lead absorbers (cm)	Background (atmospheric PS)	With carbon	Production in carbon (local PS)
0	1.106±0.069	1.455±0.082	~0.7
2, 5	0.656±0.056	1.000±0.077	0.344±0.095
5	0.562±0.037	0.728±0.037	0.166±0.052
10	0.443±0.043	—	—

IV. EXPERIMENT III

In Experiment III the PS are selected by two vertical telescopes, and variable thicknesses of lead are placed above a counter, E, located between the telescopes (Fig. 3). We measure, in this way, the penetrating power of one particle of the shower. Each tray of the telescopes consisted of three counters in parallel. Between the trays of each telescope was a permanent layer of 10 cm of lead. We recorded both the coincidences among the four trays of the telescopes and the fivefold coincidences among these four trays and counter E.

In a preliminary measurement, without absorber above counter E, we placed 5 cm of lead absorber above the upper trays of the telescopes and the fourfold coincidence rate of the background decreased appreciably, as shown in Table III. This suggests that, with only the permanent lead absorber, some electron showers were still recorded. When we further increased the absorber above the telescopes by 5 cm of lead, the

TABLE III. First part of Experiment III: Hourly rates of coincidences.

Lead thickness		0 cm	5 cm	10 cm
Background (atmospheric PS)	fourfold rate	1.493±0.083	0.853±0.031	0.978±0.070
	fivefold rate	0.930±0.066	0.518±0.024	0.643±0.057
With gasoline	fourfold rate	2.009±0.106	1.175±0.056	1.084±0.090
	fivefold rate	1.181±0.082	0.672±0.042	0.693±0.071
Production in gasoline (local PS)	fourfold rate	~0.8	0.322±0.064	0.106±0.114
	fivefold rate	~0.6	0.154±0.049	0.050±0.091

TABLE IV. Second part of Experiment III: Hourly rates of coincidences.

Lead thickness above counter E (cm)	Background		With gasoline	
	fourfold coincidences	fivefold coincidences	fourfold coincidences	fivefold coincidences
0	0.834±0.051	0.518±0.026[a]	1.301±0.074	0.730±0.034[a]
5	0.805±0.058	0.548±0.029[a]	1.195±0.069	0.751±0.034[a]
15	0.906±0.074	0.496±0.034[a]	1.234±0.073	0.669±0.036[a]
20	0.911±0.080	0.499±0.029[a]	1.186±0.064	0.679±0.030[a]
Average rate[b]	0.853±0.031	0.518±0.024	1.226±0.035	—
1	0.876±0.081	0.539±0.038[a]	1.198±0.080	0.706±0.040[a]

[a] These statistical errors can be used only when comparing measurements in the same column.
[b] The measurements with 1 cm were not included when computing the average.

background rate did not change appreciably. This shows that no more electron showers are recorded with 15 cm of lead and confirms that the absorption of the atmospheric PS is weak. Repeating the same measurements with a producing material (38 g/cm² of gasoline) we observed that the locally produced PS recorded by the two telescopes are strongly absorbed (Table III). This is in agreement with the results of Experiments I and II.

Afterwards, with a permanent absorber of 15 cm of lead in the telescopes and with 67 g/cm² of gasoline as producing material, we placed various thicknesses of lead above counter E. The fivefold coincidence rates with different thicknesses of lead are shown in Table IV.

Let us notice that the absorber covers only counter E, so that its presence cannot change the rate of fourfold coincidences due to either background or local production of PS. This is confirmed by Table IV. Also, by Table IV, we see that there is no absorption of the fivefold coincidences without the producing material, in agreement with Experiments I and II. Taking into account that the fivefold coincidences are not statistically independent of the fourfold coincidences, we normalized all our data for fivefold coincidences to the common fourfold coincidence rate and accordingly reduced the statistical errors of the fivefold rates. It is observed from Table IV that the absorption of the locally produced particles is very small.

We investigated whether or not counter E was struck by photons resulting from the decay of neutral mesons of the PS, which constitute about half of the number of charged mesons.[3] As the thickness of the wall of counter E measured in radiation lengths is much smaller than unity, this counter has a very low efficiency for the registration of photons. When covered with 1 cm of lead its efficiency will approach unity, in our range of energies. We thus expect the difference between the fivefold coincidence rates with and without 1 cm of lead to yield the frequency of these photons. Table IV shows that this frequency is low. We believe that this happens because the angular dispersion of the two photons into which the neutral mesons decay is so large that few of them strike counter E. This sets an upper limit of about 1 Bev to the mean energy of the mesons which go in the direction of counter E, if we assume the number of photons to be about equal to the number of charged mesons.[3]

[3] Carlson, Hooper, and King, Phil. Mag. 41, 701 (1950).

V. DISCUSSION

In our experiments the absorption of atmospheric PS is weak. The atmospheric PS must be produced in a mass of air at least of the order of the mass of the producing material used in our experiments because the counting rates are of the same order. By geometrical considerations we see that the center of this mass of air must be tens of meters above our arrangement. The largest part of the recorded atmospheric PS should consist of groups of particles having a very small angular dispersion and in consequence large energy, and should consist mainly of μ-mesons resulting from the decay of π-mesons. For these reasons these particles should neither disappear appreciably by ionization nor suffer nuclear interactions. It is interesting to notice that the predominant factor in the selection of the atmospheric PS is the small angular divergence rather than the thickness of lead used in our experiments so that the recorded particles of the atmospheric PS selected by our arrangement have an energy much larger than the minimum energy necessary to cross the lead shielding.

The results of Experiments I and II, and the absorption of the fourfold coincidences in Experiment III indicate that, in the conditions of these experiments, the absorption of the locally produced PS is strong, even if we take into account the fact that in order to record the absorption of a PS it is sufficient that only one particle be absorbed. However, the absorption of the particles which strike counter E in the locally produced PS (Experiment III) is weak. Because of this fact and because the cross section for nuclear absorption would need to be larger than the geometrical cross section, we do not believe that the contribution of nuclear interactions to the observed absorption of the fourfold coincidences due to the local PS is important. Thus, the principal contribution to the absorption of the PS comes from particles stopped in the lead absorber after having lost their energy by ionization. Our experimental results indicate that the main part of the particles of the local PS recorded by the two telescopes have an energy just above the minimum energy required to cross the lead absorber. We believe that the local PS are not selected by the requirement of a particularly small angular divergence but by the thickness of the lead absorber, which means that the minimum energy of the recorded particles of the local PS should be just the energy necessary to penetrate this absorber. Because the spectral distribution of these particles is believed to fall off rapidly with increasing energy, the local PS would be easily absorbed.

It is very important to know the criterion by which

the PS are selected with a given arrangement. Indeed, the PS are really "penetrating"; i.e., their frequency does not depend, within large limits, on the thickness of the lead absorber, except if they are selected by a special requirement, such as their small angular divergence. This is why showers resulting from high energy nuclear explosions (high energy stars) discovered in the atmospheric PS may be called "penetrating." The registered local PS, though of the same nature as the recorded atmospheric PS, are not really "penetrating" in the sense given above, for reasons we have already discussed; but they are penetrating, of course, in the sense that some of their particles are able to cross large thicknesses of lead.

The small absorption of the locally produced PS in the absorber placed above counter E shows that the largest part of the particles of the PS which strike this counter have an energy larger than that necessary to penetrate any of the absorbers. This fact indicates that the particles in the center of the local PS (which have the direction of the primary particle) have in the mean a larger energy than the lateral particles. This is easily understood by the laws of conservation of momentum. If ionization does not contribute to the observed absorption, the absorption length observed by us will be caused by nuclear absorption and will be of the order of or greater than 400 g/cm² of lead. There is a correction arising from the fact that counter E is sometimes struck simultaneously by more than one particle. Taking into account this correction and the statistical errors of the measurements, we are still able to state that the nuclear absorption length in lead cannot be shorter than 350 g/cm². However, because of the possible contribution of ionization, and because of the statistical errors, we cannot give an upper limit to the nuclear absorption length.

Notice that since counter *E* was not struck by photons, we are measuring the absorption length for charged particles. In the rather high energy region involved it is plausible to assume that, in the center of the locally produced PS, π-mesons constitute the main part of the total number of ionizing particles, while the protons which constitute the remainder could not change our results appreciably, because their absorption length in lead is of the order of 300 g/cm². As the distance from the producer to counter E is too small to allow the decay of the π-mesons initially produced, we can conclude that the cross section for nuclear absorption of π-mesons in lead, in our range of energies, is less than half the geometrical cross section. This conclusion is in agreement with the results of other workers.[4–9]

However, our results do not allow us to make a definite statement on the value of the nuclear interaction length in lead of the π-mesons. Our arrangement is not sensitive to small-angle scattering with a small energy transfer to the lead nucleus. But it is believed that nuclear interactions should produce, on the average, rather large angle scattering, and these were shown by Brown and McKay[4] to be 4 or 5 times less frequent than catastrophic interactions. Besides, our arrangement has a reasonable efficiency for detecting large angle scattering. Another fact which could mask a possible nuclear interaction is the production by the π-meson of penetrating secondaries in lead. It is rather difficult to meet this argument but we may remember that the energy of the particles striking counter E cannot exceed about 1 Bev. In order to reconcile our results with a geometrical cross section for nuclear interaction (this corresponds to a mean range in lead of about 150 g/cm²), as found by the Bristol group,[10] more than half of all interactions should result in the production of a PS able to strike counter E with high efficiency. We do not know whether this can happen in our range of rather low energies.

We wish to acknowledge our gratitude to the Comissão de Pesquisas Cientificas da Universidade de São Paulo and to its president, Professor Souza Campos, for having supported, financially, our experiments in Campos do Jordão. We are grateful to Mr. H. W. Hering for his hospitality.

[4] W. W. Brown and A. S. McKay, Phys. Rev. **77**, 342 (1950).
[5] Butler, Rosser, and Barker, Proc. Phys. Soc. (London) **63**, 145 (1950).
[6] J. B. Harding and D. H. Perkins, Nature **164**, 285 (1949).
[7] W. B. Fretter, Phys. Rev. **76**, 511 (1949).
[8] Lovati, Mura, Salvini, and Tagliaferri, Phys. Rev. **77**, 284 (1950).
[9] O. Piccioni, Phys. Rev. **77**, 6 (1950).
[10] Camerini, Fowler, Lock, and Muirhead, Phil. Mag. **41**, 413 (1950).

Announcement: Publication Charge for Letters to the Editor

At the meeting of the Publication Board of the American Institute of Physics on January 30, 1951, a proposed publication charge for Letters to the Editor (and similar sections) was approved. The charge will be effective with the July issues and will be at a flat rate of $10.00 for each Letter. As in the case of regular articles, the charge will be made against the institution rather than the individual author and will be on a voluntary basis. When honored, 100 reprints will be provided without further cost.

The Journals affected are the following:

Physical Review
Journal of the Acoustical Society
Review of Scientific Instruments (Laboratory and Shop Notes)
Journal of Chemical Physics
Journal of Applied Physics

Heisenberg Operators in Quantum Electrodynamics. I

F. J. DYSON
Institute for Advanced Study, Princeton, New Jersey
(Received December 11, 1950)

A new analytic continuation principle is described, by means of which the calculation of matrix elements of Heisenberg operators in any quantized field theory is greatly simplified. By a "Heisenberg operator" is meant an average over a finite space-time region of a field operator in the Heisenberg representation of the theory. The analytic continuation is made by varying the characteristic masses of the fields through real values. In this way a Heisenberg operator with the physically occurring masses is derived from an operator calculated with very large fictitious masses. In the region of large masses, where real creation of particles is impossible, the operator is identical with the S-matrix for a suitably chosen scattering problem. The calculation reduces to the calculation of an S-matrix, to which the techniques of Feynman are directly applicable.

The S-matrix itself is a nonanalytic function of the masses in the region of values where thresholds for real processes occur. A special device is introduced in order to bypass the region of nonanalyticity. The Heisenberg operator is modified by the insertion of real exponential damping factors which have the effect of making all energy denominators in a perturbation expansion complex. The modified operator is an analytic function of the masses and of the damping coefficients, for all real positive values of the masses. The analytic continuation is made by varying the masses while the damping coefficients are non-zero, letting the damping coefficients tend to zero when the physical values of the masses have been reached.

I. INTRODUCTION

IT is generally believed that quantum electrodynamics, in spite of its inherent divergences, constitutes a consistent and meaningful theory. That is to say, given any directly measurable physical effect, the theory will predict for it a finite and unambiguous value, or statistical distribution of values. It has become possible to use the theory consistently, and to circumvent the divergence difficulties, by using the idea of renormalization of constants, an idea originally suggested by Kramers[1] and Bethe,[2] and worked out in detail by Schwinger,[3] Tomonaga,[4] Feynman,[5] and others. All these authors, however, have only applied the theory to particular problems. No general proof exists that the theory will give finite values for all measurable quantities in all situations.

A start in the construction of such a proof was made by the author,[6] who showed that all matrix elements of the S-matrix in quantum electrodynamics become finite after the renormalizations of mass and charge are carried out. This analysis of the S-matrix falls short of what is required in two important respects. (i) The S-matrix is written down as a formal series expansion in powers of the coupling constant e, assuming the series to be convergent after the renormalizations are carried out; the convergence of the series is never proved, and the series is in fact certainly not convergent in problems in which bound states are involved; thus, the analysis is applicable only to pure scattering processes between free particles. (ii) The S-matrix describes the results of measurements of the over-all behavior of a system integrated over space-time; it does not include a description of local measurements, for example, measurements of field-strengths and current-densities in finite space-time regions. The purpose of the present series of papers is to remove the defect (ii) of the previous work. It will be proved that quantum electrodynamics gives well-defined finite values for all locally measurable quantities, whenever the expansion in powers of e is convergent. Incidentally, it will appear that our methods provide a basis for removing defect (i) also from the analysis; this question will be discussed in later papers of the series.

By a locally measurable quantity in quantum electrodynamics[7] is meant an operator such as the field-average

$$\mathbf{F}_{\mu\nu}(R)=(1/V)\int_R \mathbf{F}_{\mu\nu}(x)d_4x, \tag{1}$$

where $\mathbf{F}_{\mu\nu}(x)$ is an electromagnetic field-strength operator in the Heisenberg representation, and R is a finite space-time region of 4-dimensional volume V. We use heavy type for Heisenberg representation operators, light type for interaction representation operators. Another example of a measurable quantity is

$$\mathbf{j}_\mu(S)=(1/V)\int \mathbf{j}_\mu(x)S(x)d_4x; \tag{2}$$

[1] H. A. Kramers, "Non-relativistic quantum-electrodynamics and correspondence principle," Solvay Conference Report, Brussels, 1948.
[2] H. A. Bethe, Phys. Rev. **72**, 339 (1947).
[3] J. Schwinger, Phys. Rev. **74**, 1439 (1948); **75**, 651 (1949); **76**, 790 (1949).
[4] T. Tati and S. Tomonaga, Prog. Theor. Phys. **3**, 391 (1948); Fukada, Miyamoto, and Tomonaga, Prog. Theor. Phys. **4**, 47 and 121 (1949). Also earlier papers in the same journal.
[5] R. P. Feynman, Phys. Rev. **76**, 749 and 769 (1949); **80**, 440 (1950).
[6] F. J. Dyson, Phys. Rev. **75**, 486 and 1736 (1949). These papers will be referred to hereafter as (A) and (B).
[7] The author is much indebted to Professor W. Pauli and Dr. Res Jost, who pointed out to him the necessity for working in terms of such field-averages. An unpublished calculation of Dr. Jost, communicated to the author by letter in March, 1950, included many of the ideas of the present series of papers.

here $\mathbf{j}_\mu(x)$ is a current-density operator in the Heisenberg representation, and $S(x)$ is a function which is zero outside R and unity inside R, except in a thin shell in the neighborhood of the boundary of R in which it changes smoothly from 0 to 1. As is well known,[8] the smoothness of $S(x)$ at the boundary of R is necessary in case (2) in order to obtain an operator whose mean-square fluctuation is finite. Operators such as (1) and (2) can be built up by linear superposition of the Fourier-transformed operators

$$\mathbf{F}_{\mu\nu}(p)=(1/2\pi)^4\int \mathbf{F}_{\mu\nu}(x)e^{-ip\cdot x}d_4x, \tag{3}$$

$$\mathbf{j}_\mu(p)=(1/2\pi)^4\int \mathbf{j}_\mu(x)e^{-ip\cdot x}d_4x, \tag{4}$$

where p is an arbitrary 4-vector in momentum-space. The program of this and the next paper in the series will be to prove in detail that the operator (4) is finite after all renormalizations have been carried out, including a renormalization of the unit of charge in terms of which (4) is measured. A simple argument will then show that (3) is finite after a corresponding renormalization of the unit of field-strength. It will be clear that the methods are of general validity and could be applied equally well to any locally measurable operator of the same form as (1) or (2).

The scope of the present paper is to formulate a general expansion theorem, expressing Heisenberg operators such as (3) and (4) in terms of interaction representation operators.[9] The second paper of the series will carry through the renormalization program for these operators, using the expansion theorem as a mathematical basis. The statement of the expansion theorem occupies Sec. VIII of the present paper. The theorem is surprisingly simple, being formally identical with the corresponding expansion theorem for the S-matrix which was the basis of the previous analysis. The calculation of Heisenberg operators is thereby made fully as easy as the calculation of the S-matrix. There is no longer any advantage, for practical calculations, in using the S-matrix method in preference to the original contact-transformation method of Schwinger, which works in terms of Heisenberg operators. In fact, the two methods of calculation differ only when in the S-matrix a higher order radiative effect is mixed with contributions from real effects occurring in lower order; and just in these circumstances the Heisenberg operators are simpler to use, since they isolate the true higher order effects from the others. It will be found that, in general, for radiation problems which are not direct calculations of scattering matrix elements, the Heisenberg operators are a more appropriate practical tool than is the S-matrix.

[8] W. Heisenberg, Leipzig. Ber. **86**, 317 (1934).

[9] Expressions for the Heisenberg operators in terms of interaction operators have been studied previously by G. Källén, Arkiv Fysik **2**, 187 (1950). D. Feldman and C. N. Yang, Phys. Rev. **79**, 972 (1950).

II. FORMAL MANIPULATIONS

The expression for $\mathbf{j}_\mu(x)$ in terms of interaction representation operators is

$$\mathbf{j}_\mu(x)=S^{-1}(t)j_\mu(x)S(t), \tag{5}$$

where t is the time at the space-time point x, and the transformation operator $S(t)$ is [10]

$$S(t)=\sum_{n=0}^{\infty}\left(-\frac{i}{\hbar c}\right)^n\int_{-\infty}^{t}dx_1\int_{-\infty}^{t_1}dx_2 \cdots\int_{-\infty}^{t_{n-1}}dx_n H^I(x_1)H^I(x_2)\cdots H^I(x_n). \tag{6}$$

Here,

$$H^I(x)=H_1(x)+H_s(x), \tag{7}$$

$$H_1(x)=-(1/c)j_\mu(x)A_\mu(x), \tag{8}$$

$$H_s(x)=-\delta mc^2\bar{\psi}(x)\psi(x), \tag{9}$$

$$j_\mu(x)=iec\bar{\psi}(x)\gamma_\mu\psi(x), \tag{10}$$

all these being interaction representation operators. Expanding Eq. (5) gives an expression for $\mathbf{j}_\mu(x)$ as a series of multiple commutators

$$\mathbf{j}_\mu(x)=\sum_{n=0}^{\infty}\left(\frac{i}{\hbar c}\right)^n\int_{-\infty}^{t}dx_1\int_{-\infty}^{t_1}dx_2\cdots\int_{-\infty}^{t_{n-1}}dx_n[H^I(x_n), [\cdots,[H^I(x_2),[H^I(x_1),j_\mu(x)]]\cdots]]. \tag{11}$$

By a rearrangement of terms, this series may be written in the alternative form

$$\mathbf{j}_\mu(x)=\sum_{q=0}^{\infty}\sum_{p=0}^{\infty}\left(\frac{i}{\hbar c}\right)^q\left(-\frac{i}{\hbar c}\right)^p\frac{1}{q!p!}\int_{-\infty}^{\infty}dx_1\cdots\int_{-\infty}^{\infty}dx_{q+p} \bar{P}(H^I(x_1),\cdots,H^I(x_q))P(H^I(x_{q+1}),\cdots, H^I(x_{q+p}),j_\mu(x)), \tag{12}$$

where the P-bracket denotes, as usual, a chronologically ordered product, and the $\bar{P}$-bracket is a product ordered antichronologically, reading the order of factors in both cases from right to left.

In an expression such as Eq. (11), involving products of many interaction representation operators, all kinds of higher order virtual processes are implicitly included. The aim of our analysis is to find an expansion of $j_\mu(x)$ in which virtual processes are represented explicitly, so that the divergences which arise from virtual processes can be recognized and eliminated. Stated precisely, our aim is to express $j_\mu(x)$ as a sum of "normal products" multiplied by c-number coefficients; a normal

[10] The notation is not exactly the same as in references (A) and (B).

product is defined to be a product of free particle emission and absorption operators in which all emission operators stand to the left of all absorption operators,[11] so that no virtual emission and reabsorption processes are implicitly represented in it. The free particle operators are defined to be the coefficients $A_\mu(k)$, $\psi_\alpha(k)$, $\bar{\psi}_\alpha(k)$ in the momentum representations

$$\left.\begin{aligned} A_\mu(x) &= \int dk A_\mu(k)\exp(ik\cdot x) \\ \psi_\alpha(x) &= \int dk \psi_\alpha(k)\exp(ik\cdot x) \\ \bar{\psi}_\alpha(x) &= \int dk \bar{\psi}_\alpha(k)\exp(ik\cdot x) \end{aligned}\right\} \tag{13}$$

of the interaction representation operators, the coefficients with positive values of the fourth component k_0 being by definition absorption operators, those with negative values of k_0 emission operators. The reasons for expressing $j_\mu(x)$ as a sum of normal products are the following. Given any initial and final states specified by definite numbers of free particles with definite polarizations and momenta, there exists precisely one normal product with a non-zero matrix element between these two states. Therefore, a decomposition of $j_\mu(x)$ into normal products is equivalent to a complete listing of the matrix elements of $j_\mu(x)$ in the representation in which free-particle occupation numbers are diagonal. The effects of virtual processes are represented explicitly in the numerical factors multiplying the various normal products.

There is a general theorem due to Wick[12] which states that every product Q of interaction representation operators $\bar{\psi}_\alpha(x)$, $\psi_\beta(y)$, $A_\mu(z)$ has a unique decomposition into a sum of normal products. The decomposition is a consequence only of the commutation relations between the factors of Q; it is an operator identity, independent of the particular states in which we may be interested. Just for this reason, the rules for decomposing Q into a sum of normal products are simpler than the rules given in the author's earlier papers[6] for writing down the matrix elements of Q between given states. The two sets of rules are equivalent, but there is a great advantage in working with the normal product decomposition because this method makes unnecessary any explicit reference to the vacuum state of the fields.

Wick has stated and proved his theorem only for a chronologically ordered product Q. The theorem and the method of proof are valid, however, for all products. We shall here state the theorem in its general form, referring to Wick's paper for the proof.

We define a "factor pairing" of Q in the following way. A certain number (in particular this number may be all, or none, or any intermediate even number) of the factors of Q are associated together into pairs, the members of each pair being either one $\bar{\psi}$ and one ψ, or two A_μ operators. The remaining factors are left unpaired. Two factor-pairings are regarded as distinct, even when the number of pairs and the nature of the factors composing them are the same in both, provided that the positions in Q of the paired factors are different in the two cases.

To each factor-pairing corresponds a "rearranged form" of Q as follows. First, one pair of factors P_1 is brought to the left side of Q, the order of factors in the pair being kept as it was in Q. Then another pair of factors P_2 is brought to the left and placed immediately to the right of the first pair, and so on. The order in which the pairs are chosen is not significant. When all the pairs have been picked out, the unpaired factors are left, forming a product U. The rearranged form $F=P_1P_2\cdots U$ is given the sign plus or minus according as the permutation of electron-positron factors in going from Q to F is even or odd.

Corresponding to any given product U we define the "normal product" $N(U)$. First, the factors of U are decomposed according to Eq. (13) into sums of particle emission and absorption operators; U is then a sum of products of these elementary operators. $N(U)$ is formed from U by rearranging independently each of the products of elementary operators so that absorption operators stand to the right of emission operators, giving to each rearranged product independently the sign plus or minus according as the permutation of electron-positron factors was even or odd.

Finally, a "normal constituent" of Q is obtained from each rearranged form F as follows. The unpaired factors U are replaced by $N(U)$. Each pair of factors $\psi_\alpha(x)\bar{\psi}_\beta(x')$ is replaced by the C-number

$$-iS_{\alpha\beta}{}^{+}(x-x')=[-i/(2\pi)^3]\int d_4k\theta(k)\delta(k^2+m^2) \times(k_\mu\gamma_\mu+im)_{\alpha\beta}\exp[ik\cdot(x-x')]. \tag{14}$$

Each pair of factors $\bar{\psi}_\beta(x')\psi_\alpha(x)$ is replaced by

$$-iS_{\alpha\beta}{}^{-}(x-x')=[i/(2\pi)^3]\int d_4k\theta(-k)\delta(k^2+m^2) \times(k_\mu\gamma_\mu+im)_{\alpha\beta}\exp[ik\cdot(x-x')]. \tag{15}$$

Each pair $A_\mu(x)A_\nu(x')$ is replaced by

$$i\hbar c\delta_{\mu\nu}D^{+}(x-x')=[\hbar c/(2\pi)^3]\delta_{\mu\nu}\int d_4k\theta(k) \times\delta(k^2+\lambda^2)\exp[ik\cdot(x-x')]. \tag{16}$$

[11] The decomposition of an operator into normal products has been frequently used in the past, for example by E. G. C. Stueckelberg, Nature **153**, 143 (1944); A. Houriet and A. Kind, Helv. Phys. Acta **22**, 319 (1949).

[12] G. C. Wick, Phys. Rev. **80**, 268 (1950).

Here, $\theta(k)$ is the step-function defined by

$$\theta(k)=1, \quad k_0>0, \qquad \theta(k)=0, \quad k_0<0, \tag{17}$$

where k_0 is the fourth component of the 4-vector k; m is the reciprocal of the electron Compton wavelength. λ is a real constant which has the value zero when A_μ is the electromagnetic field. It is essential to our method that we carry through the analysis also for non-zero values of λ; this means that we consider A_μ to be either the electromagnetic field or a neutral vector meson field with rest-mass $(\hbar\lambda/c)$.

After these replacements, F becomes an operator E which is by definition the normal constituent of Q corresponding to the factor-pairing from which F was derived. Each E is thus a normal product multiplied by various coefficients (15), (16), (17).

The theorem of Wick can now be stated concisely. *Every product Q is identically equal to the sum of its normal constituents.*

In order to decompose $j_\mu(x)$ into a sum of normal products, we choose any particular term in the expansion (11), for example,

$$I_n(x)=\int_{-\infty}^{t} dx_1 \int_{-\infty}^{t_1} dx_2 \cdots \int_{-\infty}^{t_{n-1}} dx_n [H_1(x_n), [\cdots, [H_1(x_1), j_\mu(x)]\cdots]]. \tag{18}$$

This term can be rewritten more symmetrically as

$$I_n(x)=(1/n!)\int_{-\infty}^{\infty}\cdots\int_{-\infty}^{\infty} dx_1\cdots dx_n S, \tag{19}$$

where

$$S=\sum \theta(x-x_1)\theta(x_1-x_2)\cdots\theta(x_{n-1}-x_n)[H_1(x_n), [\cdots, [H_1(x_1), j_\mu(x)]\cdots]], \tag{20}$$

the summation being over the $(n!)$ permutations of the points $x_1, \cdots, x_n$. S is a sum of $(2^n n!)$ products, all of them made up of the same factors in various orders. By a factor-pairing of S we mean a simultaneous pairing of identical pairs of factors in each of the $(2^n n!)$ products. To each factor-pairing F of S there corresponds a normal constituent E which is the sum of $(2^n n!)$ normal constituents, one taken from each product. The enumeration of the factor-pairings of S is now identical with the enumeration of factor-pairings for the chronological product

$$P(H_1(x_n), \cdots, H_1(x_1), j_\mu(x)), \tag{21}$$

which was required for the calculation of the S-matrix.[6] Exactly as in the S-matrix analysis, each factor-pairing is represented by a Feynman graph G, with $(n+1)$ vertices $x, x_1, \cdots, x_n$ connected by lines indicating which operators are to be paired.

III. INTRODUCTION OF DOUBLED FEYNMAN GRAPHS

Since we are now dealing with multiple commutators rather than with simple products, the analysis of operators given by the Wick theorem and represented by ordinary Feynman graphs will no longer be sufficient. We shall develop a more refined analysis, which will lead to a graphical representation by means of a new kind of diagram called a "doubled Feynman graph."

For brevity, we use the word "exchange-term" to mean either a commutator of two A_μ operators or an anticommutator of a $\bar\psi$ and a ψ operator; we use "sum-term" to mean either an anticommutator of two A_μ or a commutator of a $\bar\psi$ and a ψ. We write also instead of Eq. (20),

$$S=\sum \Theta C, \tag{22}$$

C denoting any one of the multiple commutators in Eq. (20) and Θ the corresponding product of θ-functions which specifies a particular chronological order of the points $x_1, x_2, \cdots, x_n$. Let a factor-pairing F of S, with b factor-pairs, be given. Let the Feynman graph corresponding to F be G, and let S_G be the corresponding normal constituent of S. In constructing S_G, we express each of the functions (14), (15), (16) as half the sum or difference of an exchange term and a sum-term. Thus,

$$D^{\pm}(x)=\tfrac{1}{2}[D(x)\mp iD^1(x)], \qquad S^{\pm}(x)=\tfrac{1}{2}[S(x)\mp iS^1(x)], \tag{23}$$

where $D^1(x)$ is the even function

$$D^1(x)=(1/2\pi)^3\int d_4k\,\delta(k^2+\lambda^2)e^{ik\cdot x}, \tag{23.1}$$

and S^1 is similarly defined.[13] Then, S_G is of the form

$$S_G=N_G\sum_P P L_P. \tag{24}$$

Here, the summation is over the 2^b possible products P; each P is a product of b factors, one corresponding to each internal line of G; to an electron line of G corresponds either a factor S or a factor S^1 in P, and to a photon line corresponds either D or D^1. For each P, L_P is a certain linear combination of the products Θ appearing in Eq. (22). N_G is a normal product of the $(3n+2-2b)$ unpaired factors in F, and depends only on G and not on P. The representation of S_G in the form (24) is unique.

To obtain further information about the L_P, we use an alternative form of S from which Eq. (12) was derived, namely,

$$S=\sum_{q=0}^{n}(-1)^{n-q}\sum \bar P(H_1(x_1'), \cdots, H_1(x_q')) \times P(H_1(x'_{q+1}), \cdots, H_1(x_n'), j_\mu(x)). \tag{24.1}$$

The inner sum is here over the $[n!/q!(n-q)!]$ ways of

[13] J. Schwinger, Phys. Rev. 75, 651 (1949), Appendix.

choosing q points $x_1', \cdots, x_q'$ out of the n points $x_1, \cdots, x_n$. It is important that in Eq. (24.1) the θ-functions no longer appear explicitly. When S_G is constructed from Eq. (24.1), each term of the inner sum gives rise to a product of functions S^+, S^-, D^+, S_F, $\bar{S}_F$, D_F, and $\bar{D}_F$. The function $D_F(x-x')$ arises from the replacement of $P(A_\mu(x), A_\nu(x'))$ according to Eq. (16), and is given by

$$D_F(x)=D^1(x)+i[2\theta(x)-1]D(x). \tag{24.2}$$

This is the Feynman D-function, which was used extensively in (A) and (B). The function $\bar{D}_F(x-x')$ arises from the replacement of $\bar{P}(A_\mu(x), A_\nu(x'))$ and is given by

$$\bar{D}_F(x)=D^1(x)-i[2\theta(x)-1]D(x). \tag{24.3}$$

S_F and $\bar{S}_F$ are similarly defined. Now using Eqs. (23), (24.2), and (24.3), we again obtain S_G in the form (24), but with θ-functions arising only from the factors (24.2), (24.3). Therefore, L_P is a linear combination with numerical coefficients of terms W, each W being a product of factors $\theta(x'-x'')$; we say that each term W is "correct," meaning by this that to each factor $\theta(x'-x'')$ in W there corresponds at least one exchange-term factor $S(x'-x'')$ or $S(x''-x')$ or $D(x'-x'')$ in P. Thus, S_G has been expressed in a form where every θ-function is accompanied by a corresponding exchange-term.

Let W_1 be any term in L_P which contains a set of factors forming a cycle, for example,

$$\theta(x_1-x_2)\theta(x_3-x_2)\theta(x_4-x_3)\theta(x_4-x_1). \tag{24.4}$$

We may replace some of these factors by equivalent expressions according to the identity

$$\theta(x_i-x_j)=1-\theta(x_j-x_i). \tag{24.5}$$

Then W_1 is split into a sum of terms W', one of which contains the factors

$$\theta(x_1-x_2)\theta(x_2-x_3)\theta(x_3-x_4)\theta(x_4-x_1) \tag{24.6}$$

and is identically zero, while the others all contain fewer factors than does W_1. The terms W' obtained in this way are all correct. If some of them again contain cycles of factors, these W' can again be replaced by sums of terms with a smaller number of factors. In this way we shall finally arrive at an expression for L_P as a linear combination of products W, each W being correct and cycle-free.

Given any cycle-free W_2 which contains a chain of factors beginning with the point x, for example,

$$\theta(x_1-x)\theta(x_1-x_2)\theta(x_3-x_2)\theta(x_4-x_3),$$

we can replace certain factors as before by Eq. (24.5) in such a way that W_2 is replaced by a sum of correct cycle-free terms W'. One of the W' contains the chain of factors

$$\theta(x-x_1)\theta(x_1-x_2)\theta(x_2-x_3)\theta(x_3-x_4), \tag{24.7}$$

while the others contain fewer factors than W_2. Proceeding in this way, we arrive ultimately at an expression for L_P as a linear combination of products W, each W being correct and cycle-free and also "ordered with respect to x." By this last phrase we mean that every chain of factors in W beginning with x is of the special form (24.7). A cycle-free W which is ordered with respect to x has the following property. The points $x_1, \cdots, x_n$ fall into two classes, C_1 and, C_2, one of which may be empty. There does not exist any factor $\theta(x'-x'')$ in W with x' and x'' in different classes. For every x_i in C_1, there exists one and only one chain of factors in W of the form

$$\theta(x-x')\theta(x'-x'')\cdots\theta(x'''-x_i), \tag{24.8}$$

connecting the points x and x_i.

Each W may be expressed as a linear combination of products

$$Z_q=\theta(x-x_1')\theta(x_1'-x_2')\cdots\theta(x'_{q-1}-x_q')\theta(x'_{q+1}-x'_{q+2})\cdots\theta(x'_{n-1}-x_n'),$$

where q takes the values $0, 1, 2, \cdots, n$, and $x_1', \cdots, x_n'$ are any permutation of the points $x_1, \cdots, x_n$. When W is cycle-free and ordered with respect to x, then an expansion of W into a sum of Z_q can be made, using only those Z_q for which the points $x_1', \cdots, x_q'$ make up the class C_1. It was proved earlier that L_P is a linear combination of the Θ occurring in Eq. (22), that is to say, a linear combination of Z_q with $q=n$. Also, L_P is a sum of W, each W being a linear combination of Z_q with q equal to the number of points in the class C_1 corresponding to W. But the representation of L_P as a linear combination of Z_q is unique; if a linear combination of the Z_q is zero, then every coefficient must be zero. Therefore, the sum of the terms W in L_P, for which the number of points in C_1 is not n, is identically zero. We need retain only the terms W for which the class C_2 is empty.

Summarizing the results of the analysis so far, we have expressed S_G in the form (24). L_P is a linear combination of products W, with numerical coefficients. Each W is a product of factors $\theta(x'-x'')$ which is correct, and cycle-free and ordered with respect to x, and connected. By connected we mean that a chain of factors (24.8) exists in W for every point x_i. This has the important consequence that *non-zero normal constituents S_G of S are obtained only from connected graphs G.* We shall suppose henceforward that G is connected, which implies $b \geq n$.

A "doubled Feynman graph," G_T, is defined as the graph G with a certain subset T of its internal lines drawn double. The figure formed by the doubled lines T must satisfy three conditions: (i) it is connected; (ii) it is simply connected, without closed cycles; (iii) at least one line of T is incident at every vertex of G. These conditions imply that there are just n lines in T.

To each product W we associate a doubled graph G_T in the following way. To each factor $\theta(x'-x'')$ in W there corresponds one or more exchange-term factors in P involving the two points x' and x''. If there is more than one such exchange-term, we choose one arbitrarily and ignore the others. To each factor of W corresponds then one factor in P, and hence one internal line of G. The set T of lines so obtained satisfies the three required conditions for a set of doubled lines. We call T the "order-type" of W, and G_T is the corresponding doubled graph.

The order-type T implies a partial ordering of the points $x, x_1, \cdots, x_n$ defined by the following two statements: (i) x is later than x_i for all i; (ii) x_i is later than x_j if x_i lies on a polygonal arc joining x_j to x in T. Thus, T fixes W uniquely. The partial ordering is a complete ordering only if T is a single continuous arc without branches and with one end point at x.

Regrouping the terms of the sum (24), we have

$$S_G = N_G \sum_T S_1(T) S_2(T), \tag{25}$$

where the summation is over the order-types T compatible with G. Each $S_1(T)$ is a product of n factors of the form

$$\theta(x'-x'')S(x'-x''), \quad \theta(x'-x'')S(x''-x') \text{ or } \theta(x'-x'')D(x'-x''), \tag{26}$$

one corresponding to each doubled line of G_T. Each $S_2(T)$ is a linear combination of products of $(b-n)$ factors of the form

$$S(x'-x''), \quad D(x'-x''), \quad S^1(x'-x''), \text{ or } D^1(x'-x''), \tag{27}$$

one factor corresponding to each undoubled internal line of G_T.

Equation (25) is the conclusion of this lengthy analysis of S_G by means of doubled graphs. The only purpose of the analysis is to show that the θ-functions in Eq. (20) can be so rearranged that they occur always in conjunction with exchange-terms as in (26). Fortunately, the subsequent arguments will be of such a kind that we shall never need to carry out the rearrangement in practice. The final results will be very simple and will not involve θ-functions explicitly; but it seems to be essential, in order to justify the simple rules of calculation which we shall later formulate, to prove that the rearrangement of θ-functions is possible in principle.

For completeness, we must here observe that Eq. (18) is not the most general kind of term in the expansion of Eq. (11). In addition to Eq. (18), we shall need to consider terms in which a multiple commutator C_r appears involving, say, r operators H_1 and $(n-r)$ operators H_s. When Eq. (7) is substituted into Eq. (11), such commutators always appear in symmetrical combinations; thus,

$$\sum C_r = \sum [H_{1,s}(x_n), [\cdots, [H_{1,s}(x_1), j_s(x)]\cdots]], \tag{28}$$

where the summation is over the $\binom{n}{r}$ ways of choosing r suffixes 1 and $(n-r)$ suffixes S. The points $x_1, \cdots, x_n$ are not permuted in the different terms of Eq. (28). When we pass to the symmetrical form analogous to Eq. (19), we must now write

$$I_n(x) = (1/n!) \sum \int_{-\infty}^{\infty} \cdots \int_{-\infty}^{\infty} dx_1 \cdots dx_n S_r, \tag{29}$$

$$S_r = \sum \theta(x-x_1)\cdots\theta(x_{n-1}-x_n)[H_{1,s}(x_n), [\cdots, [H_{1,s}(x_1), j_s(x)]\cdots]]. \tag{30}$$

Here, the summation in Eq. (29) is over the $\binom{n}{r}$ ways in which we can associate with each of the points $x_1, \cdots, x_n$ either H_1 or H_s. The summation in Eq. (30) is over the $(n!)$ permutations of $x_1, \cdots, x_n$, the operators H_1 and H_s being permuted simultaneously so that each x_i carries its own operator around with it. By splitting up the double summation in this special way, we have arranged that S_r is a sum of products of the same factors in various orders. The different terms in Eq. (29), on the other hand, involve products of different sets of factors and are represented by different sets of graphs G. Therefore, we make the analysis into normal constituents for each S_r separately. In all other respects, the terms involving S_r can be treated in precisely the same way as the terms in S. To avoid needless complications, we dismiss the S_r with these brief remarks and carry through the analysis only for S.

IV. MOMENTUM SPACE REPRESENTATIONS

We wish to calculate the coefficient multiplying a particular normal product such as

$$N(\bar{\psi}_\alpha(p_1)\bar{\psi}_\beta(p_2)\cdots\psi_\delta(p_i)\cdots A_\lambda(p_j)\cdots A_\nu(p_l)) \tag{31}$$

in the expansion of $\mathbf{j}_\mu(p)$. Here $p, p_1, p_2, \cdots, p_l$ are given 4-vectors and $\alpha, \beta, \cdots, \lambda, \cdots, \nu$ are given spinor and vector suffixes. Let this coefficient be M. Then M is a sum of contributions $M(S)$ from different integrals of the general form

$$I_n(p) = (1/n!) \int_{-\infty}^{\infty} \cdots \int_{-\infty}^{\infty} dx_1 \cdots dx_n \int_{-\infty}^{\infty} dx e^{-ip\cdot x} S, \tag{32}$$

with S given by Eq. (20).

We now take the decisive step which will have the effect of simplifying the calculation of $M(S)$. We consider instead of $M(S)$ the corresponding coefficient $M_\Gamma(S)$ in the expansion of the generalized operator

$$I_n(\Gamma, p) = (1/n!) \int_{-\infty}^{\infty} \cdots \int_{-\infty}^{\infty} dx_1 \cdots dx_n \int_{-\infty}^{\infty} dx S \times \exp[-ip\cdot x + \Gamma_1\cdot(x-x_1) + \Gamma_2\cdot(x-x_2) + \cdots + \Gamma_n\cdot(x-x_n)]. \tag{33}$$

Here, the Γ_i are n 4-vectors with components

$$\Gamma_i=(0, 0, 0, \Gamma_{i0}) \tag{34}$$

and the Γ_{i0} are any n complex numbers with positive real parts. In Eq. (33) the integrals over $x_1, \cdots, x_n$ are exponentially convergent. The integrals in Eq. (32) are not convergent but either oscillate or diverge at infinity. We shall see later[14] that there are good physical reasons for *defining* the value of Eq. (32) to be the limit of Eq. (33) as all the Γ_{i0} tend to zero in a certain way. That is to say, we use the Abel summation method to give a meaning to Eq. (32). We shall discuss only very incompletely the physical meaning of Eq. (33) for finite Γ_{i0}, which will form the subject of a separate paper. The $I_n(\Gamma, p)$ are here used simply as mathematical auxiliaries in the evaluation of $I_n(p)$.

Let G be any Feynman graph with the correct external lines to give rise to normal constituents with the operator factor (31). Then, $M_\Gamma(S)$ is a sum of contributions $M_\Gamma'(S_G)$ from all such G. Each $M_\Gamma'(S_G)$ may be further subdivided into contributions $M_\Gamma(S_G)$ arising from a graph G with particular association of each factor in Eq. (31) to one external line of G, so that each external line is restricted to represent a particle carrying a certain definite momentum p_r. Finally, each $M_\Gamma(S_G)$ is a sum of contributions $M_\Gamma(S, G_T)$, one from each doubled graph G_T derived from G.

Let t_i be the algebraic sum of the momenta carried by the external lines of G at the vertex x_i. Then $M_\Gamma(S, G_T)$ is apart from numerical factors an integral

$$M_\Gamma(S, G_T)=\int_{-\infty}^{\infty}\cdots\int_{-\infty}^{\infty}\cdots dx dx_1\cdots dx_n S_1 S_2$$
$$\times\exp[-ip\cdot x-it_1\cdot x_1\cdots-it_n\cdot x_n+\Gamma_1\cdot(x-x_1)$$
$$+\cdots+\Gamma_n\cdot(x-x_n)], \tag{35}$$

where S_1 is a product of n factors (26), and S_2 is a sum of products of $(b-n)$ factors (27). The "numerical factors" which are omitted from Eq. (35) depend on G but are independent of T. They are unimportant because we shall finally arrive at a much simpler formula for the precise evaluation of $M_\Gamma(S_G)$ including numerical constants; we shall use Eq. (35) only in order to determine the analytic behavior of $M_\Gamma(S, G_T)$ as a function of the Γ_{i0}. Now, write f for $(b-n)$, and let λ_a, $a=n+1, \cdots, b$, be the undoubled internal lines of G_T. The electron lines of G have arrows giving them a definite sense; it is convenient also to insert arbitrarily an arrow in each photon line, so that every line has a sense. Let the end points of λ_a be $x_a'x_a''$, with the arrow pointing from x_a'' towards x_a'. Suppose that $\lambda_{n+1}, \cdots, \lambda_{n+g}$ are electron lines and $\lambda_{n+g+1}, \cdots, \lambda_b$ are photon lines. Then S_2 can be written as an f-fold integral in momentum-space

$$S_2=\int_{-\infty}^{\infty}\cdots\int_{-\infty}^{\infty}dk_{n+1}\cdots dk_b C(k_{n+1}, \cdots, k_b)$$
$$\times\prod_{a=n+1}^{n+g}(k_{a\mu}\gamma_\mu+im)\delta(k_a^2+m^2)\prod_{a=n+g+1}^{b}\delta(k_a^2+\lambda^2)$$
$$\times\prod_{a=n+1}^{b}\exp[ik_a\cdot(x_a'-x_a'')]. \tag{36}$$

Here $C(k_{n+1}\cdots, k_b)$ is some numerical function which takes only 2^f distinct values, since it depends only on the signs of the fourth components of $k_{n+1}, \cdots, k_b$. The values of $C(k_{n+1}, \cdots, k_b)$ will depend on the precise combinations of D^1, D, S^1, and S functions occurring in S_2. They are pure numbers depending only on the shape of G_T and independent of all variables such as p_i and Γ_i. The product

$$\prod(k_{a\mu}\gamma_\mu+im)$$

is a symbolic notation for a product of dirac matrices which, multiplied with a similar product arising from S_1, makes up a tensor with the correct vector and spinor suffixes to serve as a coefficient for Eq. (31) in $\mathbf{j}_n(p)$.

Next we introduce momentum representations for the factors of S_1. Let λ_i be the doubled line of G_T joining x_i to a point x_j or x which is later than x_i in T. Let y_i be the point x_j or x in question, and let

$$z_i=y_i-x_i. \tag{37}$$

If x' and x'' are any two vertices of G, let $\theta_T(x', x'')$ denote 1 if either $x'=x''$ or x' stands later than x'' in T, and zero otherwise. Then, by Eq. (37),

$$x-x_i=\sum_j\theta_T(x_j, x_i)z_j. \tag{38}$$

This implies the identities

$$\left.\begin{aligned}\textstyle\sum_i\Gamma_i\cdot(x-x_i)&=\textstyle\sum_j\Delta_j\cdot z_j,\\ \textstyle\sum_i l_i\cdot(x-x_i)&=\textstyle\sum_j u_j\cdot z_j,\\ \textstyle\sum_a k_a\cdot(x_a'-x_a'')&=\textstyle\sum_j q_j\cdot z_j,\end{aligned}\right\} \tag{39}$$

where

$$\left.\begin{aligned}\Delta_j&=\textstyle\sum\theta_T(x_j, x_i)\Gamma_i, \quad u_j=\sum\theta_T(x_j, x_i)l_i,\\ q_j&=\textstyle\sum_a[\theta_T(x_j, x_a'')-\theta_T(x_j, x_a')]k_a=\sum_a c_{ja}k_a.\end{aligned}\right\} \tag{40}$$

Always, the suffixes i and j run from 1 to n, and a runs from $n+1$ to b.

Now let

$$S_1'=\exp[\Gamma_1\cdot(x-x_1)+\cdots+\Gamma_n\cdot(x-x_n)]S_1. \tag{41}$$

By Eqs. (26) and (39), S_1' is a product of n factors, one corresponding to each doubled line λ_i. When λ_i is an electron line with the arrow in the sense x_iy_i, the factor is

$$S_{\Delta i}(z_i)=\exp(\Delta_i\cdot z_i)\theta(z_i)S(z_i). \tag{42}$$

When λ_i is an electron line with arrow in the sense y_ix_i, the factor is

$$S_{\Delta i}^*(z_i)=\exp(\Delta_i\cdot z_i)\theta(z_i)S(-z_i). \tag{43}$$

[14] In the next paper of this series. The idea of using a limiting process of this kind is due to B. Ferretti, Nuovo Cimento **7**, 79 and 375 (1950).

When λ_i is a photon line, the factor is

$$D_{\Delta i}(z_i)=\exp(\Delta_i\cdot z_i)\theta(z_i)D(z_i). \tag{44}$$

We denote the products of these three sets of factors in S_1' by

$$\Pi_e,\ \Pi_e',\ \text{and}\ \Pi_p, \tag{45}$$

respectively.

Now it happens that the special functions $S_\Delta(z)$, $S_\Delta{}^*(z)$, $D_\Delta(z)$ have particularly simple representations in momentum-space, when Δ is a vector of the form

$$\Delta_i=(0,0,0,\Delta_{i0}) \tag{46}$$

according to Eq. (40), and Δ_{i0} has a positive real part. For example, we shall prove that

$$D_\Delta(z)=-(1/2\pi)^4\int_{-\infty}^{\infty}dk e^{ik\cdot z}/[(k+i\Delta)^2+\lambda^2]. \tag{47}$$

Let I be the right-hand side of Eq. (47). The integrand is nonsingular for real k, and so there is no ambiguity in defining the integral to be along the real axis for all four components of k. We may evaluate I by using Cauchy's theorem in the complex k_0 plane, where k_0 is the fourth component of k. The poles are then at the two points

$$k_0=-i\Delta_0\pm(k_1^2+k_2^2+k_3^2+\lambda^2)^{\frac{1}{2}}. \tag{48}$$

When z_0 is negative, the integrand vanishes for large k_0 in the upper half-plane. Since the poles (48) lie below the real axis, the value of I is then zero. When z_0 is positive, I is given by the sum of the residues at the two poles, namely,

$$I=\exp(-\Delta_0 z_0)D(z).$$

This completes the proof of Eq. (47). In exactly the same way we find

$$S_\Delta(z)=[-i/(2\pi)^4]\int_{-\infty}^{\infty}dk e^{ik\cdot z}/[(k+i\Delta)_\mu\gamma_\mu-im], \tag{49}$$

$$S_\Delta{}^*(z)=[-i/(2\pi)^4]\int_{-\infty}^{\infty}dk e^{+ik\cdot z}/[(k+i\Delta)_\mu\gamma_\mu+im]. \tag{50}$$

Using now Eqs. (39), (41), (45), (47), (49), and (50) and omitting a numerical factor gives the momentum representation of S_1' as

$$S_1'=\int_{-\infty}^{\infty}\cdots\int_{-\infty}^{\infty}dk_1\cdots dk_n\prod_e\left[\frac{1}{(k_i+i\Delta_i)_\mu\gamma_\mu-im}\right]$$
$$\times\prod_e'\left[\frac{1}{(k_i+i\Delta_i)_\mu\gamma_\mu+im}\right]\prod_p\left[\frac{1}{(k_i+i\Delta_i)^2+\lambda^2}\right]\prod_{i=1}^{n}$$
$$\times\exp(ik_i\cdot z_i). \tag{51}$$

It remains only to substitute Eqs. (36) and (51) into Eq. (35). Using Eqs. (38) and (39), we may express $M_\Gamma(S,G_T)$ as an integral over the 4-vectors

$$x,\ z_1,\ \cdots,\ z_n,\ k_1,\ \cdots,\ k_b.$$

The integrations over x and the z_i are trivial, yielding only a product of $(n+1)$ δ-functions,

$$\delta(p+\textstyle\sum t_i)\delta(k_1+q_1+u_1)\cdots\delta(k_n+q_n+u_n). \tag{52}$$

The first factor in Eq. (52) is a constant multiplying factor expressing over-all conservation of energy and momentum. This factor will be replaced by a nonsingular function $f(\sum t_i)$ when the various Fourier components $\mathbf{j}_\mu(p)$ are superposed to form the physically measurable quantity (2). We omit this factor together with the other numerical factors in the discussion of Eq. (35). The remaining factors in Eq. (52) are just sufficient to express the momenta $k_1,\cdots,k_n$ as linear combinations of the $k_{n+1},\cdots,k_b$ according to Eq. (40). The resulting formula for $M_\Gamma(S,G_T)$ is

$$M_\Gamma(S,G_T)=\int_{-\infty}^{\infty}\cdots\int_{-\infty}^{\infty}dk_{n+1}\cdots dk_b C(k_{n+1},\cdots,k_b)$$
$$\times\prod_e\left[\frac{1}{(-q_i-u_i+i\Delta_i)_\mu\gamma_\mu-im}\right]$$
$$\times\prod_e'\left[\frac{1}{(q_i+u_i-i\Delta_i)_\mu\gamma_\mu-im}\right]$$
$$\times\prod_p\left[\frac{1}{(-q_i-u_i+i\Delta_i)^2+\lambda^2}\right]\prod_{a=n+1}^{n+g}[(k_{a\mu}\gamma_\mu$$
$$+im)\delta(k_a{}^2+m^2)]\prod_{a=n+g+1}^{b}\delta(k_a{}^2+\lambda^2). \tag{53}$$

V. COMPLEX INTEGRAL REPRESENTATIONS

Consider the rational function

$$\Phi\equiv\Phi(k_{n+1},\cdots,k_b)=\prod_e\left[\frac{(-q_i-u_i+i\Delta_i)_\mu\gamma_\mu+im}{(-q_i-u_i+i\Delta_i)^2+m^2}\right]$$
$$\times\prod_e'\left[\frac{(q_i+u_i-i\Delta_i)_\mu\gamma_\mu+im}{(q_i+u_i-i\Delta_i)^2+m^2}\right]$$
$$\times\prod_p\left[\frac{1}{(-q_i-u_i+i\Delta_i)^2+\lambda^2}\right]$$
$$\times\prod_{a=n+1}^{n+g}\left[\frac{k_{a\mu}\gamma_\mu+im}{k_a{}^2+m^2}\right]\prod_{a=n+g+1}^{b}\left[\frac{1}{k_a{}^2+\lambda^2}\right]. \tag{54}$$

The factors correspond, in an obvious way, to the factors in Eq. (53). We now assert that this function, Φ, depends only on G and is essentially the same for all doubled graphs, G_T, which are derived from G. To

prove this we write Eq. (54) in the form,

$$\Phi=\prod_r\left[\frac{R_{r\mu}\gamma_\mu+im}{R_r^2+m^2}\right]\prod_r\left[\frac{1}{R_r^2+\lambda^2}\right], \tag{55}$$

where there is one factor, and one 4-vector, R_r, corresponding to each internal line, λ_r, of G whether doubled or undoubled. The two products in Eq. (55) together run over the values $r=1, \cdots, b$ in some order. The R_r consist of the vectors k_a, $a=n+1, \cdots, b$, together with n vectors $\eta_i(-q_i-u_i+i\Delta_i)$, $i=1, \cdots, n$. Here, η_i is ±1 according to whether the arrow in λ_i is in the direction x_iy_i or y_ix_i. Let ϵ_{rj} be defined to be $+1$ if λ_r is a line incident at x_j with the arrow pointing away from x_j, -1 if λ_r is incident at x_j with the arrow towards x_j, and zero if λ_r is not incident at x_j. Then, in consequence of the structure of G_T, we have the identity

$$\sum_{j=1}^{n}\epsilon_{jl}\eta_j\theta_T(x_j, x_i)=\delta_{il}, \tag{56}$$

which is only an alternative statement of Eq. (38). By the definition of R_r, with Eqs. (40) and (56),

$$\begin{aligned}\textstyle\sum_r \epsilon_{rl}R_r&=\textstyle\sum_a \epsilon_{al}k_a+\sum_j \epsilon_{jl}\eta_j(-q_j-u_j+i\Delta_j)\\ &=-t_l+i\Gamma_l, \quad l=1, \cdots, n.\end{aligned} \tag{57}$$

These n linear relations between the R_r are equivalent to the n relations (40) expressing the q_j in terms of the k_a. But (57) is independent of T and depends only on G. Therefore, for all T, the function (54) is identical with (55), with the R_r related by (57). The functions Φ for different T differ only in that different sets of f of the R_r are chosen as the basic vectors k_a in terms of which Φ is expressed, the remaining R_r being eliminated by means of (57). Let L be the number of T which are compatible with G. Then these different T correspond precisely to the L possible ways of choosing a set of f of the R_r which are linearly independent.

Let the $3b$ space-components of the R_r be given any arbitrary real values consistent with (57). We consider (55) as an analytic function of the b time-components $\zeta_r=R_{r0}$, subject to the relations

$$\sum_r \epsilon_{rl}\zeta_r=-t_{l0}+i\Gamma_{l0}, \tag{58}$$

the ζ_r being complex variables. The denominator of (55) is

$$D=\prod_r[(\alpha_r-\zeta_r)(\alpha_r+\zeta_r)], \tag{59}$$

where

$$\left.\begin{aligned}\alpha_r&=(R_{r1}^2+R_{r2}^2+R_{r3}^2+m^2)^{\frac{1}{2}},\\ \alpha_r&=(R_{r1}^2+R_{r2}^2+R_{r3}^2+\lambda^2)^{\frac{1}{2}},\end{aligned}\right\} \tag{60}$$

for factors in the first and second product, respectively, in Eq. (55). D is a product of $2b$ factors which are non-homogeneous linear forms in the f complex variables k_{a0}, when Φ is represented by Eq. (54).

Suppose now that $\lambda\neq0$, so that by Eq. (60) $\alpha_r\neq0$. Then the factors of D have two properties which are essential to the discussion: (i) there exists a set of f linearly independent factors, and (ii) it is impossible for any set of $(f+1)$ factors to vanish simultaneously for any values of the variables. The proof of (ii) is as follows. If there is a set of $(f+1)$ factors vanishing simultaneously, at least one of these factors, say, F_1, is linearly dependent on a subset $F_2, F_3, \cdots, F_m$ of the others, where the $F_2, \cdots, F_m$ are themselves linearly independent. We can choose a representation of the R_r in terms of basic vectors k_a, such that $F_2, \cdots, F_m$ are of the form

$$(\alpha_a\pm k_{a0}), \tag{61}$$

with $(m-1)$ different values of a. Then F_1 is of the form

$$F_1=\alpha_1\pm(-q_{j0}-u_{j0}+i\Delta_{j0}), \tag{62}$$

where q_{j0}, according to (40), is a linear combination with real coefficients of the k_{a0} occurring in (61). The α_r are real, and therefore when all factors (61) vanish, q_{j0} is real. But u_{j0} is real, and Δ_{j0} has a positive real part, and so (62) and (61) cannot vanish simultaneously.

In consequence of properties (i) and (ii) of D, there exists an expansion of Φ in partial fractions

$$\Phi=\textstyle\sum_U[g(U)/(\zeta_\mu\pm\alpha_\mu)(\zeta_\nu\pm\alpha_\nu)\cdots(\zeta_\rho\pm\alpha_\rho)]. \tag{63}$$

Here the summation is over the $(L2^f)$ possible ways U of choosing f linearly independent factors from D. Each U involves a choice of f linearly independent variables $\zeta_\mu, \zeta_\nu, \cdots, \zeta_\rho$, from the ζ_r, forming the k_{a0} corresponding to a particular T, and a choice of f independent signs ±1. The coefficients $g(U)$ are uniquely determined and depend on the space components of the R_r but not on the ζ_r. We omit the proof that properties (i) and (ii) imply (63), since it involves only elementary but rather tedious algebra.

We see from Eq. (63) that Φ is not at all a general rational function of f complex variables, but has a very simple structure. It has precisely $L2^f$ simple poles, or points at which f linear factors in its denominator vanish. To each term in Eq. (63) corresponds a pole which we call the pole U. The function is completely determined by Eq. (63), given the positions of the poles and the constants $g(U)$, which are the residues at the poles.

In the above analysis, the fact that $\lambda\neq0$ was used only in order to ensure that the α_r given by Eq. (60) should not vanish. The discussion is still valid for $\lambda=0$, except when

$$R_{r1}=R_{r2}=R_{r3}=0 \tag{64}$$

for some value of r. We shall finally integrate Φ over the space components of the R_r, and we do not need even to define Φ at the isolated points where Eq. (64) holds. However, the behavior of the coefficients $g(U)$ in the neighborhood of such points must be gentle

enough to make the integrals well defined. In fact, the $g(U)$ become infinite at most like

$$(R_{r1}^2+R_{r2}^2+R_{r3}^2)^{-\frac{1}{2}},$$

and so the integrals over the space-components are easily convergent in the neighborhood of the singularities. This allows us to use Eq. (63) for $\lambda=0$ without danger of inconsistency.

The introduction of the Γ_i factors in Eq. (33) has entirely eliminated, from the present analysis, the two kinds of unessential but troublesome divergences which arise in the study of the S-matrix,[15] namely, accidental divergences due to vanishing energy denominators in perturbation theory and infrared divergences. The disappearance of these divergences is due directly to the fact that more than f factors in the denominator of Φ can never vanish simultaneously, which in turn is a consequence of the exponential convergence of Eq. (33). In particular, if we take $\lambda=0$ and then make all $\Gamma_i\to 0$, the integrals of $g(U)$ over the space-components of the R_r become logarithmically divergent at the points (64), and these are typical infrared divergences.

Returning to Eq. (53), carrying out the integrations over the k_{a0}, and remembering the properties of the function $C(k_{n+1}, \cdots, k_b)$ stated after Eq. (36), we have

$$M_\Gamma(S, G_T)=\int d_3R \sum_U C(U)g(U). \tag{65}$$

Here the integration is over the space components of the R_r subject to Eq. (57). The summation is over the 2^f poles U of Φ at which the δ-functions in Eq. (53) have singularities, which are just the poles corresponding to the given G_T. The coefficients $C(U)$ are derived from the 2^f values of the function $C(k_{n+1}, \cdots, k_b)$ and are numbers independent of all the variables.

Finally, we sum Eq. (65) over the G_T derived from a given G, and we find

$$M_\Gamma(S_G)=A\int d_3R \sum_U C(U)g(U), \tag{66}$$

where the summation is now over all the poles of Φ, the $C(U)$ are as before pure numbers, and A is a multiplying factor which is independent of m, λ, and the Γ_i; A incorporates the various factors which were dropped in the preceding work. By Eq. (63), we may write instead of Eq. (66),

$$M_\Gamma(S_G)=A'\int d_3R \int d\zeta_r \Phi(R_r), \tag{67}$$

where $\int d_3R$ is as before a real integral, while $\int d\zeta_r$ is some contour integral in the space of the complex ζ_r variables. The form of this contour integral will be determined in the following section.

[15] See Sec. V of reference (B).

VI. DETERMINATION OF THE CONTOUR

Let m and λ now be considered to be very large numbers, greater than any combinations of the p, Γ_i, and t_i which occur in the theory. In this case we make an alternative analysis of $\mathbf{j}_n(p)$ based on Eq. (12) instead of on Eq. (11). Consider the contribution J_{qp} to $\mathbf{j}_n(p)$ derived from the term (q, p) in the double sum on the right of Eq. (12). Let J_{qp} be expanded as a sum of normal products according to the rules of Sec. II.

The coefficient of Eq. (31) in the expansion of J_{qp} is as before a sum of contributions $M(\bar{S})$ from different integrals of the form (32) with $n=q+p$, where $\bar{S}$ is now an expression like

$$\bar{S}=\bar{P}(H_1(x_1), \cdots, H_1(x_q))P(H_1(x_{q+1}), \cdots, H_1(x_n), j_n(x)) \tag{68}$$

instead of Eq. (20). We consider instead of $M(\bar{S})$ the corresponding coefficient $M_\Gamma(\bar{S})$ in the expansion of Eq. (33). But now, since there are no θ-functions in Eq. (68), the Γ_{i0} must all have real part zero in order that Eq. (33) should not diverge exponentially.

Let $M_\Gamma(\bar{S}_G)$ as before be a contribution to $M_\Gamma(\bar{S})$ arising from a connected graph G. Suppose first that $q>0$. In this case, G will contain at least one internal line $x'x''$, where x' belongs to the $\bar{P}$-product and x'' to the P-product in Eq. (68). Let C be the set of all internal lines of G with this property. To each line of C will correspond in $M_\Gamma(\bar{S}_G)$ a factor

$$S^+(x'-x''), \quad S^-(x''-x'), \quad \text{or} \quad D^+(x'-x''), \tag{69}$$

according to Eqs. (14), (15), (16). In the momentum representations these factors contain only fourier components of the form $\exp[ik\cdot(x'-x'')]$ with $k_0>0$ and either

$$k_1^2+k_2^2+k_3^2-k_0^2+m^2=0 \quad \text{or} \quad k_1^2+k_2^2+k_3^2-k_0^2+\lambda^2=0.$$

That is to say, only fourier components occur for which

$$k_0 \geq \text{Min}(m, \lambda). \tag{70}$$

The internal lines of G not belonging to C will contribute to $M_\Gamma(\bar{S}_G)$ factors of the form $\phi(x'-x'')$, where x' and x'' both belong to the first product or both to the second product in Eq. (68). The external lines contribute a factor

$$\exp[-il_1\cdot x_1\cdot\cdots-il_n\cdot x_n].$$

Now the integral for $M_\Gamma(\bar{S}_G)$ is obtained by substituting all these factors for $\bar{S}$ in Eq. (33). We may take as independent variables $x_1, \cdots, x_q, \xi_{q+1}, \cdots, \xi_n, x$, where

$$\xi_i=x_i-x.$$

When the momentum representations of the factors (69) are used, $M_\Gamma(\bar{S}_G)$ becomes an integral over these variables and over a set of momentum variables k satisfying Eq. (70). Let the integration over x be carried out first. The factors $\phi(x'-x'')$ are independent of x.

The factors depending explicitly on x are

$$\exp[-i(\sum k+p+\sum_{q+1}^{n} t_j+i\sum_{1}^{q}\Gamma_j)\cdot x]. \quad (71)$$

When (71) is integrated over x, the result is a 4-dimensional δ-function of the vector multiplying x; but the fourth component of this vector is never zero, provided that

$$\mathrm{Min}(m,\lambda)>|p_0|+\textstyle\sum_1^n|t_{j0}|+\sum_1^n|\Gamma_{j0}|. \quad (72)$$

It is assumed that m and λ are large enough to satisfy (72). Therefore, the $M_\Gamma(S_G)$ derived from Eq. (68) vanish identically whenever $q>0$ for every connected G.

It was proved in Sec. III that the normal constituents of $\mathbf{j}_\mu(p)$ arising from disconnected G are zero. Therefore, when m and λ satisfy (72), the normal constituents of $\mathbf{j}_\mu(p)$ can be calculated as follows. We use for $\mathbf{j}_\mu(x)$ instead of Eq. (12) the expression

$$\mathbf{j}_\mu{}^F(x)=\sum_{n=0}^{\infty}\left(-\frac{i}{hc}\right)^n\frac{1}{n!}\int_{-\infty}^{\infty}\cdots\int_{-\infty}^{\infty}dx_1\cdots dx_n \times P(H^I(x_1),\cdots,H^I(x_n),j_\mu(x)), \quad (73)$$

and include contributions only from connected graphs.

The operator $\mathbf{j}_\mu{}^F(x)$ has been encountered before. It is the current operator in the "mixed representation" of reference (A), where initial states are specified at a remote time in the past, and final states at a remote time in the future. The equivalence of $\mathbf{j}_\mu(x)$ and $\mathbf{j}_\mu{}^F(x)$ for large m and λ is a consequence of the fact that there is not sufficient energy available in a measurement of $\mathbf{j}_\mu(p)$ for the real production of particles of large rest-mass.

For our present purposes, the physical interpretation of $\mathbf{j}_\mu{}^F(x)$ is unimportant. The important fact is that $\mathbf{j}_\mu{}^F(x)$ has the same structure as the S-matrix, involving chronological products only. We are able to apply to it the rules given in reference (B) for the calculation of the S-matrix, with only minor alterations. These rules lead to an alternative expression for the integral on the right of Eq. (67), namely,

$$M_\Gamma(S_G)=A'\int_{-\infty}^{\infty}\cdots\int_{-\infty}^{\infty}dk_{n+1}\cdots dk_b\Phi. \quad (74)$$

Here the integrals are along the real axis for all the $4f$ components of the vectors k_a, and Φ is given by Eq. (54), with the convention that the poles are moved an infinitesimal distance away from the real axis by replacing each m^2 and λ^2 by $(m^2-i\epsilon)$ and $(\lambda^2-i\epsilon)$, ϵ being a small positive number and the integrals being calculated in the limit $\epsilon\to+0$. This convention regarding the poles of Φ is due to Feynman,[5] and is the convention which is always correct for momentum representations of operators like (73) involving only chronological products.

It is possible now to transform the path of integration in Eq. (74) for each of the fourth components k_{a0} from the real axis to the imaginary axis, just as was done in Sec. V of reference (B). Provided that (72) is satisfied, no singularities will be encountered in transforming the path of integration through the first and third quadrants of the k_{a0} planes. There are no "displaced poles," because we assume the masses so large that Eq. (51) of reference (B) can never hold. Therefore, Eq. (67) holds, with the path of the integral $\int d\zeta_r$ defined as follows. Choosing any set of f variables ζ_r which are linearly independent, we integrate over each of these variables up the imaginary axis from $(-i\infty)$ to $(+i\infty)$. The ϵ-limiting process is no longer needed, because the path of integration is now separated from the poles.

Equation (67), with this special choice of contour, is valid under the two conditions: m and λ are sufficiently large, and each Γ_{i0} has real part zero.

VII. THE ANALYTIC CONTINUATION METHOD

We have found two alternative expressions for $M_\Gamma(S_G)$. One is the expression E_1 on the right of Eq. (66). The other is the expression E_2 on the right of Eq. (67), with the contour as defined in the preceding section. The regions within which these two expressions have been shown to be valid do not overlap. E_1 is valid in the region

$$\mathrm{Re}(\Gamma_{i0})>0, \quad (75)$$

for all values of m and λ including $\lambda=0$. E_2 is valid in the region

$$\mathrm{Re}(\Gamma_{i0})=0, \quad (76)$$

with m and λ restricted by (72).

It is clear, from the definition of $g(U)$ by Eq. (63), that E_1 is an analytic function of the Γ_{i0} throughout the region (75), for any given values of m and $\lambda\neq0$. Provided that the path of integration in E_2 is separated from the poles of Φ, E_2 is also an analytic function; therefore, E_2 is analytic for all complex values of the Γ_{i0} satisfying (72); that is to say, E_2 is an analytic function of the Γ_{i0} in a region including in its interior points satisfying (76). We use now a lemma from the theory of analytic functions.

Let $f_2(w)$ be a function of the complex variable w, analytic in a circle C. Let D be a diameter of C bounding the semicircle C_1. Let $f_1(w)$ be a function analytic in C_1, such that $f_1(w)\to f_2(w_0)$ when a point w in C_1 tends to a point w_0 on D. Then f_1 and f_2 are identical.

The proof of this lemma will not be given here. It follows easily from the Schwartz reflection principle.[16] To apply the lemma to our functions E_1 and E_2, take

$$\Gamma_{i0}=\mu_i w, \quad (77)$$

where the μ_i are positive real numbers, and write

[16] J. E. Littlewood, *Theory of Functions* (Oxford University Press, 1944), theorem 105, p. 109, and corollary, p. 130.

$E_1=f_1(w)$, $E_2=f_2(w)$. Then C_1 is a part of the region (75), and D a part of the region (76). The lemma states that $E_1=E_2$ for all Γ_{i0} given by Eq. (77) with $\mathrm{Re}(w)>0$; but, since both E_1 and E_2 are analytic functions of the μ_i, $E_1=E_2$ also for complex μ_i. The conclusion of the argument is that E_1 and E_2 are alternative representations of the same analytic function E, valid in different but overlapping domains.

Up to this point we have considered only the analyticity of E as a function of the Γ_{i0}; but E_1 is also an analytic function of m and λ in the region

$$\mathrm{Re}(\Gamma_{i0})>0, \quad m>0, \quad \lambda>0, \tag{78}$$

that is to say, for real values of m and λ and for complex values in the immediate neighborhood of the positive real axis, and E_2 is an analytic function of λ and m in the same sense, for all λ and m satisfying (72). Therefore, E is a unique analytic function of the variables $(m, \lambda, \Gamma_{i0})$ in the combined domain of all points satisfying *either* (78) *or* (72).

The procedure to be used for practical calculations is the following. Suppose that we wish to calculate a particular $M(S_G)$, the contribution from a given G to the coefficient of Eq. (31) in the normal product expansion of Eq. (32), with the physically occurring value of m and $\lambda=0$. We start by writing down the expression E_2 for $M_\Gamma(S_G)$ according to Eq. (67), with $\lambda\neq 0$. Assuming (72) to hold, the integrals in E_2 can very conveniently be evaluated analytically by means of the well-established techniques of Feynman.[6] The result of evaluating the integrals is the analytic function E. We continue this function through the region (78), keeping $\mathrm{Re}(\Gamma_{i0})>0$, and decreasing m and λ until m reaches its actual value and λ reaches a very small λ_0 less than any of the energies which are characteristic of the particular physical situation. Then we make all Γ_{i0} tend to zero, in a way which will be specified precisely in the next paper of this series. Finally, we may make $\lambda_0\to 0$ if we desire to reintroduce infrared divergences into our calculations, or we may leave λ_0 standing as a convenient cutoff parameter for these divergences.

In this paper, nothing has been said about the physically interesting ultraviolet divergences, the divergences at large momenta of the integrals (67). These are the divergences which are removed by mass and charge renormalization, as will be described in the following paper. Here we remark only that these divergent terms will be separated in a consistent way from the integrals E_2 before the integrals are evaluated analytically. The function E is therefore finite, and the ultraviolet divergences do not interfere with the process of analytic continuation.

The integrals E_2, when all Γ_{i0} are zero, are formally identical with the integrals occuring in the calculation of the S-matrix. If we maintain $\Gamma_{i0}=0$ and try to continue the function E_2 from large values of m and λ down to the values in which we are interested, we shall encounter values of m and λ at which E_2 is not analytic. These are the places where the S-matrix is nonanalytic because of the appearance of a threshold for some real process which is competing with the process under analysis. When we arrive at the actual values of m and λ, the integrals E_2 representing elements of the S-matrix differ from the values of E which we find by analytic continuation through the region (78), because of the effects of the competing processes. In practice, E will have a simpler analytic form than does E_2; this is the justification for the remarks made at the end of Sec. I.

VIII. SUMMARY OF RULES FOR THE CALCULATION OF HEISENBERG OPERATORS

A Heisenberg operator such as $\mathbf{j}_\mu(p)$ is expressed formally in terms of interaction representation operators by means of Eq. (11). By the theorem of Wick stated in Sec. II, $\mathbf{j}_\mu(p)$ may be expanded into a sum of normal products (31) multiplied by C-number coefficients M. According to Sec. IV, each M is a sum of contributions $M(S_G)$ corresponding to different terms S of the form (20) and to different connected graphs G. We calculate $M(S_G)$ as the limit when all $\Gamma_{i0}\to 0$ of the generalized coefficient $M_\Gamma(S_G)$ defined in Sec. IV.

To calculate $M_\Gamma(S_G)$, we consider m and λ to be large, satisfying (72). The operator $\mathbf{j}_\mu^F(p)$ is defined by Eq. (73). This operator having the analytic form of an S-matrix, we may calculate its decomposition into normal products by following the rules of the S-matrix analysis in (B). Let $M'(S_G)$ be the coefficient of Eq. (31) in the normal product expansion of $\mathbf{j}_\mu^F(p)$, arising from the term S and the graph G. Then $M'(S_G)$ is an integral in momentum-space of the form (67), with Φ given by Eq. (54) with all $\Delta_i=0$. From $M'(S_G)$ we obtain $M_\Gamma(S_G)$ simply by inserting the parameters Δ_i given by Eq. (40) into Φ as given by Eq. (54). The path of integration in Eq. (67) is defined in Sec. VI.

We evaluate the integrals (67) analytically, using the methods of Feynman, obtaining for $M_\Gamma(S_G)$ an expression which is an analytic function of the variables Γ_{i0}, m and λ in the region where either (72) or (78) is satisfied. By analytic continuation through the region (78), as described in Sec. VII, we derive $M_\Gamma(S_G)$ for the values of m and λ which are of physical interest. Hence, passing to the limit $\Gamma_{i0}\to 0$, and, if necessary, also letting $\lambda\to 0$, we finally obtain the coefficients $M(S_G)$ in the normal product expansion of $\mathbf{j}_\mu(p)$.

It should be observed that there is nothing in the methods of the present paper which is specific to quantum electrodynamics. Precisely the same rules can be used for the calculation of Heisenberg operators in any theory in which two or more quantized fields of any kind are in interaction.

Letters to the Editor

PUBLICATION of brief reports of important discoveries in physics may be secured by addressing them to this department. The closing date for this department is five weeks prior to the date of issue. No proof will be sent to the authors. The Board of Editors does not hold itself responsible for the opinions expressed by the correspondents. Communications should not exceed 600 words in length.

Adiabatic Oscillations in Liquid Helium*

JOHN E. ROBINSON
Chemistry Department, Duke University, Durham, North Carolina
(Received February 9, 1951)

IF a container of liquid helium is connected by a very fine slit or a capillary with a helium bath, the meniscus in the container reaches the level of the bath eventually by way of very slow and very slightly damped oscillations. Allen and Misener,[1] who first observed this phenomenon, assumed that the frequency of the oscillations is determined by the restoring force of gravitation, $A g \rho x$, where A is the area of the liquid surface in the container, ρ is the density of liquid helium, x is the level difference, and $g = 980$ cm/sec^2. The potential energy is then

$$E_{\text{pot}} = \tfrac{1}{2} A g \rho x^2.$$

To all intents and purposes the inertia of the liquid can be attributed entirely to the mass of the liquid moving in the capillary. Then, assuming that only the superfluid [velocity $v_s = (A/\sigma)(\rho/\rho_s)\dot{x}$] can pass through the capillary of length l and cross section σ, the kinetic energy is given by

$$E_{\text{kin}} = \tfrac{1}{2} l \sigma \rho_s v_s^2 = \tfrac{1}{2} \rho^2 l A^2 \dot{x}^2 / \rho_s \sigma.$$

Hence, the system represents an harmonic oscillator of frequency

$$\omega_i = 2\pi\nu_i = (\rho_s g \sigma / \rho l A)^{\frac{1}{2}}. \tag{1}$$

Atkins[2] has observed similar oscillations in a vessel connected with the bath by the Rollin film, and has used measurements of the frequency to determine the thickness of the film. In measuring these oscillations, particular care must be taken to avoid swamping them by the fountain effect. In Allen and Misener's and in Atkins' experiments, constant temperature was insured by a very good heat contact between container and bath.

If, however, the two containers are well isolated from each other, it is mainly the fountain effect and not gravitation which determines the frequency of the oscillations. We have the equations of motion[3] for the superfluid:

$$\langle \dot{V}_s \rangle + \frac{1}{l}\left\{ g x + \frac{1}{\rho}(p - p_0) - \frac{\rho_n}{\rho}(S_n - S_s)(T - T_0) \right\} = 0 \tag{2}$$

and for the normal fluid:

$$\langle \dot{V}_n \rangle + \frac{1}{l}\left\{ g x + \frac{1}{\rho}(p - p_0) + \frac{\rho_s}{\rho}(S_n - S_s)(T - T_0) \right\} + \frac{8\pi\eta_n}{\rho_n \sigma}\langle V_n \rangle = 0, \tag{3}$$

where p_0 and T_0 are the vapor pressure and temperature in the container, S_n and S_s are the entropies per gram of helium attributed to the normal and superfluid components, η_n is the viscosity of the normal fluid, and $\langle V_n \rangle$ the average of V_n over the cross section of the capillary. S_s is generally understood to be zero, or practically zero. We express the balance of entropy by

$$\rho_s \sigma (S - S_s) T_0 \langle V_s - V_n \rangle + \rho A (h + x) C_p \dot{T} + \kappa (T - T_0) = 0, \tag{4}$$

where C_p is the specific heat per gram, h is the distance from the bottom of the container to the bath level, and κ is an assumed heat leakage between bath and container. We will assume the capillary or slit so narrow that the normal fluid is immobilized by its viscosity. We may then put $\langle V_n \rangle = 0$, $\rho_s \sigma \langle V_s \rangle = \rho A \dot{x}$, and dispense with Eq. (3), writing (2) and (4) as

$$(\rho A l \dot{x}/\rho_s \sigma) + g x + (1/\rho)(p - p_0) - (S - S_s)(T - T_0) = 0, \tag{2'}$$

$$\rho A \{ T_0 (S - S_s) \dot{x} + (h + x) C_p \dot{T} \} + \kappa (T - T_0) = 0. \tag{4'}$$

The quantity $p - p_0$ can be expressed by the temperature difference and the derivative of the vapor pressure curve,

$$p - p_0 = (T - T_0)(dp/dT)_{\text{vap}}.$$

For x small compared with h, (2') and (4') are linear, homogeneous equations of the form:

$$\ddot{x} + \omega_i^2 x - \omega_i^2 \alpha \tau = 0, \tag{2''}$$

$$\dot{x} + \dot{\tau} + L\tau = 0, \tag{4''}$$

where

$$\tau = (T - T_0) h C_p / [T_0 (S - S_s)],$$

$$\alpha = \frac{T_0 (S - S_s)^2}{g h C_p}\left\{ 1 - \frac{1}{\rho (S - S_s)}\left(\frac{dp}{dT} \right)_{\text{vap}} \right\},$$

$$L = \kappa / (\rho A h C_p).$$

Equations (2'') and (4'') have solutions of the form

$$x = B' e^{\lambda t}, \quad \tau = B'' e^{\lambda t}, \tag{5}$$

where λ is determined by the secular equation:

$$\lambda^3 + L\lambda^2 + \omega_i^2 (1 + \alpha)\lambda + L\omega_i^2 = 0. \tag{6}$$

For $L \to \infty$ (complete heat exchange), we have $\lambda = i\omega_i$. These are the isothermal oscillations mentioned above.

On the other hand, for $L = 0$ (complete insulation), we have a much higher frequency:

$$\omega_a = \omega_i (1 + \alpha)^{\frac{1}{2}} = \omega_0 [\rho_s (1 + \alpha)/\rho]^{\frac{1}{2}}, \tag{7}$$

where ω_0 is the frequency at the absolute zero. Furthermore, there is a static solution $\lambda = 0$ and, from (2''), $x_0 = \alpha \tau_0$ which is the well-known equilibrium condition for the fountain pressure. The general solutions are vibrations of frequency ω_a around an equilibrium position x_0 given by the temperature difference. For $1.3° < T < T_\lambda$ the entropy is roughly proportional to $T^{3.6}$, and a crude estimate gives $\omega_a/\omega_i = (82/h^{\frac{1}{2}})(T/T_\lambda)^{3.3}$. Figure 1 displays

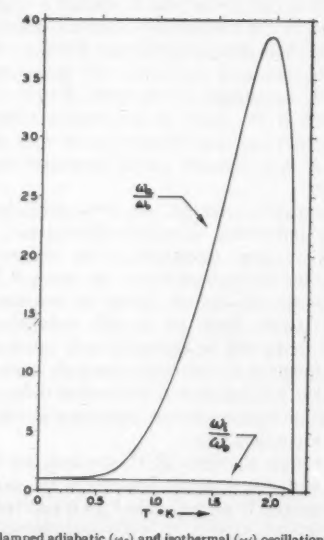

FIG. 1. Undamped adiabatic (ω_a) and isothermal (ω_i) oscillations, calculated for $h = 1$ cm. Frequencies as functions of temperature.

the temperature dependence of ω_i/ω_0 and ω_a/ω_0. (In the calculation it was assumed that $S_s=0$ and $S\sim T^{3.6}$ over the entire range.)

Examination of the discriminant Δ of (6), given by

$$27\Delta=1-\tfrac{1}{2}\left\{1+18\left(\frac{\omega_i}{\omega_a}\right)^2-27\left(\frac{\omega_i}{\omega_a}\right)^4\right\}\left(\frac{L}{\omega_a}\right)^2+\left(\frac{\omega_i}{\omega_a}\right)^2\left(\frac{L}{\omega_a}\right)^4$$

reveals that for finite L and T, three distinct situations may obtain. For $L/\omega_a<2$ we have the damped adiabatic vibrations. For $L/\omega_a>\frac{1}{2}\omega_a/\omega_i$ we have the damped isothermal vibrations. Between these values, for $2<L/\omega_a<\frac{1}{2}\omega_a/\omega_i$, the three solutions of (6) are all aperiodic.

We substitute $\lambda=is-b$, and equate real and imaginary parts of (6) to zero. The two equations so obtained yield an aperiodic solution $a=0$, and two more relations between a, b, and L from which we can derive a relationship between a and b and then calculate the dependence of each on L. The aperiodic solution can then be found by equating the constant term in (6) to the product of the roots:

$$\lambda_3=-L\omega_i^2/(\lambda_1\lambda_2)=-L\omega_i^2/(a_2^2+b_2^2).$$

In the periodic regions the general solution of (2″) and (4″) for the meniscus level x can then be written:

$$x=D'e^{-bt}\cos(at-\phi)+D''\exp[-L\omega_i^2t/(a_2^2+b_2^2)], \qquad (8)$$

where D', D'', ϕ, are arbitrary constants. Hence, we obtain an aperiodic decrease of the average temperature and pressure differences between bath and container, plus the damped vibrations.

In Fig. 2 we show the solutions calculated for $T=2°$K and $h=1$ cm, as functions of L/ω_a. The ordinates are in units of ω_a in and

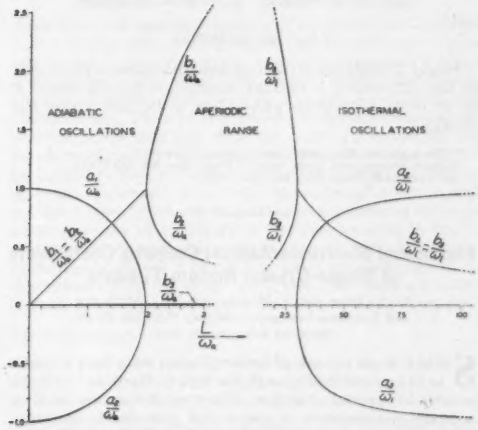

FIG. 2. Frequencies (a) and damping (b) as functions of the heat exchange L, calculated for $h=1$ cm, $T=2°$K. The aperiodic solution in the adiabatic range is $\lambda_1=-b_1$, and in the isothermal range is $\lambda_1=-b_3$.

adjacent to the adiabatic region, and in units of ω_i in and adjacent to the isothermal region. (For the scales employed, the aperiodic root, λ_3, is almost too small to be visible in the adiabatic range, and is too large in the isothermal range to be shown in the plot.) Figure 2 shows that if the adiabatic oscillations are to persist over several periods with only slight diminution in amplitude, we must have at most $L/\omega_a<0.1$. In this case we have

$$a=\omega_a\{1-\tfrac{1}{8}(L/\omega_a)^2\}; \quad b=\tfrac{1}{2}L; \quad \lambda_3=-(\omega_i/\omega_a)^2L.$$

The vibrations die out more rapidly than the average meniscus level sinks.

To see whether the adiabatic oscillations are observable we refer to Keesom and Saris,[4] who found that for one of their experimental arrangements the total heat leakage from an insulated container (volume 1 cm³) to the bath was about 40 erg deg^{-1} sec^{-1} for $T<T_\lambda$. This would give roughly $L\approx 2\times10^{-4}T^{3.6}$, where we have taken $\cdot\rho C_p\approx 4\times10^{-3}T^{3.6}$ cal deg^{-1} sec^{-1} cm^{-3}. Accordingly, it should be possible to provide insulation which will reduce the damping sufficiently to permit observation of the adiabatic oscillations. This might provide a method of measuring the temperature dependence of the entropy, or rather of $(S-S_a)$, at lowest temperatures.

The author is indebted to Professor F. London for suggesting this question and for numerous discussions.

* Supported by the ONR.

[1] J. F. Allen and A. D. Misener, Proc. Roy. Soc. (London) **A172**, 467 (1939).
[2] K. R. Atkins, Proc. Roy. Soc. (London) **A203**, 119, 239 (1950).
[3] See, for instance, R. B. Dingle, Proc. Phys. Soc. (London) **A62**, 648 (1949).
[4] W. H. Keesom and B. Saris, Physica **7**, 241 (1940). See also P. H. Keesom, Physica **11**, 339 (1945).

ft-Values and β-Decay and the Shell Models

M. TAKETANI
Tokyo, Japan

S. NAKAMURA, M. UMEZAWA, AND K. ONO
Department of Physics, University of Tokyo, Tokyo, Japan

AND

Y. YAMAGUCHI
Department of Physics, Osaka City University, Osaka, Japan

(Received March 15, 1951)

STARTING from the classification of *ft*-values of β-decay, we[1] have recently analyzed the β-decay schemes and selection rules of β-rays by Mayer's shell model.[2] Our general conclusion agrees with the result of recent researches made by Wu[3] and also by Feenberg and Trigg.[4] As regards some of the β-decays, Mayer's theory gives a more simple explanation than those of Feenberg and Hammack[5] and of Nordheim.[6] We would like to lay special stress on the following three points:

(1) Fermi's formula for the allowed transition, which has been tentatively employed in calculating the *ft*-values of β-decay, is subject, in some cases of forbidden transitions, to errors ranging up to about one hundred. For instance, Feenberg and Hammack[5] held that in a group obeying the first-forbidden selection rule $\Delta J=\pm2$, parity change yes, respective *ft*-values are too great to be included in the first-forbidden category. However, our re-examination[7] by means of the correct forbidden formula of Nakamura, Shima, and Kobayashi[8] resulted in improvement by a factor of as much as sixty. It is interesting to note that the re-examination reveals that all of the above-mentioned group with "*a*"-type spectrum have almost the same *ft*-values (see Table I), and that their magnitudes are not unreasonably great for the first-forbidden transition if allowance is made for the reduction of

TABLE I. Improvement of *ft*-values by the first-forbidden formula:*

$$f(W_0)=\left(\frac{W_0^4}{630}-\frac{59W_0^2}{5040}-\frac{407W_0^2}{10080}-\frac{1}{630}\right)(W_0^2-1)^{\frac{1}{2}}+\left(\frac{W_0^2}{24}+\frac{W_0}{96}\right)\log[W_0+(W_0^2-1)^{\frac{1}{2}}]. \qquad (1)$$

Elements of "*a*"-type	W_0 (mc^2)	t (sec)	*ft* uncorrected	*ft* corrected by Eq. (1)
V^{50}	5.29	2.2×10^5	1.1×10^8	3×10^7
A^{38}	2.108	4.5×10^5	2.1×10^8	4×10^7
Kr^{85}	2.17	2.96×10^5	3.0×10^8	4×10^7
Cl^{38}	10.43	2.3×10^5	4.0×10^7	5×10^7
Sr^{89}	3.88	4.7×10^6	4.9×10^8	6×10^7
Sr^{90}	2.05	8×10^6	1.4×10^8	7×10^7
Y^{91}	4.01	5.3×10^6	5.4×10^8	8×10^7
Rb^{86}	4.6	1.36×10^6	3.8×10^8	8×10^7
K^{42}	8	6.0×10^4	1.1×10^8	1.1×10^8

* F. B. Shull and E. Feenberg, Phys. Rev. **75**, 1768 (1949), replaced it by $(W_0^2-1)f$ and found, as a mean value, $(W_0^2-1)ft\sim10^{10}$ for the "*a*"-type group.

nuclear matrix elements due to the jump of the principal quantum number. As was pointed out by many authors, this does not contradict Mayer's shell model, but leads to some difficulties with Feenberg's model, with respect to the $3p$ level.

(2) A series of spectacular experiments started by Langer,[9] Wu,[10] and others, led to the discovery of many of "a"-type spectra concerned with the first-forbidden transitions. It may naturally be asked in this connection why no other type of spectrum associated with the first-forbidden formulas of Konopinski and Uhlenbeck,[11] for instance, with $\int \mathbf{r}$, has so far been discovered. We will try to indicate here that this question may be answered satisfactorily by the use of Mayer's shell model. The selection rule for the matrix element $\int \mathbf{r}$ is $\Delta J = \pm 1, 0$, parity change yes. However, in Mayer's level scheme, nuclei with the same principal quantum number have the same parity. Therefore, it naturally follows from this that, if parity changes in a β-transition, the principal quantum number will also jump. For example, transitions $(4f_{7/2} \leftrightarrow 3d_{5/2})$, $(2s_{1/2} \rightarrow 3p_{3/2})$, etc., in spectroscopic notation, are such cases. Of these, the transitions $(2s_{1/2} \rightarrow 3p_{3/2})$ are actually found to be less frequent than the transitions $(4f_{7/2} \leftrightarrow 3d_{5/2})$ in Mayer's shell model.[1] Moreover, for the case $\Delta J = \pm 1, 0$, $\int \boldsymbol{\alpha}$, which represents an allowed spectrum, may happen to mask the contribution of $\int \mathbf{r}$. This provides a basis for explanation of the fact that the case with $\int \mathbf{r}$ is far less frequent than the case of "a"-type. On the other hand, in the shell model where the parity and the principal quantum number may be taken independently, the explanation would require a more complicated basis.[5,6]

(3) Two divergent opinions have so far been advanced as regards the classification of the bulk of β-emitters with ft-values $10^6 \sim 10^8$; the one favoring their classification as first-forbidden, and the other proposing to classify them as allowed unfavored transitions (as seen in 1A in Table II of Konopinski).[12] If we try to make the calculation by the first-forbidden formula,[3] we will obtain considerably dispersed values for ft. However, a conventional calculation on the basis of the allowed formula gives more distinct values. If we do not regard this result as fortuitous, but take this as a result of failure to observe the seventh-power law, it follows, then, as stated by Wu[3] and also by Feenberg and Trigg,[4] that it is better to classify these transitions as allowed but unfavored.

[1] Umezawa, Nakamura, Yamaguchi, and Taketani, Prog. Theoret. Phys. 6, No. 3 (1951); Umezawa, Horie, Yamaguchi, and Yoshida, *ibid.* 6, No. 3 (1951); S. Nakamura, *ibid.* 6, No. 4 (1951).
[2] M. G. Mayer, Phys. Rev. **74**, 235 (1948); **75**, 1986 (1949); **78**, 16 (1950).
[3] C. S. Wu, Revs. Modern Phys. **22**, 386 (1950).
[4] E. Feenberg and G. Trigg, Revs. Modern Phys. **22**, 399 (1950).
[5] E. Feenberg and K. C. Hammack, Phys. Rev. **75**, 1877 (1949).
[6] L. W. Nordheim, Phys. Rev. **75**, 1894 (1949).
[7] Taketani, Nakamura, Ono, and Umezawa, Prog. Theoret. Phys. 6, No. 3 (1951).
[8] Nakamura, Shima, and Kobayashi, J. Phys. Soc. Japan **4**, 166 (1949). Under the direction of Professor Yukawa, they worked out an explicit forbidden probability, i.e., f-function, for each of the five Fermi interactions. An estimate for a special case ("a"-type spectra) was also made by Feenberg and Trigg (see reference 4).
[9] L. M. Langer and H. C. Price, Jr., Phys. Rev. **75**, 1109 (1949).
[10] C. S. Wu and L. Feldman, Phys. Rev. **78**, 318 (1950); **76**, 693 (1949).
[11] E. J. Konopinski and G. E. Uhlenbeck, Phys. Rev. **60**, 308 (1941).
[12] E. J. Konopinski, Revs. Modern Phys. **15**, 209 (1943).

Convergence of the Chapman-Enskog Method for a Completely Ionized Gas*

ROLF LANDSHOFF
University of California, Los Alamos Scientific Laboratory, Los Alamos, New Mexico
(Received March 8, 1951)

THE theory of transport phenomena in an ionized gas has recently been reconsidered by Cohen, Spitzer, and McR. Routly,[1] in an approximation which is specially adapted to inverse square forces. In this connection some results on the convergence of the Chapman-Enskog method which came up in the work reported in an earlier paper[2] may be of some interest. These results refer to the case $H=0$, where the matrix Δ of Eq. (34) is real. In this case the determinants can be evaluated with much less labor and the approximation was carried to 5×5 matrices, i.e., 2 steps beyond the approximation of reference 2. The results are given in Table I. The velocity distribution of electrons in

TABLE I. Successive approximations of the determinant ratios.

i	$Z=1$	$Z=2$	$Z=3$	$Z=\infty$
		$\Delta_{02}^{(i)}/\Delta^{(i)}$		
2	1.9320	1.1590	0.8430	$3.25/Z$
3	1.9498	1.1605	0.8430	$3.3906/Z$
4	1.9616	1.1628	0.8435	$3.3945/Z$
5	1.9657	1.1634	0.8436	$3.3950/Z$
∞	—	—	—	$3.3953/Z$
		$\Delta_{01}^{(i)}/\Delta^{(i)}$		
2	0.6213	0.4393	0.3398	$1.5/Z$
3	0.5545	0.4201	0.3425	$2.0625/Z$
4	0.55983	0.4212	0.3429	$2.0391/Z$
5	0.5583	0.4207	0.3428	$2.0377/Z$
∞	—	—	—	$2.0372/Z$
		$\Delta_{11}^{(i)}/\Delta^{(i)}$		
2	0.4142	0.2929	0.2265	$1/Z$
3	0.6636	0.5433	0.4625	$3.25/Z$
4	0.6660	0.5439	0.4628	$3.3906/Z$
5	0.6665	0.5443	0.4630	$3.3945/Z$
∞	—	—	—	$3.3953/Z$

presence of an electric field is, in the notation of reference 2, given by

$$\phi = f\left(1 - \frac{e(\mathbf{v}\cdot\mathbf{E})}{\nu kT} \sum_0^{i-1} (-1)^i \frac{\Delta_{0i}^{(i)}}{\Delta^{(i)}} L_i\right).$$

For $Z=1$, one obtains

$$\Delta_{02}^{(3)}/\Delta^{(3)} = -0.0630, \quad \Delta_{02}^{(4)}/\Delta^{(4)} = -0.018365,$$

and

$$\Delta_{02}^{(5)}/\Delta^{(5)} = 0.039955.$$

Finally, I should like to point out some corrections to reference 2. In Eqs. (21) delete q in the third equation; in Eq. (30) replace β^2 by β^3; in Eq. (62) replace $\sqrt{2}$ by $(2\pi)^{\frac{1}{2}}$; in Eq. (65) replace H_{rs}^2 by H_{rs}^i.

* This work was done under the auspices of the AEC.
[1] Cohen, Spitzer, and McR. Routly, Phys. Rev. **80**, 230 (1950).
[2] R. Landshoff, Phys. Rev. **76**, 904 (1949).

Elastic and Electromechanical Coupling Coefficients of Single-Crystal Barium Titanate

W. L. BOND, W. P. MASON, AND H. J. MCSKIMIN
Bell Telephone Laboratories, Murray Hill, New Jersey
(Received February 13, 1951)

SMALL single crystals of barium titanate have been available to us for some time through the work of Matthias.[1] Although suitable for qualitative studies, these crystals were too small for accurate measurements of elastic and piezoelectric constants. Through the cooperation of the Signal Corps Engineering Laboratory, we have obtained larger single crystals of barium titanate produced by the Harshaw Chemical Company under Signal Corps contracts.[2] These were large multi-domain single crystals, but by being polarized with a high electric field the domains could be oriented with their ferroelectric axes predominantly in the direction of the thickness of the crystal plate.

The elastic constants were measured by using the ultrasonic pulse method shown by Fig. 1. Longitudinal or transverse waves are generated or received in fused quartz rods by X- or Y-cut quartz crystals soldered to the rods. The sample is connected to the fused quartz rods by means of a quarter-wave thickness of polystyrene, which has a very low loss and the mechanical impedances of 0.45×10^6 and 0.165×10^6 mechanical ohms per cm^2 for longitudinal and shear waves, when connected to the fused quartz rods. The velocity and attenuation can be measured by observing the ratio between the incident and transmitted waves.

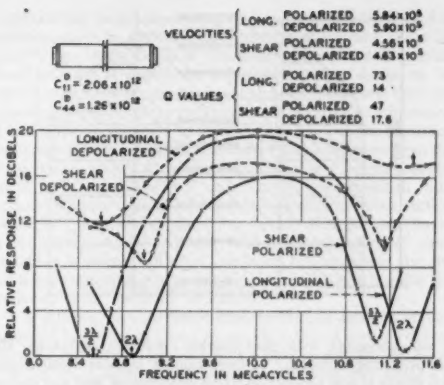

FIG. 1. Relative response as a function of frequency.

The transmitted waves are greatest at half-wavelength frequencies; and, by obtaining two of these, the velocity can be determined. If R is the ratio of the amplitude at odd quarter-wavelengths to the amplitude at half-wavelength frequencies, the attenuation can be calculated from the formula

$$\tanh Al=\left\{R\left(\frac{Z_s^2+Z_0^2}{2Z_sZ_0}\right)-1\right\}\Big/\left\{\frac{Z_s^2+Z_0^2}{2Z_sZ_0}-R\right\}, \qquad (1)$$

where Al is the attenuation in nepers, Bl the phase shift in radians, Z_s the sending and receiving impedances on either side of the sample, and Z_0 the characteristic impedance of the sample equal to the density ρ times the velocity. Figure 1 shows measurements for longitudinal and shear waves for a sample 1 cm square and 1.029 mm thick. The solid lines are for the sample polarized in the direction of the thickness, while the dotted curves are for the sample unpolarized. From these it is seen that the constant electric displacement elastic constants do not differ by more than 3 percent, which indicates that $c_{11}{}^D=c_{33}{}^D$ and $c_{44}{}^D=c_{66}{}^D$ within several percent. A much higher loss for the depolarized condition indicates a microhysteresis effect. The elastic constants are given by Fig. 1.

Measurements were also made of resonant and antiresonant frequencies of a series of orientations which were polarized along the thickness which lies along a cubic axis. The results are shown in Table I. From these we obtain the values of the constant field elastic constants:

$$\begin{aligned} &s_{11}{}^E=1.12\times10^{-12}\ \text{cm}^2/\text{dyne};\\ &\tfrac{1}{2}s_{11}{}^E+\tfrac{1}{4}(2s_{13}{}^E+s_{66}{}^E)=0.69\times10^{-12};\\ &c_{33}{}^E=1.13\times10^{12}\ \text{dynes/cm}^2. \end{aligned} \qquad (2)$$

For the square crystal the dielectric constant was 2890 at low frequencies, 2740 at frequencies below the thickness resonance, and 1500 above the resonance. From the relation between the dielectric constant above the resonance $\epsilon_{33}{}^S$ and the dielectric constant $\epsilon_{33}{}^T$ below the resonance, which can be written in the form

$$\epsilon_{33}{}^S/\epsilon_{33}{}^T=1-k^2, \qquad (3)$$

we find $k=0.67$, which is considerably higher than that found in a polarized ceramic of barium titanate. A similar relation between the elastic constants measured for constant displacement and constant field is

$$c_{33}{}^E/c_{33}{}^D=1-k^2 \qquad (4)$$

or $k=0.675$.

From the dielectric constant, the coupling constants 0.192 and 0.67 for the longitudinal length and thickness modes, respectively, and the elastic constants one can calculate the "effective" piezoelectric constants for this degree of poling as

$$\begin{aligned} d_{31}&=-310\times10^{-8}\ \text{stat coulombs/dyne},\\ d_{33}&=+950\times10^{-8}\ \text{stat coulombs/dyne}. \end{aligned} \qquad (5)$$

The elastic constants for constant electric displacement are

$$\begin{aligned} c_{11}{}^D=2.06\pm0.05\times10^{12}\ \text{dynes/cm}^2;\quad c_{13}{}^D=1.40\pm0.2\times10^{12};\\ c_{44}{}^D=1.26\pm0.05\times10^{12}. \end{aligned} \qquad (6)$$

TABLE I. Resonant and antiresonant frequencies for various orientations.

Orientation	Dimensions in mm L	W	T	Resonant frequency	Antiresonant frequency	Electromechanical coupling
Length along a cubic axis	10.13	1.15	0.5	189,973	192,950	0.192
Length 45° from a cubic axis	9.90	1.02	0.5	247,650		
Square plate	10.0	10.0	1.0	2,170,000		

[1] Blattner, Matthias, Merz, and Scherrer, Experientia 3, 148 (1947).
[2] A. de Brettville, Jr., and G. Katz, Phys. Rev. 78, 340 (1950).

Nuclear Magnetic Resonance Absorption in $NaSbF_6$

E. R. ANDREW
Department of Natural Philosophy, The University, St. Andrews, Scotland
(Received March 19, 1951)

PROCTOR and Yu[1] have demonstrated an interesting fine structure in the nuclear magnetic resonance absorption line for Sb^{121} and Sb^{123} in an aqueous solution of sodium hexafluoantimonate and hydrofluoric acid. The structure consists of an equally spaced symmetrical set of seven lines whose over-all width of ~10 gauss is unusually great for a liquid resonance. The second moment for the Sb^{121} line, computed from their illustrated experimental curve, is 5.5 gauss[2]. If the resonance had been obtained in a polycrystalline solid, a second moment of 15.3 gauss[2] would have been expected.[2,3] In solution the second moment should be less than this, since there should be random reorientation of the octahedral $[SbF_6]^-$ ion, with a frequency much greater than the frequency line width, unless the liquid has an unusually high viscosity. In fact, for equal probability of all spatial orientations, the line should be very narrow, since the average values of the terms $(3\cos^2\theta_{jk}-1)$, which occur in the interaction hamiltonian, are zero.[4]

A high viscosity could reduce the ionic reorientation frequency such that the line width is only partially reduced. It is, however, difficult to see why such a reduction caused by random reorientation should give the well-resolved fine structure. Moreover, it requires the viscosity to be $\sim2\times10^8$ poise.[5]

Suppose, however, that rapid ionic reorientation takes place about one axis only. For either uniform or random reorientation about a tetrad axis of the octahedron the second moment would be reduced to 7.2 gauss[2]; about a diad axis the value is 1.9 gauss[2], and about a triad axis it is zero. Rotation about one tetrad axis thus seems the most promising assumption. On this basis the line shape has been calculated by classical computation of the local field due to the six octahedral F^{19} nuclei at the central Sb^{121} nucleus; this procedure appears to be justifiable with this symmetry and motion for non-identical perturbing nuclei of spin ½, since it gives the correct second moment for all ionic orientations. Calculation is made for the 2^6 equally probable configurations of the six F^{19} nuclei; for each the local field is averaged for random reorientation about one tetrad axis. Finally, the line shape shown in Fig. 1(a) is obtained for a randomly oriented assembly of ions and is seen to exhibit an equally spaced symmetrical set of nine lines. When multiplied by a broadening function, a curve is obtained whose derivative is shown in Fig. 1(b). This curve agrees

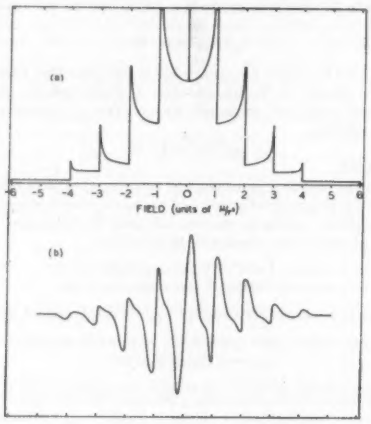

FIG. 1. (a) Calculated line shape for Sb^{121} in a polyoriented assembly of $[SbF_6]^-$ ions. (b) Line shape derivative after broadening the line shown in (a).

closely with the experimental curve of Proctor and Yu. The outer pair of lines are each derived from a configuration of weight 1 in 64 only, and for this reason scarcely show on their record. (The left-hand member is actually just visible.) This also explains why the second moment of their curve is rather less than the calculated value of 7.2 gauss[2]. The nine lines are separated by intervals of $\mu(F^{19})/r^3$ or 1.79 ± 0.05 gauss. The separation on the experimental record is 1.86 ± 0.05 gauss, in satisfactory agreement with the theory.

It now remains to explain why the ionic reorientation frequency about one tetrad axis should be higher than the frequency line width, while about other axes it is lower. A probable explanation is to be found in terms of the well-known polymerization of hydrogen fluoride. In the gas the molecules form zigzag hydrogen-bonded chains of about four units; the solid consists of infinite zigzag chains; the liquid is certainly associated although the degree is not known. Thus, it seems possible that the $[SbF_6]^-$ ion can form a link in a hydrogen fluoride chain, two subchains $(HF)_n$ being connected to two opposite fluorine atoms of the octahedral ion. If the effective length of the chain is $\sim r$ times the ionic diameter, the reorientation frequency about the tetrad axis through the connected corners will be $\sim r^3$ times that for end-over-end motion of the chain.[6] Intramolecular reorientation of the ion about this tetrad axis is also very likely. For $r\sim10$, in order that the end-over-end frequency be less than the frequency line width, the viscosity of the liquid need only be ~2 poise, which is a more reasonable value.

[1] W. G. Proctor and F. C. Yu, Phys. Rev. **81**, 20 (1951).
[2] J. H. Van Vleck, Phys. Rev. **74**, 1168 (1948).
[3] This represents the intramolecular contribution only.
[4] H. S. Gutowsky and G. E. Pake, J. Chem. Phys. **18**, 162 (1950).
[5] Bloembergen, Purcell, and Pound, Phys. Rev. **73**, 679 (1947).
[6] P. Debye, *Polar Molecules* (Dover Publications, New York, 1945), Chapter V.

Transition Effects of Star-Producing Cosmic Radiation in Lead*

E. SCHOPPER, K. H. HÖCKER, AND G. KUHN
Technische Hochschule, Stuttgart, Germany, and Forschungsstelle für Physik der Stratosphäre, Weissenau, Germany
(Received March 12, 1951)

THE frequency of cosmic-ray stars produced under various thicknesses of lead has been investigated by Bernardini, *et al.*,[1] and by George and Jason.[2] Continuing former experiments

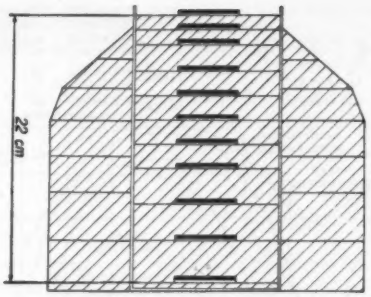

FIG. 1. Lead absorber.

of our laboratory with photographic emulsions concerning the star-producing radiation,[3] we have studied[4] in more detail transition effects of star production under absorbers of lead and carbon at the Zugspitze observatory (2950 m).

The plates (Kodak NT 4) were placed horizontally in different depths of the absorber as shown in Fig. 1 and exposed simultaneously for about 20 days in October, 1949, and May, 1950, respectively. In order to avoid fading effects the plates were kept in a nitrogen atmosphere and were developed to nearly two times minimum ionization, thereby facilitating particle discrimination.

In Fig. 2 the relative star intensity under lead has been plotted (solid circles) *versus* thickness of the absorber. We have recorded all events with at least two tracks, one of them longer than 70μ, radiating from a common center. Possible cases of scattering were excluded. We have added the data of George and Jason (open squares) and those of Bernardini and collaborators (open triangles), normalized at 0 cm Pb. They are in good agreement with our results, regarding the general shape of the absorption curve given by the mean range $L_{Pb}=320$ g/cm^2 for N-radiation. For the absolute star intensity in the unscreened plate we find $s=14.5$ stars cm^{-3} day^{-1}.

The more detailed variation of absorber thickness in our arrangement leads to a distinct maximum at about 1.2 cm Pb, confirming the existence of a transition effect. We could also find the transition effect for single protons, not plotted here, previously observed by Heitler and Powell.[5]

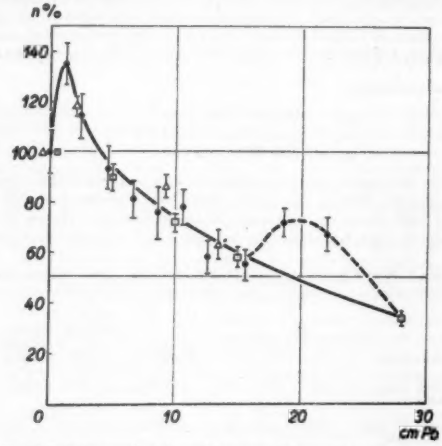

FIG. 2. Relative number of cosmic-ray stars (n percent) at 2950 m under various thicknesses of lead. The solid circles represent our data, the open squares the data of George and Jason, and the open triangles the data of Bernardini, *et al.*

Subtracting from our measured intensities the level of star intensity, given by the exponential absorption law with $L_{Pb}=320$ g/cm^{-2}, e.g., by the points of George and Jason, we find an additional intensity of mainly few-pronged stars, very similar to the transition curve of photon-produced showers.[6] However, there are some difficulties. From the comparison of the known multiplication of the cascade-component in lead with the peak of our transition maximum of stars, one is led to the conclusion that several percent of the stars in air should be initiated by photons; the cross section would be $\sigma_{air}\sim10^{-26}-10^{-27}$ cm^2. This is not consistent with recently reported results of Kikuchi,[7] showing a cross section $\sigma=4\times10^{-25}$ cm^2 for star production by 300-Mev photons. As far as our experiments go, we can, from an energy point of view, exclude a transition effect of nucleons as responsible for the additional frequency of stars at this altitude.[8] There remains the possibility of an interaction of mesons.

It is difficult, too, to understand the second increase of star frequency beginning at about 15 cm Pb, which is scarcely due to statistical deviations. Together with a point of George and Jason at 28 cm Pb, it suggests a second maximum. One may suppose a connection between this phenomenon and the second maximum of the Rossi curve, recently published by Bothe and Thurn.[9]

Further experiments aiming at a more detailed study of these phenomena are in progress.[10]

* Reported at the conference of Verband Deutscher Physikalischer Gesellschaften, Bad Nauheim, October, 1950.

[1] Bernardini, Cortini, and Manfredini, Phys. Rev. **74**, 845 (1948).
[2] E. P. George and A. C. Jason, Proc. Phys. Soc. (London) **62**, 243 (1949).
[3] K. H. Höcker and E. Schopper, Ann. Physik **6**, 338 (1949).
[4] With special nuclear track microscopic equipments supplied by Fr. Ernst Leitz, Wetzlar (Germany).
[5] Heitler, Powell, and Heitler, Nature **146**, 65 (1940).
[6] B. Rossi and L. Janossy, Proc. Roy. Soc. (London) **A173**, 88 (1940).
[7] S. Kikuchi, Phys. Rev. **80**, 492 (1950).
[8] Schopper, Höcker, and Kuhn, Phys. Rev. **82**, 445 (1951).
[9] W. Bothe and H. Thurn, Phys. Rev. **79**, 544 (1950).
[10] To be published in Z. Naturforsch.

Secondary Nucleons in Lead

E. Schopper, K. H. Höcker, and G. Kuhn
Technische Hochschule, Stuttgart, Germany, and Forschungsstelle für Physik der Stratosphäre, Weissenau, Germany

(Received March 12, 1951)

TRANSITION effects of cosmic-ray stars[1] and of low energy neutrons, observed in lead at 3000 m, suggest some considerations concerning the production of secondary nucleons in lead.

As to stars, there is good reason to believe that most of them at this altitude are produced by secondary nucleons originating in nuclear disintegrations. Thus the formation of the nuclear component is a cascadelike process, which may happen in different ways in absorber material and in air, respectively.

We have observed in our experiments an increase in the number of neutron-produced single tracks of protons, beginning and ending in the photographic emulsion (Kodak NT 4 plates), by a factor of roughly 2.5 with varying thickness of the lead absorber (Fig. 1). This is in agreement with experiments of Tongiorgi.[2]

The particles of the nucleonic component can be divided roughly into three groups. The first, containing particles of relativistic energy, produces mesons and secondary nucleons. For the second group (10^9 ev$>E>10^8$ ev) meson production is negligible. The third group ($E<10^8$ ev), containing mainly neutrons, gives rise to single protons but not to stars.

Assuming the probability of nuclear collisions per gram to be proportional to A^{-1} (A=mass number) and the number of secondary nucleons starting in a nuclear disintegration to be proportional to $A^{2/3}$, we find the number N of secondaries per gram proportional to A^{+1}, and the ratio $N_{Pb}/N_{air}=2.4$. The energy transferred to these secondary nucleons is due to the energy loss

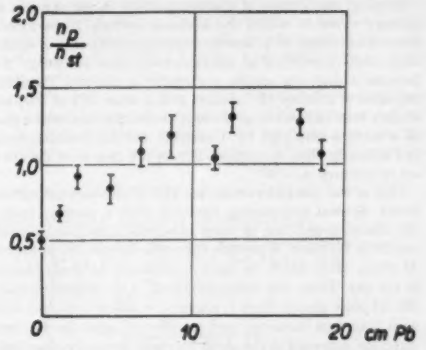

FIG. 1. Intensity of neutron-produced single proton tracks (n_p) under Pb screens, relative to the star intensity of the unscreened plate (n_{st}).

of their primaries, that is, proportional to A^{-1}. Thus, we have a greater number of secondaries in lead with smaller energy.

Nucleons of the first group being rather rare at 3000 m, the main contribution to star production will be made by nucleons of the second group. From the foregoing considerations their secondaries in lead are not expected to initiate further stars at a sizable rate, since they belong mainly to the third group. It seems, therefore, not probable that the transition effect of stars in lead[4,5] can be attributed to secondary nucleons produced in lead, regardless of the shape of the transition curve itself. This is, however, not conclusive for higher altitudes, where a nucleonic transition effect of star intensity in lead may occur because of the comparatively greater frequency of first-group nucleons.[4]

[1] Schopper, Höcker, and Kuhn, Phys. Rev. **82**, 444 (1951).
[2] V. C. Tongiorgi, Phys. Rev. **76**, 517 (1949).
[3] Bernardini, Cortini, and Manfredini, Phys. Rev. **74**, 845 (1948); **76**, 1792 (1949).
[4] G. N. Whyte, Phys. Rev. **78**, 630 (1950).

A Cloud-Chamber Study of the New Unstable Particles*

H. S. Bridge and M. Annis
Department of Physics and Laboratory for Nuclear Science and Engineering, Massachusetts Institute of Technology, Cambridge, Massachusetts

(Received March 12, 1951)

IN a set of pictures taken with a large multiple-plate cloud chamber at 700 g cm^{-2} atmospheric depth, we have observed 10 examples of tracks that deviate suddenly in the gas of the chamber. These are similar to the "V" tracks reported by Rochester and Butler,[1] by Seriff, Leighton, Hsiao, Cowan, and Anderson,[2] and recently by Fretter.[3] Of these 10 events, 4 can be interpreted as neutral-particle decays, 4 as charged-particle decays, while 2 are uncertain as to type.

Of the 4 neutral-particle decays, 2 show one of the decay products ionizing heavily and stopping in a plate. In 2 cases it is possible to say from ionization, range, and scattering that one of the decay products is probably a meson.

In general, we could not ascertain whether the plane of the "V" contained the origin of the event which gave rise to the neutral particle. However, in one case in which many penetrating particles were seen to traverse the chamber vertically, the plane of the "V" was nearly horizontal. In most events of this type reported up to the present, the triggering system was such as to favor events in which the V was vertical.

In all of the 4 cases of charged-particle decay one can see the primary event in which the unstable particle is produced. Two cases show decay of a heavily ionizing parent into a lightly ionizing product which, if an electron, must have an energy >2 Mev because it does not scatter noticeably in the gas. Possibly these are cases of β-decay (B^{12} decays with a mean life of 0.02 second), or they may be cases of $\mu \rightarrow e$ decay. From the production spectrum of π-mesons obtained by Camerini and his collaborators,[4] one can estimate that the probability to see two $\mu \rightarrow e$ decays in our set of pictures is $\sim 10^{-2}$.

One of the charged events (see Fig. 1) can be analyzed in some detail. Several penetrating particles from a nuclear event enter the chamber and one of them produces a nuclear interaction in the third Pb plate. A particle from this interaction penetrates one Al plate, after which its track is deviated suddenly through 90° in the gas. From this point the track, *a*, goes upward and enters the Al plate above. Here it appears to suffer a nuclear scattering with little loss in energy and is deflected again in the downward direction, stopping in the ninth Pb plate. From the observed range, scattering, and ionization, particle *b* must be a meson. In 4 plates, this particle is scattered through an angle greater than twice the average value of the scattering angle calculated under the assumption that the particle is a proton. One proton in 10^4 will be scattered in this way. If the charged-decay product is a meson, it must be a π-meson, since it suffers a nuclear scattering in an Al plate.

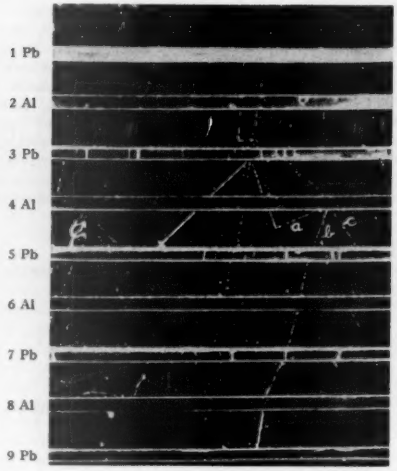

FIG. 1. A particle executing a right-hand turn in the gas of a cloud chamber. Track *a* and track *b* reproject to the same height in plate 3 in both views. Track *c* does not reproject to the same point in the plate and is probably one of the electrons of the pair seen above the plate. Alternate plates are 0.25-inch Pb and 0.31-inch Al.

Assuming the process is a two-body decay, one can calculate the mass, m_1, of the unstable particle assuming different masses, m_0, for the neutral-decay product. Provided m_0 lies between zero and m_π, m_1 is not sensitive to the choice of m_0. Using these limits for the mass of the neutral particle and extreme values for the ionization, we obtain a mass for the parent between 600 and $1200 m_e$. This spread is mostly the result of assuming that the estimated specific ionization is uncertain by a factor of 1.7. The choice of m_0 has little effect on the result if m_0 is taken lighter than a π-meson.

We have also observed 7 cases in which a particle enters the chamber from above, slows down, and apparently stops in a plate (Fig. 2). From this plate there emerges a thin track with no other products visible. In one of these pictures (Fig. 2) the secondary particle traverses ~ 35 g cm^{-2} of Pb with no multiplication. The average scattering angle in 3 plates is 3°. If the secondary particle were an electron, the minimum value of the energy loss due to collision processes alone would be 43 Mev, while the average radiation loss would be at least 850 Mev. The particle is thus not an electron from a $\mu \rightarrow e$ decay. We think that at least some of the other cases are not $\mu \rightarrow e$ decays, yet we can think of no process other than a decay which would explain these events.

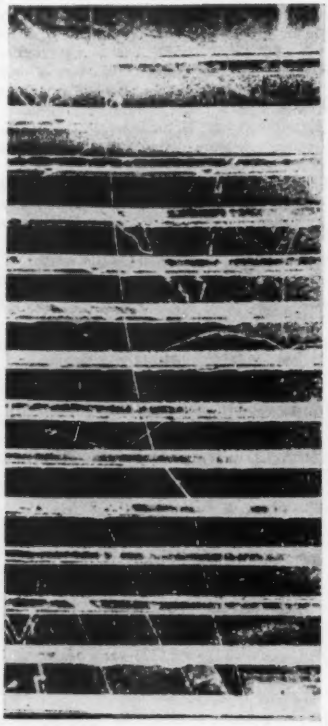

FIG. 2. Particle stopping in a lead plate and giving rise to a lightly ionizing product. All plates are 0.25-inch Pb.

One can show that the time of flight in the cloud chamber of a particle heavier than $200 m_e$ which stops in the chamber after traversing 8 Pb plates is at least 10^{-9} second. The mean life of these stopped particles is thus not much shorter than 10^{-9} seconds, although it might be appreciably longer.

The analysis of these particles is being continued.

We are indebted to Professor R. W. Williams and to Mr. F. B. Harris for aiding us during the experiment, and to Professor B. Rossi for aid in the analysis of the pictures.

* This work was supported in part by the joint program of the AEC and ONR.

[1] G. D. Rochester and C. C. Butler, Nature **160**, 855 (1947).
[2] Seriff, Leighton, Hsiao, Cowan, and Anderson, Phys. Rev. **78**, 290 (1950).
[3] W. B. Fretter, Phys. Rev. **82**, April 15 A (1951).
[4] Camerini, Fowler, Lock, and Muirhead, Phil. Mag. **41**, 413 (1950).

Neutron Deficient Isotopes of Lanthanum

M. M. Gransden and W. S. Boyle
Radiation Laboratory, McGill University, Montreal, Canada
(Received March 19, 1951)

A BARIUM target bombarded by protons with energies up to 90 Mev has been found to yield the new isotopes La^{132} (4.5 hr) and La^{131} (58 min) which were isolated by a 180° mass spectrograph.

The filament of the thermal ion source in the mass spectrograph was coated with the chemically separated La, and the isotopes were collected on a thin Dural foil. Transfer plates were made with x-ray no-screen film; and the new products, which were identified with reference to known active La isotopes,[1] were then cut from the foil and studied separately. These individual strips showed activities from 10,000 to 40,000 cpm, sufficient to permit not only good values for the half-lives but also absorption experiments to determine the energy of the γ-rays and the positrons which had been identified in a rough magnetic analysis. Results are given in Table I.

The time interval between bombardment and counting would prevent the observation of half-lives of less than about 20 min.

Owing to the large number of Ba isotopes in appreciable abundance, the energy of proton bombardment for best yield of any particular isotope is not sharply defined. The ratio La^{132}/La^{131} increases by a factor of 20 between 20 and 90 Mev.

Table I. Observed half-lives and energies.

Isotope	Half-life	Radiation
La^{132}	4.5 hr	β^+ 3.5 Mev γ 1.0 Mev
La^{131}	58 min	β^+ 1.6 Mev

Whereas the period of La^{131} fits into the steadily decreasing series of half-lives for La isotopes of even neutron number, that of La^{132} (4.5 hr) might be expected to be measured in minutes, in view of the corresponding series of known isotopes of odd neutron number. Indeed, the energy of the positron suggests that this isotope may have a complex decay scheme involving an isomeric state. This point is being investigated.

We express our best thanks to Professor J. S. Foster for his interest in this work.

[1] Naumann, Reynolds, and Perlman, Phys. Rev. 77, 398 (1950).

Absorption of 280-Mev Photons*

J. W. DeWire, A. Ashkin, and L. A. Beach
Cornell University, Ithaca, New York
(Received March 12, 1951)

TOTAL cross sections for 280-Mev photons in various elements have been determined by measuring the transmission through samples placed in the bremsstrahlung beam from the 300-Mev synchrotron. The photons above 250 Mev were detected by an electron pair spectrometer,[1] in order to avoid effects due to degradation of the photon energies in the absorbers. The results are given in Table I, together with the ratio of the calculated values to the experimental results. The theoretical values are based on the Bethe-Heitler theory[2] for pair production in the nuclear field, the Wheeler and Lamb calculations[3] on pair production in the electronic field, and the Klein-Nishina formula for Compton scattering.

Table I. Total cross sections for 280-Mev photons.

Absorber	Experimental cross section (cm^2/g)	Probable statistical error (%)	Ratio of theory to experiment
Be	0.01060	1.2	0.982
Al	0.0284	1.2	0.988
Cu	0.0528	0.9	1.011
Sn	0.0776	1.0	1.032
Pb	0.1069	1.2	1.105
U	0.1148	1.4	1.114

The results show a relation to the theoretical cross sections which is similar to the results of Lawson[4] at 88 Mev and of Adams[5] and Walker[6] at still lower energies. The beryllium cross section agrees with the theory, in contrast to the disagreement found by Lawson.[4]

Further details will be given in a paper to be published later.

* Assisted by the joint program of the ONR and AEC.
[1] DeWire, Ashkin, and Beach, Phys. Rev. 79, 210 A (1950).
[2] H. Bethe and W. Heitler, Proc. Roy. Soc. (London) 146, 83 (1934).
[3] J. A. Wheeler and W. E. Lamb, Phys. Rev. 55, 858 (1939).
[4] J. L. Lawson, Phys. Rev. 75, 433 (1949).
[5] G. D. Adams, Phys. Rev. 74, 1707 (1948).
[6] R. L. Walker, Phys. Rev. 76, 527 (1949).

Erratum: A Canonical Transformation in the Theory of Particles of Arbitrary Spin

[Phys. Rev. 81, 290 (1951)]

W. A. Hepner
Department of Mathematics, Imperial College of Science and Technology, London, England

THE equations in the first line of Eq. (2) should have the letters (a), (b), (c) attached to them, and those in the second line (d), (e), (f), respectively. Also, insert "assuming that S^3 anticommutes with β_3" before Eq. (5), and add "as assumed," after Eq. (7).

Note on Total Yield of Alphas from $Li^6(d, \alpha)\alpha$

Robert Resnick
Department of Physics, University of Pittsburgh, Pittsburgh, Pennsylvania
(Received March 15, 1951)

THE fit of the theoretical curves[1] of angular distribution of alphas in $Li^6(d, \alpha)\alpha$ with experiment[2] and the reasonable values of the parameters required for such a fit suggest that the assumptions of one sharp state and one broad state are valid in the energy range investigated (0 to 4 Mev). The rise in the $Y(E, 90°)$ curve beyond the observed resonance at $E \simeq \frac{3}{4}$ Mev is attributed to increasing penetrability of the $l=2$ wave at higher energies. Attempts to fit the $Y(E, 90°)$ curve with these assumptions, using values of the parameters determined from the angular distribution curves, fail to give good results for a range of reasonable values of E_3 and γ_3, the resonant energy and half-width of the sharp state. One obtains $Y(\frac{3}{4}\text{ Mev})/Y(2\text{ Mev}) = 6.1$, compared with the experimental value 2.3, for the best fit. The choice of a nuclear radius smaller than the assumed $R = 1.83e^2/mc^2$ improves the situation somewhat.

Hence, the existence of a second resonant state around 4 Mev seems necessary to account for the high minimum in $Y(E, 90°)$ beyond the first resonance. Such an assumption in the theory results in an increase in the number of arbitrary parameters and more complicated relationships between these parameters and the interaction matrix elements.[1] A good fit to all experimental results thus becomes possible but less significant than in the simpler theory. Extension of the energy range of the experiments is necessary to determine whether such a resonance exists, and the conditions imposed by the total yield and angular distribution over this increased range may reduce the arbitrariness sufficiently to allow unique assignment of the parameters involved.

[1] R. Resnick and D. R. Inglis, Phys. Rev. 76, 1318 (1949).
[2] Heydenburg, Hudson, Inglis, and Whitehead, Phys. Rev. 74, 405 (1948).

Calculation of Matrix Elements

J. S. R. CHISHOLM
Christ's College, Cambridge, England
(Received March 12, 1951)

ANY line in a Feynman-Dyson[1,2] graph gives a factor in the integrand of the matrix element. If k denotes a linear combination of the internal energy-momenta over which we subsequently integrate, scalar bosons have (apart from constant factors) a propagation factor $(k^2+\kappa^2)^{-1}$; and fermions have a factor[2]

$$\left[-\kappa-(i\gamma/2)(\partial/\partial p)\int_{\kappa^2}^{\infty}d\sigma\right]\{(p-k)^2+\sigma\}^{-1}. \quad (1)$$

p is either an external momentum or a "false external momentum" introduced when closed loops of fermion lines occur, and eventually equated to zero. A different symbol p is used for each line.

Thus, the internal momenta always occur as in a scalar boson factor (this can include scalar meson-photon interaction). These factors, combined by Feynman's methods, result in an integral of the type

$$\int_{-\infty}^{\infty}d^4k\cdots\int_{-\infty}^{\infty}d^4k^{(n)}[Q(k,k',\cdots,k^{(n)})], \quad (2)$$

where Q is a quadratic function of the internal momenta. The integral is invariant under orthogonal transformations and simple translations of the k's with jacobian $+1$, and Q is reducible to diagonal form with positive coefficients. Evaluating this integral by Feynman's methods, and by using invariance properties, it follows that Eq. (2) is a constant multiple of $\Lambda^{r-2n-2}\chi^{2n-r}$, where χ is the discriminant of Q, and Λ is the discriminant of the purely quadratic part of Q; both are invariants. Λ is independent of p's and σ's and so commutes with the square bracket in Eq. (1). Therefore, we need simply consider the effect of a product of these brackets (perhaps interspersed by γ-matrices) on χ^{-m}, $(m=r-2n)$.

If a graph contains self-energy (s.e.) parts, Eq. (2) is divergent in some k variables; and following Ward,[4] we differentiate with respect to some σ in the s.e. parts. Then Eq. (2) converges and is a constant multiple of $\Lambda^{(r+1)-2n-2}\chi^{2n-(r+1)}$. The divergences appearing later, partly caused by reintegration with respect to σ, are all eliminated by subtraction procedure. Apart from subtraction, the same formula for Eq. (2) holds in every case.

χ is linear in the σ's and quadratic in the p's; $\partial\chi/\partial\sigma=\chi_\sigma$ is independent of p's and σ's, and the "derivative" of χ defined by $\chi_p=(2\chi_\sigma)^{-1}\partial\chi/\partial p$ is easily found. The "second derivative," $\chi_{pp'}=(4\chi_\sigma\chi_{\sigma'})^{-1}\partial^2\chi/\partial p\partial p'$, is a multiple of the unit (metric) tensor and has diagonal components, say, $\Omega_{pp'}$. Defining $\Omega_p=-\kappa+i\gamma\chi_p$, all matrix elements are expressible in terms of Ω_p, $\Omega_{pp'}$, χ, Λ, and γ-matrices.

For example, in considering a product of fermion operators occurring in Eq. (1), we use the formula

$$\left[-\kappa-(i\gamma/2)(\partial/\partial p)\int_{\kappa^2}^{\infty}d\sigma\right]F(\chi)\chi^{-l}$$
$$=[\Omega_p+I(\chi)(2\chi_\sigma)^{-1}\partial/\partial p](\chi^{-l};F(\chi)). \quad (3)$$

In Eq. (3), $F(\chi)$ is a function of the derivatives of χ (all independent of the σ's); $I(\chi)$ is an operator defined by

$$I(\chi)\chi^{-l}=(1-l)^{-1}\left[\int_m^{\beta}d\alpha(\chi+\alpha)^{-l}\right]_{\beta=0}.$$

$I(\chi)$ operates on χ^{-l} and $\partial/\partial p$ operates on $F(\chi)$ only; the resulting factors are multiplied together. Hence, a term

$$\left[-\kappa-(i\gamma/2)(\partial/\partial p)\int_{\kappa^2}^{\infty}d\sigma\right]\gamma_\mu\left[-\kappa-(i\gamma/2)(\partial/\partial p')\int_{\kappa^2}^{\infty}d\sigma'\right]\gamma_\nu\cdots$$
$$\times\left[-\kappa-(i\gamma/2)(\partial/\partial p^{(n)})\int_{\kappa^2}^{\infty}d\sigma^{(n)}\right]\chi^{-m} \quad (4)$$

is evaluated as follows. The "basic term" is

$$\Omega_p\gamma_\mu\Omega_{p'}\gamma_\nu\cdots\Omega_{p(n)}\chi^{-m}. \quad (5)$$

We can substitute for any pair $\Omega_{p(i)}\cdots\Omega_{p(j)}$ the terms $\gamma_\alpha\cdots\times\gamma_\alpha\Omega_{p(i)}{}_p(j)I(\chi)$, retaining the original order of the γ-matrices. The value of Eq. (4) is Eq. (5) plus all possible terms derived by any number of these substitutions. Occurrence of several $I(\chi)$ implies repeated integration of χ^{-m}.

Difficulty arises when $I(\chi)\chi^{-1}$ and $I(\chi)I(\chi)\chi^{-1}$ appear. $I(\chi)\chi^{-1}$ terms enter in vertex (v.) and fermion self-energy (f.s.e.) parts, and $I(\chi)I(\chi)\chi^{-1}$ occurs in boson self-energy (b.s.e.) parts in electrodynamics. These are just the parts involving subtraction procedure. For s.e. parts, the earlier differentiation with respect to one σ in that part is balanced by the introduction of another factor $I(\chi)$. Subtractions, made successively, starting with the "innermost" divergence, are performed before applying $I(\chi)$, so that we have to subtract from terms containing only inverse powers of χ. If an unsubtracted term is $T=T(p,p',\cdots)$ and T_f is T with the p's put equal to free particle momenta, then, for v. and f.s.e. parts, the term after subtraction is $T-T_f$. For b.s.e. parts, we subtract the first *two* terms of the Taylor expansion of T. Subtraction eliminates all difficulties in interpreting $I(\chi)$. Both the original term and those subtracted are derived directly by the general method.

The problem of integration over Feynman auxiliary variables has not yet been undertaken.

[1] R. P. Feynman, Phys. Rev. **76**, 749 and 769 (1949).
[2] F. J. Dyson, Phys. Rev. **75**, 486 and 1736 (1949).
[3] R. Karplus and N. M. Kroll, Phys. Rev. **77**, 548 (1950), Eq. (58).
[4] J. C. Ward, Phys. Rev. **78**, 182 (1950) and Proc. Phys. Soc. (London) **64** (Pt. 1), 54) 1951).

Distribution of Energy Loss of Electrons in Aluminum

R. D. BIRKHOFF
Department of Physics, University of Tennessee, Knoxville, Tennessee
and
Health Physics Division, Oak Ridge National Laboratory, Oak Ridge, Tennessee
(Received February 23, 1951)

THE conversion electrons of Ba^{137} have been examined before and after passing through a thin foil (13.4 mg/cm² of Al) by means of a beta-spectrograph similar to that described by DuMond.[1,2] The results are shown in Fig. 1, where the ordinates

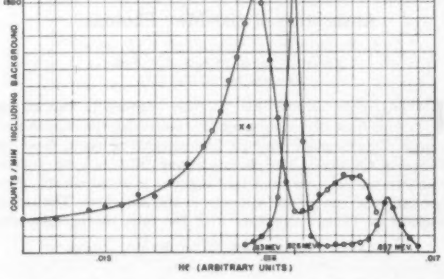

FIG. 1. Conversion lines of 0.663-Mev γ-ray from Ba^{137} with and without 13.4-mg/cm² aluminum absorber.

for the electrons which have traversed the foil have been multiplied by four. The separation of the K and L conversion lines and the large decrease in the number of counts at the maximum of the K line when a foil is introduced are indicative of the high resolution obtainable with this type of instrument. Calculations of the areas under the K lines with and without the foil indicate a loss of

about 23 percent of the incident electrons due to scattering out of the beam.

Previous experiments have been characterized by a spread in incident energy of the same order as the spread due to straggling in the foil,[2-6] or by the use of a sharp beta-spectrum superimposed on a continuous beta-spectrum, or both.[6] It was the purpose of this experiment to make unnecessary the corrections which have had to be applied to these experiments in order to compare with energy loss theory.

In Fig. 2 the experimental counts less the background of 45 cpm have been plotted together with the theories of Landau[7]-Williams[8]

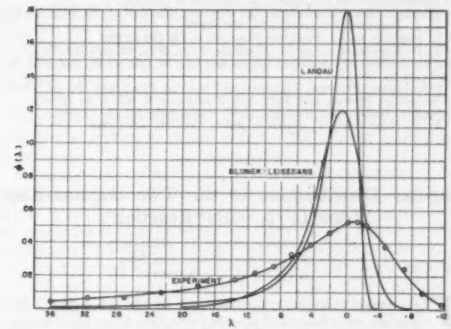

FIG. 2. Normalized energy loss distribution according to Landau, Blunck-Leisegang, and experiment.

and Blunck-Leisegang.[9] The variation in the most probable energy loss among the theories and the experiment of about 1.5 lambda-units is the same order as the experimental error and hence may or may not be significant. The width of the energy loss distribution is considerably greater than predicted by either theory, a result noted previously in the work of White and Millington[6] with mica foils. Here (in the notation of Landau[7]) λ is a dimensionless variable proportional to the energy loss, and $\Phi(\lambda)d\lambda$ is the normalized probability for an energy loss between λ and $\lambda+d\lambda$. The experimental curve has been normalized to unity in order to facilitate comparison with the theory. The electron energy before passing through the foil lies at $\lambda=-11.6$.

When completed, the spectrograph should have a resolution superior to that obtained here of about 0.5 percent without sacrificing the 1 percent of the solid angle from the source. Further experiments with the spectrograph and an electrostatic accelerating arrangement will permit measurement of electron straggling at any energy up to 2 Mev. A description of the spectrograph will appear in the literature in the near future.

[1] J. W. M. DuMond, Rev. Sci. Instr. **20**, 160 (1949).
[2] J. W. M. DuMond, Rev. Sci. Instr. **20**, 616 (1949).
[3] W. Paul and H. Reich, Z. Physik **127**, 429 (1950).
[4] Birkhoff, Hays, and Goudsmit, Phys. Rev. **79**, 199 (1950).
[5] S. D. Warshaw and J. J. L. Chen, Phys. Rev. **80**, 97 (1950).
[6] P. White and G. Millington, Proc. Roy. Soc. (London) **A120**, 701 (1928).
[7] L. Landau, J. Phys. (U.S.S.R.) **8**, 201 (1944).
[8] E. J. Williams, Proc. Roy. Soc. (London) **A125**, 420 (1929).
[9] O. Blunck and S. Leisegang, Z. Physik **128**, 500 (1950).

Radioactivity of Cerium

R. D. HILL
Physics Department, University of Illinois, Urbana, Illinois*
(Received March 9, 1951)

A SEARCH for further isomers at the end of the 5th nuclear shell has led to a reinvestigation of the activities of $_{58}Ce_{79}^{137}$ and $_{58}Ce_{81}^{139}$. Within the experimental limitation of a lifetime greater than about a day, no isomeric activity was observed. This would be consistent with level trends discernible[1] from neighboring isomers of barium, xenon, and tellurium.

Normal and enriched samples of cerium isotopes were bombarded by neutrons in the piles at the Oak Ridge and Argonne National Laboratories. The compositions of the samples were:[2]

Sample 1: 0.19 percent (136), 0.25 percent (138), 88.48 percent (140), 11.07 percent (142);
Sample 2: 0.10 percent (136), 4.42 percent (138), 92.00 percent (140), 3.48 percent (142);
Sample 3: 8.94 percent (136), 0.81 percent (138), 84.98 percent (140), 5.27 percent (142).

All bombarded samples showed strongly the 30-day activity of Ce^{141}. A γ-transition of 145 ± 0.5 kev was found to be associated with this activity. The transition is converted in praseodymium, and the N_K/N_L ratio is approximately seven. These observations are in good agreement with the latest reported values of Freedman and Engelkemeir.[3]

Sample 2 showed lines in the electron spectrum from a 165.5 ± 0.5-kev γ-transition, most probably converted in lanthanum. These lines, when compared with those of the 145-kev transition in Ce^{141}, decayed with a long half-life of between 100 and 400 days. They are undoubtedly to be attributed to the 140-day Ce^{139} activity discovered by Pool and Krisberg.[4] Owing to the weakness of the activity, arising from only a 4 percent abundance of the capture isotope Ce^{138}, an approximate value of $\geqslant 4$ could only be determined for the N_K/N_L ratio.

The electron spectrum from sample 3 exhibited lines from a 257 ± 1-kev γ-transition, decaying with a half-life of approximately 2 days. These lines were not evident in the spectra from samples 1 and 2; and, therefore, the 257-kev transition cannot be ascribed to the activity of Ce^{143}, of similar lifetime. It is rather to be identified with the 280-kev γ-transition of 36-hour Ce^{137} discovered by Chubbuck and Perlman.[5] The activity in the present experiments was again too weak to obtain either an accurate determination of the position of the L conversion line, for an assignment of its conversion atom, or an accurate measurement of the N_K/N_L ratio, which was estimated to be ~ 4.

* Assisted in part by the joint program of the ONR and AEC.
[1] R. D. Hill, Phys. Rev. **79**, 102 (1950).
[2] Obtained from Y-12 Plant, Carbide and Carbon Corporation, Oak Ridge, Tennessee.
[3] M. S. Freedman and D. W. Engelkemeir, Phys. Rev. **79**, 897 (1950).
[4] M. L. Pool and N. L. Krisberg, Phys. Rev. **73**, 1035 (1948).
[5] J. B. Chubbuck and I. Perlman, Phys. Rev. **74**, 982 (1948).

Radiations from I^{126}

M. L. PERLMAN AND G. FRIEDLANDER
*Chemistry Department, Brookhaven National Laboratory, Upton, Long Island, New York**
(Received March 8, 1951)

IODINE 126 is known to decay with a half-life of 13 days, emitting negative beta-particles and gamma-rays.[1] However, the yields reported for the reactions $I^{127}(\gamma, n)I^{126}$,[2] $Sb^{123}(\alpha, n)I^{126}$,[3] and $Bi^{209}(d, \text{fission})$,[4] as determined from the I^{126} beta-activity, seem low. An investigation of the decay scheme of I^{126} has therefore been undertaken, and preliminary results are reported here.

The I^{126} was produced at MIT by the reaction $I^{127}(n, 2n)I^{126}$, and it was concentrated by a Szilard-Chalmers separation from the irradiated solid potassium iodate. The activity, with some inactive iodine carrier, was purified and finally converted to aqueous I_2 solution which was placed over a copper foil. The activity deposited itself onto the foil as a result of the reaction $2Cu+I_2 \rightarrow 2CuI$.[5]

Tellurium K x-rays were observed in the decay of I^{126} by use of a proportional counter[6] and pulse height analyzer.[7] The counter had a 107-mg/cm^2 beryllium window, and it was filled to three atmospheres pressure with a mixture of 97 percent krypton and 3 percent ethane. The counting efficiency for tellurium K x-rays was about 90 percent. Figure 1 shows a typical I^{126} pulse height

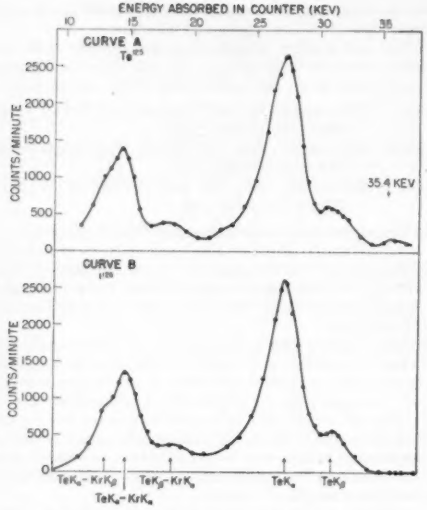

FIG. 1. Pulse spectra from x-rays of Te^{125} and I^{126}.

spectrum measured through sufficient beryllium to absorb the beta-particles and L x-rays. For comparison, the tellurium K x-ray spectrum resulting from the isomeric transition in Te^{125} is also shown. The correspondence of the two curves proves that the I^{126} radiations are tellurium K x-rays. Xenon K x-rays arising from internal conversion following β^- decay cannot contribute more than 2 percent of the x-ray intensity.

The absolute K-electron capture rate of an I^{126} sample was calculated from the x-ray pulse height distribution by the method previously described.[6] A fluorescence yield of 0.75 was assumed.[8] The L capture rate may be estimated[9] to be 12 percent of the K rate. The absolute beta-disintegration rate was measured for an I^{126} sample of known capture activity by correction of the measured Geiger activity for solid angle, absorption in air and counter window, back scattering, coincidence loss, and x- and gamma-activities. The ratio of the electron capture probability to the beta-decay probability for I^{126} was found to be 1.44 ± 0.15.

Beta-ray spectrometer measurements made by Alburger demonstrated, in agreement with earlier data,[1] the existence of two beta-transitions of energies 1.24 ± 0.02 Mev (~25 percent) and 0.85 ± 0.03 Mev (~75 percent), and of conversion electrons of a 0.382 ± 0.004-Mev gamma-ray.

Gamma-ray energies were measured with a scintillation spectrometer, in collaboration with E. der Mateosian. A 640 ± 20-kev gamma-ray line was found, low in intensity compared with the previously known 390-kev line. The energies of the two lines were established by comparison with the gamma-rays of Cs^{137} (663 kev) and of Au^{198} (411 kev). In addition, a faint line was observed of energy corresponding to annihilation radiation.

With an I^{126} source, coincidences were observed between pulses from two NaI(Tl) scintillation counters placed at right angles and shielded from each other by 4 mm of lead. Measurements with copper and lead absorbers showed that approximately one-half the observed coincidence rate represented x-γ events and one-half γ-γ events. A comparison of the coincidence rates at 180° and at 135°, when both counters were covered with 3 g/cm² of lead absorber, established the presence of annihilation radiation. A preliminary estimate of 2 percent positron decay may be deduced from the data. Beta-gamma coincidences were measured with the use of a Geiger counter and a NaI-scintillation counter. Comparison of the β-γ coincidence counts per β-count for I^{126} and for Au^{198} (which has a 960-kev beta-transition followed by a 411-kev gamma-ray) and coincidence absorption measurements showed the following: (1) the 1.24-Mev betas do not coincide with gamma-rays and therefore presumably go to the ground state of Xe^{126}; (2) the 0.85-Mev betas are followed by a single gamma-ray transition, probably the observed 0.38-Mev gamma. The γ-γ coincidences and the 640-kev gamma-ray must therefore be in the electron capture branch. The coincidence work was done in collaboration with Dr. A. W. Sunyar.

We thank Mr. J. Bulkley of MIT for the neutron irradiation and Miss E. Wilson for assistance with some of the measurements.

* Research carried out under the auspices of the AEC.
[1] Mitchell, Mei, Maienschein, and Peacock, Phys. Rev. **76**, 1450 (1949).
[2] M. L. Perlman, Phys. Rev. **75**, 988 (1949).
[3] L. Marquez and I. Perlman, Phys. Rev. **78**, 189 (1950).
[4] R. H. Goeckermann and I. Perlman, Phys. Rev. **76**, 628 (1949).
[5] This method of preparing iodine samples as thin as 0.1 mg/cm² was developed by Dr. W. Orr.
[6] Friedlander, Perlman, Alburger, and Sunyar, Phys. Rev. **80**, 30 (1950).
[7] Bernstein, Brewer, and Rubinson, Nucleonics **6**, No. 2, 39 (1950).
[8] Steffen, Huber, and Humbel, Helv. Phys. Acta **22**, 167 (1949).
[9] M. E. Rose and J. L. Jackson, Phys. Rev. **76**, 437 (1949).

Angular Distributions of the Two Gamma-Rays from $Li^7(p, \gamma)Be^8$ Reaction*

M. B. STEARNS AND B. D. MCDANIEL
Cornell University, Ithaca, New York
(Received March 22, 1951)

THE separate angular distributions of the 14- and 17-Mev gamma-rays from $Li^7(p, \gamma)Be^8$ reaction have been studied at two proton bombarding energies. From these measurements it has been possible to draw certain conclusions concerning the angular momentum of the energy levels involved. Earlier published experiments[1-5] have left considerable uncertainty both with regard to the angular distribution and to the nature of these levels.

The two gamma-ray lines were resolved using the gamma-ray pair spectrometer.[6] The angular aperture of the spectrometer was limited to ±7 degrees; then, by varying the angular position of the spectrometer with respect to the target and incident proton beam, it was possible to measure the intensity of each of the lines as a function of angle. A Pb radiator of 84 mg/cm² was used in the spectrometer.

The two proton bombarding energies were 0.50 ± 0.03 Mev and 1.15 ± 0.05 Mev. At the bombarding energy of 0.50 Mev a thick target was used, yielding mostly 440-kev resonance radiation. At the proton energy of 1.15 Mev a target thickness of 250 ± 50 kev was used. This yields mainly "nonresonant" radiation. For each proton energy, observations were made of the intensities of the two gamma-ray components at three angles of emission. Two stationary Geiger counters were used to monitor the primary beam intensity.

The data may be considered in two different ways. One may first obtain the ratio of intensity of the 17- to 14-Mev component at each angle of observation. For isotropic distributions this ratio should be independent of the angle. One may also obtain the variation of intensity of the individual gamma-ray components as a function of the angle, thus obtaining the separate angular distribution functions. Because of corrections for gamma-ray absorption in the target and the necessity to rely on the counters for long time stability, these values are less accurate. The results are given in Table I.

Within the limits of error, the resonant radiation is isotropic for both components. This is in agreement with the results of Devons and collaborators,[1,2] who find that under these conditions the total radiation differs from isotropy by only 4 percent and also that a pair spectrometer measurement indicates each component to be isotropic to within the accuracy of their measurements (about 20 percent). These results are in sharp disagreement with those of Nabholtz, Stoll, and Wäffler,[3] who obtained the value of 2.2 for R_{90}/R_0 using photographic plates and the $C^{12}(\gamma, 3\alpha)$ reaction for energy discrimination.

TABLE I. Angular distributions of the 14-Mev and 17-Mev gamma-rays. Relative intensity $=I$. Ratio of relative intensity, $R=I_{17}$ Mev/I_{14} Mev. Absolute intensity ratio, 17 Mev/14 Mev $=cR$.

Type of radiation	Angle in degrees	I_{14} Mev	I_{17} Mev	R	c*
440-kev resonance radiation. $E_p=0.50$ Mev	0	1.00±0.07	1.00±0.07	1.00±0.06	1.70±0.20
	35	0.97±0.07	1.03±0.07	1.06±0.06	
	70	0.98±0.07	0.99±0.07	1.01±0.06	
Nonresonant radiation. $E_p=1.15$ Mev	0	1.00±0.05	1.00±0.05	1.00±0.05	0.62±0.07
	35	0.74±0.06	0.69±0.06	0.94±0.08	
	75	0.77±0.05	0.56±0.05	0.72±0.05	

* The value of c, the ratio of absolute intensities in the forward direction, was obtained from a weighted average of the present data and earlier data of Walker and McDaniel. Corrections have been made for the variation with energy of the spectrometer detection efficiency. Resolution width, loss from vertical scattering, and pair cross section have been considered. Stated errors are standard deviations based on statistics and estimated accidental errors.

The nonresonant radiation is strongly anisotropic, and the angular distribution is clearly different for the two gamma-ray components.

Following Devons' arguments concerning the resonance radiation, one may suggest the following level assignments. Because of the isotropy of both components under resonance excitation, the resonance level is produced by s-protons and has an angular momentum $J=1$ and odd parity. Since the separate angular distributions of the two lines for nonresonant excitation are anisotropic and different from each other, it is likely, though not necessary, that the 2 lower states have different angular momenta. The long lifetime[7] of the Be^8 ground state would seem to favor the assignment of $J=2$, even, to that state and $J=0$, even, to the 3-Mev level. The separate angular distributions of the two components of the nonresonant radiation are not consistent with the angular distribution $(1+a\cos^2\theta)$ which would exist if p-protons alone caused this radiation. It is therefore likely that the s-protons which produce the resonant radiation, or d-protons forming some higher level, are interfering with the p-protons in producing the nonresonant radiation at these energies.

* Assisted by the ONR.

[1] S. Devons and M. G. N. Hine, Proc. Roy. Soc. (London) **A199**, 56 (1949).
[2] S. Devons and G. R. Lindsey, Proc. Phys. Soc. (London) **A63**, 1202 (1950).
[3] Nabholtz, Stoll, and Wäffler, Helv. Phys. Acta **23**, 858 (1950).
[4] E. R. Cohen, Phys. Rev. **75**, 1463A (1949).
[5] R. F. Christy, Phys. Rev. **75**, 1464A (1949).
[6] R. L. Walker and B. D. McDaniel, Phys. Rev. **74**, 315 (1948).
[7] C. H. Millar and A. G. W. Cameron, Phys. Rev. **79**, 182L (1950).

Microwave Collision Diameters and Associated Quadrupole Moments*

R. M. HILL AND WILLIAM V. SMITH
Department of Physics, Duke University, Durham, North Carolina
(Received February 23, 1951)

IN recent papers[1,2] Smith and Howard reported an investigation of the broadening of the 3-3 inversion line of NH_3 by other gases. From the data obtained, they calculated a collision diameter for the NH_3-foreign gas collision. In the cases for which this diameter was markedly greater than that obtained from kinetic theory, the collision was ascribed to the interaction of the NH_3 dipole moment and a permanent electric quadrupole moment (averaged over the rotation)[3] of the foreign gas. The quadrupole moments for these gases were calculated.

Anderson[3] has since shown that the interaction of the quadrupole moment of NH_3, calculated from its structure, and the dipole induced in the foreign gas gives a collision diameter in good agreement with those molecules whose experimental collision cross sections approached kinetic theory values. However, for N_2 and others this diameter is too small, and the assignment of a permanent electric quadrupole to these molecules seems justified.

TABLE I. Collision diameters (b) of NH_3 with various colliding molecules.

Gas	$b\times10^8$ (cm) (microwave)	$b\times10^8$ (cm) (kinetic theory)	Polarization (α) $\times10^{24}$ [a]	$b\times10^8$ (cm) (Anderson)	Quadrupole moment (Q) $\times10^{26}$ (cm^2)
C_2H_2	8.79		3.33	3.92	1.1
C_2H_4	6.67	4.79[b]	4.27	4.09	0.48
C_2H_6	5.64	4.86[b]	4.53	4.15	(0.28)
C_6H_6	9.76	4.50[c]	10.32	4.85	1.3
N_2O	7.32	4.35[d]	2.99	3.89	0.59
NO	5.64	3.90[d]	1.72	3.52	0.28
CO	5.97	3.96[d]	1.95	3.39	0.34

[a] H. A. Stuart, *Molekulstruktur* (Verlag. Julius Springer, Berlin, 1934).
[b] E. H. Kennard, *Kinetic Theory of Gases* (McGraw-Hill Book Company, Inc., New York, 1938), p. 149.
[c] Landolt-Bornstein, *Phys. Chem. Tab.*, Eg. I (a), p. 105.
[d] L. Loeb, *Kinetic Theory of Gases* (McGraw-Hill Book Company, Inc., New York, 1934), p. 651.

The NH_3 3-3 line breadth has been measured for mixtures of NH_3 with several more gases, using the same experimental technique as in reference 1. The results obtained are listed in Table I. For the gases investigated, either the dipole moment or its average over a collision was zero, and the collision may be described by an interaction other than dipole-dipole.

The diameters calculated from Anderson's formula are quite a bit lower than those found from broadening data, and except for C_2H_6 a quadrupole moment has been given. For C_2H_6 the microwave diameter is sufficiently close to the kinetic theory diameter that the quadrupole moment is given only as an upper limit.

For the C_2H_2, C_2H_4, C_2H_6 series the microwave diameter and associated quadrupole moment are seen to increase with the order of the C−C bond, indicating an increase in the asymmetry of the charge distribution. The moments obtained for NO and CO are very close to that for N_2 found by Smith and Howard, while the quadrupole moment for N_2O agrees very well with their values for COS, CS_2, and CO_2.

Further work in the interpretation of these data is in progress.

* The research reported in this document has been made possible through support and sponsorship extended by the Geophysical Research Directorate of the Air Force Cambridge Research Laboratories. It is published for technical information only and does not represent recommendations or conclusions of the sponsoring agency.
[1] R. R. Howard and W. V. Smith, Phys. Rev. **79**, 128 (1950).
[2] W. V. Smith and R. Howard, Phys. Rev. **79**, 132 (1950).
[3] P. W. Anderson, Phys. Rev. **80**, 511 (1950).

Survey Experiment on Elastic Scattering*

JACK W. BURRIG AND BYRON T. WRIGHT
Department of Physics, University of California, Los Angeles, California
(Received March 19, 1951)

USING cameras similar to those described by Fulbright and Bush[1] two survey experiments on the elastic scattering of protons have been performed.

In one, the angular dependence of the differential elastic cross section in the range 26° to 106° was measured at 15° intervals for the elements W, Pd, Ni, and Al. The proton beam energy, as determined from the magnetic field strength and the camera geometry, was 18.6±0.4 Mev. The total energy spread at the half-maximum intensity of the incident beam was less than 1 Mev. The circulating beam was scattered by wires 0.001 in. in diameter.

The camera used in this experiment had three slits. In a single run the relative values of the elastic scattering at three angles could be obtained. The measurements were extended to other angles by overlapping sets of observations.

The relative values of the cross sections were then determined by counting the number of tracks per unit area in the elastic lines which appear on the developed film.

The results of this experiment are shown in Fig. 1. We have plotted $\ln(\sigma_o/\sigma_R)$ *vs* θ, where σ_o is the observed cross section, σ_R is that expected for Rutherford scattering, and θ is the angle

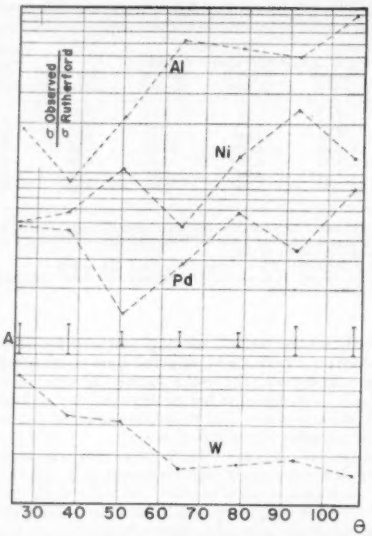

FIG. 1. A plot of the logarithm of the ratio of the observed elastic scattering to Rutherford scattering *vs* the scattering angle θ for 18.6-Mev. protons. The relative vertical position of the four curves has no significance.

through which the protons are scattered. No scale for the ordinates is indicated, since none would be significant. The relative vertical position of the four curves is not significant. They are presented on the same figure merely as a matter of convenience. The vertical lines along the horizontal line A indicate the probable errors in the various observations. The procedure of overlapping sets of observations leads to a larger probable error for the smallest and largest angles.

The W elastic scattering decreases monotonically below the Rutherford dependence; the Ni scattering has an average dependence the same as that expected for Rutherford scattering; and the Al definitely decreases less rapidly than would be expected for the case of Rutherford scattering. In addition, there are considerable deviations for Pd, Ni, and Al about their average angular dependence. A certain amount of progress has been made toward the description of the Al results in terms of a nuclear model which gives a sticking probability dependent on the angular momentum.[3]

By using a pair of cameras very near one another, the cross section for elastic scattering at 78.7±0.5° of a number of elements

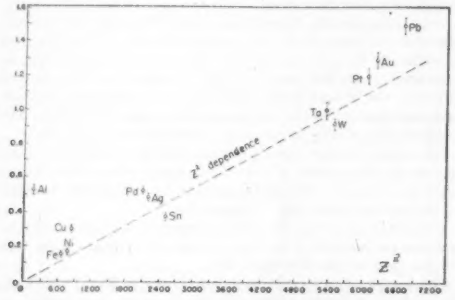

FIG. 2. For scattering at 78.7°, a plot of the ratio of the scattering by various elements relative to W *vs* the square of the atomic number Z.

relative to W was measured. The mass per unit length of the scattering wires was obtained with a quartz torsion microbalance. The reference wire was W in all cases except for four cross check runs. The results of this experiment are shown in Fig. 2. The ratios have probable errors varying from six to nine percent. In view of the marked angular dependence indicated in Fig. 1, the results of the scattering at a fixed angle, shown in Fig. 2, would appear to have little chance of interpretation at the present time.

* This work was supported in part by the joint program of the ONR and AEC.

[1] H. W. Fulbright and R. R. Bush, Phys. Rev. **74**, 1323 (1948).

[2] R. LeLevier and D. S. Saxon (private communication).

Relative Back-Scattering of Electrons and Positrons

WILLIAM MILLER
National Bureau of Standards, Washington, D. C.
(Received March 13, 1951)

RECENT measurements by Seliger[1] have indicated a significant difference in the back-scattering coefficients, β^- and β^+, for electrons and positrons. For isotropic sources of electrons and positrons with energies of the order of 0.5 Mev, and several scattering media with Z values ranging from 4 to 82, it was found that $\beta^-/\beta^+\sim 1.3$.

Seliger suggested that this different behavior of electrons and positrons might result simply from their different cross sections for elastic single scattering at relativistic energies.[2] The ratio of the electron and positron cross sections for 90° scattering at 1.7 Mev is as large as 4, but the ratio approaches 1 at lower energies and for small angle scattering. The cumulative effect of small angle single scatterings constitutes the main source of the diffusion and back-scattering of electrons. Therefore, it is not immediately apparent that the difference of electron and positron scattering, while obviously in the right direction, is actually adequate to account quantitatively for the observed effect.

No detailed theory of back-scattering is available, but Bothe[3] has evaluated the back-scattering coefficient β approximately by considerations modeled on the neutron "albedo" theory. In the treatment of Bothe, the main parameter controlling the value of β is the ratio of the "true" range R of a particle in the scattering medium to the "scattering length" λ_s (inversely proportional to $\int_0^\pi \sigma(\theta)(1-\cos\theta)\sin\theta d\theta$), that is, $\beta=\beta(R/\lambda_s)$. Bothe computed λ_s from a nonrelativistic differential single-scattering cross section $\sigma(\theta)$, i.e., in essence a Rutherford cross section, equal for electrons and positrons.

A new evaluation based on relativistic cross sections has been made for the purpose of estimating the magnitude of the effect under consideration. The theoretical data of Bartlett, Watson, and Massey[2] on the cross section for single scattering of 500-kev electrons and positrons in mercury were inserted in the Bothe formulas. The λ_s values for electrons and positrons were calculated by approximating the $\sigma(\theta)$ by simple functions and doing the integral analytically. Since there is no reason to expect an appreciable difference in the ranges of the two types of particles, the range R for 500-kev electrons and positrons in mercury was taken as 0.030 cm.

The resulting values of R/λ_s for electrons and positrons are 18.1 and 12.4, respectively. Table I shows a comparison of the values of λ_s, R, R/λ_s from the present calculation and of the corresponding values derived from Bothe's nonrelativistic for-

TABLE I. Comparison of calculated values with those of Bothe's theory.

		$1/\lambda_s$ (cm^{-1})	R (cm)	R/λ_s	β
Present calculation	Electrons	$605=1.39Z^2\rho/A$	$0.03=0.163A/Z\rho$	18.1	0.59
	Positrons	$414=0.95Z^2\rho/A$		12.4	0.51
Bothe		$(400/V)^2Z^2\rho/A$ $=0.64Z^2\rho/A$	$1.25\times10^{-6}V^2A/Z\rho$ $=0.31A/Z\rho$	$0.2Z$ $=16$	0.56

mulas. (The Bothe values for λ_s and R are actually not relevant to 500-kev particles. Nevertheless, Bothe was able to apply his method to 680-kev electrons with success, because, as shown in Table I, the Bothe value for the ratio R/λ_s departs from the improved estimate much less than the separate values of R and λ_s.[4])

Estimates of the back-scattering coefficient β were derived from the various values of R/λ_s according to the Bothe theory. The resulting asymmetry, $\beta^-/\beta^+\sim 1.16$, is roughly comparable to the observed effect. This result is taken as an indication that the differences in single scattering alone may well be responsible for the observed differences in back-scattering. Much better agreement with the experimental results should not have been expected in view of the approximations involved. In particular, it should be noted that the observed values of β correspond to an isotropic source at the boundary of the back-scatterer, whereas the values calculated on Bothe's theory do not apply to an isotropic source but rather to one intermediate between that and a normally incident one. For this reason the observed and calculated values of β cannot be expected to agree in an absolute sense.

I would like to thank Dr. U. Fano for suggesting this investigation and for many helpful discussions.

[1] H. H. Seliger, Phys. Rev. **78**, 491 (1950).
[2] See, e.g., N. F. Mott and H. S. W. Massey, *The Theory of Atomic Collisions* (Oxford Univerdity Press, New York, 1945), p. 81ff.
[3] W. Bothe, Ann. Physik **6**, 44 (1949).
[4] See also C. H. Blanchard and U. Fano, Bull. Am. Phys. Soc. **26**, No. 2, G10(A) (1951).

Concerning Certain Anomalous Small Angle Diffraction Effects

GEORGE H. VINEYARD
Department of Physics, University of Missouri, Columbia, Missouri
(Received March 19, 1951)

HALPERN and Gerjuoy[1] have pointed out that radiation scattered from a parallelopiped will (on the basis of the usual theory) extend to anomalously large angles when the incident beam is very nearly parallel to any face. Recently, Forrester and Mittenthal[2] have attempted to observe this effect in the diffraction of light by a glass cube immersed in a liquid of nearly equal index. They show that extremely large intensities at these angles should be expected, providing the optical path length through the glass cube is many wavelengths larger than in the surrounding medium. Their experiments fail to reveal this intense scattering, and they suggest several explanations, one of them being that the Born approximation (single scattering) underlying Halpern and Gerjuoy's formulas is inapplicable here.

We wish to point out that smallness of the phase shift through the scatterer is a common criterion for the validity of the Born approximation,[3] and that, further, for the case in which the refractive index of the scatterer differs from the surrounding index by much less than unity, a different type of approximate calculation can be made which is valid for both large and small phase shifts and which reduces to the Born approximation in the latter case. In this method, the radiation field is calculated on a plane situated just beyond the scatterer and perpendicular to the incident beam; from this, the far-field is found by the Kirchhoff form of Huygen's principle. The field on this intermediate plane is approximated sufficiently well by (a) the undisturbed incident field at all points outside the geometrical shadow of the scatterer, and (b) a field inside the shadow having the same amplitude but with its phase modified at each point according to the optical path length on a line straight through the scatterer and reaching that point. These approximations seem rather drastic at first sight, but their validity is demonstrated by work of van de Hulst,[4] who considers spherical scatterers and shows that the rigorous Mie solution for electromagnetic radiation agrees with such computations under similar limitations. It is also easy to show directly that the Born approximation emerges (for scattering angles small compared with 1 radian) when the phase shift is small. This can be shown for any shape of scatterer.

We have carried through such a calculation for the case of a cube with two opposite faces parallel to the incident beam, and we have calculated the differential cross section for scattering in a plane perpendicular to these faces. When the phase shift through the center of the cube is large compared with unity, the differential cross section never exceeds that of an equal sized rectangular aperture by more than a factor of 4. Also, at intermediate values of the phase shift, the cross section is always of the same order of magnitude as that of an equal sized aperture. These results can be readily understood on the basis of a physical interpretation of this mode of calculation, also owing to van de Hulst.[4] The contribution from the radiation in the geometrical shadow corresponds closely, for large cubes, to rays refracted by geometrical optics; the remainder correspond to radiation diffracted around the cube. Here, the field arising from the "ray" portion cannot exceed that of a simple aperture, and the field arising from the diffraction portion equals that of a simple aperture. Their combined intensity, then, depends on relative phase and cannot exceed 4 times the intensity scattered by an aperture.

The negative results of Forrester and Mittenthal are thus to be explained entirely on the basis of the breakdown of the Born approximation in their case.

[1] O. Halpern and E. Gerjuoy, Phys. Rev. **76**, 1117 (1949).
[2] A. T. Forrester and L. Mittenthal, Phys. Rev. **81**, 268 (1951).
[3] D. Bohm, *Quantum Theory* (Prentice-Hall, Inc., New York, 1951), p. 553.
[4] H. C. van de Hulst, *Optics of Spherical Particles* (J. F. Duwaer en Zonen, Amsterdam, 1946). This excellent work deserves wider circulation than it seems to have attained.

Ionization by the Collision of Pairs of Metastable Atoms

MANFRED A. BIONDI
Westinghouse Research Laboratories, East Pittsburgh, Pennsylvania
(Received March 20, 1951)

MICROWAVE techniques are used to measure the variation in electron density following the interruption of a discharge.[1] It is found that the electron density actually increases for approximately a millisecond after the electric field is removed from a helium or neon discharge (see Fig. 1). Analysis of the data indicates that the delayed ionization results from the collisions of pairs of metastable atoms, as suggested by T. Holstein.

After the maintaining field is removed from the discharge, ionization by electron impact ceases; however, electrons continue to be produced by metastable-metastable collisions. The electrons, which quickly (<100 μsec) come into thermal equilibrium with the gas, diffuse to the walls ambipolarly.[2] The metastable atoms produced during the discharge are lost by diffusion to the walls, by de-exciting collisions with gas atoms, and by metastable-metastable ionizing collisions. Experimental data indicate that the ionization loss is small compared to the diffusion and collision loss; hence, the metastable concentration is given by

$$M \simeq M_0 \exp(-t/T_m), \tag{1}$$

where M_0 is the metastable concentration immediately following the discharge and

$$1/T_m = (D_m/\Lambda^2) + \nu_d. \tag{2}$$

Here T_m is the metastable mean decay time, D_m is the metastable diffusion coefficient, ν_d is the frequency of de-exciting collisions with gas atoms, and Λ is the characteristic diffusion length of the container.[2] The electron density is given by

$$n = A \exp(-t/T_D) - B \exp(-2t/T_m), \tag{3}$$

where

$$T_D = \Lambda^2/D_a, \tag{4}$$

D_a being the ambipolar diffusion coefficient.[2]

Figure 1 shows typical data for helium. At late times, the pro-

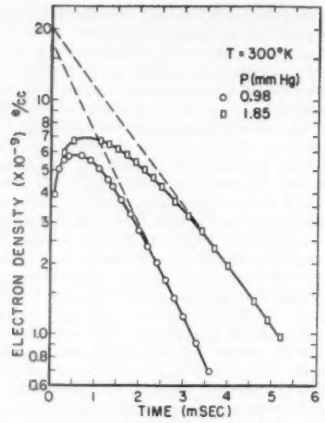

FIG. 1. Production of electrons in helium.

duction of electrons by metastables becomes negligible, and the electron density decays according to the first term of Eq. (3). We extrapolate this terminal slope toward zero time and take the difference between the actual curve and the extrapolated curve. This yields the second term of Eq. (3), which is shown plotted in Fig. 2.

If we consider the volume loss of metastables to arise from binary collisions between metastables and normal atoms, we may

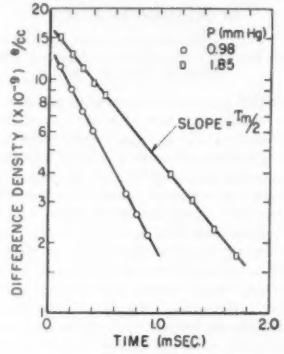

FIG. 2. Loss of metastables in helium.

replace the term ν_d of Eq. (2) by Cp, where C is a constant, and p is the gas pressure.[8] Multiplying Eq. (2) by p we have

$$p/T_m=(D_m p/\Lambda^2)+Cp^2. \tag{5}$$

In Fig. 3 are plotted values of p/T_m *vs* p^2. The intercept of the curve gives the value $D_m p/\Lambda^2$, and the slope of the curve yields C. The diffusion takes place in a container with diffusion length $\Lambda=0.735$ cm.[2] From Fig. 3 we find $D_m p=520\pm20$ (cm²/sec)·(mm Hg) and $C=55\pm6$ (mm Hg·sec)$^{-1}$. Runs on several samples of helium give values differing from these results by less than ten percent. Optical absorption experiments by Ebbinghaus yield values of $D_m p=535$ and $C=107$.[4] The difference in the values of the volume loss coefficient, C, may be attributed to differences in gas purity. With specially purified helium[5] (estimated impurity $<1:10^8$), we obtain the value $C=55$, given above; however, with Airco reagent helium (estimated impurity $\sim1:10^4$), we obtained

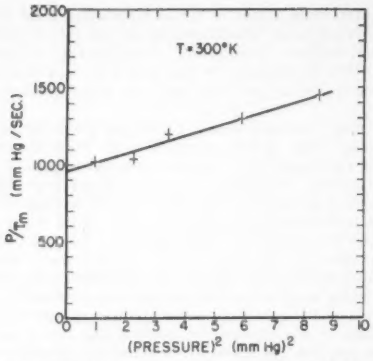

FIG. 3. Diffusion and volume loss of metastables in helium.

a value $C=100$. A more complete investigation of the volume loss of metastables is in progress.

Data similar to that shown in Figs. 1–3 have been obtained for neon, giving values of $D_m p=200\pm20$ and $C=230\pm20$. These results may be compared with Phelps' and Molnar's[6] value of $D_m p=150\pm30$, obtained by optical absorption. The rather good agreement between the diffusion coefficients obtained from the present measurements and from the optical absorption experiments indicates that the proposed metastable-metastable origin of the ionization is correct. Independent confirmation of the metastable origin of the ionization has been obtained by irradiating the discharge with light of the proper wavelength to raise a metastable atom to a radiating state. A decrease in the metastable concentration results, and we observe a corresponding decrease in the electron density rise of Fig. 1.

In a recent article Johnson *et al.*[7] reported on electron density measurements in helium. They explain their failure to observe an increase in density following the discharge by the fact that their higher electron densities and gas pressures destroy the metastables. Actually, the 10-μsec discharge period they use is too short to permit the metastables to reach more than a fraction of a percent of their equilibrium concentration. As we decrease our discharge time from its usual value of 300 μsec to 10 μsec, we find that the initial density rise diminishes and finally disappears.

The author wishes to thank Dr. T. Holstein for his assistance during the course of this work.

[1] M. A. Biondi, "Measurement of the electron density in ionized gases by microwave techniques," Rev. Sci. Instr., to be published. The apparatus is similar in principle to that described by M. A. Biondi and S. C. Brown, Phys. Rev. **75**, 1700 (1949).
[2] M. A. Biondi, Phys. Rev. **79**, 733 (1950), and the references cited therein.
[3] See Mitchell and Zemansky, *Resonance Radiation and Excited Atoms* (Cambridge University Press, London, 1934), pp. 246 ff.
[4] Ebbinghaus, Ann. Physik **7**, 267 (1930); and reference 3, p. 249.
[5] M. A. Biondi, "Preparation of extremely pure helium gas," Rev. Sci. Instr., to be published.
[6] A. V. Phelps and J. P. Molnar, Bell Telephone Laboratories, private communication.
[7] Johnson, McClure, and Holt, Phys. Rev. **80**, 376 (1950).

The Spin of O^{18}

S. L. MILLER,* A. JAVAN, AND C. H. TOWNES
Columbia Radiation Laboratory, Columbia University, New York, New York†
(Received March 12, 1951)

OBSERVATION of the microwave absorption spectrum of $O^{16}O^{18}$ and $O^{18}O^{18}$ in the 5-mm region shows that the spin of O^{18} is zero.

In the region between 58,300 Mc and 59,900 Mc, all of the expected $O^{16}O^{18}$ and $O^{18}O^{18}$ lines have been observed and identified.

TABLE I. Oxygen lines between 58,300 Mc and 59,900 Mc.

Molecule	Transition	Frequency (Mc)
$O^{16}O^{18}$	$K=9$ $J=8\rightarrow9$	58,310
$O^{16}O^{16}$	$K=9$ $J=8\rightarrow9$	58,324
$O^{16}O^{16}$	$K=3$ $J=4\rightarrow3$	58,446
$O^{16}O^{18}$	$K=3$ $J=4\rightarrow3$	58,650
$O^{16}O^{18}$	$K=8$ $J=7\rightarrow8$	58,670
$O^{16}O^{16}$	$K=3$ $J=4\rightarrow3$	58,900
$O^{16}O^{16}$	$K=7$ $J=6\rightarrow7$	58,965
$O^{16}O^{16}$	$K=7$ $J=6\rightarrow7$	59,075
$O^{16}O^{16}$	$K=7$ $J=6\rightarrow7$	59,163
$O^{16}O^{16}$	$K=4$ $J=5\rightarrow4$	59,220
$O^{16}O^{16}$	$K=6$ $J=5\rightarrow6$	59,540
$O^{16}O^{16}$	$K=5$ $J=6\rightarrow5$	59,590
$O^{16}O^{18}$	$K=5$ $J=6\rightarrow5$	59,685
$O^{16}O^{16}$	$K=5$ $J=6\rightarrow5$	59,810
$O^{16}O^{16}$	$K=5$ $J=4\rightarrow5$	59,875

These are listed in Table I. Their positions are predicted closely by Schlapp's formula, as modified by Burkhalter *et al.*[1] with appropriate changes in constants because of the change in isotopic masses.

A sample of enriched oxygen was very kindly supplied by Professor A. O. Nier. After a brief discharge was run in this gas to approximate an equilibrium distribution, the relative intensities of $O^{18}O^{18}$ to $O^{16}O^{18}$ to $O^{16}O^{16}$ lines were roughly 1:5:15, as may be

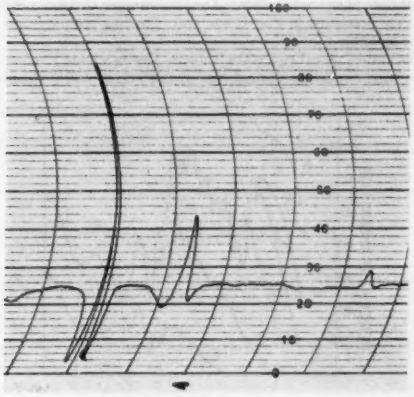

FIG. 1. The $K=7$, $J=6\rightarrow7$ transition for the isotopic combinations $O^{16}O^{18}$, $O^{16}O^{18}$, and $O^{16}O^{18}$ (from left to right).

seen from Fig. 1. The three lines shown are the $K=7$, $J=6\rightarrow7$ transition for the three different isotopic combinations.

Other observations[2] on O^{18} had failed to disclose quadrupole hyperfine structure, and the $O^{16}O^{18}$ lines show no evidence of magnetic hyperfine structure, which indicates a zero spin for O^{18}. However, real proof that the O^{18} spin is zero must rest on the method of alternating intensities in the homonuclear molecule $O^{16}O^{18}$.

The $K=8$, $J=7\rightarrow8$ transition, which should be at about 58,600 Mc; the $K=6$, $J=5\rightarrow6$ transition at about 59,375 Mc; and the $K=4$, $J=5\rightarrow4$ transition at about 59,400 Mc for $O^{16}O^{18}$ are all missing. Figure 2 shows the region of the latter two missing lines, bounded by the corresponding transitions for $O^{16}O^{18}$ which are off scale. In the case of spin=1, these missing lines should be approximately 15 units high, and for higher spin values still stronger. Therefore, it can be concluded that the spin of O^{18} is zero, since the alternate rotational levels of $O^{18}O^{18}$ do not exist. The O^{18} nucleus also follows Bose-Einstein statistics, as does O^{16}, since the same rotational levels are forbidden in both cases.

Magnetic hyperfine structure has been found in the same sample

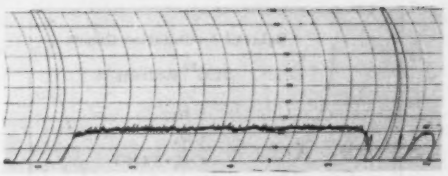

FIG. 2. Recording trace from the $K=4$, $J=5\rightarrow4$ transition for $O^{16}O^{18}$ (on the right) to the $K=6$, $J=5\rightarrow6$ transition for $O^{16}O^{16}$ (on the left). The missing $O^{16}O^{18}$ lines $K=4$, $J=5\rightarrow4$ and $K=6$, $J=5\rightarrow6$ should be about midway between them.

for $O^{16}O^{17}$. Although no definite spin determination has as yet been made from this structure, the O^{17} spin is evidently greater than $\frac{1}{2}$.

The microwave lines were detected with a recording Zeeman modulation spectrometer constructed by A. L. Schawlow, T. M. Sanders, and W. A. Hardy.

* AEC Predoctoral Fellow.
† Work supported partly by the AEC and partly by a joint Signal Corps-ONR contract.
[1] Burkhalter, Anderson, Smith, and Gordy, Phys. Rev. **79**, 651 (1950).
[2] Townes, Holden, and Merritt, Phys. Rev. **74**, 1113 (1948).

Evidence for the Formation of Positronium in Gases*

MARTIN DEUTSCH
Laboratory for Nuclear Science and Engineering, and Department of Physics, Massachusetts Institute of Technology, Cambridge, Massachusetts
(Received March 13, 1951)

THE distribution of time delays between the emission of a nuclear gamma-ray from the decay of Na^{22} and the appearance of an annihilation quantum has been measured for positrons stopping in a large number of gases and gas mixtures, extending earlier measurements.[1] A complete interpretation of the results appears to be fairly complex and will be attempted in a more extensive communication. At this time we want to report on some definite proof of the abundant formation of positronium, the bound electron-positron system analogous to the hydrogen atom. The ground state of this atom is expected[2] to have a lifetime against two-quantum annihilation of about 10^{-10} sec if the spins are antiparallel and slightly over 10^{-7} sec if they are parallel,[3] decaying by three-quantum annihilation. Ore[4] has shown that, in general, there is no mechanism for the rapid destruction of the triplet state at low energies. One may expect, however, that in a gas containing molecules with an odd number of electrons, such as nitric oxide, the triplet state would be converted very rapidly to the singlet by an electron exchange. In NO this requires essentially no energy at room temperature, the energy difference for the two spin orientation being only about 13 millivolts. The cross section for this process may be very large, since it is a resonance effect involving the coulomb interaction rather than a magnetic conversion. (The latter is expected to be very slow.[4]) Thus, even a small admixture of NO should cause the very rapid annihilation of those positrons which would otherwise have decayed by three-quantum annihilation with a period of the order of 10^{-7} sec. Figure 1 shows this phenomenon. In nitrogen the number of delayed counts is reduced by a factor of three by the addition of 3 percent NO. These counts then appear instead in the "prompt" channel, not shown in Fig. 1. In freon the effect is even greater, hardly any delayed coincidences remaining upon addition of NO. The residue in N_2 is probably due to free positrons.

Oxygen has a similar but less pronounced action. In pure O_2 the number of delayed coincidences is about half as great as in N_2 (Fig. 1).

Confirmation of the above interpretation comes from the direct observation of the continuous gamma-ray spectrum due to the

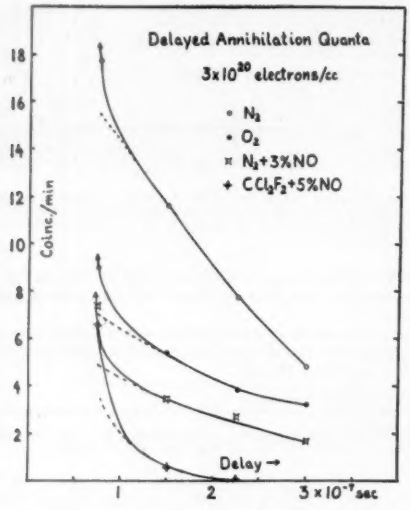

FIG. 1. Decay curves of positrons in several gases. The dotted lines are corrected for time resolution of the instrument.

three-quantum annihilation of triplet positronium in nitrogen. Figure 2 shows pulse height spectra obtained in a NaI scintillation spectrometer deliberately adjusted for low resolution to gain stability. It is seen that the photoelectron peak of the 510-kev radiation is markedly lower in pure N_2 while there is an increase of the number of lower energy electrons, compared with the spectrum from N_2+NO in which we expect almost pure two-

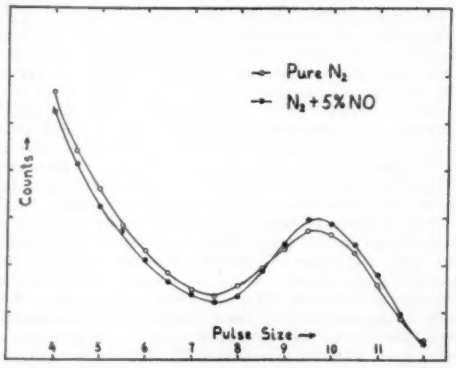

FIG. 2. Part of the scintillation spectrum of two-quantum (solid circles) and two-quantum plus three-quantum (open circles) annihilation. The uncertainty of individual points is indicated by the size of the circles.

quantum annihilation. The large number of small pulses present in both curves is due to scattered radiation from the walls of the gas vessel. The annihilation spectrum in pure O_2 resembles that in N_2+NO.

The slight shift of the photoelectron peak to lower energies in N_2 is due to the large number of quanta just below 510 kev from the three-quantum process[5] falling within the experimental width of the two-quantum line. A similar phenomenon may explain the low value of the annihilation energy obtained by DuMond.[6]

* Supported in part by the joint program of the AEC and ONR.
[1] J. W. Shearer and M. Deutsch, Phys. Rev. **76**, 462 (1949).
[2] J. Pirenne, Arch. Sci. phys. et nat. **29**, 257 (1947).
[3] A. Ore and J. L. Powell, Phys. Rev. **75**, 1696 (1949).
[4] A. Ore, Yearbook 1949 (University of Bergen), No. 12.
[5] J. W. M. DuMond, Phys. Rev. **81**, 468 (1951).

Infrared Absorption and Intrinsic Semiconductivity of Condensed Aromatic Systems

EDWARD A. KMETKO
Department of Physics, University of Buffalo, Buffalo, New York
(Received March 8, 1951)

IN order to explain the temperature dependence of the resistivity of polycrystalline graphite and carbons, it seems necessary to assume the existence of an energy gap between the filled and upper bands.[1] The familiar progressive change in color of condensed aromatic compounds with the size of the molecule is believed to be a manifestation of the change in this energy gap, which, as it decreases to zero, leads to the semimetallic properties of graphite.

The presence of aromatic rings in pyrolyzed cellulose products is known.[2] The writer has studied the infrared absorption of Cellophane char films (~20μ thick). The transmission curves for several films are presented in Fig. 1, and their charring temperatures are given in Table I.

The curves reveal two main features. One is a band of complete absorption extending through the visible region and terminating

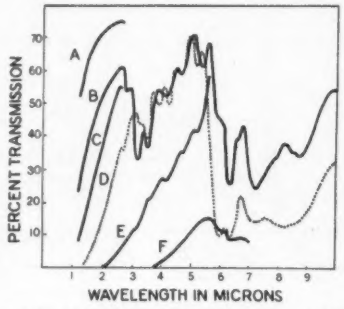

FIG. 1. Infrared transmission curves for Cellophane char films.

in the infrared. The limit of this band is seen to move progressively toward longer wavelengths as the treatment temperature increases. The other feature is the presence of characteristic bands corresponding to different types of bonds present in the char. As will be shown, the shifting band is of an electronic origin and corresponds, probably, to motion of electrons in the aromatic lattice. Midpoints of the transparency expressed in electron volts

TABLE I. Transparency and resistance data.

Sample	Treatment temp. °C	Midpoint of transparency in ev	ΔE in ev from R *vs* T
A	300	1.2	···
B	350	0.87	···
C	425	0.71	0.8
D	500	0.50	0.62
E	540	≥0.33	0.41
F	630	≤0.28	0.22
G	700	~0.2	0.09
H	800	···	0.03

are given in Table I. For the 540° and 630°C films, the uncertainty is caused by the strong bond absorptions. The films treated to 700°C and higher are almost completely opaque. However, the band edges are detectable at large slit widths, and the approximate position for the film charred at 700°C is given in Table I.

The resistances of several films were measured over the range 20° to 120°C and were found to be very strongly temperature dependent. This dependence was approximated by the relationship for intrinsic semiconductors, $R \sim \exp \Delta E/2kT$; and values of ΔE thus obtained are presented in Table I.

The rough agreement evident between the energy values given in columns 3 and 4 of Table I up to 630°C shows that the advancing absorption band corresponds to an electronic excitation. Furthermore, it demonstrates that the size of the energy gap decreases as the condensing process progresses. At higher charring temperatures, the agreement is gradually destroyed by the presence of an increasing number of excess electrons in the upper band (peripheral valence electrons becoming mobile after removal of the attached hydrogen atoms[1]). The slopes of the resistance *versus* temperature curves are decreased by the presence of such electrons; hence, the ΔE's evaluated from the formula become smaller than the real values in column 3. In samples treated to higher temperatures i.e., $\geqslant$630°C, these excess electrons probably cause the large overall absorption in the infrared. The general trend of the variation of size of the gap seems consistent with the value 0.1 ev predicted for calcined cokes.[1]

The variable cut-off feature of these films suggests their use as infrared filters. Further studies of their properties are in progress.

The author is indebted to Professor S. Mrozowski for suggesting this problem and for continued advice and encouragement, and to Mr. G. W. LeSuer and other members of the laboratory for their valuable assistance.

[1] S. Mrozowski, Phys. Rev. **77**, 838 (1950).
[2] R. C. Smith and H. C. Howard, J. Am. Chem. Soc. **59**, 234 (1937).

Beta-Spectrum of Cl^{36}

C. S. Wu and L. Feldman
*Pupin Physics Laboratories, Columbia University, New York, New York**
(Received February 23, 1951)

IN 1949 we reported[1] our work on the beta-ray spectrum of Cl^{36} and showed the pronounced curvature of its Kurie plot toward the energy axis down to the very low energy region. This was the first shape of this kind ever observed among the forbidden spectra.

Because of the unfavorable source thickness used (0.3 mg/cm² to 1 mg/cm²), the energy region of the spectrum below 180 kev was not extensively investigated, as its true shape is probably somewhat distorted. Nevertheless, we found a good fit from 200 kev to the upper energy limit 713 kev between the observed spectrum and the so-called D_2 correction factor (using Marshak's notation),[2] which is the unique forbidden correction factor for a transition where the spin change is ± 3. Meanwhile, Townes[3] determined the spin of Cl^{36} to be 2. Since argon 36 contains an even number of both neutrons and protons, its spin is probably zero. With a spin change of 2, and parity change either yes or no, a beta-transition can be any one of the many transitions allowed by the selection rules. Although the fitting of this spectrum with the theoretical factors C_{2S}, C_{2A}, C_{2P}, or C_{2V} is out of the question (see Fig. 1), the factors C_{2V} and C_{2T} (for $I=2\rightarrow I=0$) contain several nuclear matrix elements which, at present, one is free to adjust to obtain the best fit. In other words, the fitting of C_{2V} and C_{2T} to the observed results involves considerable arbitrariness; thereby, it offers the greatest latitude in matching.

The previously reported unsatisfactory matching of C_{2V} or C_{2T} with the measurements in the case of Cl^{36} required the introduction of a linear combination to account for the spectrum shape.[4] The possibility of fitting the C_{2T} correction factor with the Cl^{36} spectrum has been recently brought to our attention by Fulbright and Milton.[5] Since the spectrum shape which they observed is essentially the same as the one which we reported in 1949, it is obvious that the unsatisfactory fitting of either C_{2V} or C_{2T} to the observed spectrum must be owing to the unfavorable ratios of the matrix elements used.

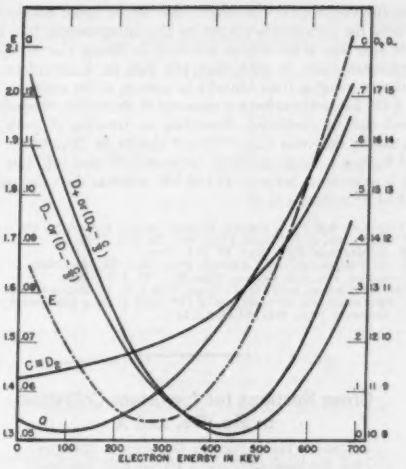

FIG. 1. The correction factors for each distinct matrix element in the second forbidden transitions of Cl^{36} ($\Delta I=2\rightarrow 0$). The notation is that of E. J. Konopinski, Revs. Modern Phys. **15**, 209 (1943):
$C_{2S}=\Sigma_{ij}|R_{ij}|^2[D_-]$; $C_{2A}=\Sigma_{ij}|T_{ij}|^2(\frac{1}{3})[D_- -\frac{1}{2}c]$,
$C_{2V}=\Sigma_{ij}|R_{ij}|^2[D_+]+\Sigma_{ij}|A_{ij}|^2[3a]-i\Sigma_{ij}(R_{ij}A_{ij}^*+\text{c.c.})[E]$,
$C_{2T}=\Sigma_{ij}|T_{ij}|^2(\frac{1}{3})[D_+ -\frac{1}{2}c]+\Sigma_{ij}|A_{ij}|^2[3a]-\Sigma_{ij}(T_{ij}A_{ij}^*+\text{c.c.})[E/2]$.

With the following ratio of matrix elements,

$$|T_{ij}|^2:|A_{ij}|^2:|A_{ij}^*T_{ij}+\text{c. c.}|=1:18:2(18)^{\frac{1}{2}},$$

we obtain a good fit for C_{2T} to the experimental spectrum from about 200 kev to the upper limit of 716 kev, in contradiction to the previously reported unsuccessful attempt.[4] Figure 2 shows the Kurie plot of the Cl^{36} spectrum corrected by C_{2T}, yielding indistinguishable results from that obtained with the D_2 correction

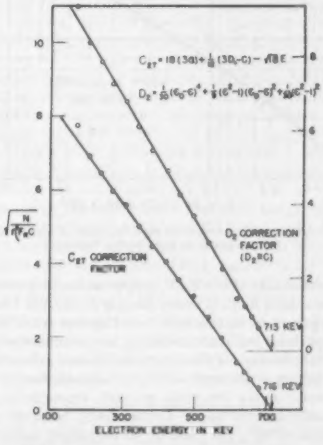

FIG. 2. Corrected Kurie plots of Cl^{36} spectrum.

With the following ratio of matrix elements,

$$|T_{ij}|^2:|A_{ij}|^2:|A_{ij}^*T_{ij}+\text{c. c.}|=1:18:2(18)^{\frac{1}{2}},$$

we obtain a good fit for C_{2T} to the experimental spectrum from about 200 kev to the upper limit of 716 kev, in contradiction to the previously reported unsuccessful attempt.[4] Figure 2 shows the Kurie plot of the Cl^{36} spectrum corrected by C_{2T}, yielding indistinguishable results from that obtained with the D_2 correction

factor (plotted above). The slight shift in the upper energy limit is within the uncertainty caused by the extrapolation. It is to be noted that the arbitrariness involved in fitting C_{ST} or C_{SV} to experimental data is such that one can fit Kurie plots with curvatures ranging from concave to convex, as for example, RaE and Cl[38]. The arbitrariness is removed if the matrix elements involved can be evaluated. According to Greuling's[6] method of estimation, the ratio $|A_{ij}|^2:|T_{ij}|^2$ should be $5(\gamma_0)^2/9\rho^2$. With $(\gamma_0)^2$ having a value probably between 0.01 and 0.1, this ratio then is somewhere between 30 and 300, whereas the value used to fit the Cl^{36} spectrum is 18.

* This work was made possible through partial support by the AEC.
[1] C. S. Wu and L. Feldman, Phys. Rev. **76**, 693 (1949).
[2] R. E. Marshak, Phys. Rev. **75**, 513 (1949).
[3] C. H. Townes and L. C. Aamodt, Phys. Rev. **76**, 691 (1949).
[4] Longmire, Wu, and Townes, Phys. Rev. **76**, 695 (1949).
[5] We are indebted to H. W. Fulbright and J. C. D. Milton for informing us of their results on the spectrum of Cl^{36} prior to their publication.
[6] E. Greuling, Phys. Rev. **61**, 568 (1942).

Cross Sections for Ion-Atom Collisions in He, Ne, and A

JOHN A. HORNBECK AND GREGORY H. WANNIER
Bell Telephone Laboratories, Murray Hill, New Jersey
(Received March 8, 1951)

A METHOD has been developed by one of us which permits accurate measurement of the drift velocity v_d of a positive ion as it moves through a gas under the influence of a constant electric field E. We wish to discuss, in the following, the results of these measurements for the ions He^+, Ne^+, and A^+ in their respective parent gases.

Theory predicts that v_d should depend only on the gas temperature and on the combination E/N, N being the gas number density. When $v_d \gg$ thermal velocity, theory predicts further that v_d should depend only on E/N. This prediction is confirmed by experiment. A log-log plot showing v_d *versus* E/N for neon is shown in Fig. 1. Similar plots for helium and argon have been obtained.

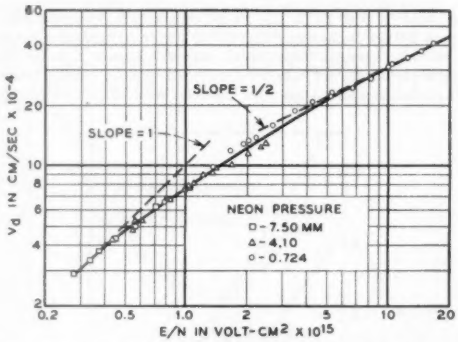

FIG. 1. Drift velocity of Ne^+ in neon as a function of the ratio of electric field strength to gas number density.

It may be noted that at low E/N, v_d approaches proportionality to E/N, while at high E/N, v_d varies directly as $(E/N)^{\frac{1}{2}}$. Dimensional arguments permit us to conclude from this last result that λ, the mean free path for ion-atom collisions, has become approximately constant. Examination of the interaction forces indicates that the law of scattering is isotropic to a good approximation. Isotropy and a constant mean free path uniquely characterize the hard sphere model of kinetic theory. This model is, therefore, applicable to the motion of He^+, Ne^+, and A^+ in the parent gases, provided we limit ourselves to the "high field" range.

The problem of ionic motion in high fields has been solved by one of us for the hard sphere model and yields for the drift velocity $v_d = 1.147(a\lambda)^{\frac{1}{2}}$. Here a stands for the acceleration imposed by the field upon the ion. We can apply this formula to the high field measurements discussed above and obtain from them a value of λ and hence the collision cross section σ_i, which is listed in the first column of Table I. The viscosity cross section σ_a for the gas atoms

TABLE I. Cross sections and mobilities.

	$\sigma_i \times 10^{15}$ cm²	$\sigma_a \times 10^{15}$ cm²	$\mu_L\left(\frac{\text{cm}^2}{\text{volt-sec}}\right)$	$\mu_0\left(\frac{\text{cm}^2}{\text{volt-sec}}\right)$
He	54.3	14.9	13.4	10.8[a]
Ne	65.2	21.0	4.85	4.4
A	134	41.7	1.67	1.63

[a] The value computed by Massey and Mohr (reference 1) is 11.

is given in the second column for comparison. In all cases, σ_i is larger than σ_a, as expected. We should point out that it is improper to reduce σ_i by standard methods to yield an "ionic radius." Massey and Mohr[1] have shown that the collision of He^+ with a helium atom has anomalous resonance features that make σ_i abnormally large. Our experiment shows that a similar situation must prevail for neon and argon.

It is interesting to substitute the hard sphere cross sections σ_i, together with known values of the dielectric constants for the gases, in the classical Langevin mobility formula and thereby obtain predicted values for the low field mobility (defined as v_d/E) of the ions He^+, Ne^+, and A^+ in their respective parent gases. This value, μ_L, is given in the third column of the table for standard gas density, while the fourth column shows a low field value, μ_0, obtained by extrapolation of our measurements to zero field. The rough agreement between them leads us to the conclusion that the Langevin treatment of ion mobilities is more satisfactory for these cases than has been supposed.

[1] H. S. W. Massey and C. B. O. Mohr, Proc. Roy. Soc. (London) **A144**, 188 (1934).

Electromagnetic Relaxation in Superconductors

JULIAN EISENSTEIN
University of Wisconsin, Madison, Wisconsin
(Received March 19, 1951)

LONDON'S macroscopic electrodynamic theory of superconductivity[1] has been generalized by von Laue[2] in a series of papers. Steady-state solutions of the fundamental equations have been obtained by F. and H. London and by von Laue for various simply shaped superconductors. Schubert[3] has solved the time-dependent equations for the cases where the specimen is an infinite half-space or an infinite slab with parallel faces. This note is concerned with the solution of the time-dependent equations for an infinite circular cylinder. The basic equations of the theory will be found in Schubert's paper.

Let us consider first the transition of a long cylinder from the normal to the superconducting state in a constant magnetic field maintained by external sources. The characteristic parameter, λ, of the London theory will be assumed to be a function of the time which varies from an infinite value at all temperatures above the transition point to an arbitrary finite value λ_0 at the final temperature. If one neglects the small displacement current, one obtains the following equation for the magnetic field inside the specimen:

$$(\partial^2 H/\partial r^2)+(\partial H/r\partial r)-(\sigma\partial H/c^2\partial t)-H/c^2\lambda(t)=0. \quad (1)$$

Cylindrical coordinates have been chosen. The ohmic conductivity σ is assumed the same in both normal and superconducting states.

The initial condition on H is that it be uniform throughout all space. The boundary condition is that H have a value H_0 independent of time on the surface of the cylinder ($r=r_0$). The solution of Eq. (1) subject to these conditions is

$$H(R,\tau)=\frac{H_0}{\psi(\tau)}\left\{1+\frac{2}{a}\sum_{n=1}^{\infty}\exp(-\alpha_n^2\tau)\alpha_n\frac{J_0(R\alpha_n)}{J_1(a\alpha_n)}\times\int_0^{\tau}\exp(\alpha_n^2 u)[\psi(u)-1]du\right\}. \quad (2)$$

Here, we have

$$R=r/c\lambda_0^{\frac{1}{2}},\quad \tau=t/\sigma\lambda_0,\quad \lambda_0/\lambda(l)=f(\tau),\quad a=r_0/c\lambda_0^{\frac{1}{2}},$$
$$\psi(\tau)=\exp\left[\int_0^{\tau}f(u)du\right];$$

and the $a\alpha_n$ are the positive zeros of the bessel function J_0.

One can show that Eq. (2) approaches asymptotically the well-known solution $H_0J_0(iR)/J_0(ia)$. The relaxation time for the nth summand in Eq. (2) is

$$\tau_n=\sigma\lambda_0/(\alpha_n^2+1)=\sigma\lambda_0[(j_n^2c^2\lambda_0/r_0^2)+1]^{-1},$$

where $j_n=a\alpha_n$. The longest relaxation time, τ_0, is of the order of milliseconds in a one-centimeter diameter cylinder.

The supercurrent and the ordinary ohmic current can be calculated from Eq. (2). One finds that the asymptotic form of the supercurrent agrees with the solution obtained by F. and H. London, while the ohmic current goes to zero for large values of the time.

An explicit solution of Eq. (1) with appropriate boundary conditions can also be obtained for the superconducting to normal transition. It can be shown that H approaches H_0 asymptotically. The initial stages of the relaxation are rather complicated, since they depend in detail on the function $f(\tau)$.

Superconductivity can also be destroyed by passing a large current through a specimen. If the currents are parallel to the axis of the cylinder, the following equation for H can be derived:

$$(\partial^2H/\partial R^2)+(\partial H/R\partial R)-(H/R^2)-(\partial H/\partial\tau)-f(\tau)H=0. \quad (3)$$

The displacement current has again been neglected. The solution of Eq. (3) subject to appropriate boundary and initial conditions is

$$H(R,\tau)=\frac{H_0}{\psi(\tau)}\left\{1+\frac{2}{a}\sum_{n=1}^{\infty}\exp(-\beta_n^2\tau)\beta_n\frac{J_1(R\beta_n)}{J_2(a\beta_n)}\times\int_0^{\tau}\exp(\beta_n^2u)[\psi(u)-1]du\right\},$$

where the $a\beta_n$ are the zeros of J_1.

One sees from the form of the solution that the conclusions reached in the case of a constant external field hold without essential modification in this case also. Since the smallest zero of J_1 is larger than that of J_0, one can expect slightly smaller relaxation times in the constant current case. For large values of the time, H approaches asymptotically the known solution $H_0J_1(iR)/J_1(ia)$.

[1] F. and H. London, Proc. Roy. Soc. (London) **A149**, 71 (1935).
[2] M. von Laue, Ann. Physik **32**, 253 (1938); **42**, 65 (1942); Physik. Z. **43**, 274 (1942); Ann. Physik **3**, 31 (1948).
[3] G. U. Schubert, Ann. Physik **5**, 213 (1949).

Excitation Function of $Ta^{181}(d, p)Ta^{182}$

K.-H. SUN, F. A. PECJAK, AND R. A. CHARPIE*
Westinghouse Research Laboratories, East Pittsburgh, Pennsylvania
AND
J. F. NECHAJ
University of Pittsburgh, Pittsburgh, Pennsylvania†
(Received March 16, 1951)

THE excitation function of $Ta^{181}(d, p)Ta^{182}$ was measured[1] by the well-known stack foil technique. Forty 0.00025-in. thick (~10 mg/cm²) Ta foils were bombarded with the deuteron beam from the University of Pittsburgh cyclotron. The energy of the deuteron beam was measured by its range in air to be 15.0 Mev. The range-energy relationship of deuterons in Ta was calculated from data on stopping power as a function of energy obtained from interpolation of the limited information available.[2] The beam current was not measured. However, to evaluate the absolute cross section, two 0.0003-in. aluminum foils were added to the stack. Since the excitation function of $Al^{27}(d, p\alpha)Na^{24}$ is known,[3] the relative yield of Na^{24} in Al foil to Ta^{182} in Ta foil provides a measure of the absolute cross section for the Ta reaction.

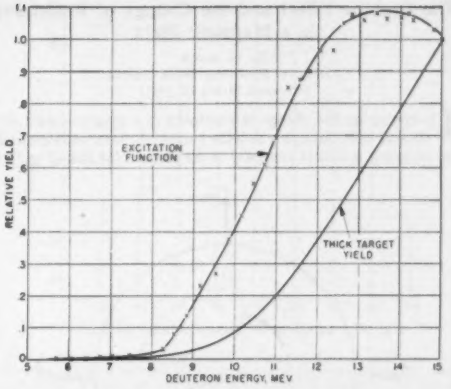

FIG. 1. Relative yield function of the reaction $Ta^{181}(d, p)Ta^{182}$.

When Ta^{181} foils were bombarded with deuterons, three activities, with half-lives 16.3 min, 115 days, and 8.2 hours, were observed. The first two activities are owing to isomers of Ta^{182} formed by the (d, p) process, and the third one is owing to Ta^{180} through the $(n, 2n)$ reaction, fast neutrons being always present in deuteron bombardment. About 5 days after bombardment, however, only the 115-day activity remained. An aluminum-absorption study of this long-lived activity revealed that it contains about 1 percent of 1.1-Mev β^-, 45 percent of 0.52-Mev β^-, and the rest are low energy electrons. The self-absorption formula for these low energy electrons was found to be $C=C_0(1-e^{-0.067\rho})/\rho$, where C is counts/sec, ρ is the surface density, in mg/cm² of the Ta foil, and C_0 is a constant. The 115-day Ta^{182} concentration in the Ta foils was accounted for by the 0.52-Mev activity as determined by the process of "peeling" and "extrapolation" to the zero absorber.

An hour after the deuteron bombardment, and up to a few days later, only one activity with a 15-hour half-period was observed in the Al foils. It was caused by Na^{24} from the reaction $Al^{27}(d, p\alpha)Na^{24}$. This was also confirmed from the absorption curve of the activity, which indicates a single β^- with an energy of 1.4 Mev.

The relative excitation function of the 115-day Ta^{182} and also the relative thick target yield were thus obtained, and they are shown in Fig. 1. At 15.0 Mev, it was found that the relative cross-section ratio for the reactions $Ta^{181}(d, p)Ta^{182}$ and $Al^{27}(d, p\alpha)Na^{24}$ was 25, assuming the end window Tracerlab Geiger counter has the same efficiency for β^- particles of 0.52 Mev and 1.4 Mev. By using 0.028 barn as the extrapolated cross section value for 15.0-Mev deuterons for the reaction $Al^{27}(d, p\alpha)Na^{24}$ after Clarke,[4] it was found that the cross section for 15.0-Mev deuterons from the reaction $Ta^{181}(d, p)Ta^{182}$ was 0.5 barn. The total thick target yield at this deuteron energy was then calculated as $0.5_6\times10^8$ disintegrations/sec per μa hr of deuterons. The cross sections and thick target yield at other deuteron energies can be obtained from these values and the relative yield-curves shown in Fig. 1.

† Assisted by the joint program of the ONR and AEC.
* Now at Oak Ridge National Laboratories, Oak Ridge, Tennessee.
[1] Sun, Pecjak, Charpie, and Nechaj, Phys. Rev. **78**, 338 (1950).
[2] M. S. Livingston and H. A. Bethe, Revs. Modern Phys. **9**, 272 (1937).
[3] E. T. Clarke, Phys. Rev. **71**, 187 (1947).

The Corbino Effect and the Change of Resistance in a Magnetic Field

K. M. Koch
Technische Hochschule, Wien, Austria
(Received March 12, 1951)

IN measuring the change of resistance in a magnetic field in a circular disk through which the current J_r flows radially, while the magnetic field acts vertically to the plane of the disk (Fig. 1), it

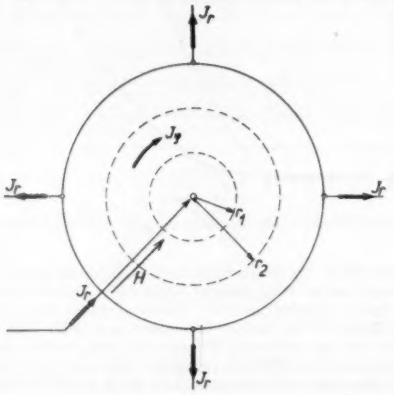

FIG. 1. Arrangement for measuring change of resistance in a magnetic field.

is found that $(\Delta R/R)_H$ decreases appreciably if the flow of the Corbino current J_φ is prevented or at least hindered by a radial slit. We have examined this phenomenon, already observed by Ettingshausen,[1] with Bi at a temperature of 80°K and found that $(\Delta R/R)_H$ decreases from 51.8 percent to 38 percent ($H=700$ oersted) if the disk is slit in the manner described above. (Of course, the slit cannot cause a change in the value of R at $H=0$; this constitutes a control for the radial character of the current.) The Hall constant also could be measured on the slit disk; it decreases perceptibly at this temperature if the field strength increases (especially in Bi which is not extremely pure). At $H=700$ oersted, we found $R_H=28$ emu.

The knowledge of R_H enables us to calculate J_φ and the Joule heat Q generated by it. It can be assumed that Q corresponds to the work necessary to overcome the additional resistance ΔR.[2] If we put the results of our measurements into the equation $Q=J_r^2\Delta R$, we find that Q accounts for only approximately $\frac{1}{3}$ of $J_r^2\Delta R$. Better conformity is achieved by putting $Q=J_r^2(\Delta R-\Delta R')$, where $\Delta R'$ means the change of resistance in the magnetic field which remains after the slitting of the disk.

To examine these relations under somewhat altered conditions, we measured the Hall electromotive force E_H in a plate, as shown in Fig. 2. The broadened side parts were intended to make possible

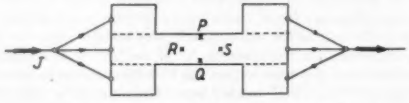

FIG. 2. Arrangement for measuring Hall emf.

a partial compensation of E_H. After measuring E_H and $(\Delta R/R)_H$ on this sample, the side parts were sawed off along the dotted lines. As expected, the measurement now showed approximately an 18 percent increase of E_H but a 2 percent decrease of change of resistance. (These measurements were carried out at 293°K.)

Detailed theoretical and experimental research is now in progress to ascertain whether more than one mechanism of change of resistance must be considered for the explanation of the results described above. At any rate, it will be necessary to consider these effects as a source of error in determining the change of resistance in a magnetic field.

[1] A. v. Ettingshausen, Wien. Berichte **XCV**, II, 737 (1887).
[2] P. W. Bridgman, Phys. Rev. **24**, 644 (1924).

π^+ Meson Mass Determination*

W. F. Cartwright
Radiation Laboratory, Department of Physics, University of California, Berkeley, California
(Received February 9, 1951)

IN a previous letter,[1] initial results were reported on measurements made, at the 184-in. synchrocyclotron, of the cross section for the production of π^+ mesons at zero degrees by proton-proton interaction.

The high peak in the meson spectrum at maximum meson energy results from the strong interaction of the product nucleons. This sharp peak provides a method of measuring the π^+ meson mass, since the meson energy at the peak depends only on the meson mass, the proton beam energy, and the total mass of the resulting nucleons. (The possibility of deuteron formation had been suggested earlier.[2,3] If a deuteron is formed, its binding energy is available to the reaction.)

The effect of the interaction of the product nucleons on the meson production cross section has been investigated theoretically by Watson and Brueckner,[4] following a suggestion by Brueckner, Chew, and Hart. We have improved the measurement of the meson spectrum so that, with the increased resolution, we can now more critically compare the experimental results with the theoretical spectra. We have concluded from this comparison that meson production at maximum meson energy is accompanied by the formation of a deuteron.[5]

The resolution, determined by the proton beam energy spread, the straggling in range, and the multiple small angle scattering of the mesons, has been estimated. Figure 1 shows the result of folding the resolution into two of the theoretical curves of Watson and Brueckner. Curve I is for the case in which the product nucleons are in the triplet S state. Some deuteron formation would be expected in this case. Since the main feature of this spectrum

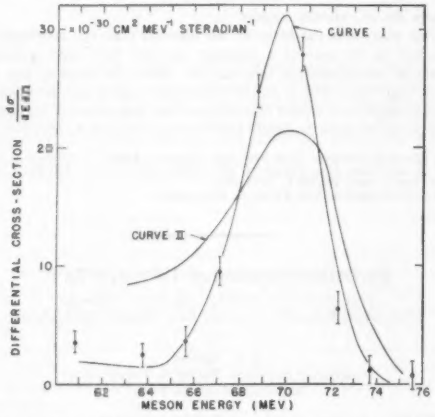

FIG. 1. Differential cross section for the production at zero degrees of π^+ mesons by 340-Mev protons on protons. Curve I: product nucleons in ^3S state. Curve II: product nucleons in ^1S state. The curves have been normalized so that the area under each, from 65.5 Mev to 76.0 Mev, is equal to the area under the experimental points in the same energy interval.

is a line displaced upward by 4 Mev from a continuum, this curve is essentially a plot of the estimated resolution. Curve II, for the case in which the product nucleons are in the singlet S state, also exhibits a peak because of the resonance resulting from the low energy virtual state. It is clear that the experimental points, also plotted, are not in agreement with either the half-width or the asymmetric character of curve II. On the other hand, the close fit of curve I with the experimental results is strong evidence that the peak corresponds to deuteron formation. Therefore, it is the deuteron mass which should be used in the calculation of the π^+ meson mass from the meson energy at the peak.

The proton beam energy was measured from its Čerenkov radiation by R. Mather to an accuracy of about ±1 Mev. The energy of each meson was found from its range, as calculated from the most recent range-energy curves.[6–8]

The π^+ meson mass, as determined by this experiment, is 275.1±2.5 electron masses. The estimated systematic errors account for most of the quoted probable error.

The details of the entire experiment will be published later.

It is a pleasure to acknowledge the help and encouragement of Professors C. Richman and H. A. Wilcox, and Dr. K. M. Watson.

* This work was performed under the auspices of the AEC.

[1] Cartwright, Richman, Whitehead, and Wilcox, Phys. Rev. **78**, 823 (1950).
[2] Morand, Cüer, and Moucharafyeh, Compt. rend. **226**, 1974 (1948).
[3] Walter Barkas, Phys. Rev. **75**, 1109 (1949).
[4] K. M. Watson and K. A. Brueckner, to be published.
[5] In addition to the evidence presented below, Crawford, Crowe, and Stevenson recently detected directly the deuteron in this reaction. [Phys. Rev. **82**, 97 (1951)].
[6] Aron, Hoffman, and Williams, AECU 663 (unpublished).
[7] C. J. Bakker and E. Segrè, Phys. Rev. **81**, 489 (1951).
[8] R. Mather and E. Segrè, private communication (to be published later).

Photonuclear Effects in Carbon from 100-Mev Betatron X-Rays

E. R. Gaerttner and M. L. Yeater
General Electric Research Laboratory, Schenectady, New York
(Received March 16, 1951)

A METHANE-FILLED cloud chamber[1] has been used to observe the photodisintegration of carbon nuclei by x-rays from a 100-Mev betatron. The disintegrations are produced in the gas at one-half atmosphere pressure by a collimated beam of x-rays which passes diametrically through the cloud chamber. The present results are based on the examination of 1800 disintegrations involving the emission of charged particles.

The observed disintegrations form "stars," consisting of three or more tracks with a common origin, and "flags," consisting of a short heavy track from the residual nucleus and a longer, lighter track from a single emitted charged particle. The ratios of flags to 3-prong stars to 4-prong stars are found to be 31:5.5:1 at a peak x-ray energy of 100 Mev and 60:5.5:1 at a peak x-ray energy of 50 Mev. Two 5-prong stars were observed.

About ninety percent of the flags from carbon represent the emission of a charged particle alone, without an accompanying neutron. The identification procedure is the same as previously described.[2] Not more than ten percent of the flags can be ascribed to $C^{12}(\gamma, n\hat{p})B^{10}$. It is believed that the $C^{12}(\gamma, \hat{p})B^{11}$ reaction is principally involved, although a contribution from the $(\gamma, \hat{d})$ or (γ, He^3) reactions is not ruled out by the present evidence. The reaction $C^{12}(\gamma, He^4)Be^8$ is, of course, excluded as an origin of flags by the instability of the Be^8, but it is undoubtedly responsible for some of the observed 3-prong stars.

The yield of flags in methane has been referred to the yield of flags in nitrogen,[3] for which the approximate integrated cross section has been previously determined, by comparing x-ray intensities with an ionization chamber. In this way, we obtain an integrated cross section for the carbon flags, which is 0.22±0.09 Mev-barn, for a peak x-ray energy of 100 Mev.

The angular distribution of the flags from carbon for a peak x-ray energy of 100 Mev is shown in Fig. 1. The angle measured is

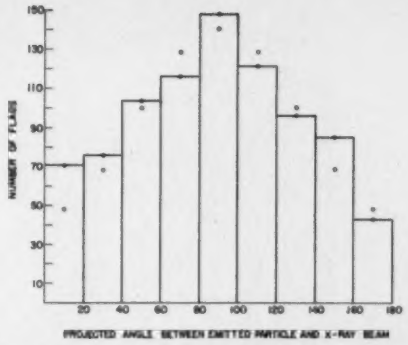

FIG. 1. The angular distribution of the carbon flags in methane. The angles are measured between the x-ray beam and the projection in the plane of the cloud chamber of the track of the emitted particle. The points indicated by open circles are calculated from the space distribution $f(\theta)d\Omega \sim (1+3\sin^2\theta)d\Omega$ by a transformation appropriate to the cloud chamber geometry.

that between the x-ray beam and the projection in the plane of the cloud chamber of the track of the emitted particle. Flags which obviously involve neutron emission are not included. This angular distribution, when transformed into a space distribution, can be represented approximately by the function

$$f(\theta)d\Omega \sim (1+a\sin^2\theta)d\Omega,$$

where θ is the space angle between the x-ray beam and the path of the emitted particle, and $a \cong 3$. This differs from the helium photo-proton distribution,[4] which is compatible with a pure $\sin^2\theta$ function.

We wish to thank Dr. E. E. Charlton for support of our research program with the 100-Mev betatron. The cloud chamber equipment was developed with funds from the ONR.

[1] E. R. Gaerttner and M. L. Yeater, Rev. Sci. Instr. **20**, 588 (1949).
[2] E. R. Gaerttner and M. L. Yeater, Phys. Rev. **79**, 401 (1950).
[3] E. R. Gaerttner and M. L. Yeater, Phys. Rev. **77**, 714 (1950).
[4] E. R. Gaerttner and M. L. Yeater, Phys. Rev. (to be published).

Coincidence Studies on the Radiations from Ba^{131}

W. H. Cuffey
*Physics Department, Indiana University, Bloomington, Indiana**
(Received February 26, 1951)

THE half-life of Ba^{131} is 12 days, and it can be formed by neutron capture in barium. It is the parent in the chain $Ba^{131} \rightarrow Cs^{131} \rightarrow Xe^{131}$. The properties of the radiations from Ba^{131} were first investigated by Yu, Gideon, and Kurbatov[1] using absorption and cloud-chamber techniques. These investigations showed that no positrons were emitted and established the fact that Ba^{131} decays by orbital electron capture. Internal conversion electrons were found. Absorption experiments in lead of the gamma-rays showed three gamma-rays of energies 0.220, 0.500, and 1.7 Mev. Katcoff[2] performed similar absorption experiments and found gamma-rays of energy 0.26, 0.5, and 1.2 Mev. In addition, he measured the absorption of the electrons in aluminum and found two groups at energies of 0.42 and 0.24 Mev. Finally, Dale, Richert, Redfield, and Kurbatov[3] and Zimmerman. Dale, Thomas, and Kurbatov[4] have measured the spectrum of the gamma-rays in a magnetic lens spectrograph and found two lines—one at 0.496 and the other at 0.213 Mev.

Since the investigation of the $Ba^{131} \rightarrow Cs^{131}$ chain is under investigation in this laboratory, the present experiments were undertaken to obtain more information, especially on the high energy gamma-ray.

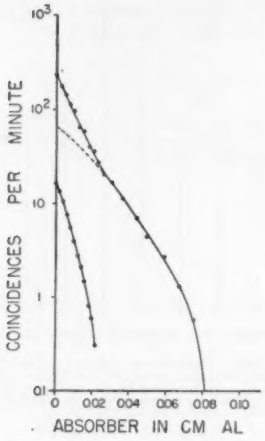

FIG. 1. Coincidence absorption curve.

Barium was irradiated by neutrons in the Oak Ridge pile, and after a chemical separation the barium fraction was investigated using coincidence counting techniques. Since Cs^{131} emits only x-rays and Auger electrons,[5] the growth of the daughter poses no problems. An absorption curve in lead was taken on the gamma-rays of Ba^{131}, with a lead lined counter whose gamma-ray efficiency is known as a function of energy. These experiments showed three gamma-ray groups at energies 0.16, 0.42, and 1.2 Mev, of relative intensities 1:1:0.25.

A coincidence absorption curve of Compton electrons ejected from a brass radiator by the gamma-rays was taken and is shown in Fig. 1. An analysis of the data by the method of Bleuler and Zunti shows two gamma-rays of energies 0.83 and 0.46 Mev.

Absorption in aluminum of the electrons from Ba^{131} showed two groups of energies approximately 0.5 and 0.2 Mev. These are presumably conversion electrons.

A measurement of gamma-gamma coincidences was made using two lead-lined counters. Coincidences were found, and a value of $N_{\gamma\gamma}/N_{\gamma}=0.24\times10^{-3}$ obtained. The interposition of 0.37 cm of lead reduced the gamma-gamma coincidence rate by a factor of 17. From consideration of counter efficiencies it seems likely that the gamma-gamma coincidences are between the gamma-ray at 0.46 Mev (actually 0.497 Mev) and one of the lower energy gamma-rays, around 0.2 Mev. Efficiency considerations exclude the 0.46- and the 0.83-Mev lines being in coincidence.

Spectroscopic experiments in this laboratory[6] show that Ba^{131} has a number of gamma-rays. These come at 0.497, 0.371, 0.241, 0.213, 0.196, and 0.122 Mev with the 0.497 being the strongest. The present experiments are in agreement with these findings, confirm the results of earlier workers, and establish a lower value, 0.83 Mev, for the highest energy gamma-ray. In addition, the coincidence experiments show that the gamma-ray at 0.46 Mev is in cascade with lower energy gamma-rays.

The author is indebted to Professor A. C. G. Mitchell, who suggested this problem, for his interest in the work.

* Supported by the joint program of the ONR and AEC.

[1] Yu, Gideon, and Kurbatov, Phys. Rev. 71, 382 (1947).
[2] S. Katcoff, Phys. Rev. 72, 1160 (1947).
[3] Dale, Richert, Redfield, and Kurbatov, Phys. Rev. 80, 763 (1950).
[4] Zimmerman, Dale, Thomas, and Kurbatov, Phys. Rev. 80, 908 (1950).
[5] Canada and Mitchell (private communication).

THE AMERICAN INSTITUTE OF PHYSICS

INCORPORATED

57 East [illegible] New York 21, N.Y.

MEMBER SOCIETIES:

American [illegible] Society
[illegible], *Secretary*, Columbia University, New York 27.

Optical Society of America
[illegible], *Secretary*, Massachusetts Institute of Technology 39, Massachusetts.

American Society of Mechanical Engineers
[illegible], *Secretary*, 29 West 39th Street, New York 22.

Society of Rheology
[illegible], *Secretary*, North American Aviation, Inc., P. O. Box [illegible], California.

American Association of Physics Teachers
[illegible], *Secretary*, University of Illinois, Urbana, Illinois.

AFFILIATED SOCIETIES:

American Crystallographic Association
Electron Microscope Society of America
Physics Society of Pittsburgh
Physics Club of Chicago
Physics Club of Philadelphia
Cleveland Physics Society
Physics Club of the Lehigh Valley

ASSOCIATES:

Over [illegible] leading industrial laboratories and other institutions which contribute to the support of the Institute.

JOURNALS:

The Physical Review
[illegible], *Editor*, Brookhaven National Laboratory, Upton, Long Island, New York.

Reviews of Modern Physics
[illegible], *Editor*, University of Minnesota, Minneapolis, Minnesota.

Journal of the Optical Society of America
[illegible], *Editor*, National Bureau of Standards, Washington 25, D. C.

The Journal of the Acoustical Society of America
[illegible], *Editor*, 57 East 55th Street, New York 22.

American Journal of Physics
[illegible], *Editor*, Michigan State College, East Lansing, Michigan.

The Review of Scientific Instruments
[illegible], *Editor*, Mellon Institute and Sarah Mellon Scaife Laboratories of the University of Pennsylvania, Pittsburgh, Pennsylvania.

The Journal of Chemical Physics
[illegible], *Editor*, Institute for Nuclear Studies, University of Chicago, Chicago 37, Illinois.

Journal of Applied Physics
[illegible], *Editor*, Case Institute of Technology, Cleveland, Ohio.

Physics Today
[illegible], *Editor*; Robert R. Davis, Managing Editor, American Institute of Physics, 57 East 55 Street, New York 22, New York.

CORPORATION

Gaetano R. [illegible], *Chairman*
Massachusetts Institute of Technology

Gaetano E. [illegible], *Treasurer*
Columbia University

GOVERNING BOARD

I. W. [illegible]
C. Pabst [illegible]
Wallace R. [illegible]
W. [illegible], Jr.
S. A. [illegible]
G. P. [illegible]
George B. [illegible]
F. [illegible]
Ronald [illegible]
Paul [illegible]
F. [illegible]
I. R. [illegible]
George [illegible]
I. I. [illegible]
Dean [illegible]
Harold C. [illegible]
Frederick [illegible]
Frederick [illegible]
John [illegible]

Committee on Printing
[illegible], *Chairman*

ADMINISTRATIVE STAFF

Henry [illegible], *Director*
Wallace [illegible], *Executive Secretary*
Thurston [illegible], *Associate Manager and Assistant Treasurer*
Ruth P. Bryans, *Publication Manager*
Betty H. Goodridge, *Assistant Secretary*
Eleanor G. Rhoades, *Circulation Manager*
Kenneth Seeds, *Senior Associate*

THE American Institute of Physics was founded in 1931 as a federation of leading societies in the field of physics. It combines into one operating agency those functions on behalf of physics which can best be done by the Societies jointly. The purpose is the advancement and diffusion of physics and its applications to human welfare. It publishes and is publisher or [illegible] of the [illegible] journals listed on this page; promotes unity and effectiveness of effort among all who are interested in physics; renders numerous services to physicists and to the public; and cooperates with governmental agencies, various associations, educational institutions, technical industries, and others in such manner as to realize the opportunities and fulfill the responsibilities of physics as an important and constructive human activity.